REPORT NUMBER 157

MARCH 1965

Volume I
NAL SYSTEMS ANALYSIS AND
FLIGHT SIMULATION REPORT

DDC AVAILABILITY NOTICES

1. Distribution of thid document is unlimited.

2. This document is subject to special report controls and each transmittal to foreign governments or foreign nationals may be made only with prior approval of US Army Aviation Materiel Laboratories, Fort Eustis, Virginia 23604.

3. In addition to security requirements which must be met, this document is subject to special export controls and each transmittal to foreign governments or foreign nationals may be made only with prior approval of USAAVLABS, Fort Eustis, Virginia 23604.

4. Each transmittal of this document outside the agencies of the US Government must have prior approval of US Army Aviation Materiel Laboratories, Fort Eustis, Virginia 23604.

5. In addition to security requirements which apply to this document and must be met, each transmittal outside the agencies of the US Government must have prior approval of US Army Aviation Materiel Laboratories, Fort Eustis, Virginia.

6. Each transmittal of this document outside the Department of Defense must have prior approval of US Army Aviation Materiel Laboratories, Fort Eustis, Va.

7. In addition to security requirements which apply to this document and must be met, each transmittal outisde the Department of Defense must have prior approval of US Army Aviation Materiel Laboratories, Fort Eustis, Virginia 23604.

8. This document may be further distributed by any holder only with specific prior approval of US Army Aviation Materiel Laboratories, Fort Eustis, Va. 23604.

9. In addition to security requirements which apply to this document and must be met, it may be further distributed by the holder only with specific prior approval of US Army Aviation Materiel Laboratories, Fort Eustis, Virginia 23604.

DISCLAIMER

DISPOSITION INSTRUCTIONS

13. Destroy this report when no longer needed. Do not return it to originator.

14. When this report is no longer needed, Department of the Army organizations will destroy it in accordance with the procedures given in AR 380-5. Navy and Air Force elements will destroy it in accordance with applicable directions. Department of Defense contractors will destroy the report according to the requirement of Section 14 of the Industrial Security Manual for Safeguarding Classified Information. All others will return the report to US Army Aviation Materiel Laboratories, Fort Eustis, Virginia 23604.

REPORT NUMBER 157

FINAL SYSTEMS ANALYSIS AND

FLIGHT SIMULATION REPORT

VOLUME I

XV-5A Lift Fan
Flight Research Aircraft Program

March 1965

ADVANCED ENGINE AND TECHNOLOGY DEPARTMENT
GENERAL ELECTRIC COMPANY
CINCINNATI, OHIO 45215

CONTENTS

LIST OF FIGURES

BLANK PAGE

SYMBOLS AND NOMENCLATURE

A_F — Main Fan Area, total for two fans, ft^2

A_{NF} — Nose fan area, ft^2

AVE — Subscript denoting average of right and left wing fans.

b — Wingspan, ft.

$\bar{c}$ — Wing mean aerodynamic chord, ft.

$\bar{c}_e$ — Elevator mean aerodynamic chord, ft.

c. g. — Center of gravity

C_D — Drag coefficient, $\dfrac{D}{qS_w}$

$C_D{}^s$ — Slipstream drag coefficient, $\dfrac{D}{q^s A_F}$

C_{D_o} — Drag coefficient at zero lift

C_{D_t} — Tail drag coefficient, $\dfrac{D_t}{qS_t}$

C_L — Lift coefficient, $\dfrac{L}{qS_w}$

$C_L{}^s$ — Slipstream lift coefficient, $\dfrac{L}{q^s A_F}$

C_{L_t} — Tail lift coefficient, $\dfrac{L_t}{qS_t}$

CM — Complete model

C_m — Pitching moment coefficient, $\dfrac{M}{qS_w \bar{c}}$

C_m^s Slipstream pitching moment coefficient, $\dfrac{M}{q^s A_F D_F}$

C_N Normal force coefficient, $\dfrac{N}{q S_w}$

C_N^s Slipstream normal force coefficient, $\dfrac{N}{q^s A_F}$

C_{N_t} Tail normal force coefficient, $\dfrac{N_t}{q S_w}$

C_X Axial force coefficient, $\dfrac{X}{q S_w}$

C_X^s Slipstream axial force coefficient, $\dfrac{X}{q^s A_F}$

C_{X_t} Tail axial force coefficient, $\dfrac{X_t}{q S_w}$

C_Y Sideforce coefficient, $\dfrac{Y}{q S_w}$

C_Y^s Slipstream sideforce coefficient, $\dfrac{Y}{q^s S_w}$

C_ℓ Rolling moment coefficient, $\dfrac{\ell}{q S_w b}$

C_ℓ^s Slipstream rolling moment coefficient, $\dfrac{\ell}{q^s S_w b}$

C_n Yawing moment coefficient, $\dfrac{N}{q S_w b}$

C_n^s Slipstream yawing moment coefficient, $\dfrac{N}{q^s S_w b}$

$C_{N_\alpha}^s$ $\dfrac{\partial C_N^s}{\partial \alpha}$

C_N^s Slipstream normal force coefficient, $\dfrac{N}{q^s A_F}$

$C_{N_o}^s$ Slipstream normal force coefficient at $\beta_v = \beta_v = \alpha = 0$

cps   Cycles Per Second

$$C_{L_q} \qquad \frac{\partial C_L}{\partial \left(\frac{q\bar{c}}{2V}\right)}$$

$$C_{L_{\dot{\alpha}}} \qquad \frac{\partial C_L}{\partial \left(\frac{\dot{\alpha}\bar{c}}{2V}\right)}$$

$$C_{m_q} \qquad \frac{\partial C_m}{\partial \left(\frac{q\bar{c}}{2V}\right)}$$

$$C_{m_{\dot{\alpha}}} \qquad \frac{\partial C_m}{\partial \left(\frac{\dot{\alpha}\bar{c}}{2V}\right)}$$

$$C_{Y_r} \qquad \frac{\partial C_Y}{\partial \left(\frac{rb}{2V}\right)}$$

$$C_{Y_p} \qquad \frac{\partial C_Y}{\partial \left(\frac{pb}{2V}\right)}$$

$$C_{n_r} \qquad \frac{\partial C_n}{\partial \left(\frac{rb}{2V}\right)}$$

C_{n_p} $\qquad$ $\dfrac{\partial C_n}{\partial \left(\dfrac{pb}{2V}\right)}$

C_{ℓ_r} $\qquad$ $\dfrac{\partial C_\ell}{\partial \left(\dfrac{rb}{2V}\right)}$

C_{ℓ_p} $\qquad$ $\dfrac{\partial C_\ell}{\partial \left(\dfrac{pb}{2V}\right)}$

C_{h_e} $\qquad$ Elevator hinge moment coefficient, $\dfrac{H_e}{q S_e \bar{c}_e}$

$C_{h_{\delta_e}}$ $\qquad$ $\dfrac{\partial C_{h_e}}{\partial \delta_e}$

C_{h_α} $\qquad$ $\dfrac{\partial C_{h_e}}{\partial \alpha}$

$\Delta C_{N_{\beta_v}}^s$ $\qquad$ $\dfrac{\partial C_N^s}{\partial \beta_v}$, evaluated at $\beta_s = 0$

$\Delta C_{N_{\beta_s}}^s$ $\qquad$ $\dfrac{\partial C_N^s}{\partial \beta_s}$, evaluated at β_v corresponding to proper T_c^s value.

$C_{N_T}^s$ $\qquad$ $\dfrac{\partial C_{N_\alpha}^s}{\partial T} = \left(\dfrac{\partial C_{N_\alpha}^s}{\partial T}\bigg|_{\beta_v=0}\right)\alpha + \dfrac{\partial}{\partial \beta_v}\left(\dfrac{\partial C_{N_\alpha}^s}{\partial T}\right)\alpha\beta_v$,

$\qquad$ variation of $C_{N_\alpha}^s$ with wing fan thrust and vector angle

$\dfrac{\partial C_{N_T}{}^s}{\partial \alpha}\bigg|_{\beta_v = 0}$ Slope of $C_{N_T}{}^s$. Change in slipstream normal force

coefficient due to fan thrust with angle of attack at $\beta_v = 0$.

$\dfrac{\partial}{\partial \beta_v}\left(\dfrac{\partial C_{N_\alpha}{}^s}{\partial T}\right)$ Variation of $\dfrac{\partial C_{N_\alpha}{}^s}{\partial T}$ with vector angle change.

$\Delta C_N{}^s$ (Sin α)   Low speed variation of $C_N{}^s$ with angle of attack over

entire range of angles of attack.

$C_{X_\alpha}{}^s$ $\dfrac{\partial C_X{}^s}{\partial \alpha}$

$\Delta C_{X_{\beta_s}}{}^s$ $\dfrac{\partial C_X{}^s}{\partial \beta_s}$, evaluated at β_v corresponding to proper $T_c{}^s$

value.

$\Delta C_{X_{\beta_v}}{}^s$ $\dfrac{\partial C_X{}^s}{\partial \beta_v}$, evaluated at $\beta_s = 0$

$C_{X_T}{}^s$ Same as $C_{N_T}{}^s$ term, with N replaced by X

$C_{L_{\delta_e}}$ $\dfrac{\partial C_L}{\partial \delta_e}$

$C_{N_{\delta_e}}$ $\dfrac{\partial C_N}{\partial \delta_e}$

$C_{m_o}{}^s$ Slipstream pitching moment coefficient at $\beta_v = \beta_s = \alpha = 0$

$C_{m_\alpha}^s$ $\qquad$ $\dfrac{\partial C_m^s}{\partial \alpha}$

$\Delta C_{m_{\beta_s}}^s$ $\qquad$ $\dfrac{\partial C_m^s}{\partial \beta_s}$, evaluated at β_v corresponding to proper T_c^s value.

$\Delta C_{m_{\beta_v}}^s$ $\qquad$ $\dfrac{\partial C_m^s}{\partial \beta_v}$, evaluated at $\beta_s = 0$.

$\dfrac{\partial C_m}{\partial |\beta|}$ $\qquad$ Variation of pitching moment coefficient with sideslip angle.

$C_D S$ $\qquad$ Fuselage side force coefficient multiplied by the fuselage projected side area, $\dfrac{Y_{fuse}}{q}$.

$\Delta C_m^s (\text{Sin} (\alpha - 50^\circ))$ $\qquad$ Low speed variation of C_m^s with angle of attack over entire range of angles of attack.

$C_{Y_\beta}^s$ $\qquad$ $\dfrac{\partial C_Y^s}{\partial \beta}$

$C_{Y_{\delta_a}}$ $\qquad$ $\dfrac{\partial C_Y}{\partial \delta_a}$

$C_{n_\beta}^s$ $\qquad$ $\dfrac{\partial C_n^s}{\partial \beta}$

$C_{n_{\delta_a}}$ $\qquad$ $\dfrac{\partial C_n^s}{\partial \delta_a}$

$C_{n_{\delta_r}}$ $\qquad$ $\dfrac{\partial C_n}{\partial \delta_r}$

$C_{\ell_\beta}{}^s$ $\qquad$ $\dfrac{\partial C_{\ell}{}^s}{\partial \beta}$

$C_{\ell_{\delta_a}}$ $\qquad$ $\dfrac{\partial C_\ell}{\partial \delta_a}$

$C_{\ell_{\delta_r}}$ $\qquad$ $\dfrac{\partial C_\ell}{\partial \delta_r}$

$C_{p_{NF}}{}^s$ $\qquad$ Nose-fan power coefficient, $\dfrac{P_{NF}\,\rho^{1/2}}{\left(\dfrac{T_{o_{NF}}}{A_{NF}}\right)^{3/2} A_{NF}}$

$C_{p_{o_{NF}}}$ $\qquad$ Nose-fan power coefficient at $T_{c_{NF}}{}^s = 1.0$

$C_p{}^s$ $\qquad$ Main fan power coefficient, $\dfrac{P_F\,\rho^{1/2}}{\left(\dfrac{T_{ooo}}{A_F}\right)^{3/2} A_F}$

$C_{p_o}{}^s$ $\qquad$ Main fan power coefficient at $T_c{}^s = 1$, $\beta_v = \beta_s = 0$

$C_{p_{\beta_s}}{}^s$ $\qquad$ Main fan power coefficient increment due to β_s

$C_{L_{\alpha_t}}$ $\qquad$ $\dfrac{\partial C_{L_t}}{\partial \alpha_t}$

$\Delta C_N{}^s(\alpha)$	Original low-speed data from which $\Delta C_N{}^s(\text{Sin } \alpha)$ was derived.
$\Delta C_X{}^s(\alpha)$	Original low-speed data not used in this simulation. Its omission is explained in Section 2.2.2.
$\Delta C_m{}^s(\alpha)$	Original low-speed data from which $\Delta C_m{}^s(\text{Sin }(\alpha - 50^\circ))$ was derived.
$C_{N_{o}}{}^S{}_{NF}$	Nose fan normal force coefficient. Not used in this simulation.
$C_{X_{o}}{}^s{}_{NF}$	Nose fan axial force coefficient. Not used in this simulation.
D	Drag, lbs., damping, lb./ft./sec.
D_t	Drag of the horizontal tail, lbs.
D_F	Fan Diameter, feet.
E_{IN}	Input voltage.
E_O	Output voltage
F	Force, lbs., Also Subscript Denoting Main Fan.
F_N	Net J-85 thrust in the turbojet mode.
f	frequency, cycles per second.
g	gravitational acceleration, ft./sec.^{2}
g_x	gravity component along body x axis.
g_y	gravity component along body y axis.
g_z	gravity component along body z axis.

$G(jw)$	Frequency response of a system or component.
h	altitude, ft.
$\dot{h}$	rate of climb, $-(u\ell_z + vm_z + wn_z)$, ft./sec.
H_x	Angular momentum component along body x axis.
H_y	Angular momentum component along body y axis.
H_z	Angular momentum component along body z axis.
H_e	Elevator hinge moment, ft. lbs.
i_t	Tail incidence angle, degrees nose up from waterline.
$\hat{i}$	Unit vector along body x axis.
IN	Input
I_x	Body moment of inertia about x axis.
I_y	Body moment of inertia about y axis.
I_z	Body moment of inertia about z axis.
I_{xz}	Body product of inertia between x and y axes.
i	Complex operator, $\sqrt{-1}$
$\hat{j}$	Unit vector along body y axis.
$\hat{k}$	Unit vector along body z axis.
K_e	Elevator system spring constant referred to elevator hinge line.
K_i	Term used in calculating induced drag on horizontal tail.

$K_T \eta_T$	Horizontal tail efficiency factor.
K_{TS}	Thrust spoiler effectiveness.
$K_{N_{NF}}$	Function describing variation of nose fan thrust with thrust reverser door position.
$K_{X_{NF}}$	Not used in this simulation.
ℓ	Rolling moment, ft. lbs.
L	Lift, lbs.
LT	Refers to left wing fan.
ℓ_x	Cosine of angle between body x axis and inertial x axis.
ℓ_y	Cosine of angle between body x axis and inertial y axis.
ℓ_z	Cosine of angle between body x axis and inertial z axis.
ℓ_t	tail moment arm, feet.
ma	Milliamps
mv	Millivolts
$\mathcal{M}$	Pitching moment, ft. lbs.
m_x	Cosine of angle between body y axis and inertial x axis.
m_y	Cosine of angle between body y axis and inertial y axis.
m_z	Cosine of angle between body y axis and inertial z axis.
MF	Refers to main fans.
m	Mass, slugs.

$\dot{m}_{MF}$ Main fan mass flow rate, slugs/sec. (both fans).

$\dot{m}_{NF}$ Nose fan mass flow rate, slugs/sec.

MNF   "MODIFIED NEW FUNCTION", used in conjunction with ΔC_m^s (Sin (α-50°)) in generating the low speed angle of attack caused variations in pitching moment.

N   Normal force, lbs.; also $100 - N_g$, percent

$\mathcal{N}$ Yawing moment, ft. lbs.

n_x Cosine of angle between body z axis and inertial x axis, also load factor in x direction, g's.

n_y Cosine of angle between body z axis and inertial y axis, also load factor in y direction, g's.

n_z Cosine of angle between body z axis and inertial z axis, also load factor in z direction, g's.

N_{RWF} Right wing fan RPM, percent of maximum.

N_g Percent gas generator RPM.

N_{LWF} Left wing fan RPM, percent of maximum.

N_F Wing fan RPM, percent of maximum.

N_{NF} Nose fan RPM, percent of maximum.

OUT   Output

P_F Wing fan power, a function of N_g, ft. lb./sec.

P_{NF} Nose fan power, a function of N_g, ft. lb./sec.

POT   Potentiometer

PSF	Pounds per square foot.
POF #1	First phasing function used with low speed terms.
POF #2	Second phasing function used with low speed terms.
p	Body axis roll rate, rad./sec.
q^s	Slipstream dynamic pressure, $\dfrac{T_{ooo}}{A_F} + \rho \dfrac{V_T^2}{2}$, lbs/ft.^{2}
q^s_{AVE}	Average q^s for right and left wing fans.
q^s_{RT}	Right wing fan slipstream dynamic pressure.
q^s_{LT}	Left wing fan slipstream dynamic pressure.
q	Dynamic pressure, $\dfrac{\rho}{2} V_T^2$, lbs./ft.^{2}
q	Body axis pitch rate, rad./sec.
r	Body axis yaw rate, rad./sec.
R_q	Ratio of free stream to slipstream dynamic pressure, $\dfrac{q}{q^s}$. Also is equivalent to $1-T_c^s$.
RT	Refers to right wing fan.
RMS	Root mean square.
S_w	Wing area, ft.^{2}
$\dot{S}_x$	Velocity along inertial x axis, $u\ell_x + vm_x + wn_x$, ft./sec.
SA	Stability augmentation

$\dot{s}_y$ Velocity along inertial y axis, $u\ell_y + vm_y + wn_y$, ft./sec.

$\dot{s}_z$ Velocity along inertial z axis, $-\dot{h}$, $u\ell_z + vm_z + wn_z$, ft./sec.

s_x $\int \dot{s}_x dt$, ground distance in inertial x direction.

s_y $\int \dot{s}_y dt$, ground distance in inertial y direction.

s_z $\int \dot{s}_z dt$, ground distance in inertial z direction.

s_t Tail area, ft.^{2}

s_e Elevator area, ft.^{2}

s Laplace operator

t time, seconds

T_j Turbojet thrust. Equivalent to F_N.

$T_{\text{ooo}_{RT}}$ Right wing fan thrust if β_s, β_v and V_T were reduced to zero. A function of N_F and ρ only.

$T_{\text{ooo}_{LT}}$ Same as above for left wing fan.

T_{NF} Nose fan thrust.

$T_{o_{NF}}$ Nose fan thrust if V_T were reduced to zero. A function of N_{NF} and ρ only.

TF Short Notation for Transfer Function

$T_c{}^s$ Thrust coefficient, $\dfrac{T_{ooo}/A_F}{\rho \dfrac{V_T{}^2}{2} + T_{ooo}/A_F}$

Also average $T_c{}^s$.

$T_{1/2}$ Time to one-half amplitude

T_2 Time to double amplitude

u Inertial velocity along body x axis.

u_w Component of wind velocity along body x axis.

u_a Aerodynamic velocity along body x axis. $u_a = u + u_w$.

$V,\ V_T$ Total velocity, ft./sec., $\sqrt{u^2 + v^2 + w^2}$.

v Volts

v Inertial velocity along body y axis.

v_w Component of wind velocity along body y axis.

v_a Aerodynamic velocity along body y axis. $v_a = v + v_w$.

W Weight, lbs.

w Inertial velocity along body z axis.

X Axial force, lbs.

x Distance along body x axis, ft., Positive fwd.

$\bar{x}$ Distance along body x axis from a point to c.g.

$\bar{x}_{NF}$ Distance from center of nose-fan to c.g., ft.

$\bar{x}_T$ Tail moment arm, ft.   Equivalent to ℓ_t.

y Distance along body y axis, ft., positive out rt. wing.

Y Sideforce, lbs.

y_F Wing fan moment arm, ft.

$\bar{y}$ Distance along body y axis from a point to c.g.

z Distance along body z axis, ft.   Positive downward.

z_t Tail moment arm in xz plane.

$\bar{z}$ Distance along body z axis from a point to c.g.

Z Force along body Z axis,   -N, pounds

α Angle of attack, $\sin^{-1} \dfrac{w}{\sqrt{u^2 + w^2}}$, degrees.

α_{LIM} Angle of attack, limited to some maximum value for purposes of this simulation, average.

β Sideslip angle, $\sin^{-1} \dfrac{v}{V_T}$, degrees.

β_{LIM} Sideslip angle, limited to some maximum value for purposes of this simulation.

$\beta_{s_{RT}}$ Right wing louver stagger angle, $\beta_{2_R} - \beta_{1_R}$, degrees.

$\beta_{s_{LT}}$ Left wing louver stagger angle, $\beta_{2_L} - \beta_{1_L}$, degrees.

β_v Average louver vector angle, $\dfrac{\beta_{v_{RT}} + \beta_{v_{LT}}}{2}$, degrees.

$\beta_{v_{RT}}$ Right wing louver vector angle, $\dfrac{\beta_{1_R} + \beta_{2_R}}{2}$, degrees.

$\beta_{v_{LT}}$ Left wing louver vector angle, $\dfrac{\beta_{1_L} + \beta_{2_L}}{2}$, degrees.

β_{RT} Forward right wing louver set angle, degrees, measured from the z axis direction, positive aft. The reference on the louver is a tangent to the rear louver surface, and the 7th louver used as the reference.

$\beta_{1_{RT}}$ Aft right wing louver set angle, degrees, measured from the z axis direction, positive aft. The 8th louver is used as the reference.

$\beta_{2_{LT}}$ Forward left wing louver angle.

$\beta_{1_{LT}}$ Aft left wing louver angle.

γ Flight path angle, equal to pitch angle minus angle of attack.

δ_{LAT} Percent lateral stick, positive right.

δ_e Elevator deflection, positive trailing edge down.

δ_a Total aileron angle, $\delta_{a_L} - \delta_{a_R}$.

δ_{a_R} Right aileron angle, positive trailing edge down.

δ_{a_L} Left aileron angle, positive trailing edge down.

δ_f Flap angle, positive trailing edge down.

δ_p — Nose fan thrust reverser position, positive in decreasing thrust direction, measured from maximum thrust position.

δ_d — Aileron droop angle, positive trailing edge down.

δ_r — Rudder position, positive trailing edge left.

ϵ — Downwash angle at tail.

ξ — Damping ratio.

η_T — Tail efficiency factor.

θ — Euler pitch angle.

θ_{RB} — Rigid body pitch angle.

θ_T — Tail total pitch angle.

θ_{BT} — Tail pitch angle due to bending at the tail.

ρ_o — Sea level standard day density, .002378 slugs/ft.^{3}

ρ — Air density, slugs/ft.^{3}

σ — Density ratio, $\dfrac{\rho}{\rho_o}$, density at altitude compared to density at sea level.

σ — Standard Deviation of normal distribution.

$\sigma_j^{(i)}$ — Normalized slope of ith flexible body mode at point j.

τ — Time constant, seconds, or torque, foot-pounds.

Φ — Euler Roll Angle.

$\Phi (jw)$ — Power Density spectrum.

Ψ Euler yaw angle.

Ψ_w Wind direction, measured from $\Psi = 0$.

ω Angular frequency, rad./sec.

ω_N Natural frequency of second order system, rad./sec.

Ω Ohms

$\phi_j^{(i)}$ Normalized deflection of ith flexible body mode at point j.

BLANK PAGE

PREFACE

Results of flight simulation and analysis of systems during the final design phase of the XV-5A Aircraft Program are given herein. This is Volume I which discusses procedures used in mechanization, checkout, and validation of the six-degree-of-freedom flight simulator. Volume II, under separate cover, presents the results of the simulator studies as well as details of supplementary analyses.

The work accomplished during this later design period and the coverage of this report is restricted principally to operation in the lift fan mode. It was necessary, however, to set up the simulator to permit conventional flight in the preconversion configuration in order to study the conversion maneuver. The simulation ultimately utilized a large analog computer facility; a six-degree-of-freedom wide screen visual display; cockpit with aircraft type controls and display instruments, and a hydraulic-electrical-mechanical controls fixture made up of actual airplane components. Aerodynamic control surface inertias and hinge moments for pilot-feel were also simulated.

The simulation program was conducted in phases, as aircraft equipment became available. This served to validate conclusions drawn earlier in the program which had provided the basis for hardware acquisition. The simulator was also used for pilot familiarization, including system failure effects and development of measures for correction. Pilot procedural and systems optimization studies also were conducted. Additionally, the simulator permitted extensive installed functional testing of components, demonstrating a high level of reliability and providing operational maintenance experience.

Analysis and simulation results are:

1.   Stability augmentation (SA) system gains were optimized by piloted flight simulator evaluation of hovering under gusty wind conditions. A Cooper rating of 2.3 was derived for the aircraft with the selected gains. The final SA system configuration provides pitch and yaw rate damping without position reference; both rate and position signals are used in roll with the position

reference removed as a result of lateral stick control command. In the primary SA system, individual pitch, roll or yaw channels may be independently selected and gains are adjustable by the pilot. The secondary system configuration is ground-adjustable over the same range as the primary system.

2.   Stability augmentation was not required above 40 knots IAS.

3.   For the 2,500 feet hot day conditions simulated, the rapidity with which a constant altitude transition from hovering could be accomplished was limited by power available and, at the more aft c.g. locations when using a nose fan thrust reversal capability of 30%, by longitudinal trim capability. No power or control limitations appear to exist in a landing transition.

4.   An automatic horizontal trim feature has been selected for transition which programs the tail to the full 20 degree incidence limit louver vector angles of 40 degrees or less. For vector angles greater than 40 degrees, tail trim may be manually commanded at 2.8 deg./sec.

5.   Conversion between conventional and fan flight modes is accomplished by timed sequencing of the wing fan door opening and horizontal tail incidence change as a function of diverter valve motion. The introduction at the proper time of a constant horizontal tail trim rate of 7.5 deg./sec. programmed to a pre-established end point was shown to permit smooth conversions over a range of initiation flight velocities.

6.   Failure studies have shown that uncommanded tail motion could result in a dangerous flight condition. As a result, both aural and visual cockpit signals have been incorporated into the aircraft to indicate lack of commanded tail motion or tail runaway.

2

1.0   INTRODUCTION

This report presents system analysis and flight simulation results
and methods covering work performed during the final design phase for
the U.S. Army XV-5A Lift Fan Flight Research Aircraft.   The XV-5A
was designed and built by the Ryan Aeronautical Company for flight
test evaluation of the General Electric X353-5 lift fan propulsion
system.   It is a V/STOL aircraft capable of conventional operation at
high subsonic speeds. Preliminary systems analysis and simulator
studies accomplished during the earlier phases of design are detailed
in Report No. 127.

In general, because of the timing, the work discussed herein involved
somewhat less design synthesis and more systems design validation
than that reported for the earlier stages of the aircraft development.
The effort was restricted primarily to investigation of the aircraft
in the low speed flight regimes which included hovering, transition,
conversion, and conventional flight in the conversion configuration.
The simulator provided the principal tool for the investigations.
A comprehensive documentation of the flight simulator study is given
by this publication. Simulator investigations of high speed
conventional flight are described in the first report. Given herein
is an explanation of the methods by which the present simulator
study was made, as well as results of the study.

The large amount of material to be presented makes it necessary to
publish this report in two volumes. The construction of the XV-5A
flight simulator from initial development of methods for incorporation
of the aircraft aero-propulsion characteristics into the analog
computer to final checkout of the completed hydraulic and controls
simulator is given in Volume I. The results of studies carried out
on the simulator are given in Volume II under separate cover.

Volume II also contains the Appendix, Section 6.0, covering work of
special interest. More detailed explanations of some items discussed
in the main body of the report are presented, along with results of
studies of real or suspected problems that arose in the initial
phases of the flight test program.

Methods presented herein will be useful as a guide in future simulation programs, especially of lift fan aircraft, and useful to flight test personnel in the present program.

1.1 GENERAL FLIGHT SIMULATION OBJECTIVES

The objectives of the flight simulation study can be summarized as follows:

- Determine the compatibility of the aircraft and its control system.

- Determine the adequacy of the stability augmentation system.

- Provide a check of the low speed conventional flight and fan powered flight performance predictions made in earlier design phases of the XV-5A Program.

- Provide future test pilots of the XV-5A with preliminary simulated flights of the aircraft which would be realistic enough to allow development of preliminary flight procedures.

- Perform studies of possible problem areas.

The simulation program was performed using ANA Bulletin 421 Hot Day atmospheric conditions for an altitude of 2,500 feet. This selection was made because of the plan for conducting the initial flight test program at Edwards AFB and was considered to be consistent with the objectives stated above. This condition was also given by the U.S. Army as a basis for quotations of VTOL performance objectives.

2.0 CONSTRUCTION AND CHECKOUT OF THE
XV-5A SIMULATOR

Volume I is devoted principally to a presentation of the build-up and check-out of the XV-5A simulator. Aerodynamic and propulsion system characteristics developed for the aircraft are given along with weights data. The manner in which these characteristics have been mechanized for analog computer solution of the equations of motion are presented. The hydraulics, controls, and cockpit display portion of the simulator is described in detail. This is followed by discussion of the simulator checkout procedures.

2.1 DESCRIPTION OF THE AIRCRAFT

2.1.1 Weights Data

Weight data is referred to fuselage axes.
Nominal weight is 9,200 pounds.
c.g. at Fuselage Station 246.

I_x	moment of inertia about x-axis	4,252 slug-ft^2
I_y	moment of inertia about y-axis	15,139 slug-ft^2
I_z	moment of inertia about z-axis	17,418 slug-ft^2
I_{xz}	product of moments of inertia	919 slug-ft^2

Geometry:

S_w	Wing Area	260 ft^2
S_t	Tail Area	52.86 ft^2
$\bar{c}$	Mean Chord	9.4 feet
ℓ_t	X Tail Moment Arm	20.6 feet

Geometry: (Continued)

z_t	Z Tail Moment Arm	7.82 feet
x_{NF}	Nose Fan Moment Arm	15.6 feet
A_F	Total Main Fan Area	42.6 ft^2
A_{NF}	Nose Fan Area	7.07 ft^2
D_F	Diameter Main Fans	5.2 feet
b	Wing Span	29.83 feet
y_F	y Fan Moment Arm	5.07 feet
x_F	x Fan Moment Arm	10 inches
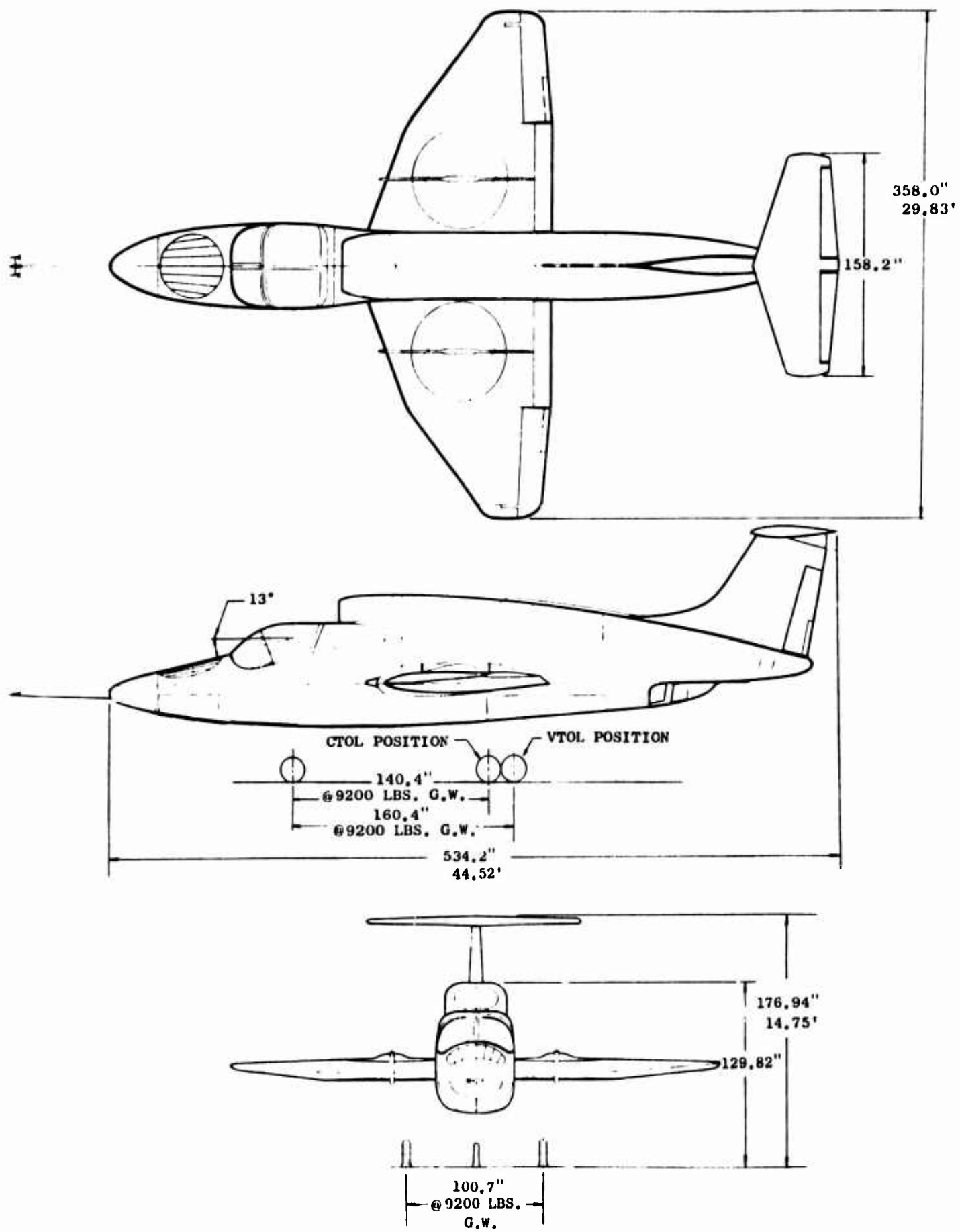
3-View of XV-5A
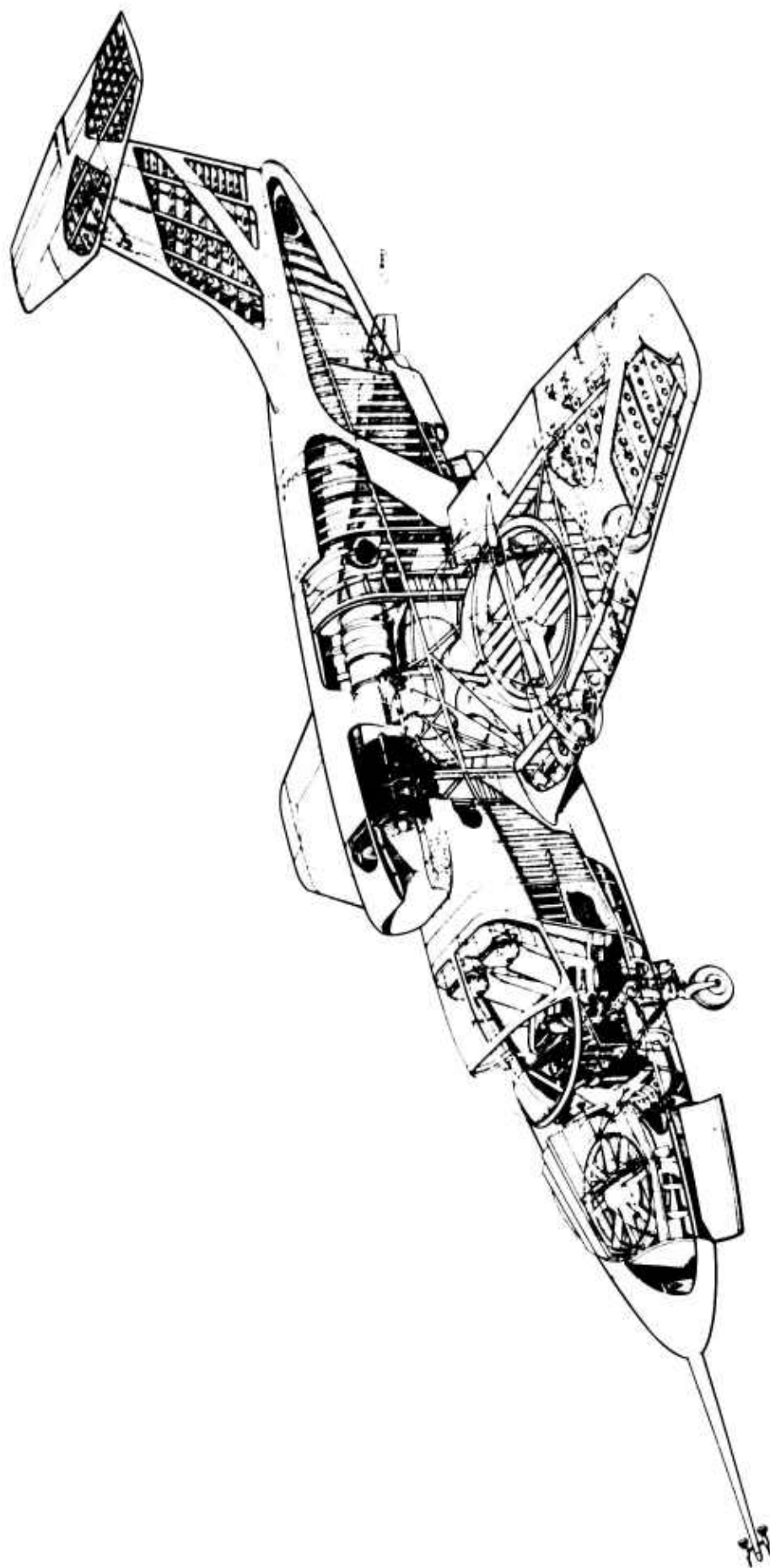
XV-5A

2.1.2 Aerodynamic Functions Presented for Simulation

The following Figures 1 through 33 are aerodynamic characteristics developed by the XV-5A Aerodynamics Group for the aircraft simulation.
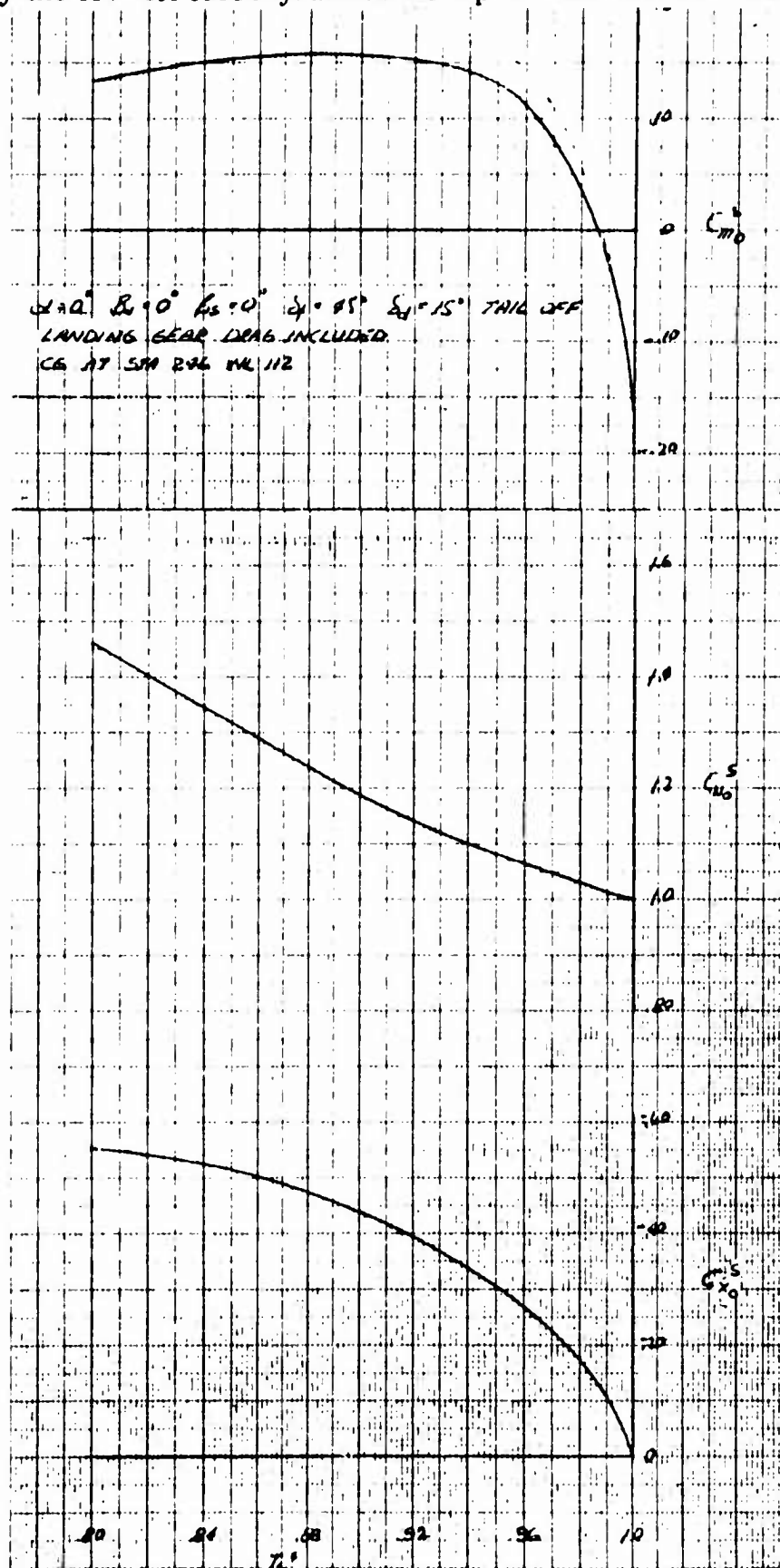
Figure 1 Estimated Basic Longitudinal Characteristics in Fan
Mode Based on Ames XV-5A Model and 1/6 Scale Data
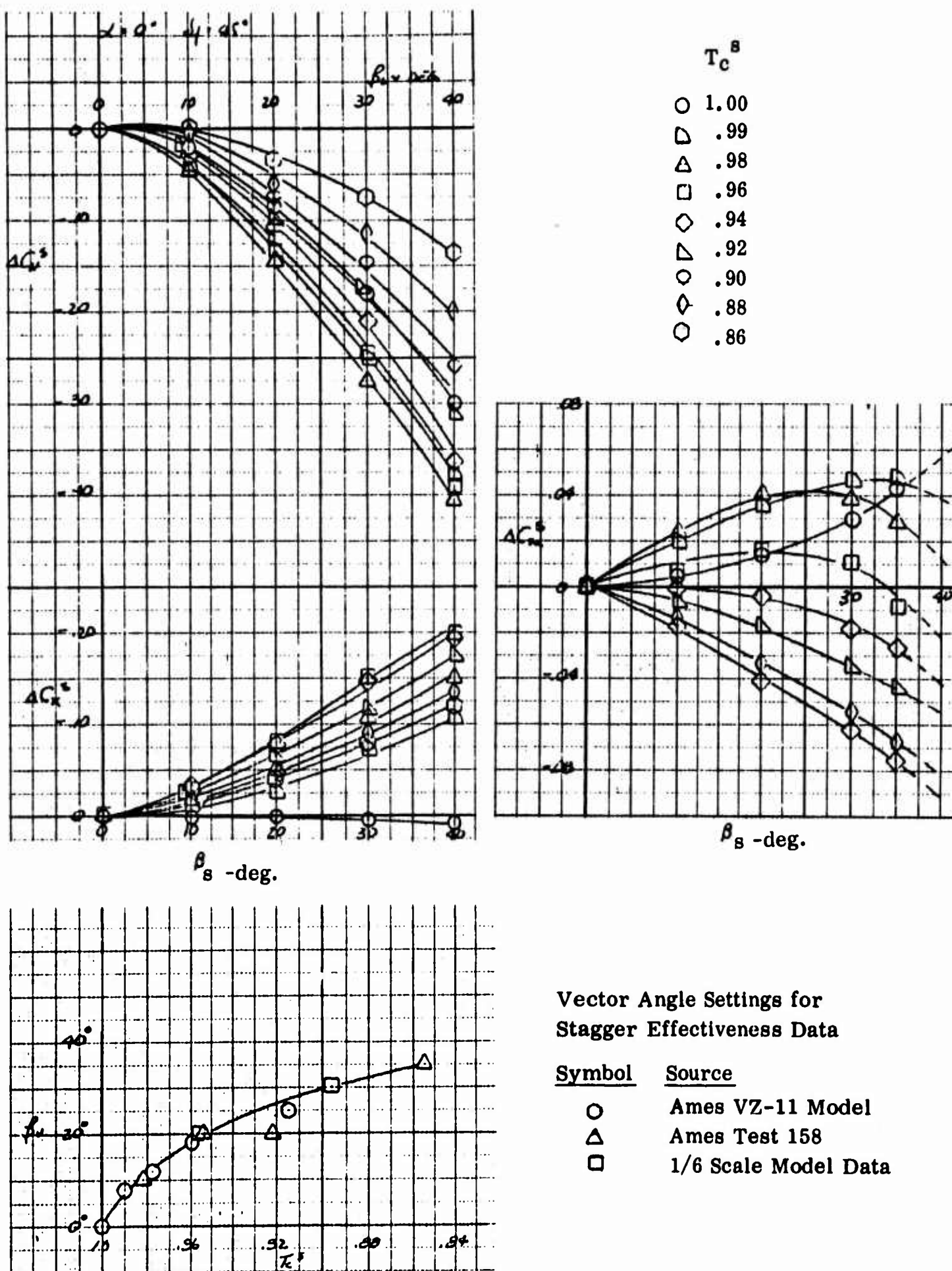
Figure 2 Effect of Exit Louver Stagger on Longitudinal Characteristics
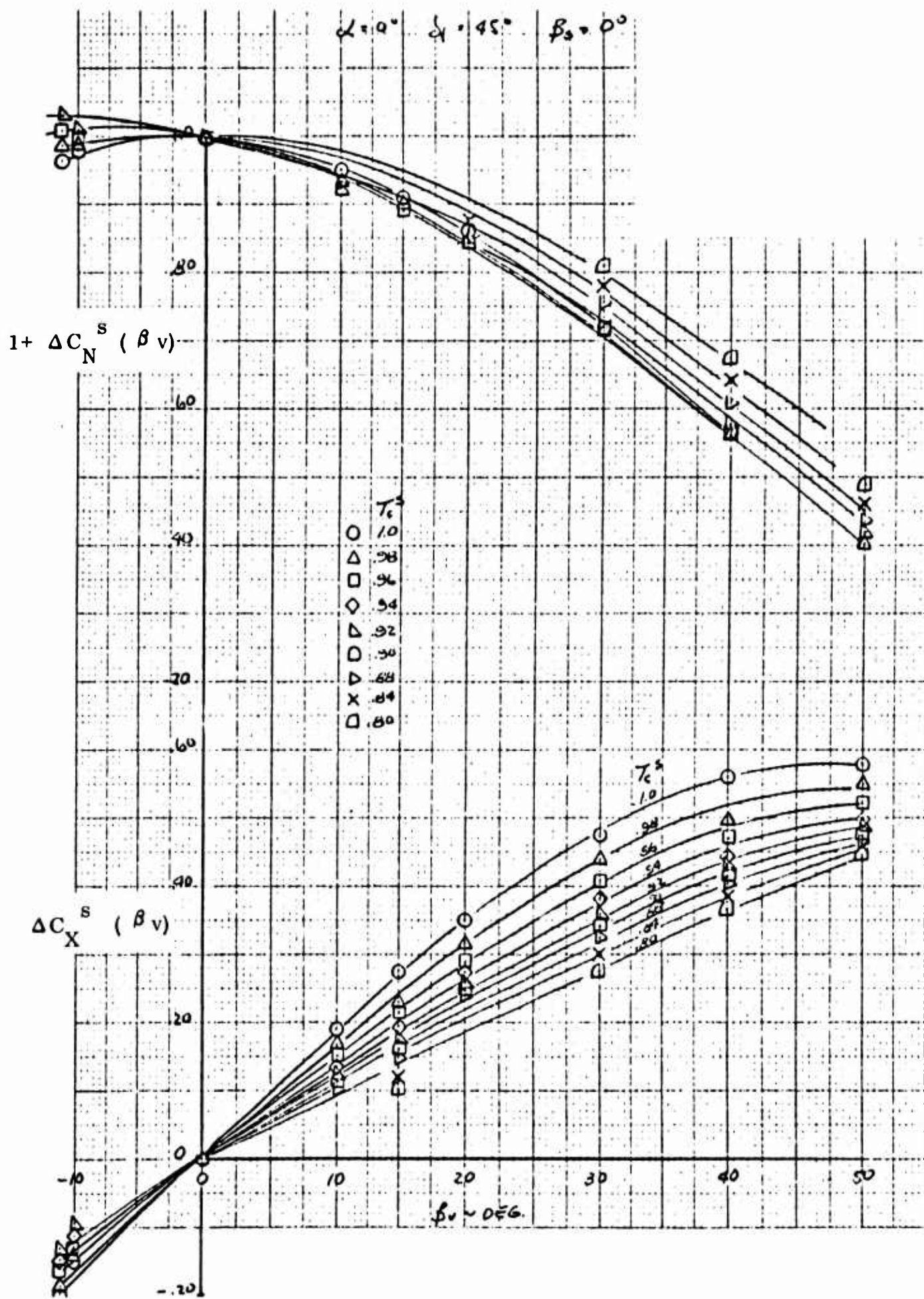
Figure 3 Exit Louver Vector Effectiveness
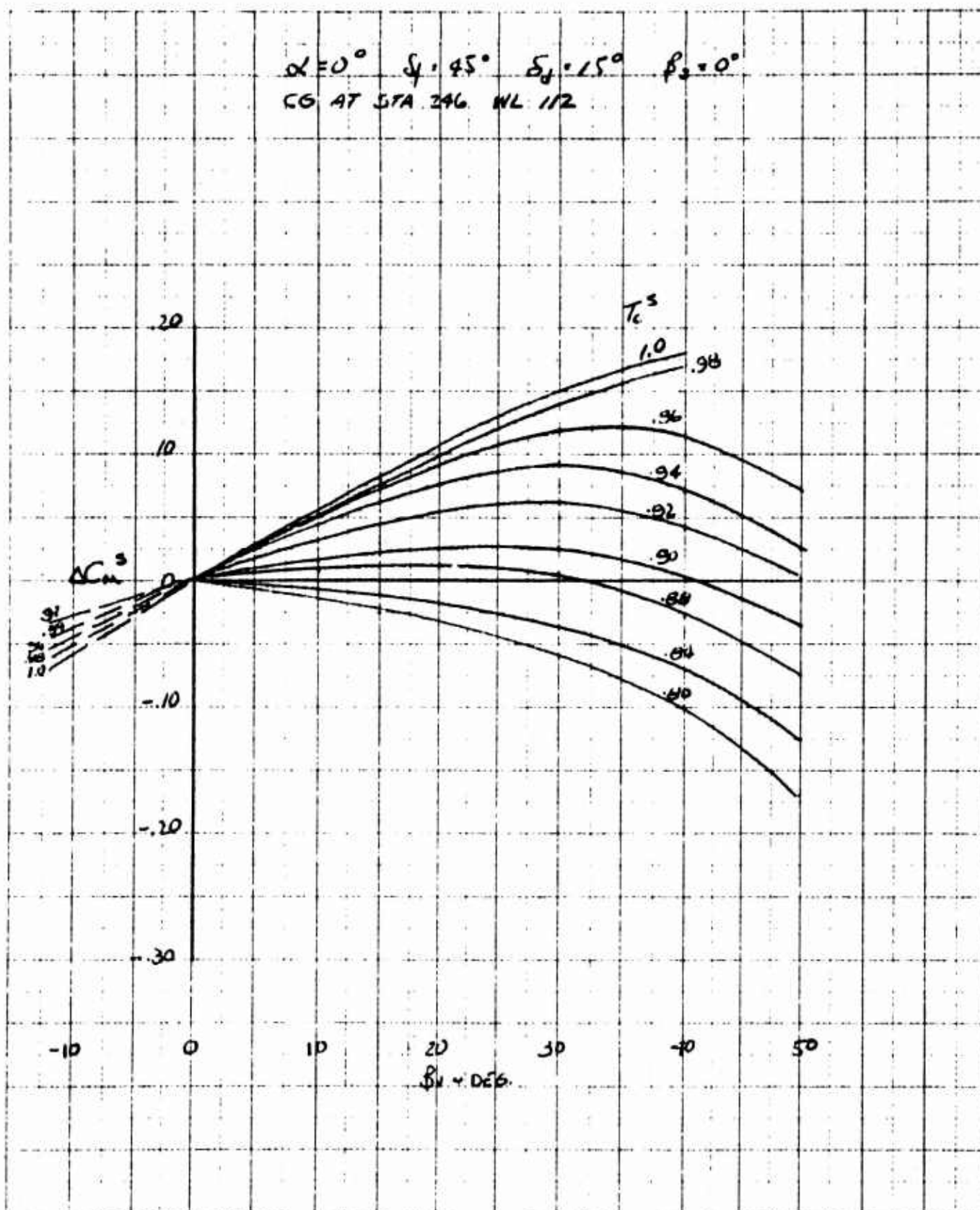
Figure 4 Incremental Pitching Moment Coefficient Due to Exit
Louver Vector Angle

Figure 5 Incremental Longitudinal Force Coefficient Variation With Angle of Attack ($\beta_V = 0°$)

Figure 6 Incremental Normal Force Coefficient Variation With Angle of Attack ($\beta_V = 50°$)
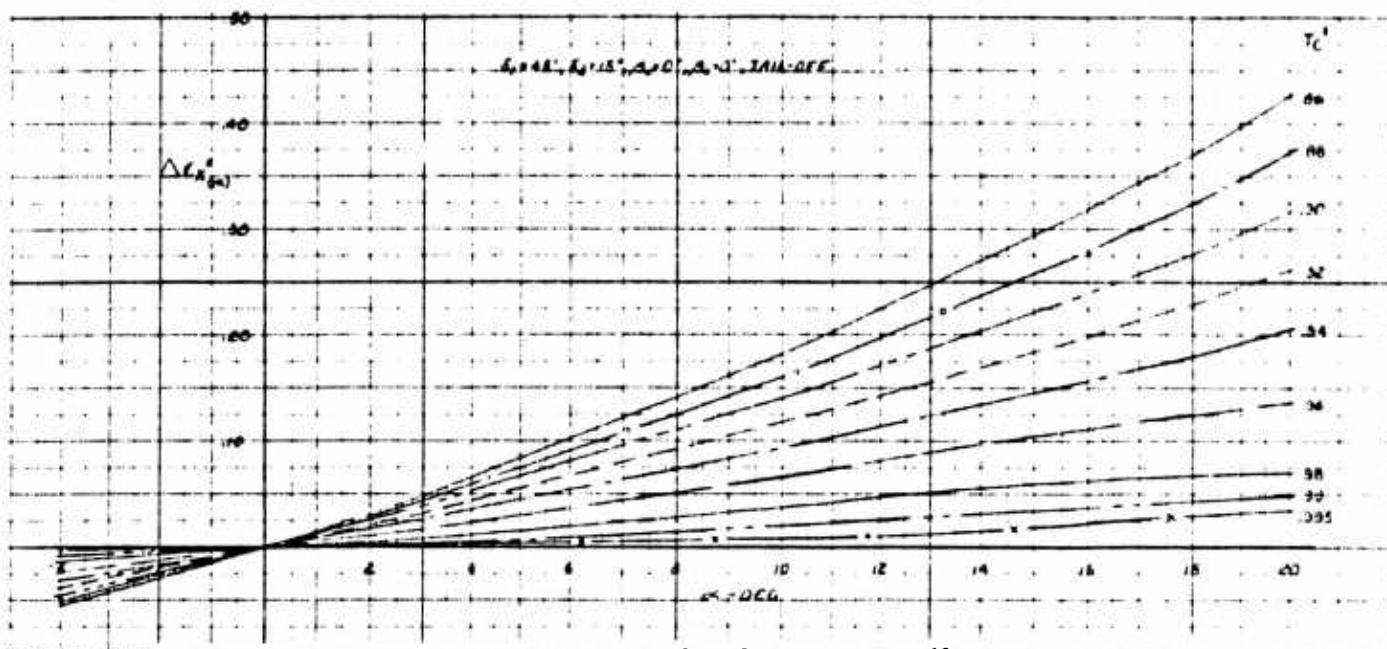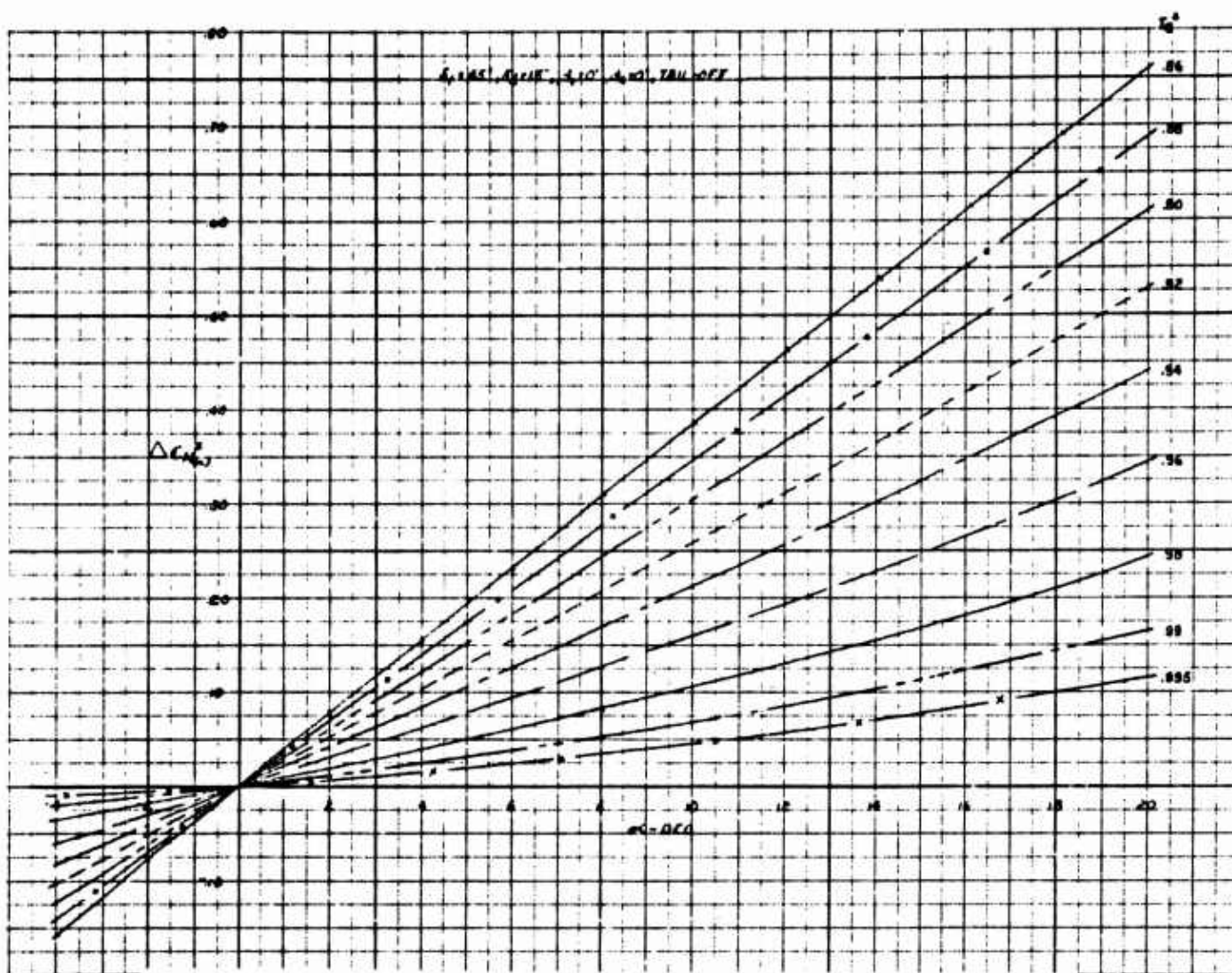
Figure 7 Incremental Longitudinal Force Coefficient Variation
With Angle of Attack ($\beta_V = 50°$)
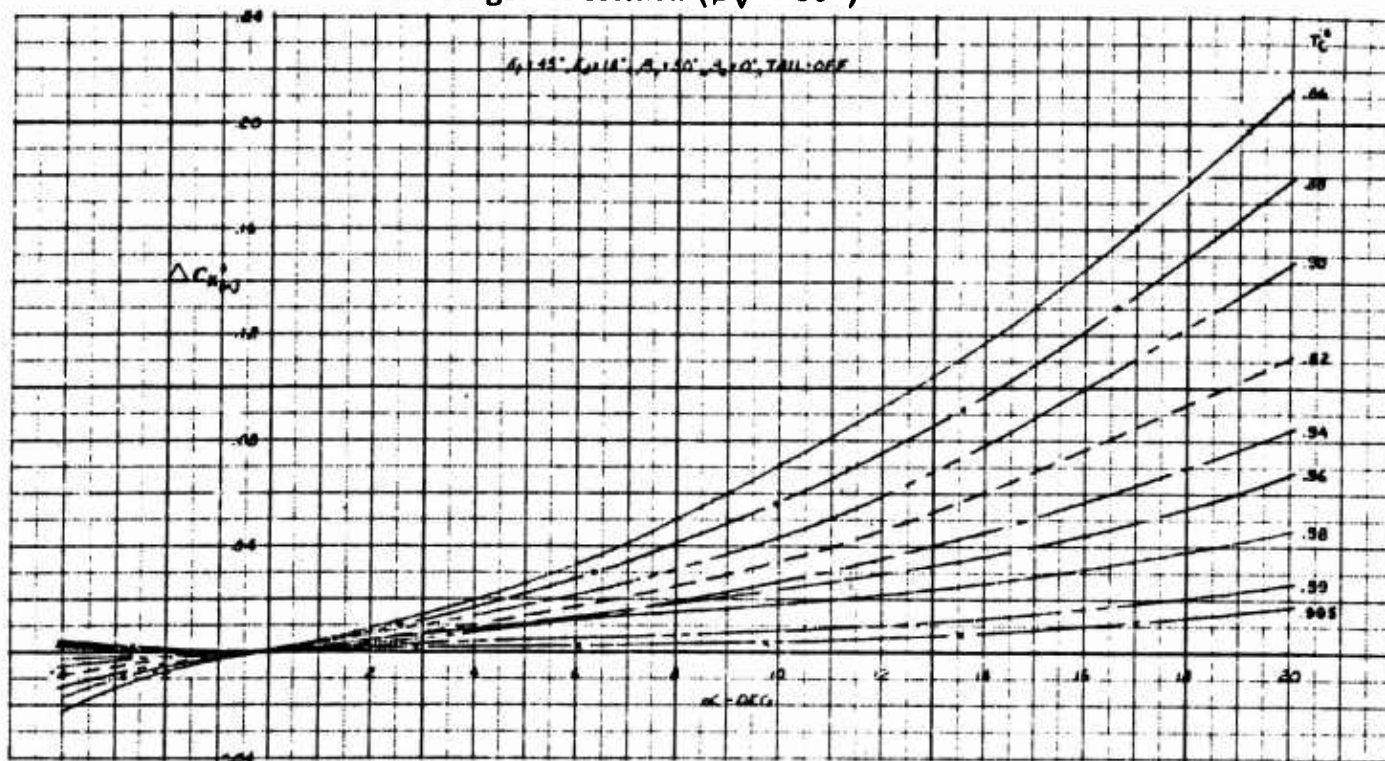
Figure 8 Incremental Normal Force Coefficient Variation
With Angle of Attack ($\beta_V = 0°$)
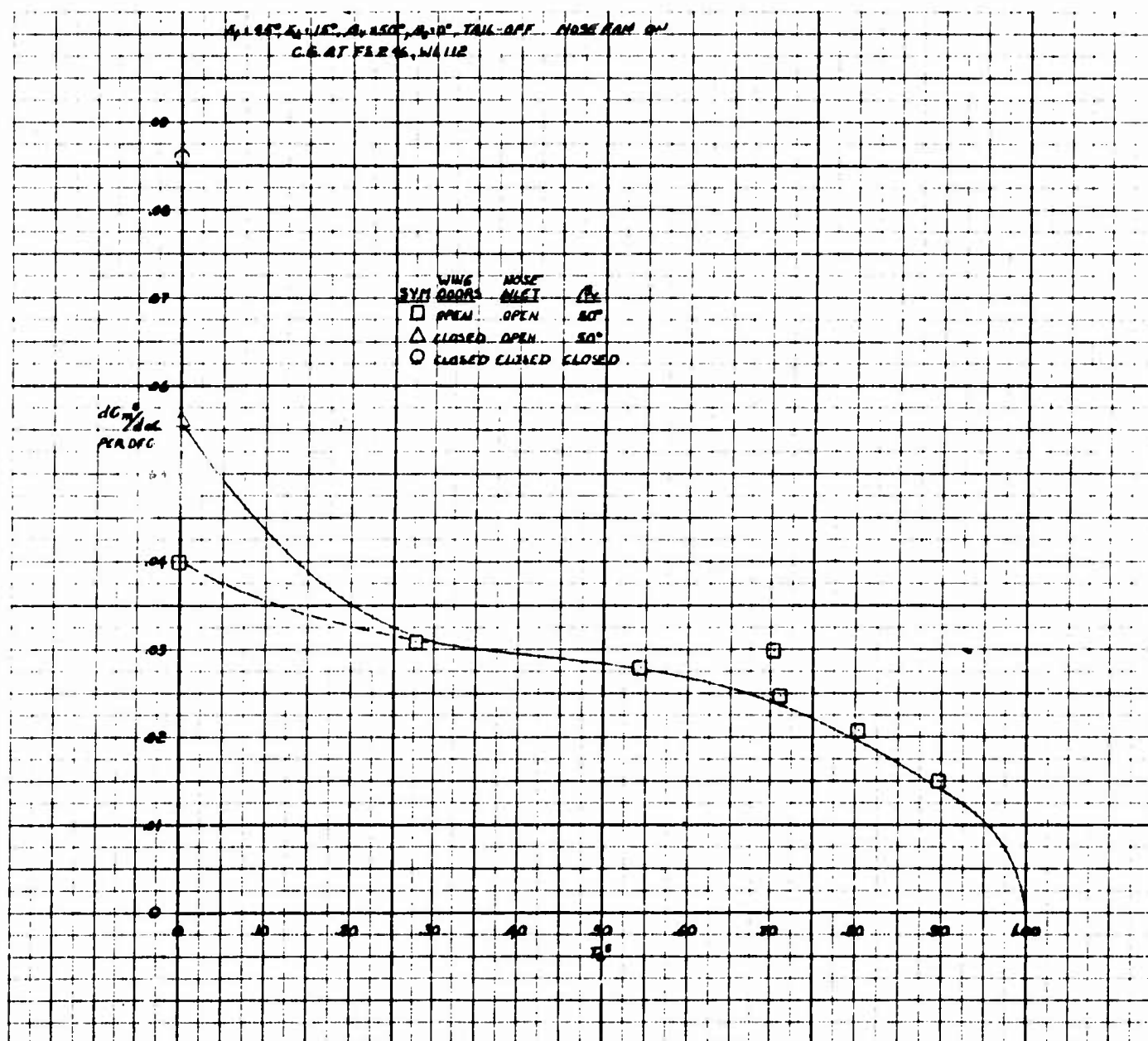
Figure 9 Pitching Moment Coefficient Curve Slope
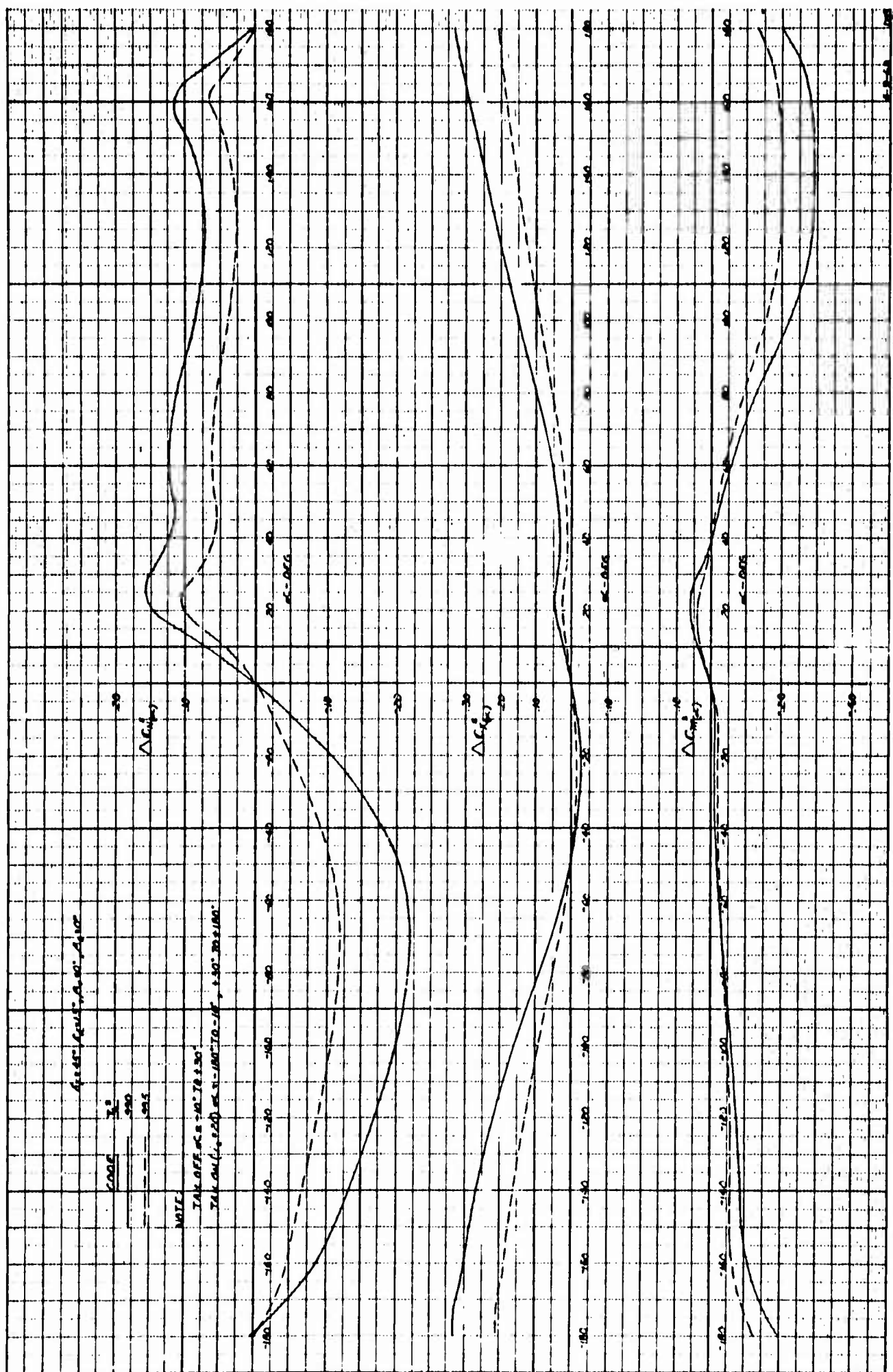
Figure 10 Low Speed Longitudinal Characteristics at Large
Angles of Attack
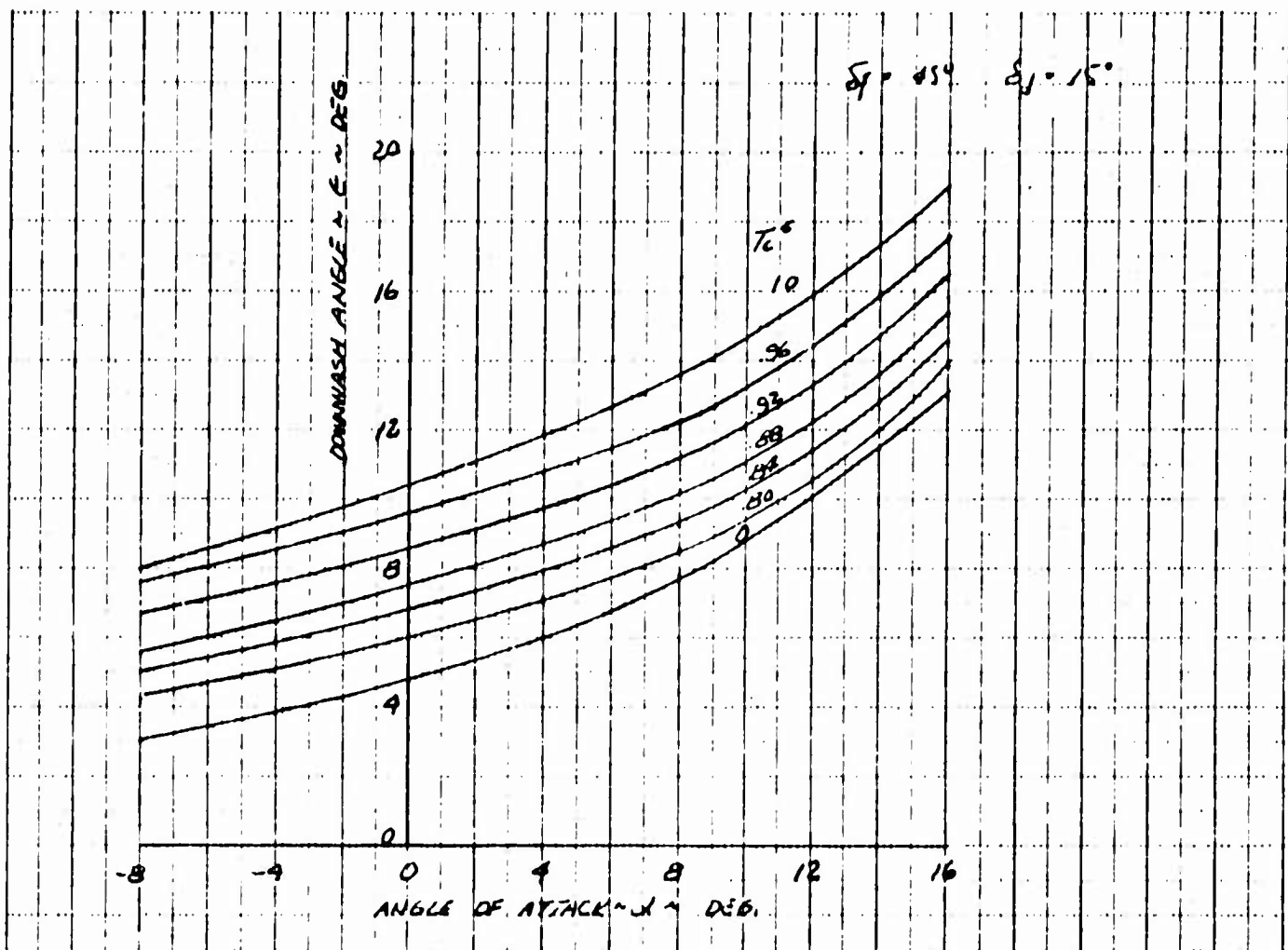
Figure 11 Downwash Angle at Horizontal Tail
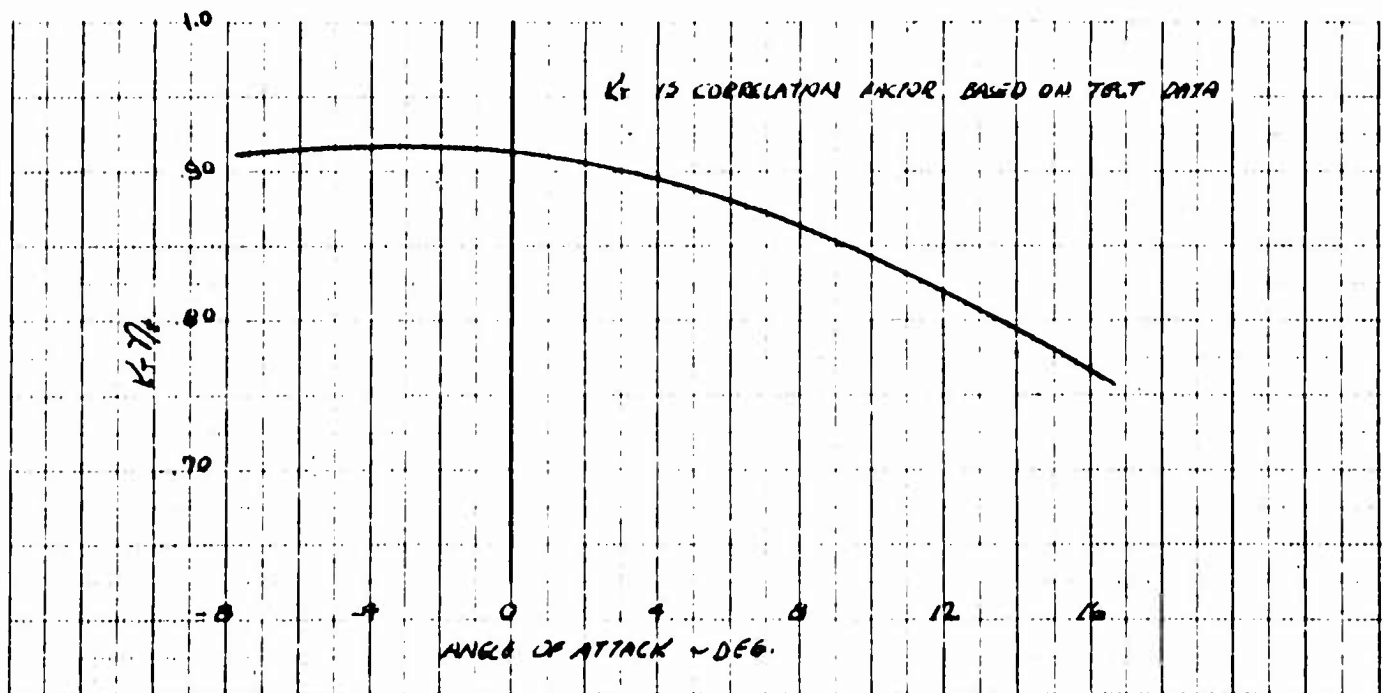
Figure 12 Horizontal Tail Efficiency Factor
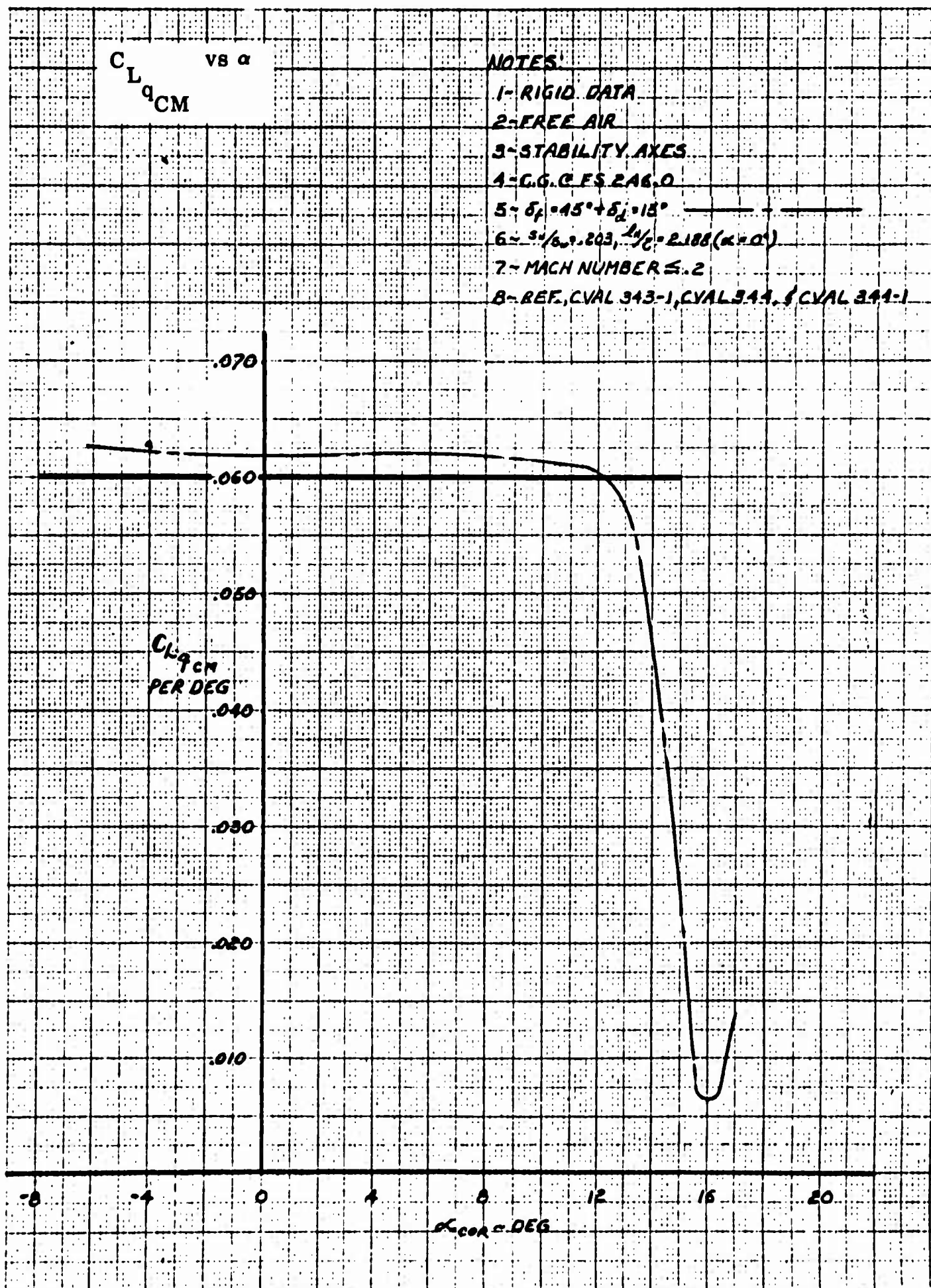
Figure 13 Basic Airframe Change of Lift Coefficient with Pitch Rate
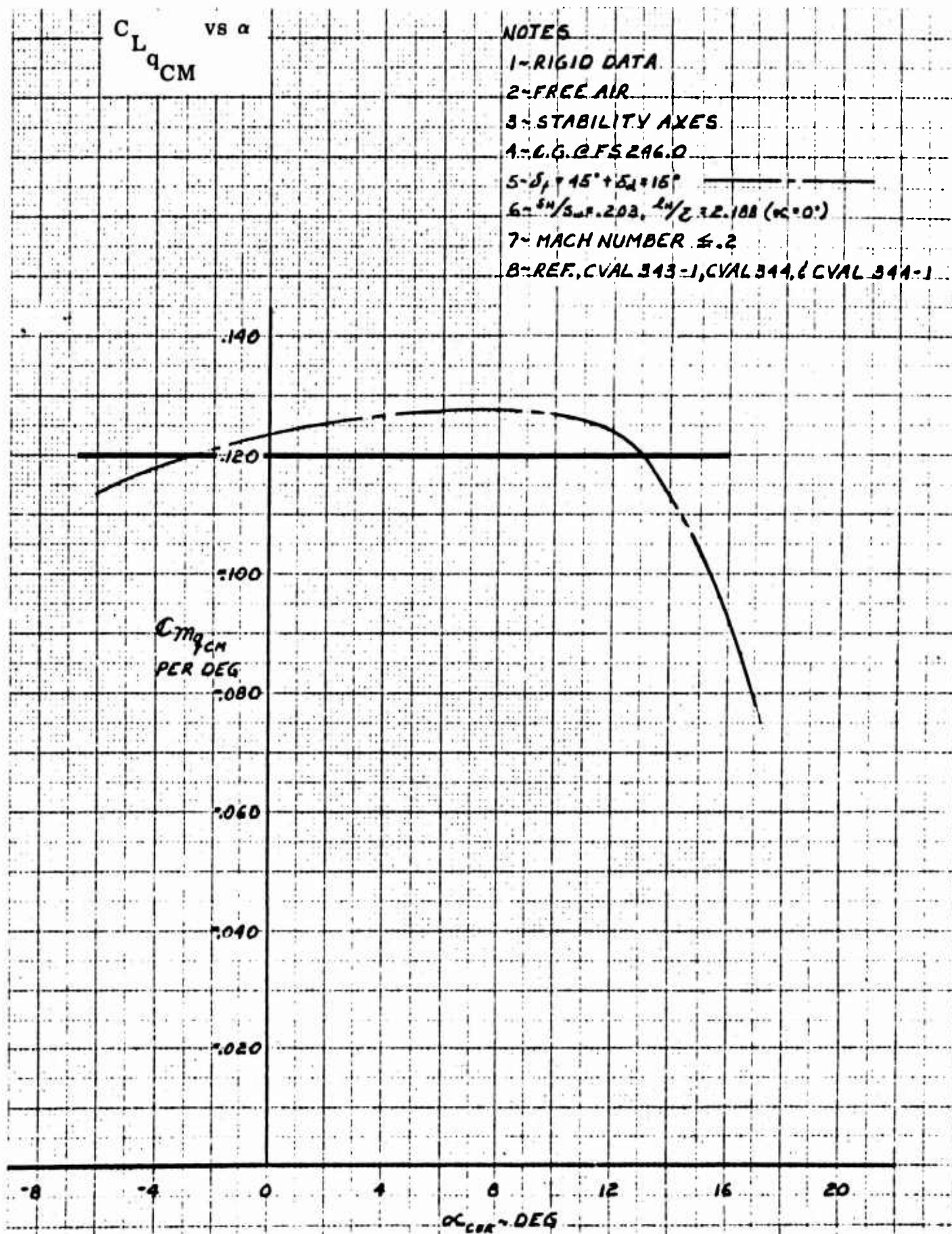
Figure 14 Basic Airframe Pitch Rate Damping Coefficient
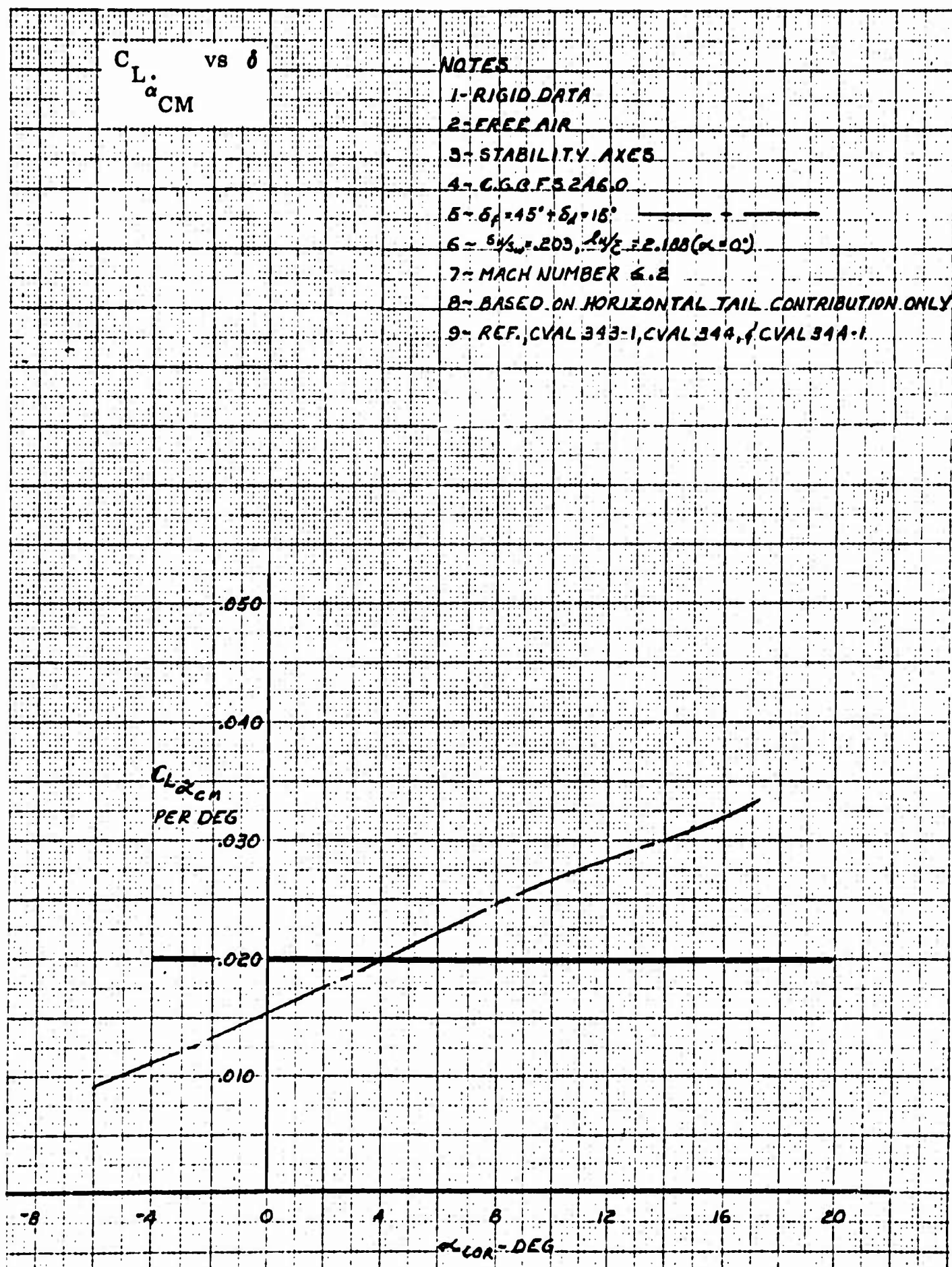
Figure 15 Basic Airframe Lift Coefficient Due to Rate of Change
Of Angle of Attack
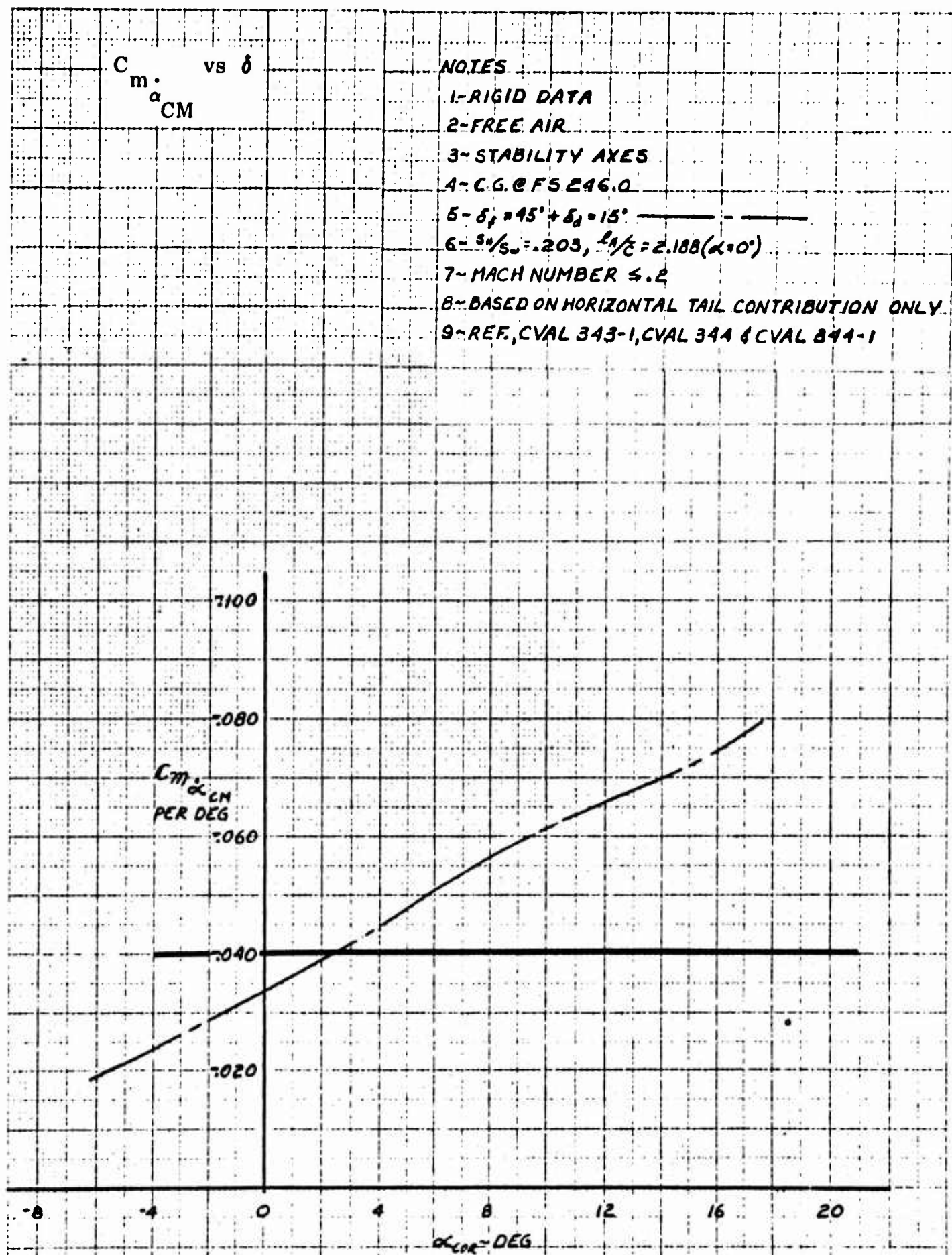
Figure 16 Basic Airframe Pitching Moment Coefficient Due to
Rate of Change of Angle of Attack
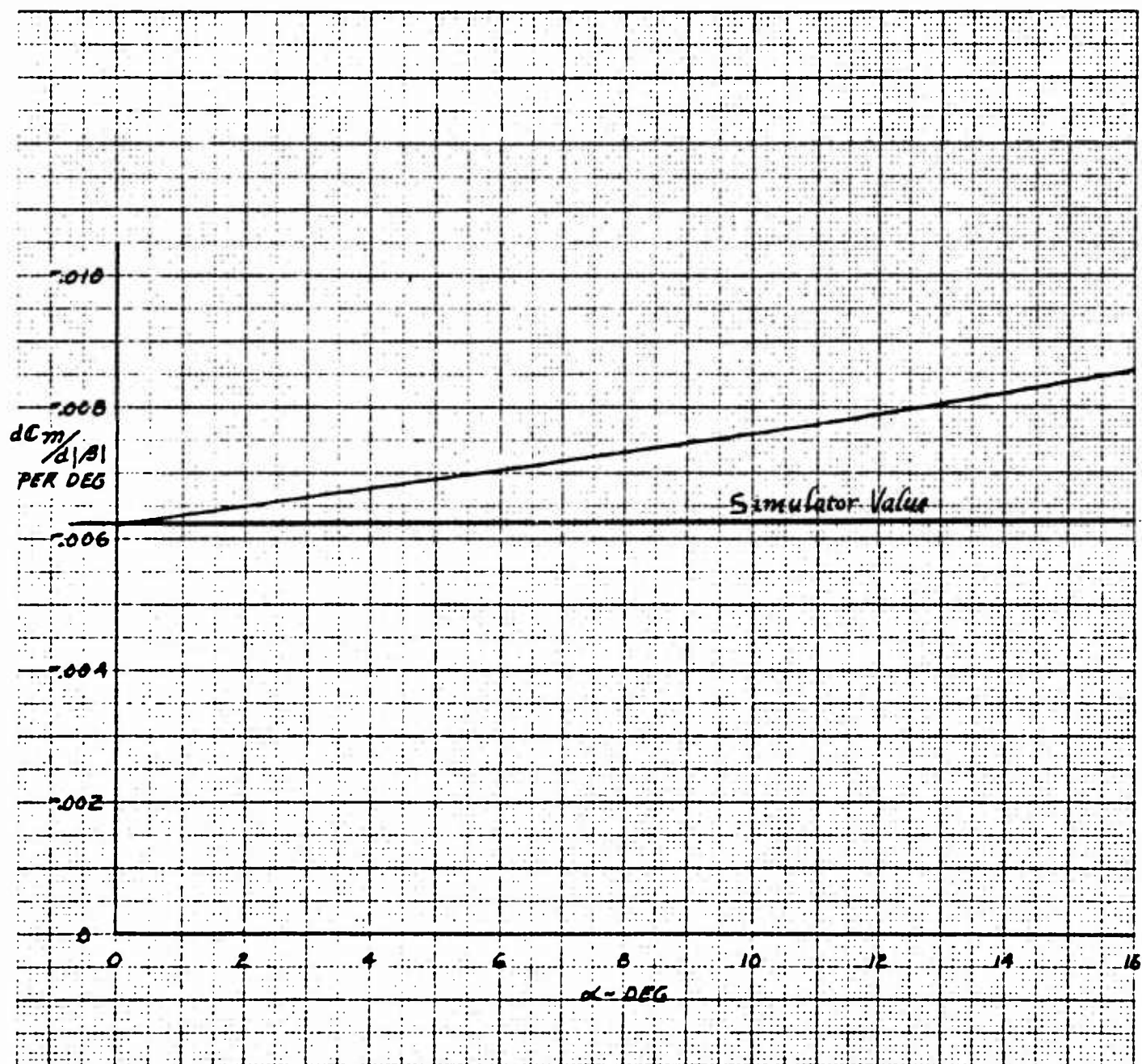
Figure 17 Change in Pitching Moment Coefficient With Sideslip Angle

Figure 18 Longitudinal Characteristics Coefficient During Conversion
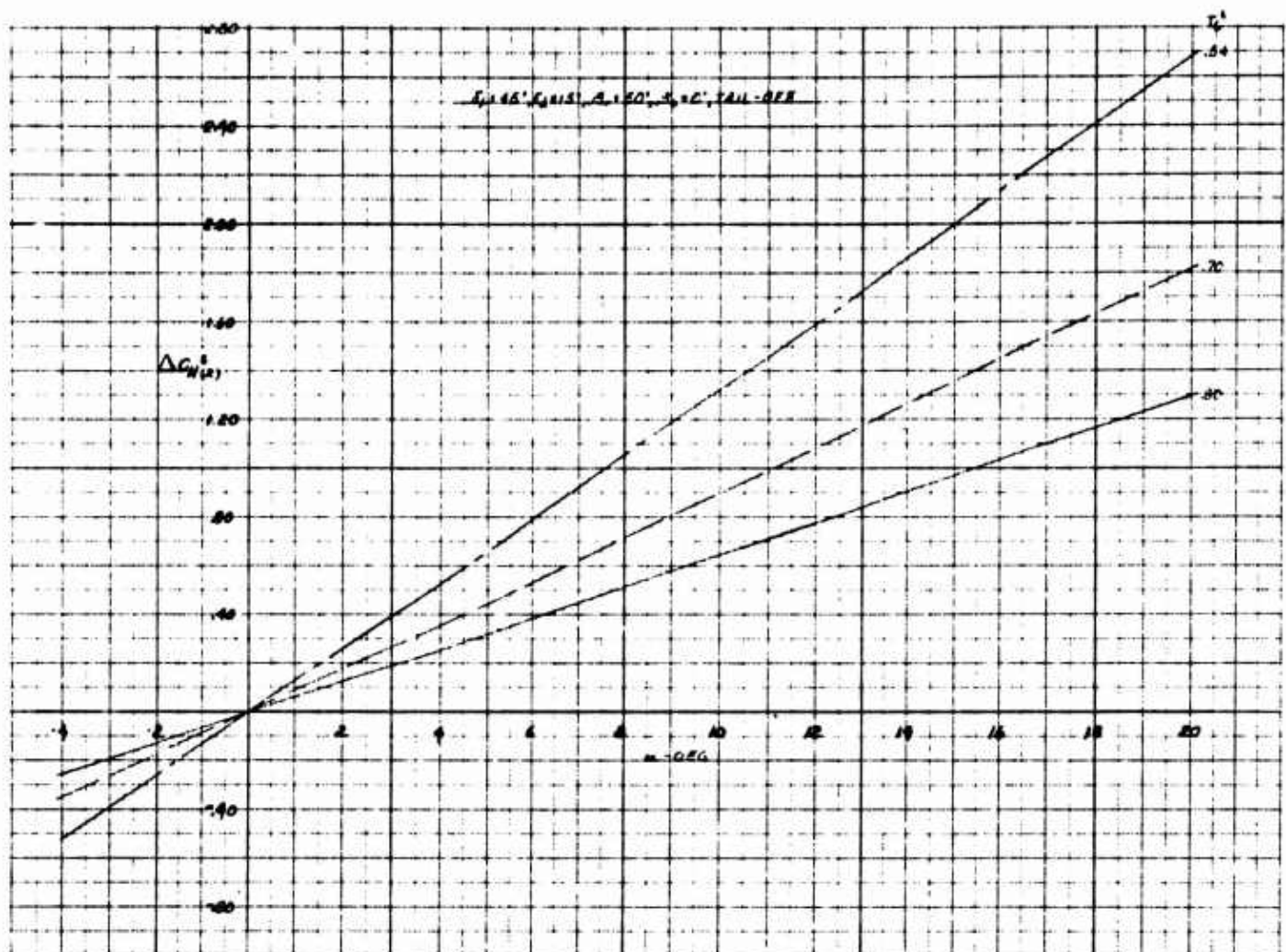
Figure 19 Incremental Normal Force Coefficient Variation with
Angle of Attack ($\beta_V = 50°$)
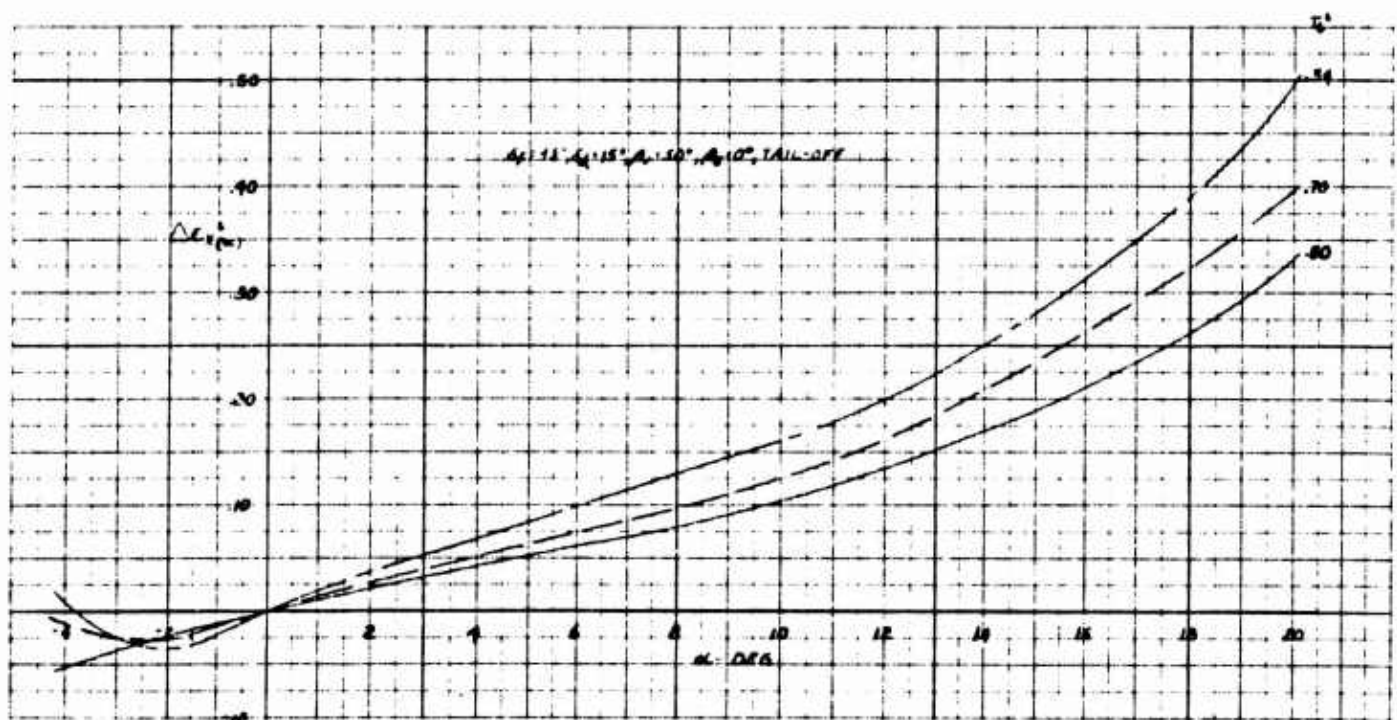
Figure 20 Incremental Longitudinal Force Coefficient Variation
With Angle of Attack ($\beta_V = 50°$)
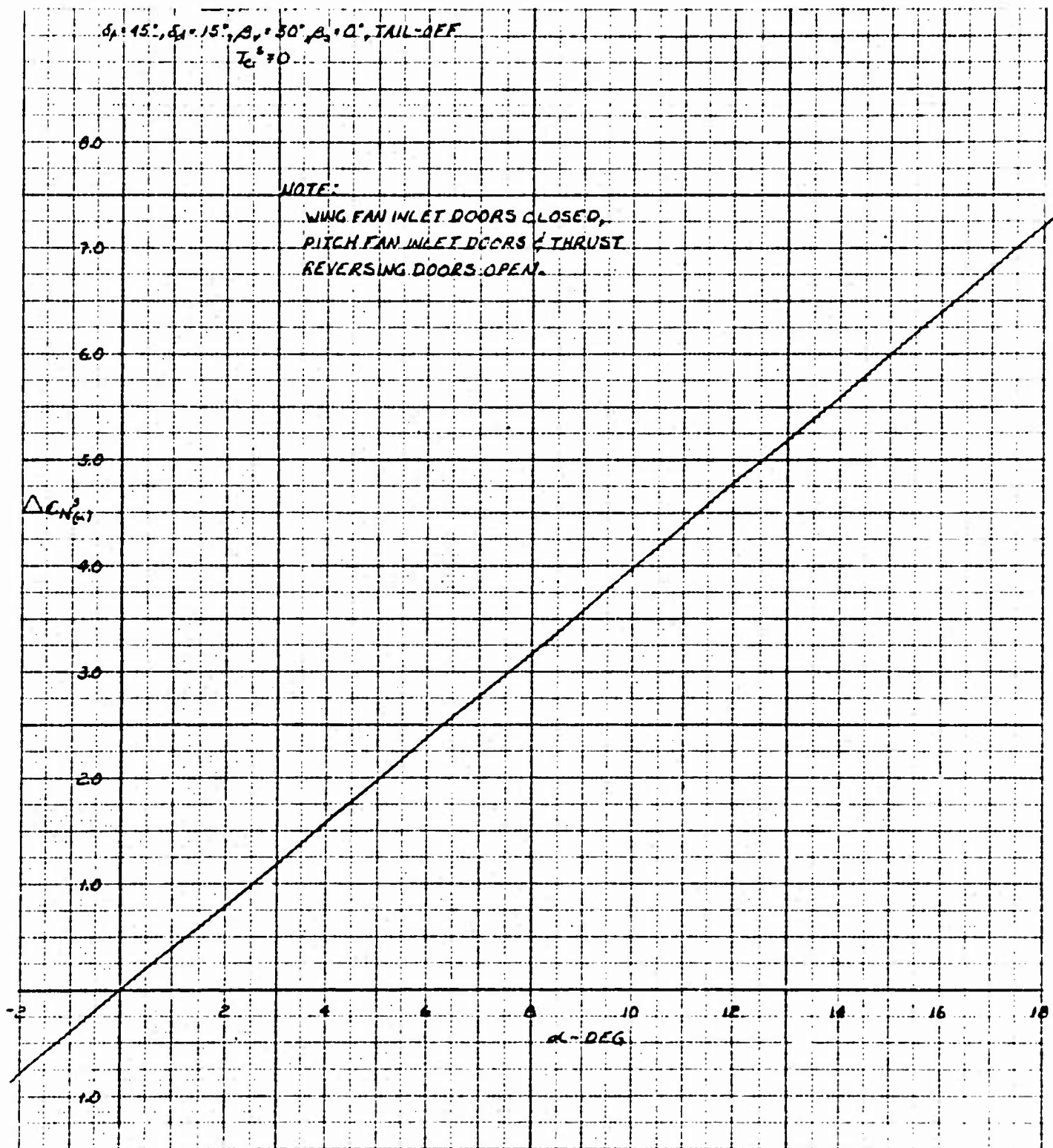
Figure 21 Incremental Normal Force Coefficient Variation with
Angle of Attack ($\beta_V = 0°$)
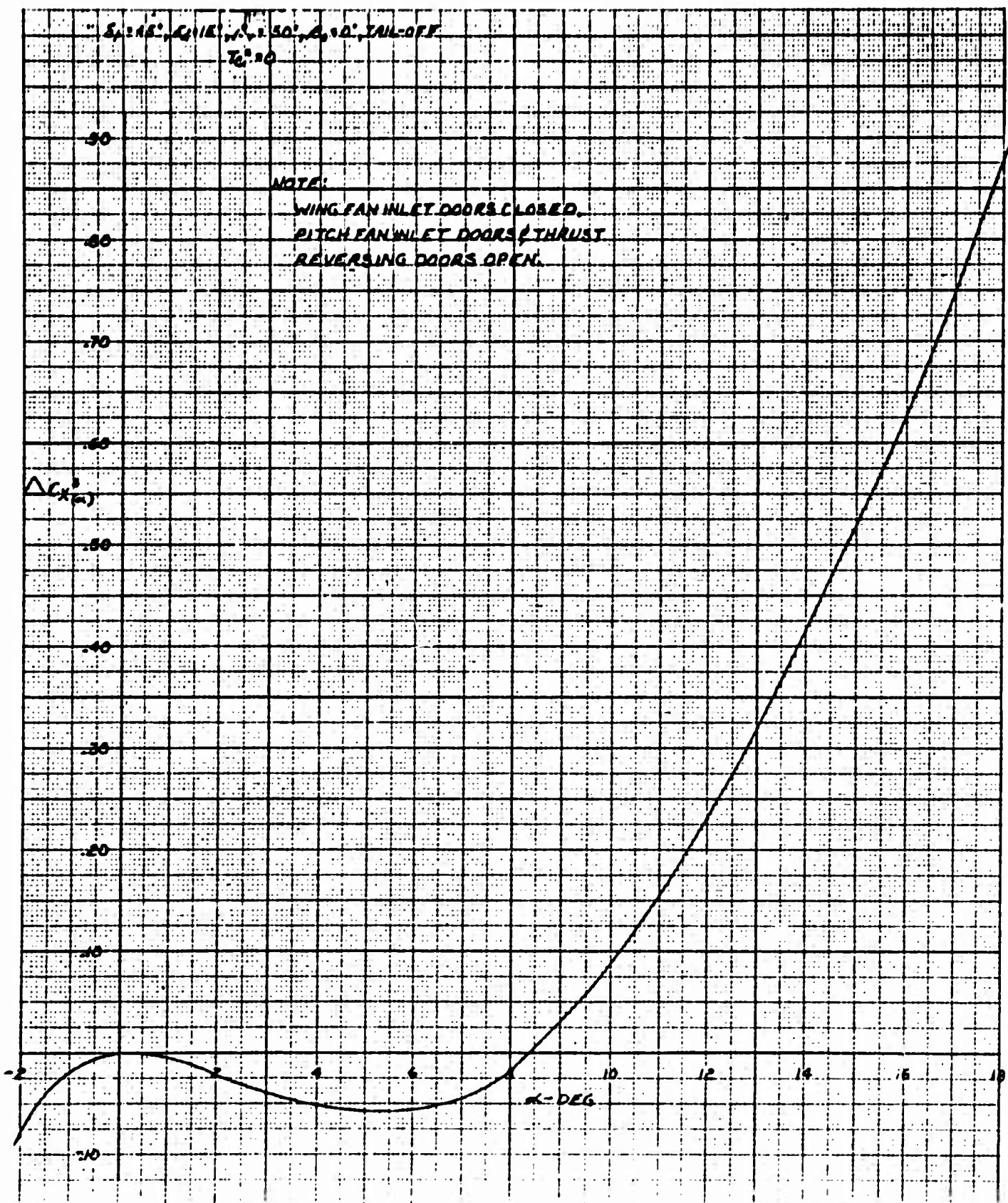
Figure 22 Incremental Longitudinal Force Coefficient Variation
With Angle of Attack ($\beta_V = 50°$)
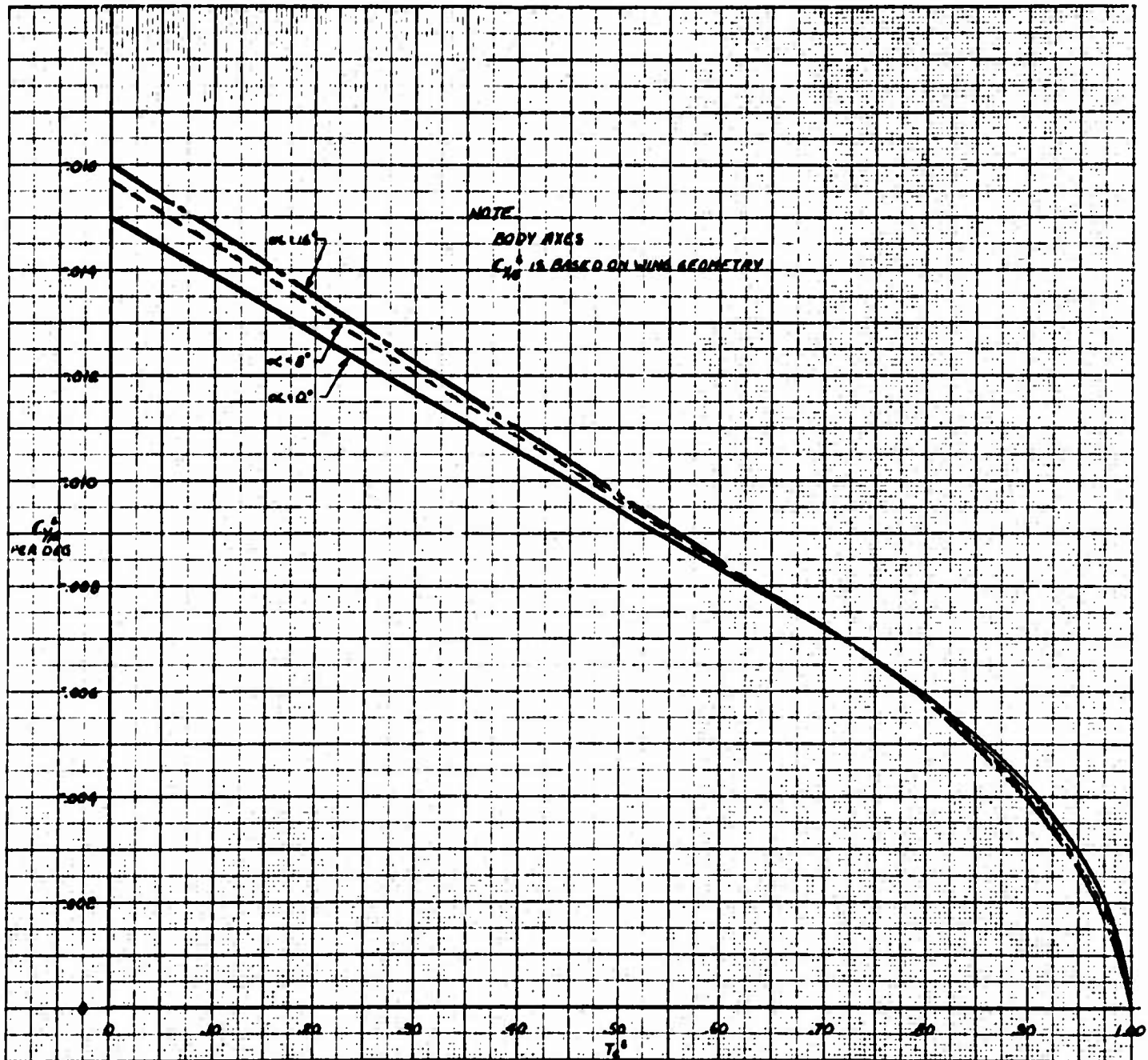
Figure 23   Variation of Sideforce Coefficient Due to Sideslip with
Thrust Coefficient
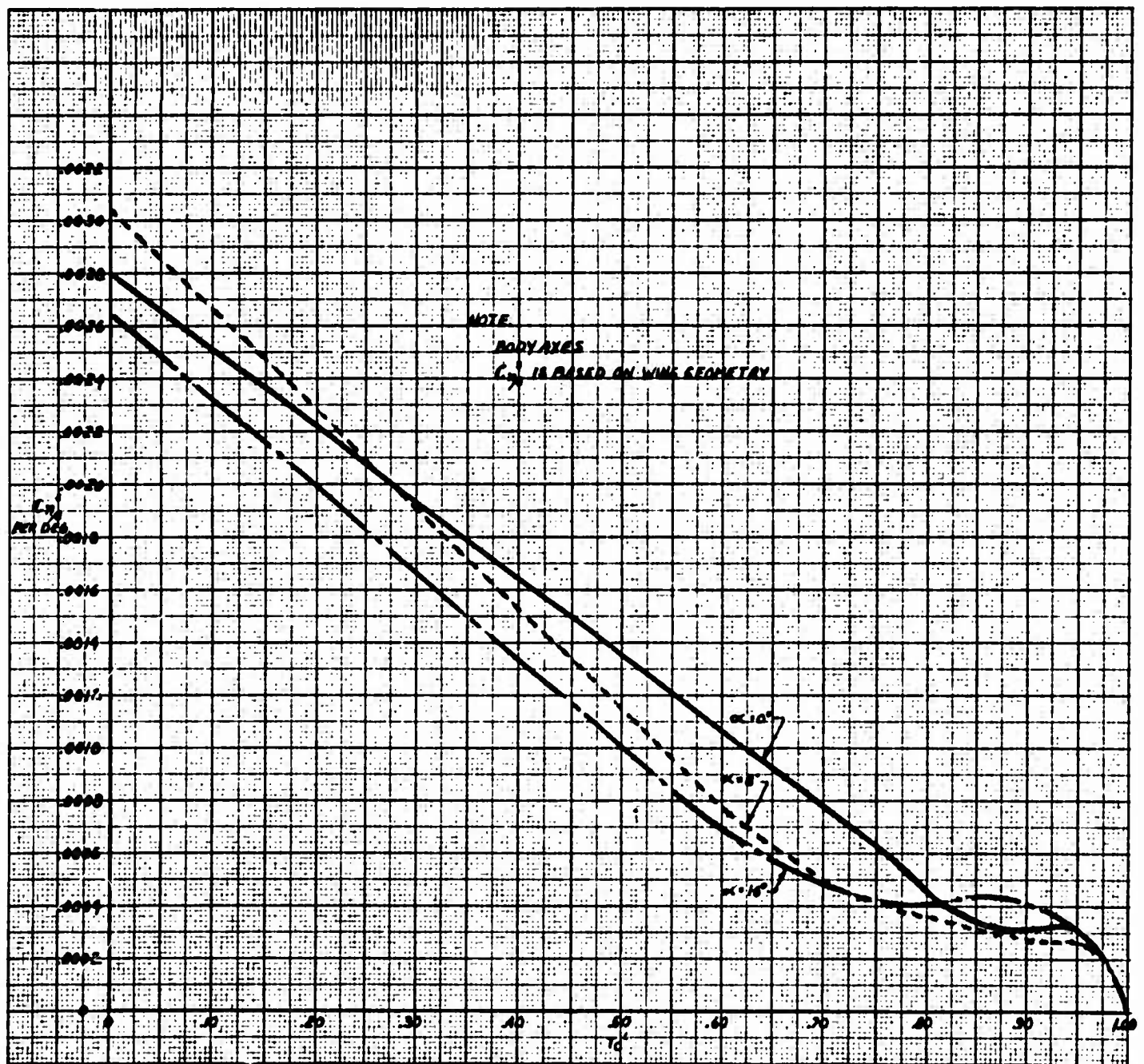
Figure 24 Variation of Yawing Moment Coefficient Due to Sideslip
With Thrust Coefficient
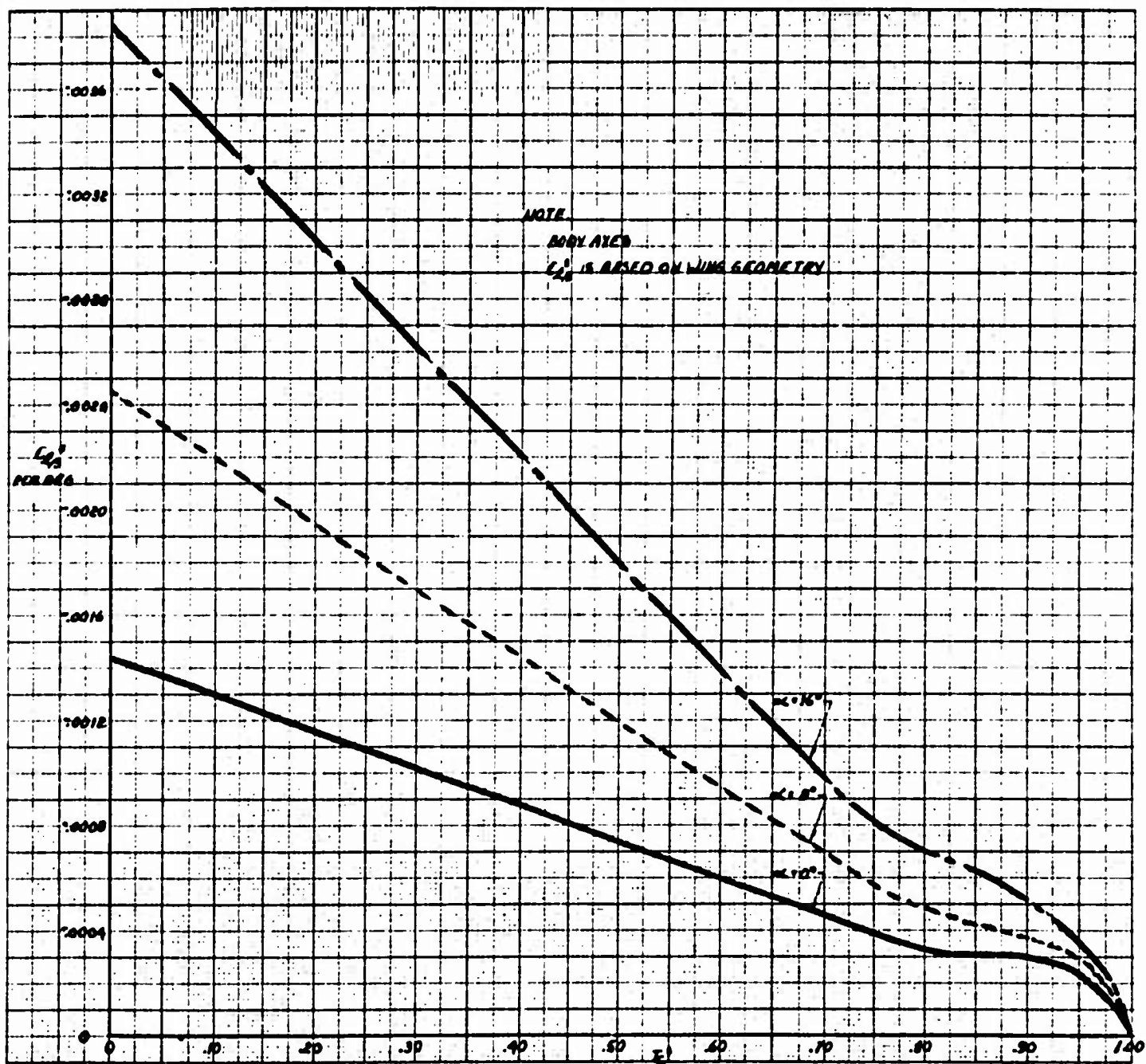
Figure 25 Variation of Rolling Moment Coefficient Due to Sideslip
With Thrust Coefficient
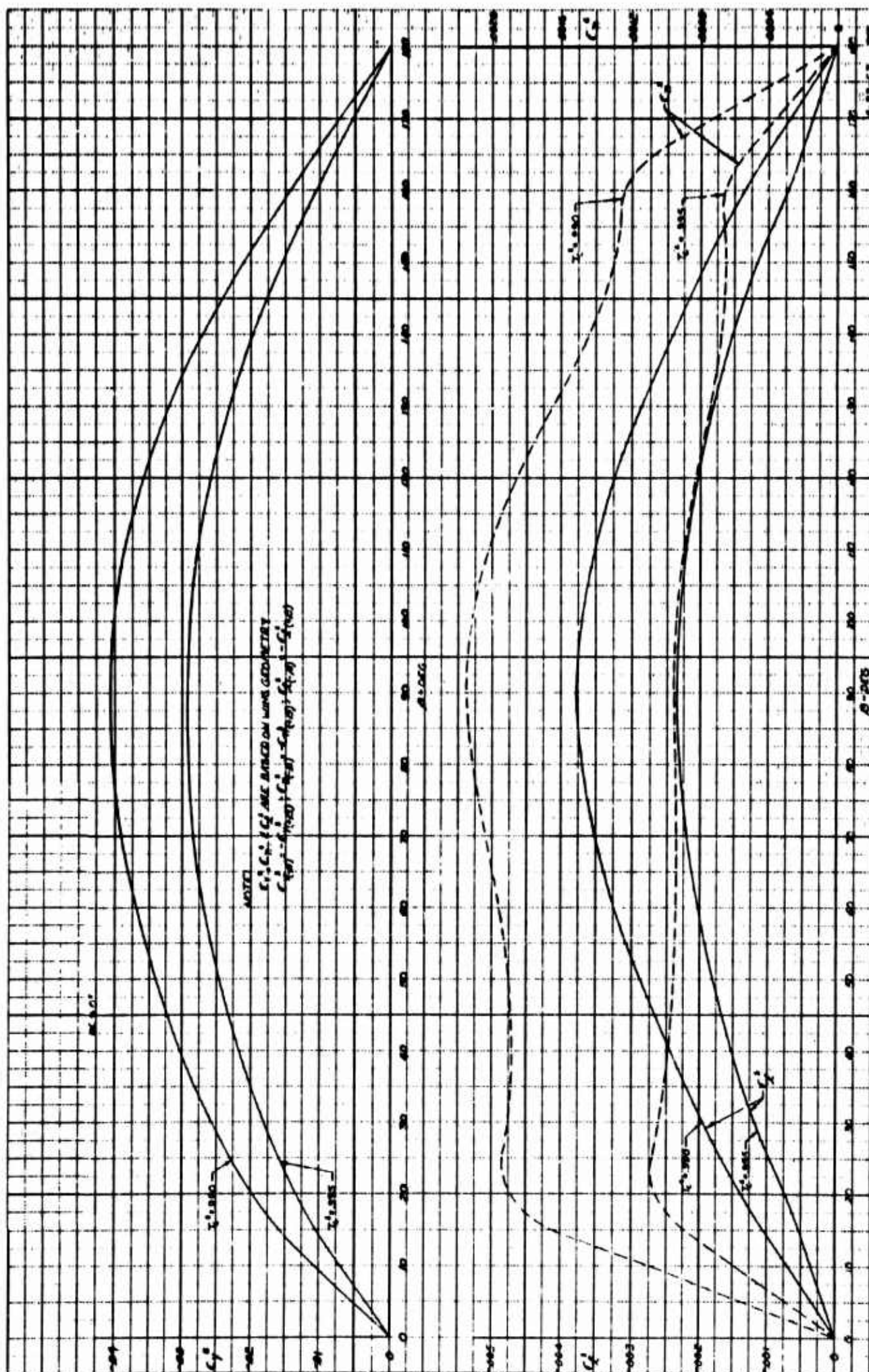
Figure 26 Low Speed Lateral Directional Characteristics at Large Angles of Sideslip
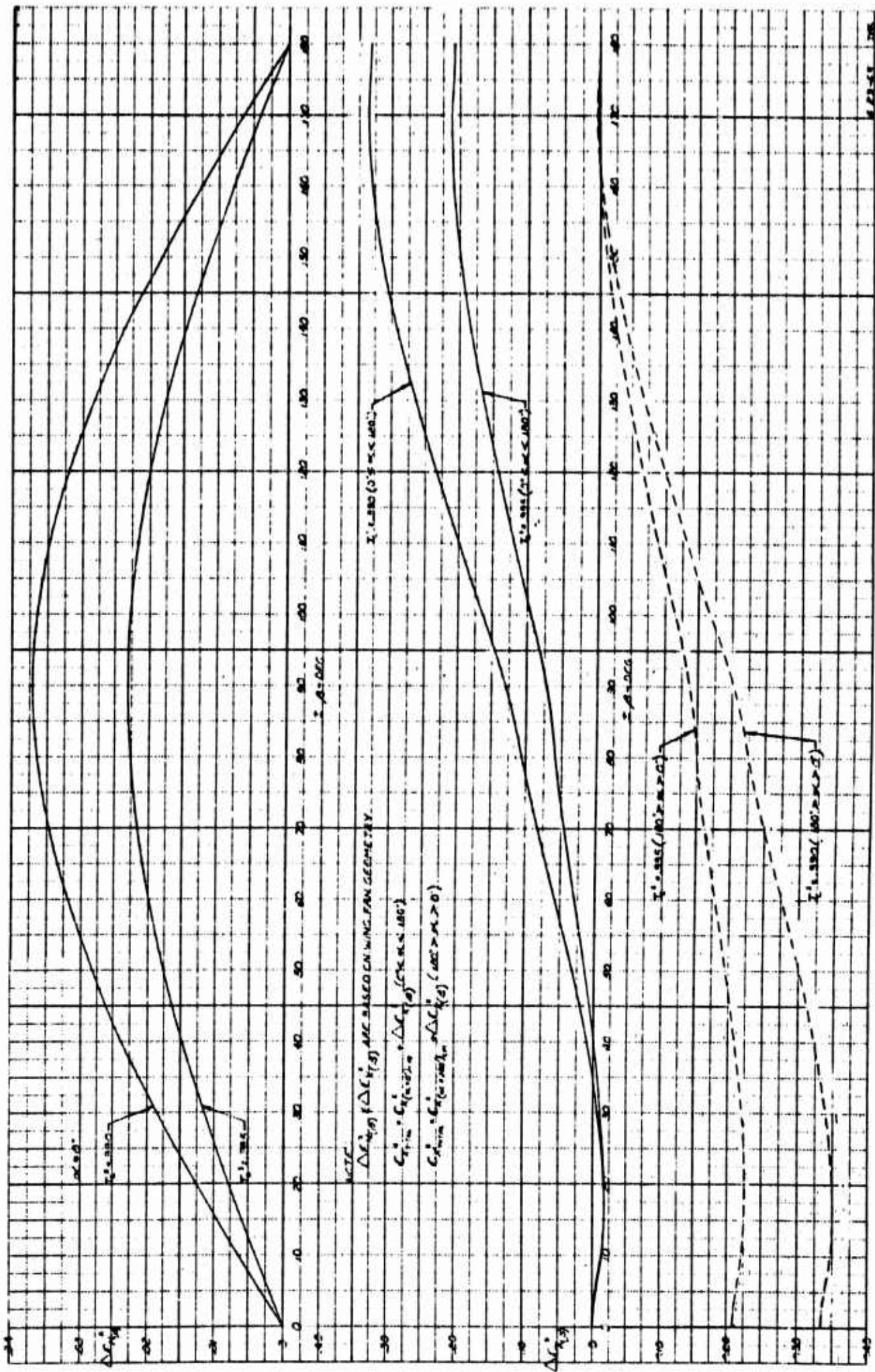
Figure 27 Low Speed Normal and Axial Force Coefficient
Characteristics at Large Angles of Sideslip
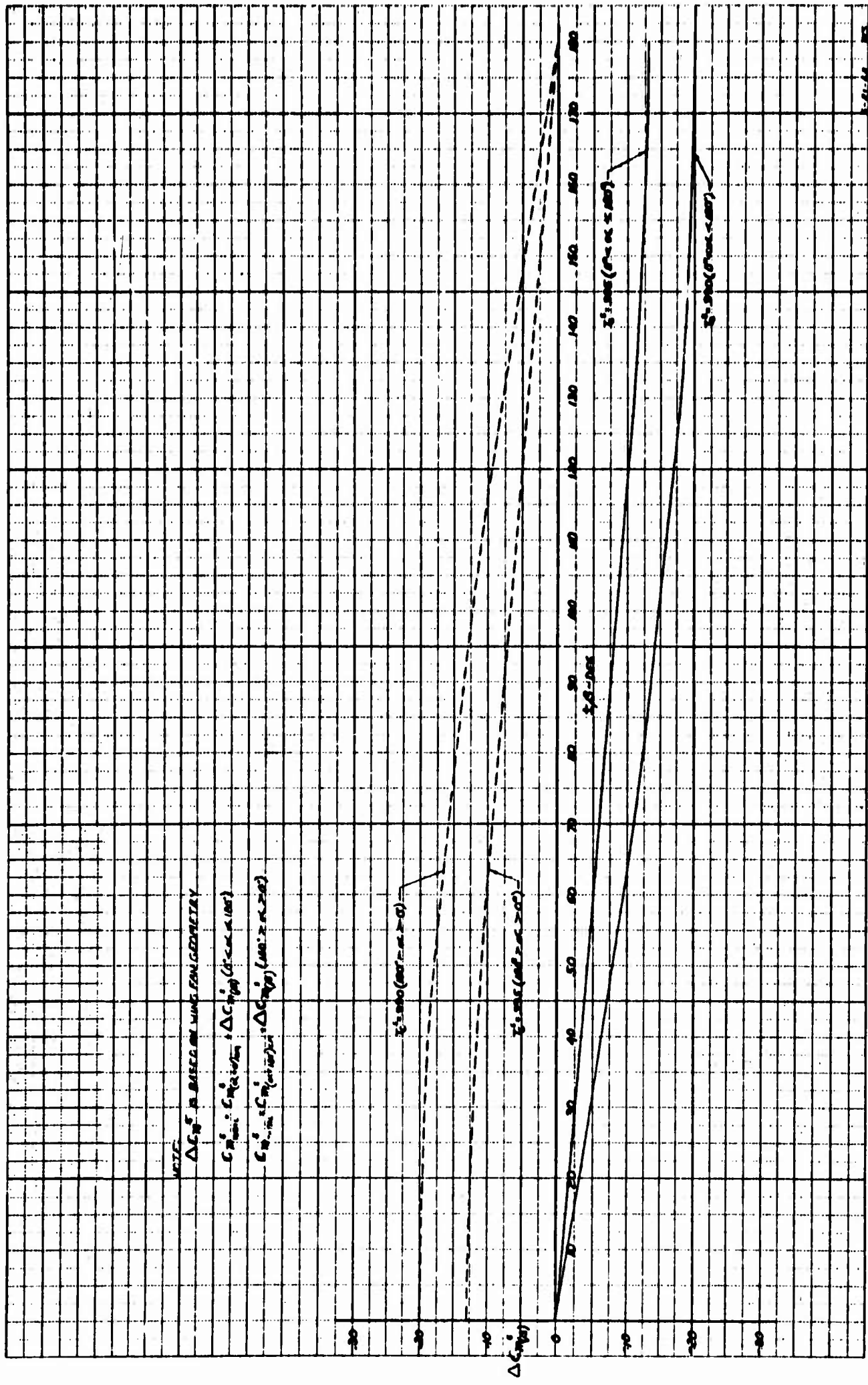
Figure 28 Low Speed Pitching Moment Coefficient Increment
At Large Angles of Sideslip

$$C_{y_{r_{CM}}} \text{ vs } \alpha$$

$$\delta_f = 45°, \quad \delta_d = 15°$$
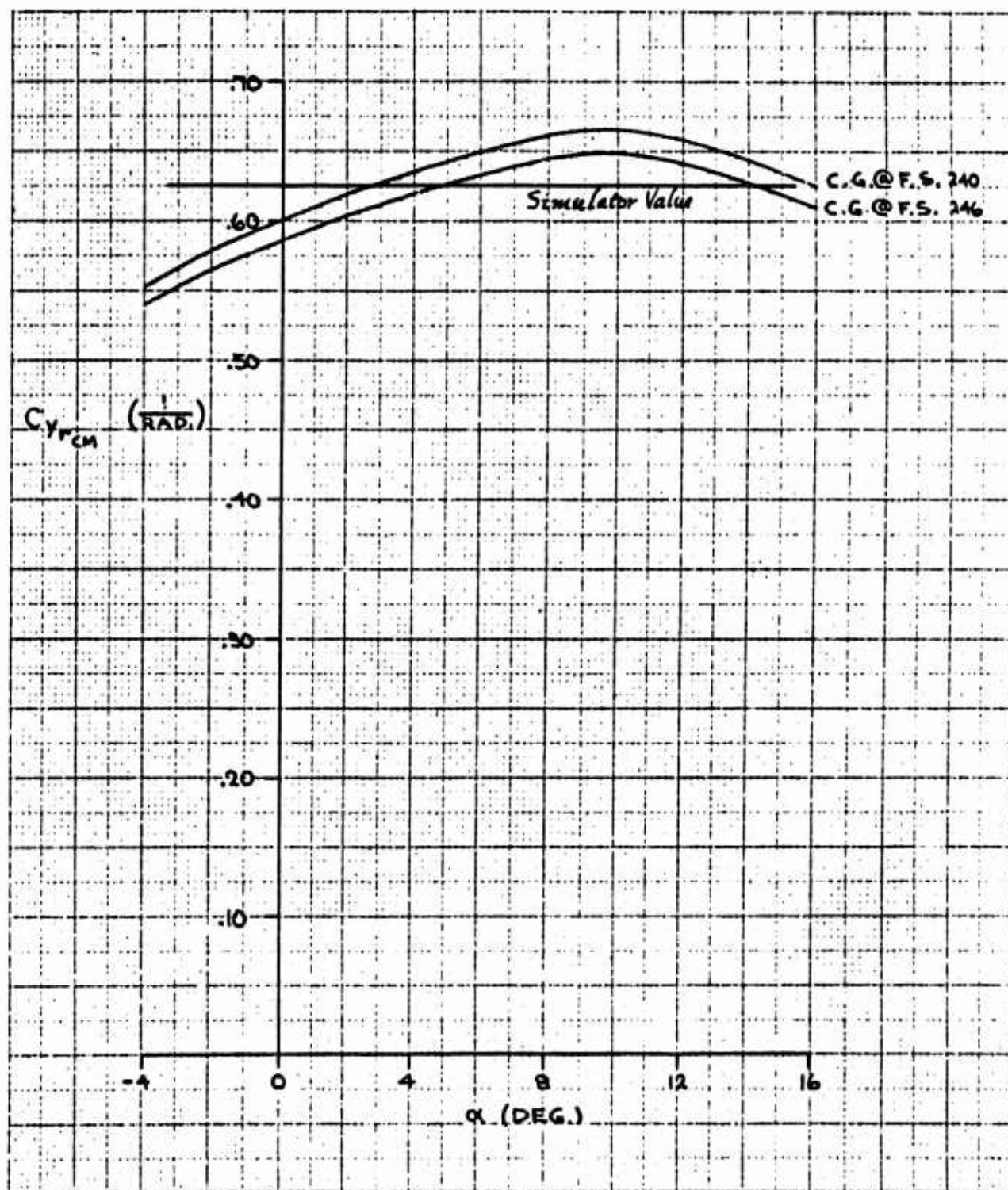
Figure 29 Basic Airframe Sideforce Coefficient Due to Yaw Rate
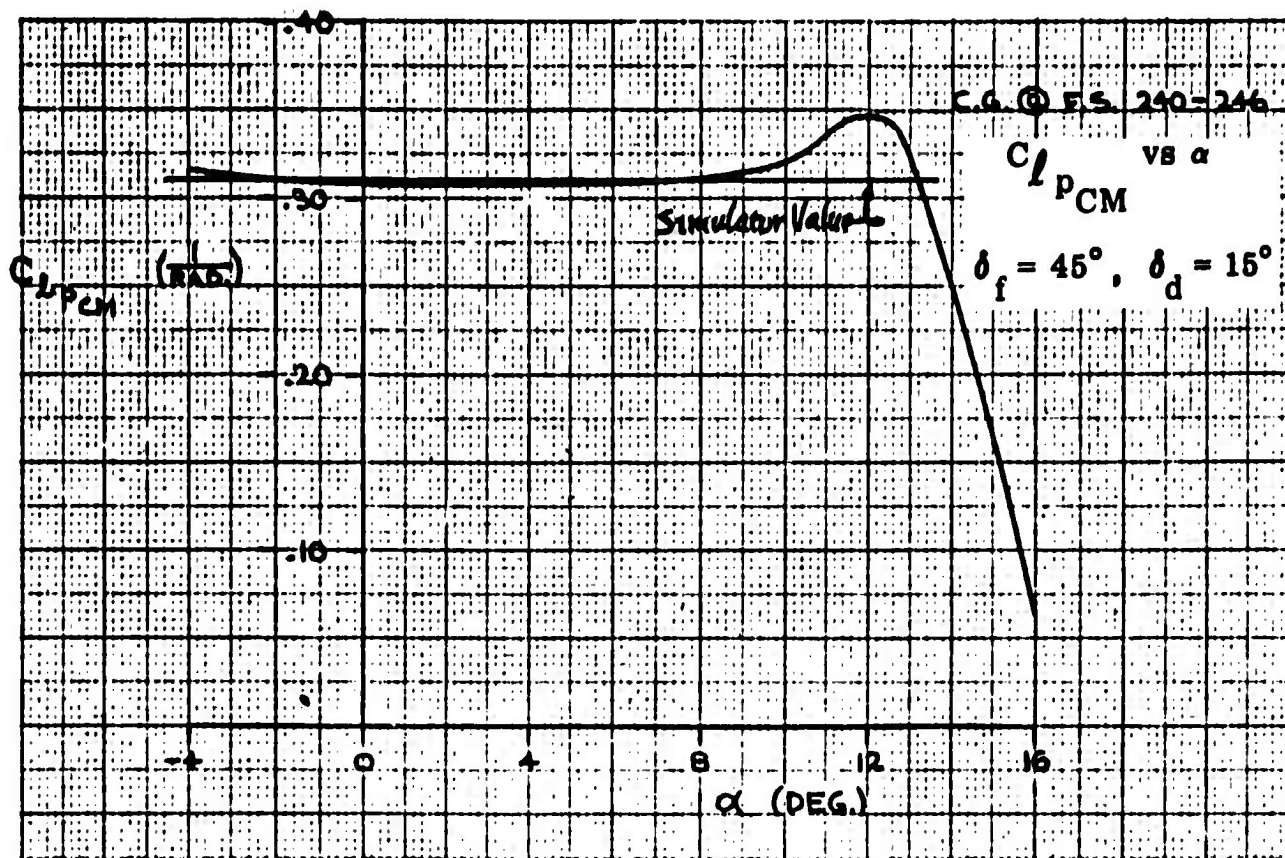
Figure 30 Basic Airframe Roll Damping Coefficient
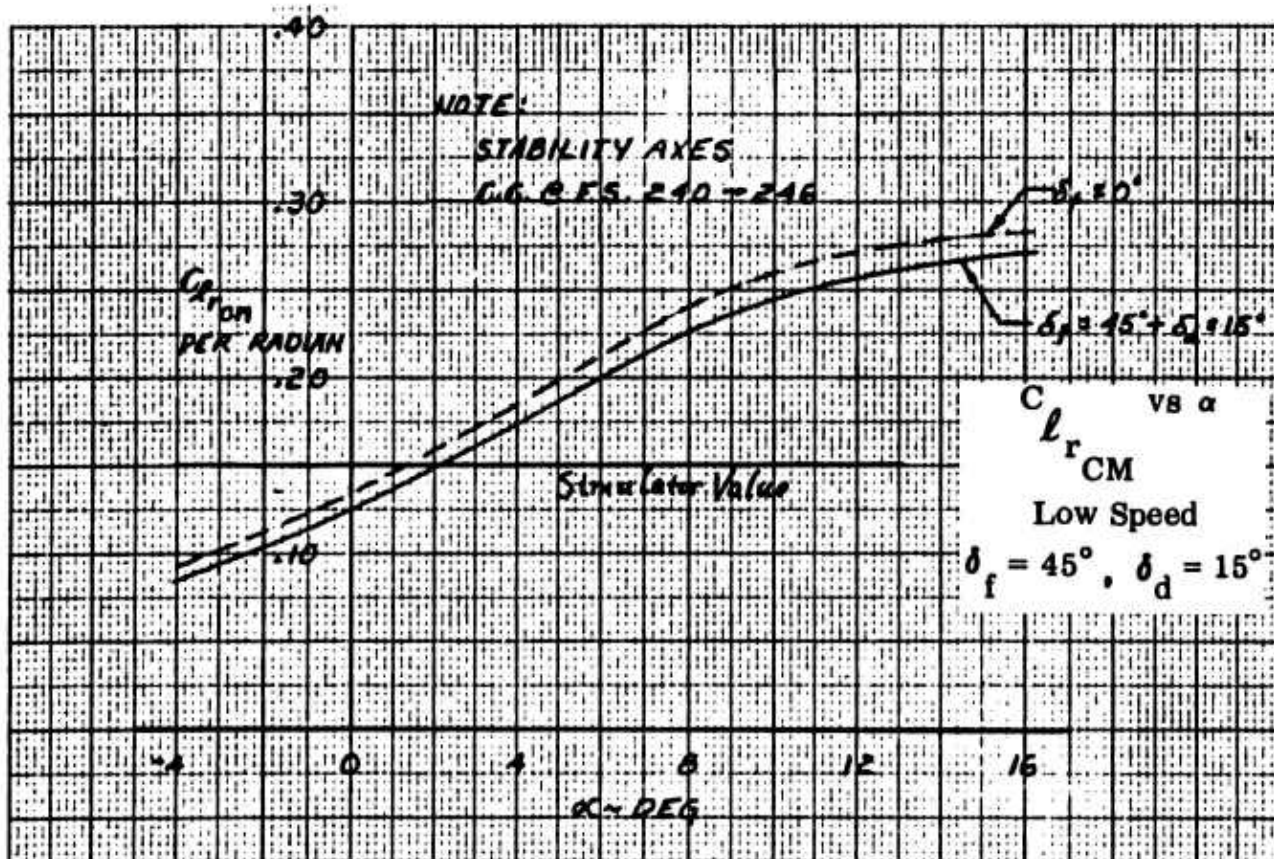
Figure 31 Basic Airframe Rolling Moment Coefficient Due to Yaw Rate

34

$$C_{n_{r_{CM}}} \quad \text{vs} \quad \alpha$$

Low Speed

$$\delta_f = 45°, \quad \delta_d = 15°$$
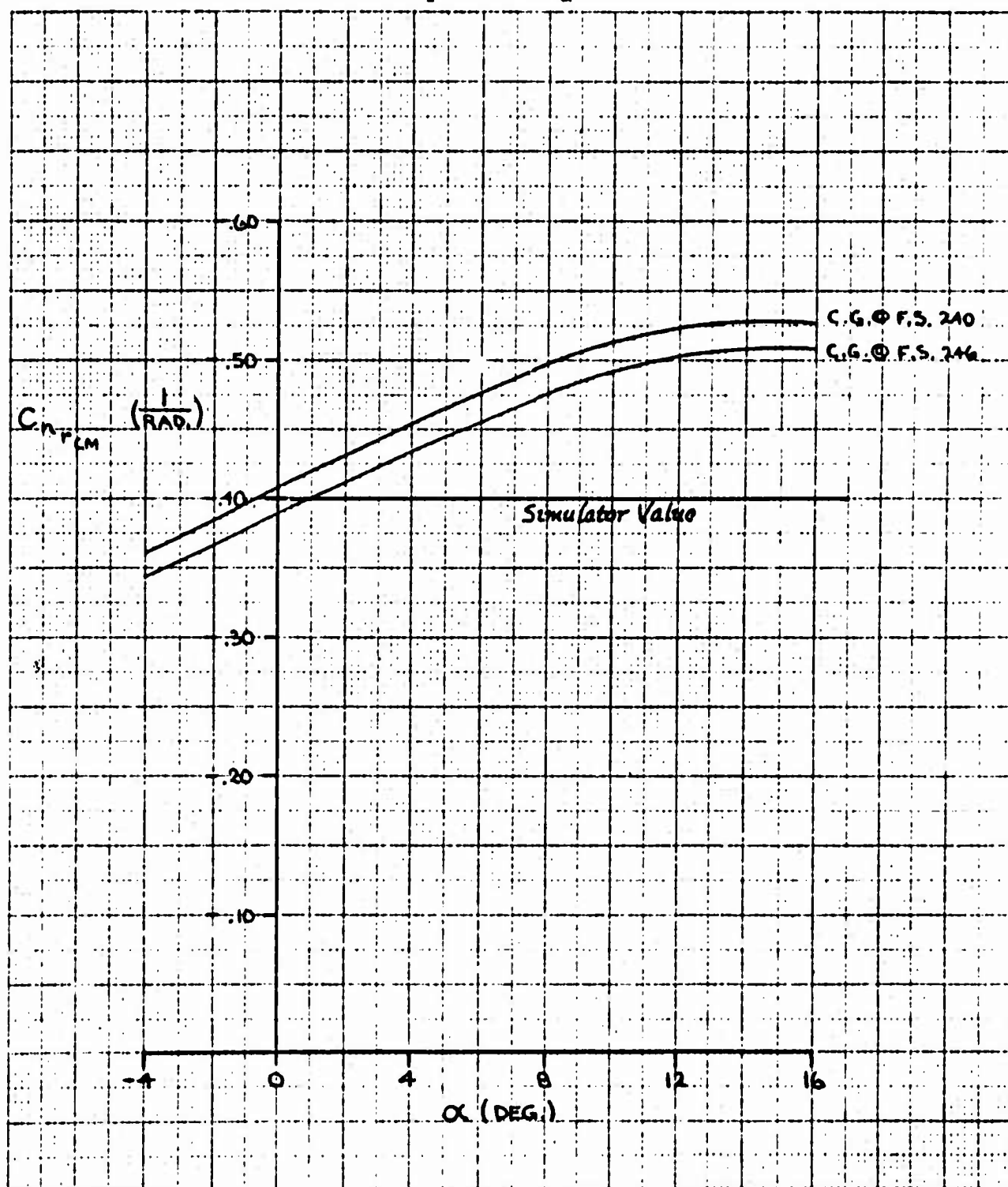
Figure 32 Basic Airframe Yaw Damping Coefficient

35

$$C_{n_{p_{CM}}} \quad vs \quad \alpha$$

Low Speed

$$\delta_f = 45°, \quad \delta_d = 15°$$
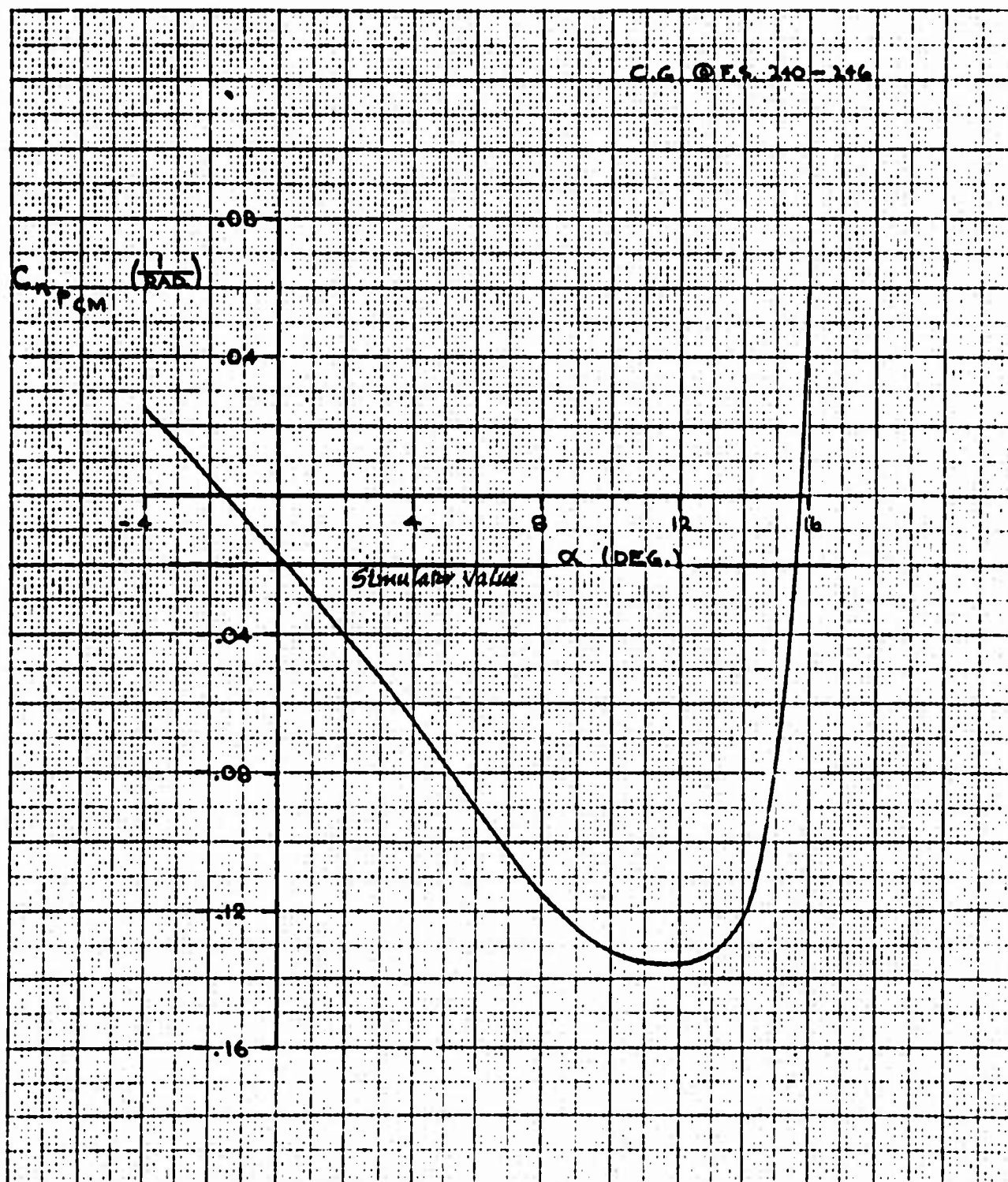
Figure 33 Basic Airframe Yawing Moment Coefficient Due to
         Roll Rate

2.1.3 Tabulated Aerodynamic Coefficients

$C_{L_{\alpha_t}}$ Tail Lift Curve Slope   .053/degree

$dC_{L_t}/d\delta_e$ Elevator Effectiveness   .023/degree

$C_{D_{o_t}}$ Tail Zero Lift Drag Coefficient .015

K_i Tail Induced Drag Coefficient   .10

$C_{y_{\delta_r}}$ Side Force Due to Rudder Deflection   .00195/degree

$C_{y_{\delta_a}}$ Side Force Due to Aileron Deflection   -.006/degree

$C_{n_{\delta_r}}$ Yawing Moment Due to Rudder Deflection   -.00122/degree

$C_{n_{\delta_a}}$ Yawing Moment Due to Aileron Deflection $-.0001 -.00031\ T_c^s$/degree

$C_{\ell_{\delta_r}}$ Rolling Moment Due to Rudder Deflection   .00025/degree

$C_{\ell_{\delta_a}}$ Rolling Moment Due to Aileron Deflection   .00088/degree

2.1.4　Fan and Engine Functions Presented for Simulation

The following Figures 34 through 43 are fan and engine characteristics developed for simulation of the aircraft.

$$C_p^s = \frac{P_F \rho^{1/2}}{\left(\frac{T_{c,n\rho}}{A_F}\right)^{3/2} A_F}$$

NOTE:
ANA 421 ST'D HOT DAY, 2500 FT. ALTITUDE

⌀ SINGLE ENGINE (MILITARY)

WING FAN POWER ~ P_F, FT-LB/SEC. $\times 10^{-6}$

% TURBOJET POWER (RPM)
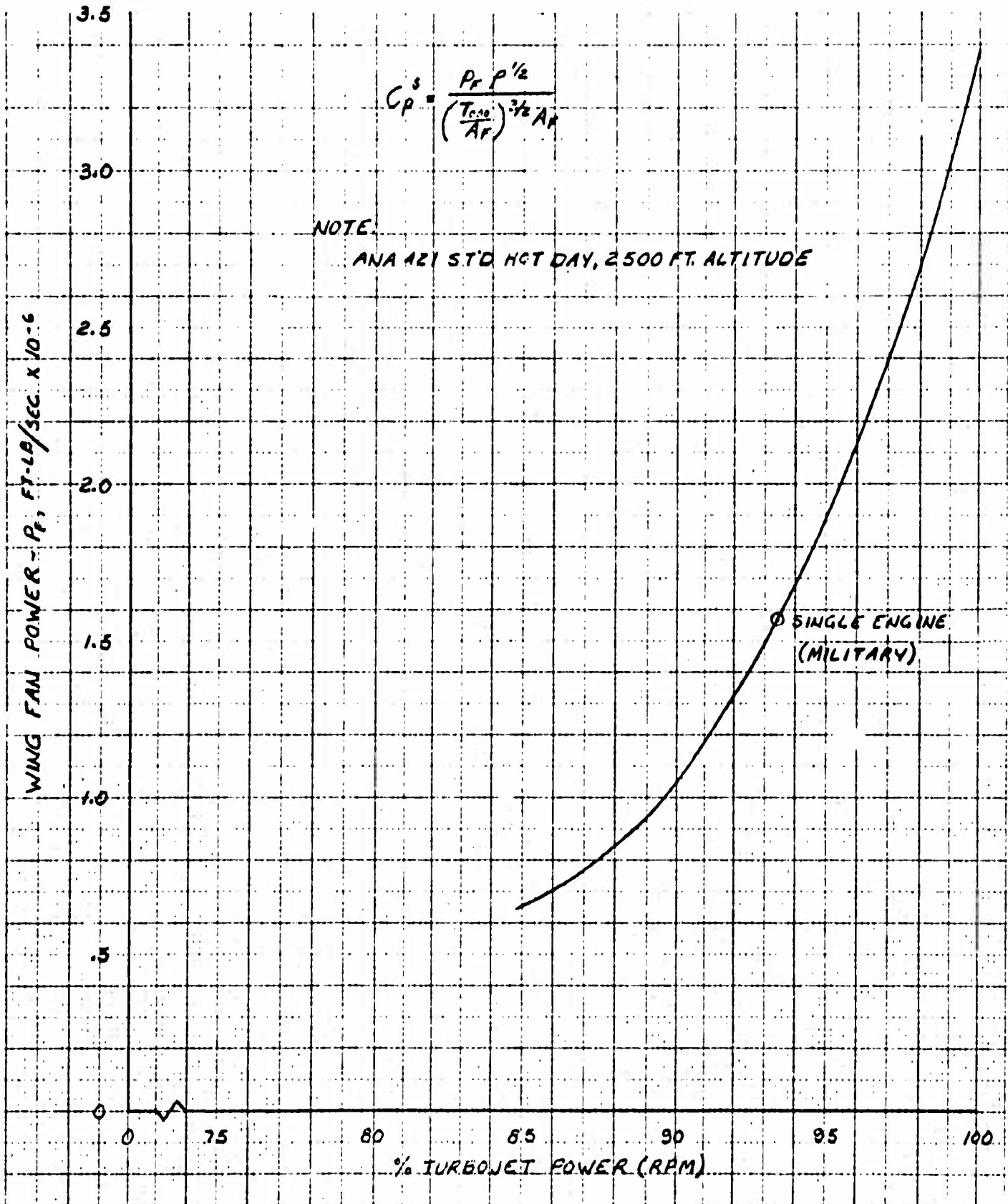
Figure 34 Wing Fan Power Curve

$$\beta_s = 0°$$

$$C_{p_O}{}^s = 1.0$$

$$C_p{}^s = \frac{P_F \rho^{1/2}}{\left(\dfrac{T_{ooo}}{A_F}\right)^{3/2} A_F}$$
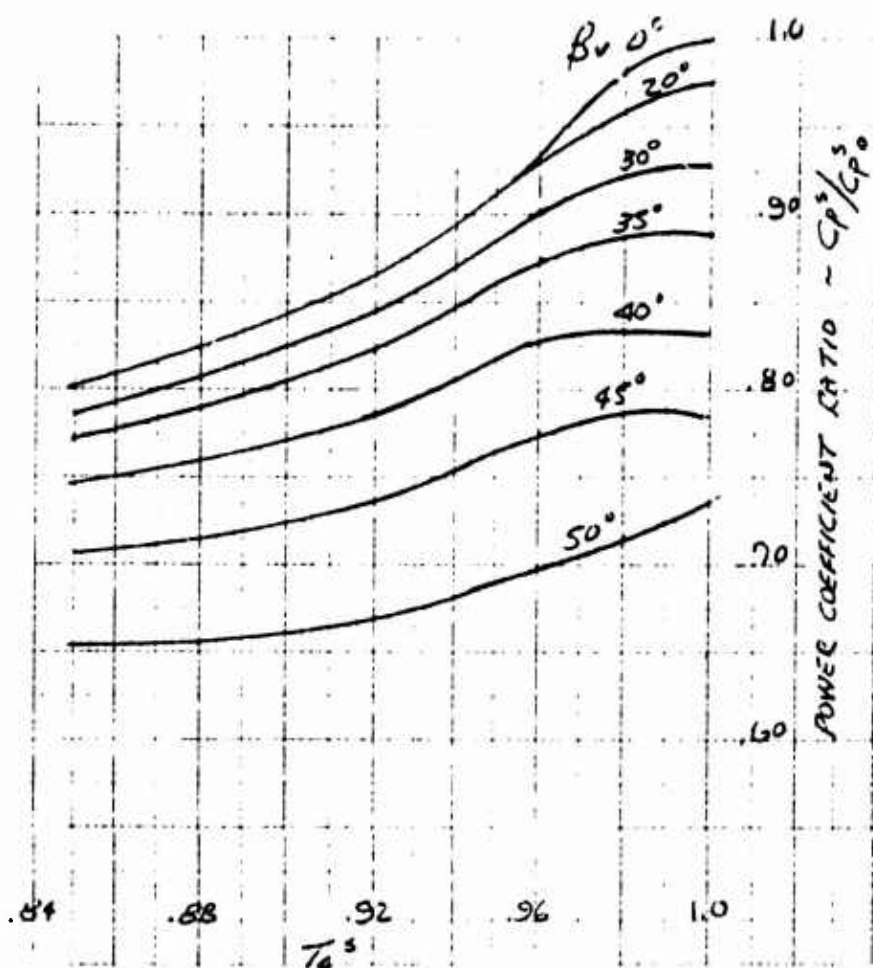
Source: Ames Test 173 and 177
1/6 Scale Data ($T_c{}^s = 1.0$)

Figure 35 Variation of Fan Power Coefficient Ratio with Vector
Angle and Thrust Coefficient
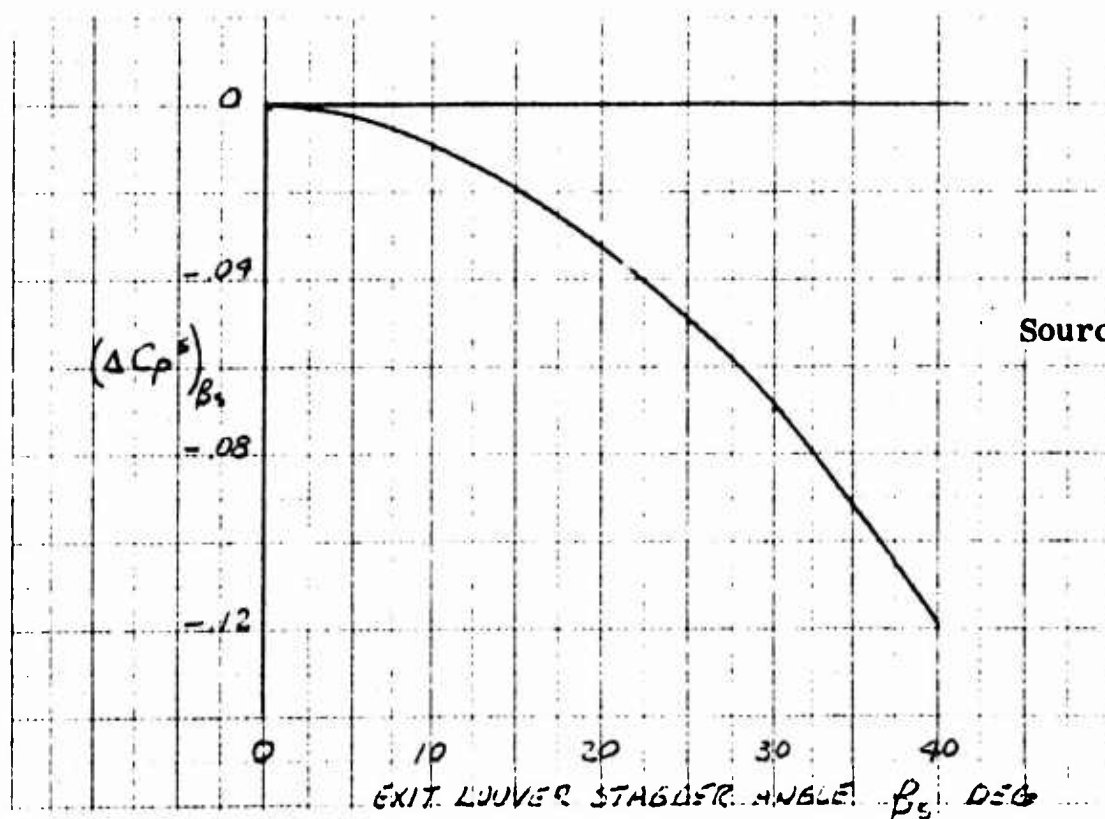
Source: Ames Test 173

Figure 36 Incremental Change in Fan Power Coefficient Ratio
Due to Exit Louver Stagger

39
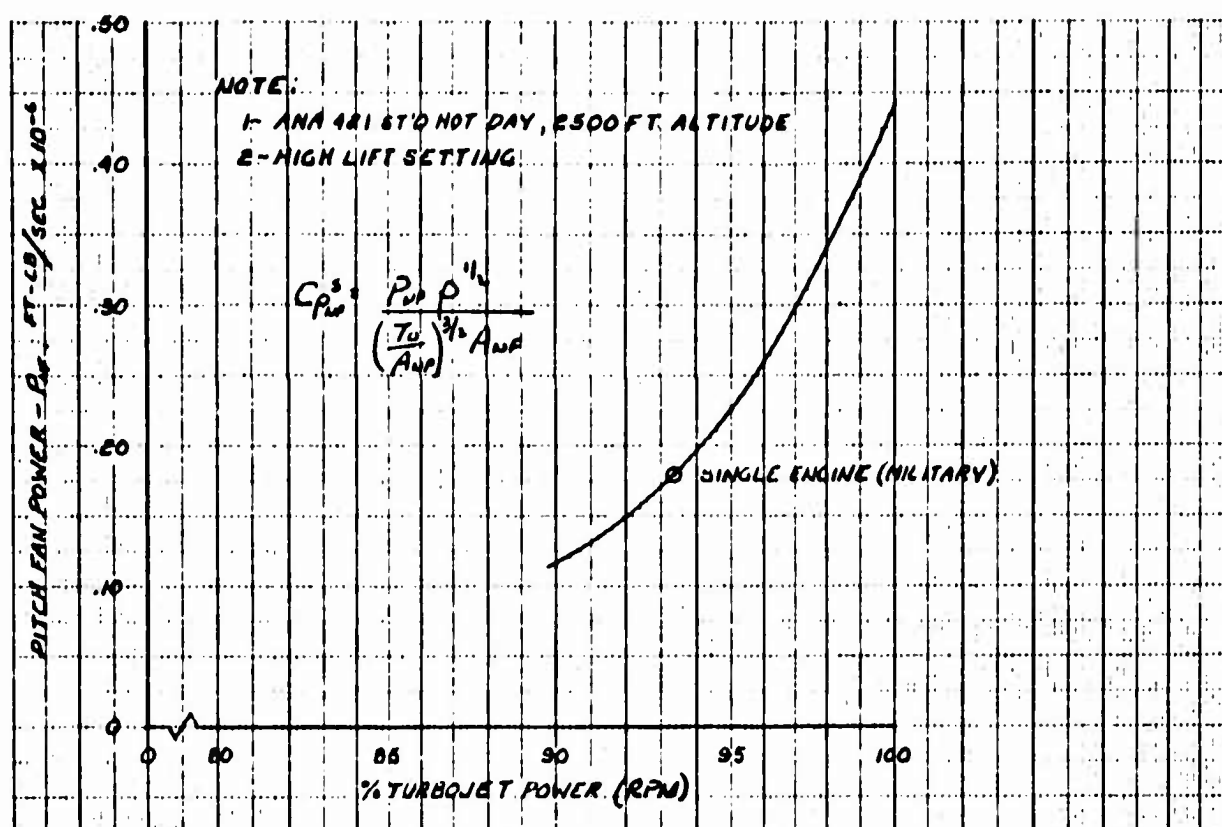
Figure 37 Pitch Fan Power Curve
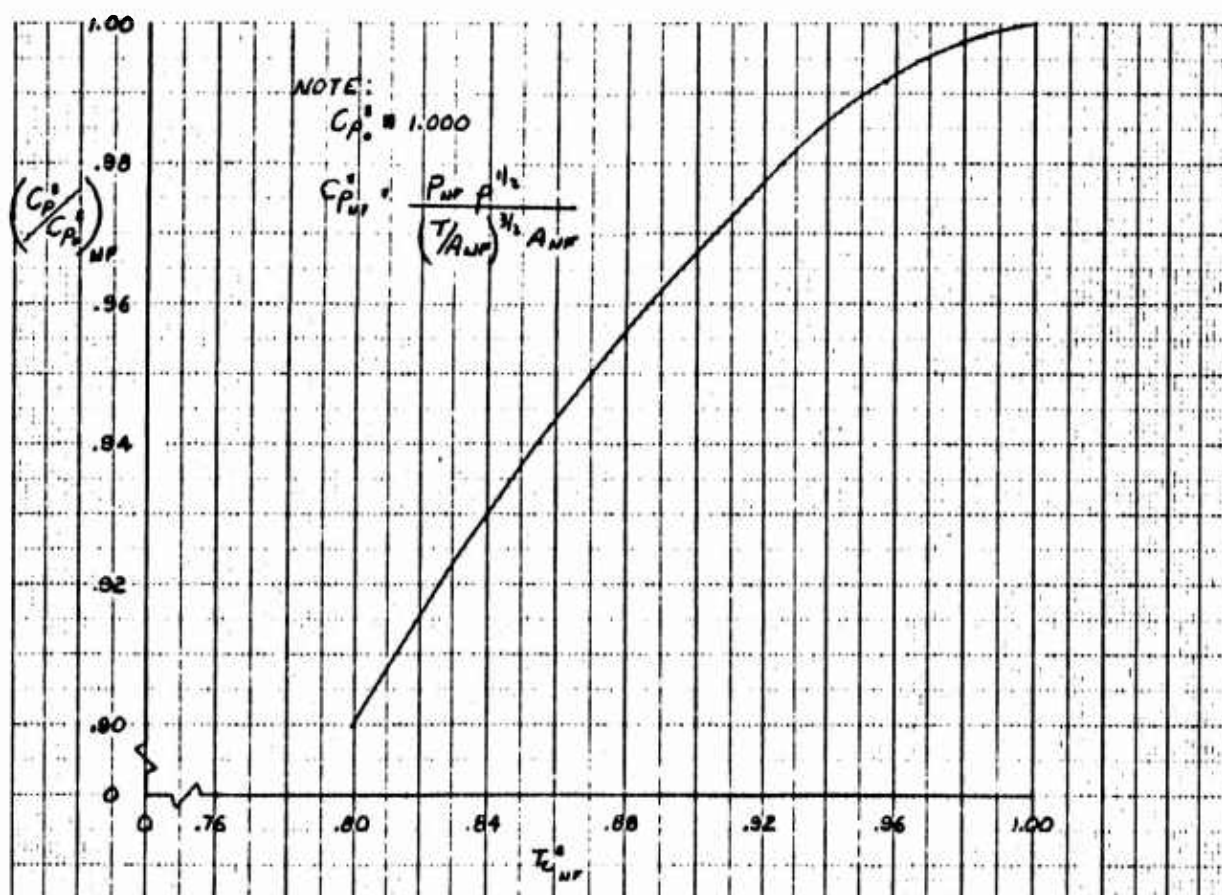
Figure 38 Variation of Pitch Fan Power Coefficient Ratio with
Thrust Coefficient
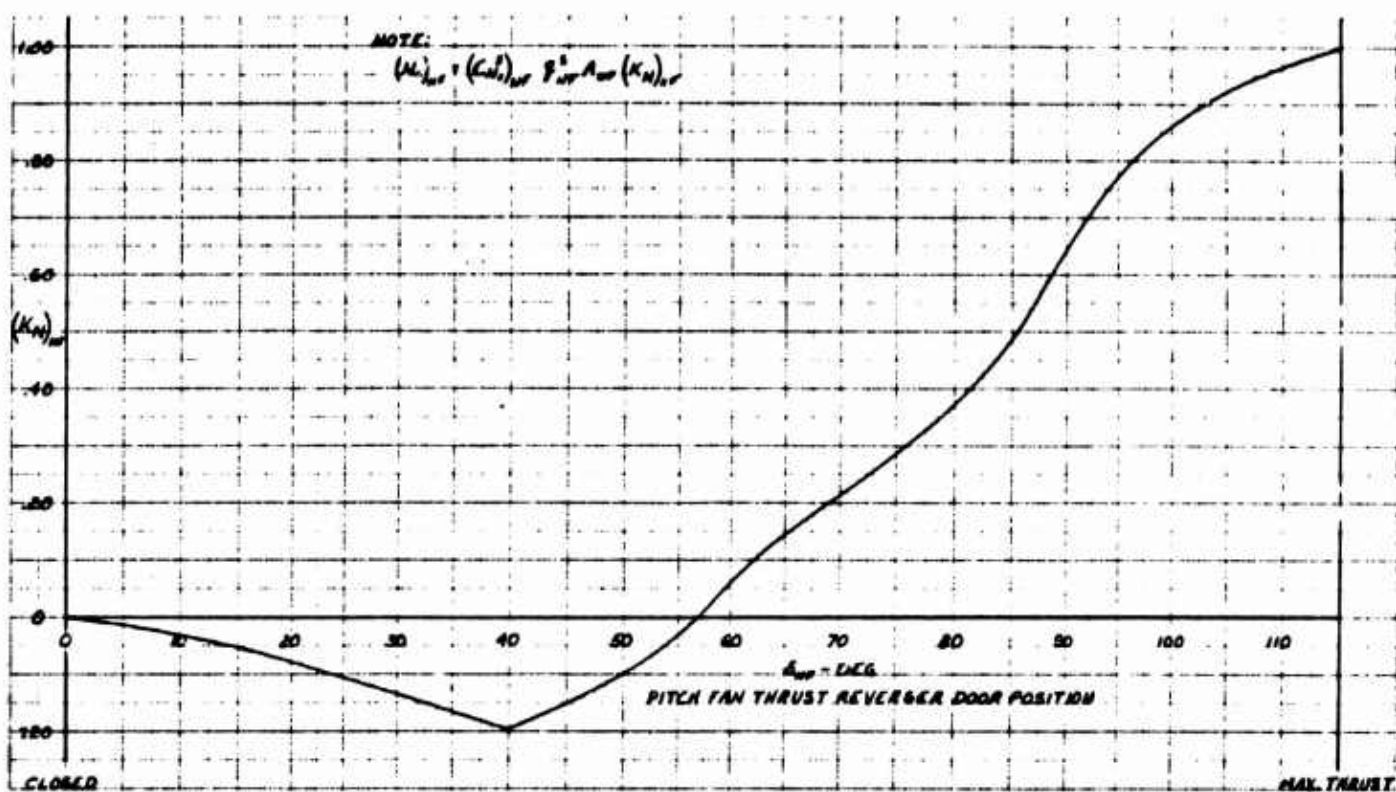
Figure 39 Pitch Fan Lift Variation Ratio with Thrust Reverser
Door Position
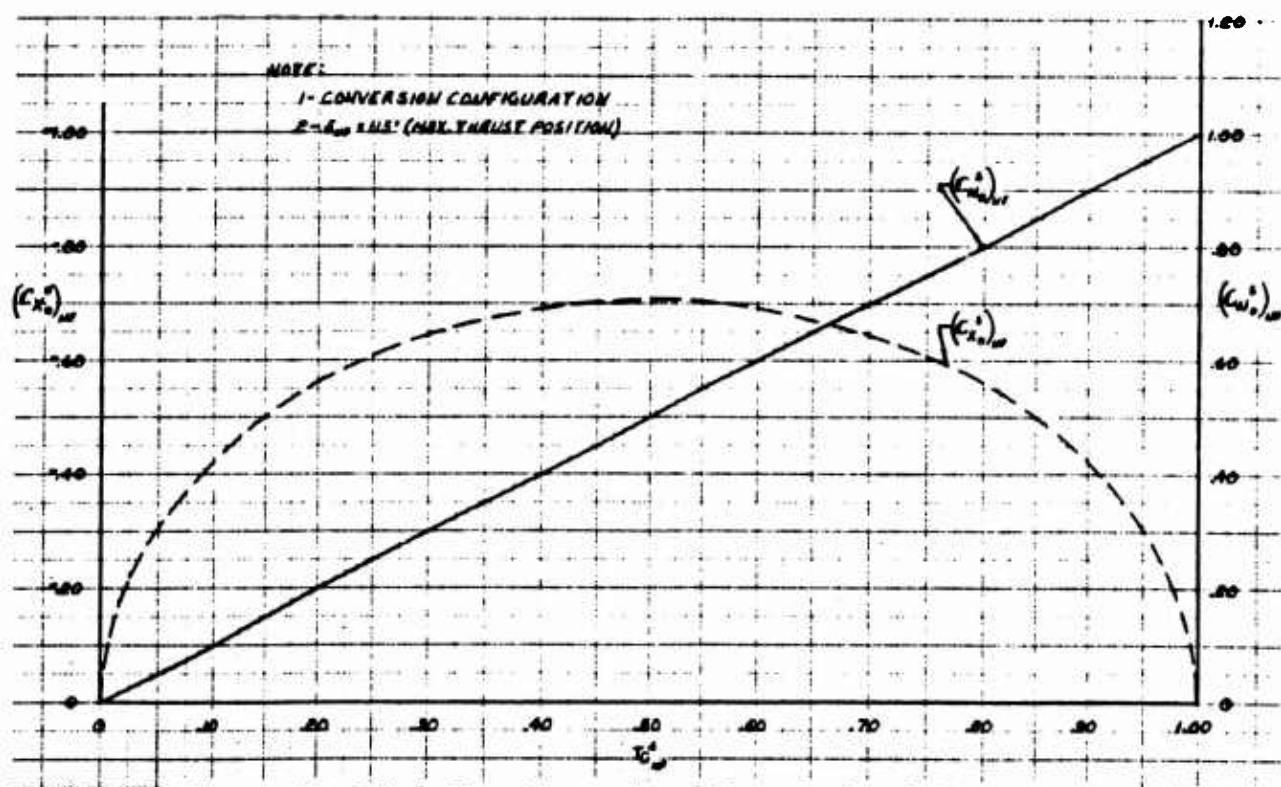
Figure 40 Pitch Fan Normal and Longitudinal Force Ratio
Characteristics
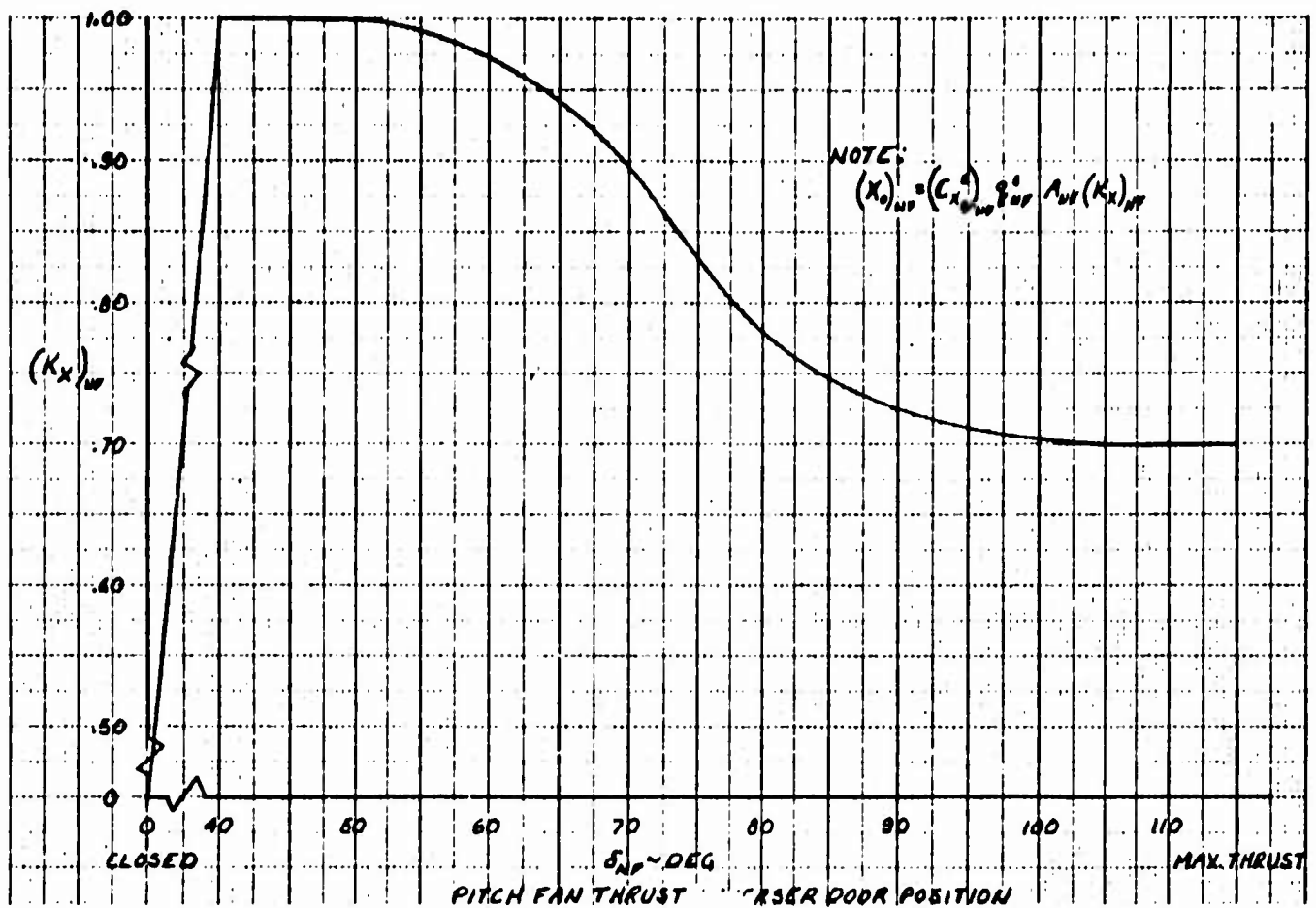
Figure 41 Pitch Fan Longitudinal Force Variation Ratio with Thrust Reverser Door Position
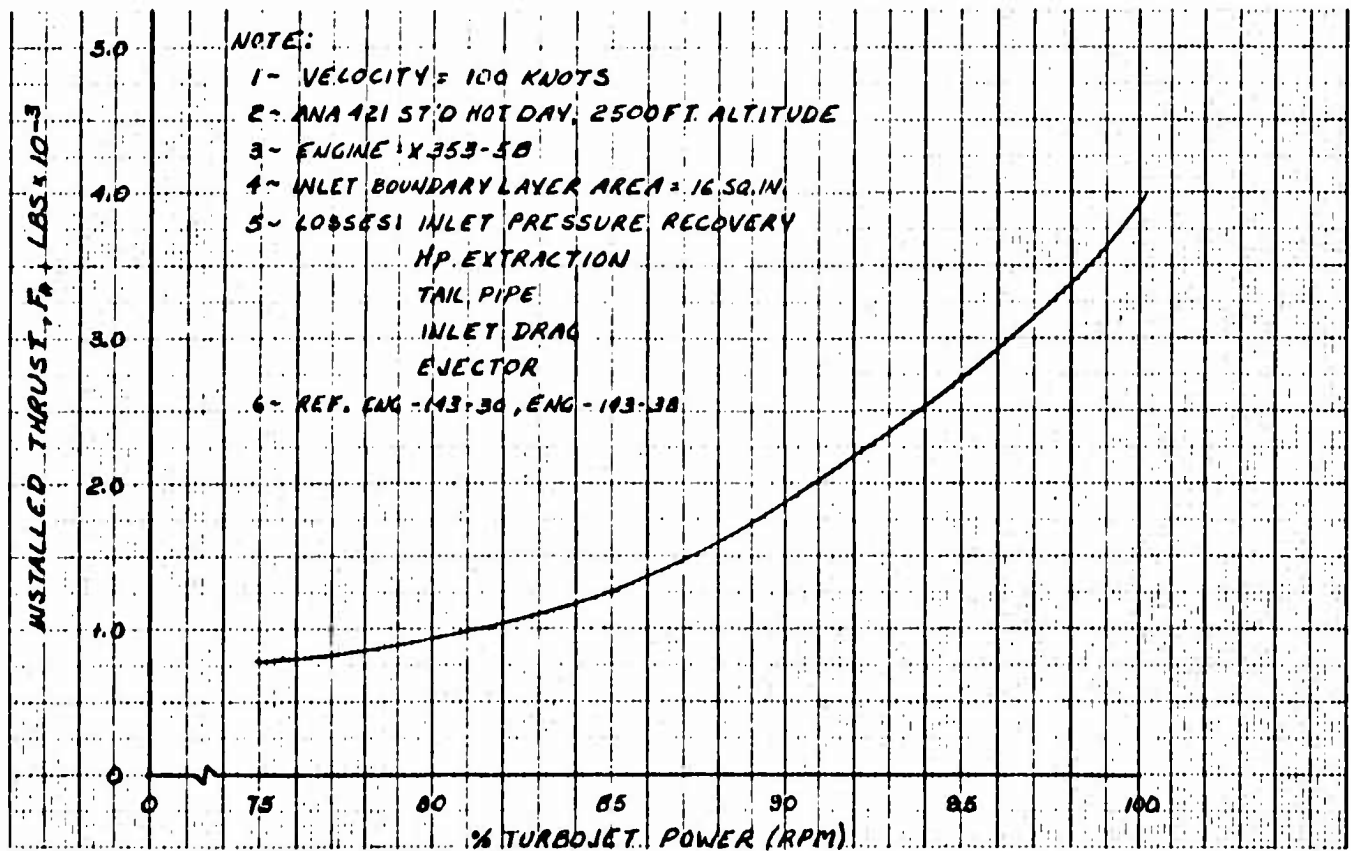
Figure 42 Installed Thrust vs Power Setting in Turbojet Mode
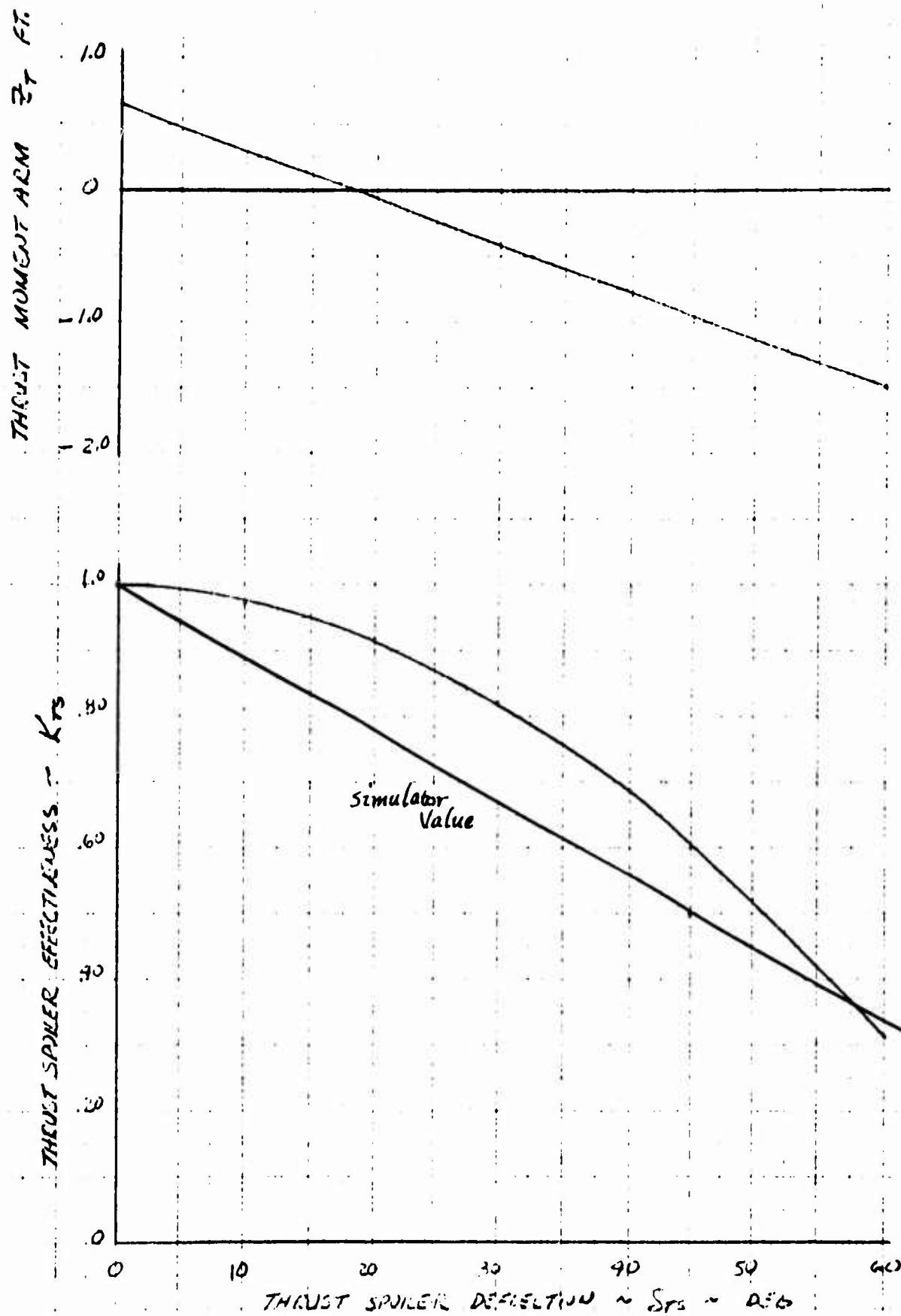
Figure 43   Estimated Thrust Spoiler Characteristics

BLANK PAGE

2.2   GENERATION OF FORCES AND MOMENTS

The analog computer generation of forces and moments acting on the vehicle required considerable thought and analysis.

In the low speed region of flight, from 0 to 50 feet per second, the vehicle has unlimited freedom of translation. In the higher speed region of flight from 50 feet per second up to the maximum transition and converted velocities of the aircraft, the motions of the aircraft tend to be restricted to the longitudinal axis, with only small perturbations laterally, around zero sideslip and zero roll angle.

The difficulty in representing the low speed force and moment behavior lies in the necessary use of data presented using flight speed correlating parameters.

Since all the coefficients, both lateral and longitudinal, are functions of T_c^s, velocities along any axis (which will cause a T_c^s variation) will cause force and moment coefficient changes along all other axes. For example, side translations couple into the longitudinal mode through variations in C_m^s, C_X^s and C_N^s with T_c^s. This coupling does not in reality occur, and if all moments and forces were generated indiscriminately as functions of T_c^s in all flight regimes, "correction" functions would have to be generated to wipe out these erroneous variations. These correction functions themselves would lead to errors if there were combinations of velocities along 2 or 3 axes.

With this problem in mind, and the realization that low speed behavior is governed mostly by fan effects, the lateral and longitudinal low speed coefficient data were converted to force and moment data and plotted versus velocity along the three aircraft body axes. The resulting data agreed closely with momentum theory for the 0 - 50 feet per second velocity range in which T_c^s coupling is a problem.

With this basic information in mind, the generation of force and moment data was divided into two separate regions. Terms generated in the low speed region are generated on the basis of momentum calculations, with force and moments calculated based on velocity components along the three body axes, while the data was "used as presented" for the higher speed flight region where the flight path (total velocity) was referred to the body axes.*

---

*"Used as presented" is a phrase meant to signify no basic change has been made in the input information. See also Paragraph 2.2.2.

Transfer from low speed terms to high speed terms is accomplished with two phasing functions explained in the term explanation portion of this report. In some cases, the higher speed terms are phased out without using these phasing functions, simply by forcing the output of whatever function generation equipment employed for generation of the term in question to go to zero at T_c^s's at and above those corresponding to a velocity of 50 feet per second.

Presented in the following Paragraph 2.2.1 is a summary of the equations used to generate the total forces and moments about each axis of the aircraft.

2.2.1 Simulation Force and Moment Equations

Normal Force   Term No.

$$\Sigma N = \frac{\rho V_T^{\,2}}{2} \, A_F \left(C_{N_\alpha}^{\,s} \Big|_{T_c^{\,s}=0} \, \alpha_{LIM} \right) \tag{1N}$$

$$+ \left(C_{N_o}^{\,s} \right) \, A_F \left(\frac{q_{RT}^{\,s} + q_{LT}^{\,s}}{2} \right) \tag{2N}$$

$$+ \, q_{RT}^{\,s} \, \frac{A_F}{2} \left(\Delta C_{N_{\beta_{s_{RT}}}}^{\,s} \, \beta_{s_{RT}} + \Delta C_{N_{\beta_{v_{RT}}}}^{\,s} \, \beta_{v_{RT}} \right) \tag{3N}$$

$$+ \, q_{RT}^{\,s} \, \frac{A_F}{2} \left(\frac{\partial C_{N_T}^{\,s}}{\partial \alpha} \Big|_{\beta_v = 0} + \frac{\partial}{\partial \beta_v} \left(\frac{\partial C_{N_T}^{\,s}}{\partial \alpha} \right) \frac{\beta_v}{50} \right) \alpha_{LIM} \tag{4N}$$

$$+ \, q_{LT}^{\,s} \, \frac{A_F}{2} \left(\Delta C_{N_{\beta_{s_{LT}}}}^{\,s} \, \beta_{s_{LT}} + \Delta C_{N_{\beta_{v_{LT}}}}^{\,s} \, \beta_{v_{LT}} \right) \tag{5N}$$

46

Normal Force (Continued)

$$+ q^s_{LT} \frac{A_F}{2} \left(\left. \frac{\partial C^s_{N_T}}{\partial \alpha} \right|_{\beta_v = 0} + \frac{\partial}{\partial \beta_v} \left(\frac{\partial C^s_{N_T}}{\partial \alpha} \right) \frac{\beta_v}{50} \right) \alpha_{LIM} \qquad \text{6N}$$

$$+ \frac{T_o}{A_{NF}} A_{NF} K_{N_{NF}} \qquad \text{7N}$$

$$+ 4.38 (w - q\bar{x}_{NF}) \qquad \text{8N}$$

$$+ \frac{\rho V_T S_w \bar{c}}{4} \left(C_{L_q} + C_{L_{\dot{\alpha}}} \right) q \qquad \text{9N}$$

$$+ \frac{\rho V_T^2}{2} S_w \left(C_{N_t} K_T \eta_T \right) \qquad \text{10N}$$

$$+ .174 \, T_j \, K_{TS} \qquad \text{11N}$$

$$+ (3 |u| + 10 |v|) \, (POF \, \#1) \qquad \text{12N}$$

$$+ q^s_{AVE} A_F \left(\Delta C^s_N (\sin \alpha) \right) \, (POF \, \#2) \qquad \text{13N}$$

Axial Force

$$\Sigma X = \frac{\rho V_T^2}{2} A_F \left(\left. C^s_{X_\alpha} \right|_{T^s_c = 0} \alpha_{LIM} \right) \qquad \text{1X}$$

$$+ A_F \left(C^s_{X_o} \right) \left(\frac{q^s_{RT} + q^s_{LT}}{2} \right) \qquad \text{2X}$$

Axial Force (Continued) — Term No.

$$\Sigma X = + \; q^s_{RT} \frac{A_F}{2} \left(\Delta C_X{}^s{}_{\beta_{s_{RT}}} \beta_{s_{RT}} + \Delta C_X{}^s{}_{\beta_{v_{RT}}} \beta_{v_{RT}} \right) \qquad 3X$$

$$+ \; q^s_{RT} \frac{A_F}{2} \left(\left. \frac{\partial C_{X_T}{}^s}{\partial \alpha} \right|_{\beta_v = 0} + \frac{\partial}{\partial \beta_v} \left(\frac{\partial C_{X_T}{}^s}{\partial \alpha} \right) \frac{\beta_v}{50} \right) \alpha_{LIM} \qquad 4X$$

$$+ \; q^s_{LT} \frac{A_F}{2} \left(\Delta C_X{}^s{}_{\beta_{s_{LT}}} \beta_{s_{LT}} + \Delta C_X{}^s{}_{\beta_{v_{LT}}} \beta_{v_{LT}} \right) \qquad 5X$$

$$+ \; q^s_{LT} \frac{A_F}{2} \left(\left. \frac{\partial C_{X_T}{}^s}{\partial \alpha} \right|_{\beta_v = 0} + \frac{\partial}{\partial \beta_v} \left(\frac{\partial C_{X_T}{}^s}{\partial \alpha} \right) \frac{\beta_v}{50} \right) \alpha_{LIM} \qquad 6X$$

$$+ \; \frac{\rho V_T{}^2}{2} \; S_w \, C_{X_t} \, K_T \eta_T \qquad 7X$$

$$+ \; T_j \, K_{TS} \qquad 8X$$

$$- \; 4.38 \, u \qquad 9X$$

$$+ \; (q^s_{AVE} \, A_F \, \mathrm{Sin} \, 4^o - 27.42 \, u) \, (\text{POF \#1}) \qquad 10X$$

Pitching Moment — Term No.

$$\Sigma \mathcal{M} = q^s_{AVE} \, A_F D_F \left(C_{m_o}{}^s \right) \qquad 1\mathcal{M}$$

$$+ \; q^s_{AVE} \, A_F D_F \left(C_{m_\alpha}{}^s \, \alpha_{LIM} \right) \qquad 2\mathcal{M}$$

$$+ \; q^s_{RT} \frac{A_F D_F}{2} \left(\Delta C^s_{m_{\beta_s}} \beta_{s_{RT}} + \Delta C^s_{m_{\beta_v}} \beta_{v_{RT}} \right) \qquad 3\mathcal{M}$$

$$+ \; q^s_{LT} \frac{A_F D_F}{2} \left(\Delta C^s_{m_{\beta_{s_{LT}}}} \beta_{s_{LT}} + \Delta C^s_{m_{\beta_{v_{LT}}}} \beta_{v_{LT}} \right) \qquad 4\mathcal{M}$$

$$+ \frac{\rho V_T^2}{2} S_w \bar{c} \left(\frac{\partial C_m}{\partial |\beta|} \, |\beta| \;\; _{LIM} \right) \qquad 5\mathcal{M}$$

$$+ \; \frac{\rho V_T^2 S_w \bar{c}}{2} \left(C_{X_t} \frac{z_t}{\bar{c}} - C_{N_t} \frac{\ell_t}{\bar{c}} \right) K_T \eta_T \qquad 6\mathcal{M}$$

$$+ \; \frac{\rho V_T S_w \bar{c}^2}{4} \left(C_{m_q} + C_{m_{\dot\alpha}} \right) q \qquad 7\mathcal{M}$$

$$+ \frac{T_o}{A_{NF}} A_{NF} K_{N_{NF}} \bar{x}_{NF} \qquad 8\mathcal{M}$$

$$+ \; 4.38 \left(w - q\bar{x}_{NF} \right) \bar{x}_{NF} \qquad 9\mathcal{M}$$

$$+ \left(134u - q^s_{ave} A_F \bar{x}_F \right) \;\; (POF \; \#1) \qquad 10\mathcal{M}$$

$$+ \; q^s_{AVE} A_F D_F \left(\Delta C_m^s (Sin(\alpha - 50^\circ) + MNF \right) (POF \; \#2) \quad 11\mathcal{M}$$

<u>Side Force</u>   <u>Term No.</u>

$$\Sigma Y = C_{Y_\beta}^s \; \beta_{LIM} q_{AVE}^s S_w$$ 1Y

$$+ \; S_w \frac{\rho V_T^2}{2} \left[C_{\delta_A} \left(\delta_{a_L} - \delta_{a_R} \right) \right]$$ 2Y

$$+ \; S_w \frac{\rho V_T^2}{2} \left(C_{Y_{\delta_r}} \delta_r \right)$$ 3Y

$$+ \; \frac{\rho V_T S_w b^2}{4} \left(C_{Y_r} r \right)$$ 4Y

$$+ \left(-31.8v - \dot{m}_{NF} \overline{x}_{NF} \, r - \frac{\rho V_T^2}{2} (C_D S) \frac{v}{V_T} \right) \text{(POF \#1)}$$ 5Y

<u>Yawing Moment</u>   <u>Term No.</u>

$$\Sigma N = C_{n_\beta}^s \; \beta_{LIM} \; q_{ave}^s \; S_w \, b$$ 1 N

$$+ \; \frac{\rho V_T^2 S_w b}{2} \left(C_{n_{\delta_a}} \left(\delta_{a_L} - \delta_{a_R} \right) \right)$$ 2 N

$$+ \; \frac{\rho V_T^2 S_w b}{2} \left(C_{n_{\delta_r}} \delta_r \right)$$ 3 N

$$+ \frac{\rho V_T S_w b^2}{4}\left(C_{n_r} r\right) \qquad\qquad 4N$$

$$+ \frac{\rho V_T S_w b^2}{4}\left(C_{n_p} p\right) \qquad\qquad 5N$$

$$+ q^s_{LT} \frac{A_F}{2} y_F \left(\Delta C^s_{X_{\beta_{s_{LT}}}} \beta_{s_{LT}} + \Delta C^s_{X_{\beta_{v_{LT}}}} \beta_{v_{LT}}\right) \qquad 6N$$

$$- q^s_{RT} \frac{A_F}{2} y_F \left(\Delta C^s_{X_{\beta_{s_{RT}}}} \beta_{s_{RT}} + \Delta C^s_{X_{\beta_{v_{RT}}}} \beta_{v_{RT}}\right) \qquad 7N$$

$$- \overset{\bullet}{m}_{NF} \overline{x}^2_{NF} r \qquad\qquad 8N$$

$$+ \left(47.0\,v + 560\frac{\rho V_T^2}{2} \frac{v}{V_T} - 2r\overset{\bullet}{m}_{MF}\overline{y}^2_{MF}\right) (POF\ \#1) \qquad 9N$$

Rolling Moment   Term No.

$$\Sigma \ell = C^s_{\ell_\beta} \beta_{LIM} q^s_{ave} S_w b \qquad\qquad 1\ell$$

$$+ \frac{\rho V_T^2}{2} S_w b\left(C_{\ell_{\delta_A}}\left(\delta_{a_L} - \delta_{a_R}\right)\right) \qquad\qquad 2\ell$$

$$+ \frac{\rho V_T^2}{2} S_w b\left(C_{\ell_{\delta_r}} \delta r\right) \qquad\qquad 3\ell$$

$$+ \frac{\rho V_T S_w b^2}{4} \left(C_{\ell_p} p \right) \qquad\qquad 4\ell$$

$$+ \frac{\rho V_T S_w b^2}{4} \left(C_{\ell_r} r \right) \qquad\qquad 5\ell$$

$$+ q^s_{LT} \frac{A_F}{2} y_F \left(C_{N_o}{}^s + \Delta C_{N_{\beta_{s_{LT}}}}{}^s \beta_{s_{LT}} + \Delta C_{N_{\beta_{v_{LT}}}}{}^s \beta_{v_{LT}} \right) \quad 6\ell$$

$$- q^s_{RT} \frac{A_F}{2} y_F \left(C_{N_o}{}^s + \Delta C_{N_{\beta_{s_{RT}}}}{}^s \beta_{s_{RT}} + \Delta C_{N_{\beta_{v_{RT}}}}{}^s \beta_{v_{RT}} \right) \quad 7\ell$$

$$+ \left(-134v - 2\dot{m}_{MF} \bar{y}^2_F p \right) \text{ (POF \#1)} \qquad\qquad 8\ell$$
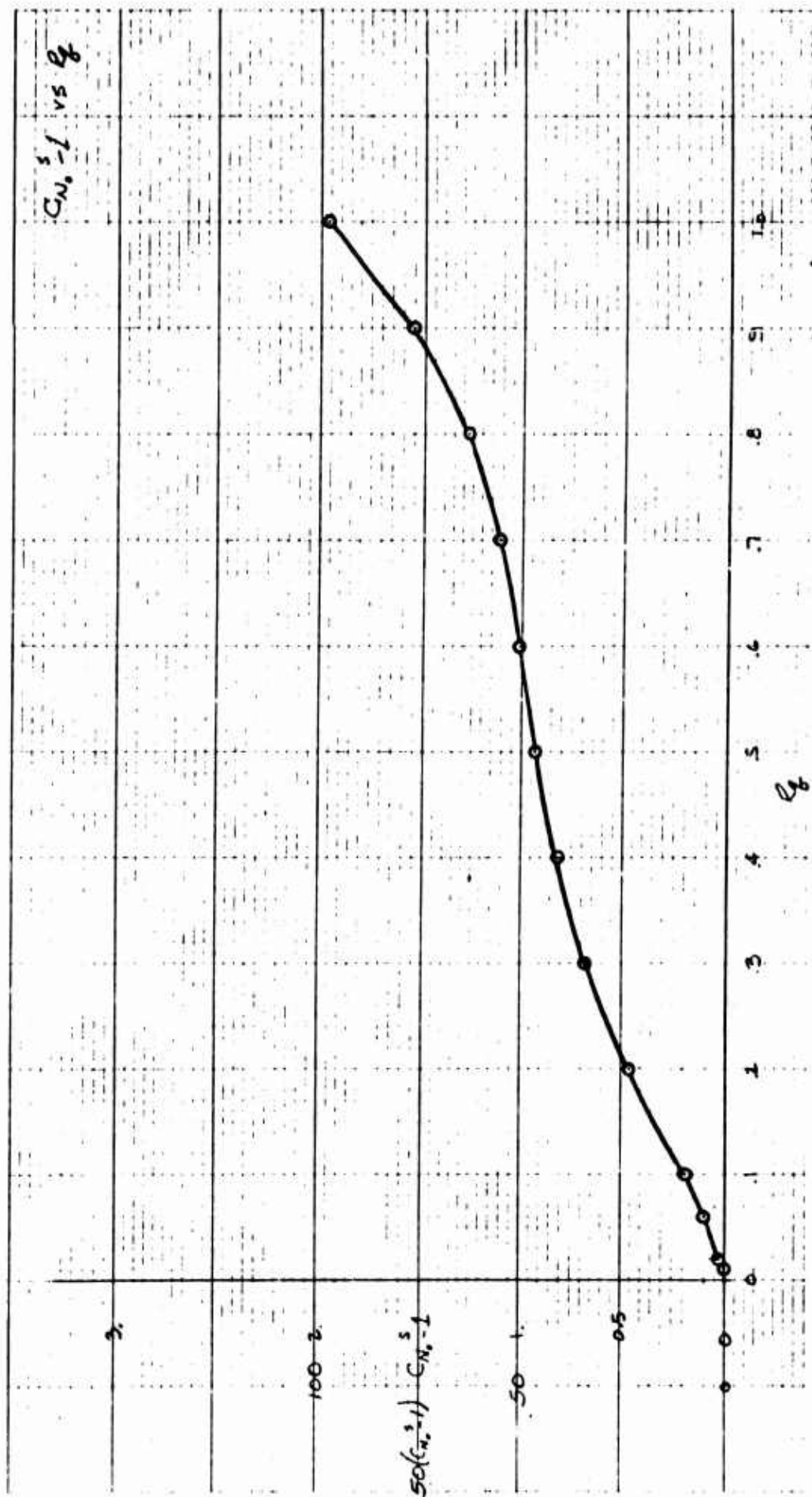
Figure 44 Basic Airframe Normal Force Coefficient Variation
With R_q, as Set Up on Diode Function Generator F68

2.2.2 Explanation of Generated Terms

The following is an explanation of the terms shown in the previous section, in terms of its function in the corresponding force or moment summation, and its modifications, if any, from the corresponding term presented for simulation by aerodynamics.

The terms POF #1 and POF #2 deserve special note. These terms are explained in the over-all explanation of the terms in which they first appear, 12N and 13N. Their use in subsequent terms is identical.

It should be further noted that the statement "used as presented" is only meant to signify no basic change has been made in the input information. The approximation of any piece of data by a constant value is a possibility covered in the section on function generation.

1N: This term is the power off normal force variation with angle of attack. It is based on fan area instead of wing area and is taken directly from Figure 21 of the presented aerodynamic coefficients.

2N: This term is the basic fan normal force coefficient for both fans at $\beta_s = \beta_v = 0$. It is phased toward 1.0 starting at a $T_c{}^s$ of .98 and ending at a $T_c{}^s$ of .99. It is held to 1.0 for $.99 \leq T_c{}^s \leq 1.0$. Variations in fan thrust due to velocity changes at higher $T_c{}^s$ values near hover are taken care of by low speed ram drag terms which are phased in at this time. This term is developed for both right and left fans by using the average value of $T_c{}^s$, or $\left(T_{c_{RT}}{}^s + T_{c_{LT}}{}^s \right) \div 2$ as the independent variable. However, the normal force is calculated individually for both the right and left fans by using separately calculated values of $q^s{}_{RT}$ and $q^s{}_{LT}$. The basic information is taken from Figure 1 of the presented aerodynamic coefficients, modified as called out above and generated as presented in Figure 44.

3N: This term represents the changes in normal force due to deviations of the right fan exit louvers from their $\beta_v = \beta_s = 0$ positions. The first part of the term generates changes corresponding to stagger deflections and the second part generates changes corresponding to vector louver deflections. Both portions of the over-all term are generated as functions of the $T_c{}^s$ specifically computed for the right wing fan.

The term is retained after conversion at the $\beta_v = 50°$ value in order to sum with $C_{N_o}{}^s$ to give zero total contribution to lift from the fans after

conversion. This is merely an artifice used to simplify simulation of the conversion. Both $\Delta C_{N_{\beta_s}}{}^s$ and $\Delta C_{N_{\beta_v}}{}^s$ are taken directly from the presented aero coefficients. Refer to Figures 2 and 3, of the presented aerodynamic coefficients.

4N: This term represents the variations in normal force with angle of attack that are due to the right wing fan. This term is shut off when the fan doors close. The data for this term is presented in Figures 6, 8, and 21 of the input aerodynamic coefficients which shows $C_N{}^S$ varying with α, $T_c{}^s$, and β_v. To understand the conversion of the coefficients presented to the coefficients of this term, it is necessary to understand the method of converting a standard aerodynamic function to slipstream notation.

As defined in the list of symbols:

$$1. \quad q^s = \frac{T_{ooo} + \dfrac{\rho V_T^2}{2}}{A_F}$$

and

$$2. \quad T_c{}^s = \frac{\dfrac{T_{ooo}}{A_F}}{\dfrac{T_{ooo}}{A_F} + \dfrac{\rho V_T^2}{2}} = \frac{\dfrac{T_{ooo}}{A_F}}{q^s}$$

and

$$3. \quad R_q = 1 - T_c{}^s = \frac{q}{q + \dfrac{T_{ooo}}{A_F}} = \frac{q}{q^s}$$

where: $q = \dfrac{\rho}{2} V_T^2$

Now if there is a standard, constant aerodynamic function such as C_{N_α}, we may write:

$$N(\alpha) = C_{N_\alpha} \cdot \alpha \cdot \frac{\rho V_T^2}{2} S_w = q S_w C_{N_\alpha} \cdot \alpha$$

If we wish to put the coefficient into slipstream notation and base it on fan area we write:

$$N(\alpha) = C_{N_\alpha}{}^s \cdot \alpha \cdot q^s \cdot A_F$$

Since $N(\alpha)$ in either notation must be the same,

$$C_{N_\alpha}{}^s \cdot \alpha \cdot q^s \cdot A_F = C_{N_\alpha} \cdot \alpha \cdot q \ S_w$$

or

$$C_{N_\alpha}{}^s = \frac{C_{N_\alpha} \ q \ S_w}{q^s \ A_F} = C_{N_\alpha} \left(\frac{S_w}{A_F}\right) \frac{q}{q^s}$$

$$= C_{N_\alpha} \left(\frac{S_w}{A_F}\right) \left(1 - T_c{}^s\right)$$

It is seen that a constant conventional aerodynamic coefficient slope transforms into a family of slopes when based upon slipstream notation.

With this in mind we may now operate on the curves of Figures 6 and 8 of Paragraph 2.1.2 using the curve of Figure 21 of Paragraph 2.1.2 as a basis.

Figure 21 was ratioed to the various $T_c{}^s$ values and then two new families of curves were determined by subtracting the ratioed Figure 21 values from Figures 6 and 8.

The slopes of $\beta_V = 0$ and $\alpha = 10°$, and $\beta_V = 50°$ and $\alpha = 4°$ of the families thus derived are plotted in Figure 45.

It is noted that the $\beta_V = 0$ slopes are only plotted down to $T_c{}^s = .86$, while the $\beta_V = 50°$ slopes are plotted to $T_c{}^s = .54$. This is a sufficient range for both, since a $T_c{}^s$ of .99 is the minimum attainable $T_c{}^s$ at a $\beta_V = 0$ and at $\beta_V = 50°$, the minimum attainable $T_c{}^s$ in fan powered mode is about .5, which occurs as the fan doors close and all the fan thrust terms disappear.
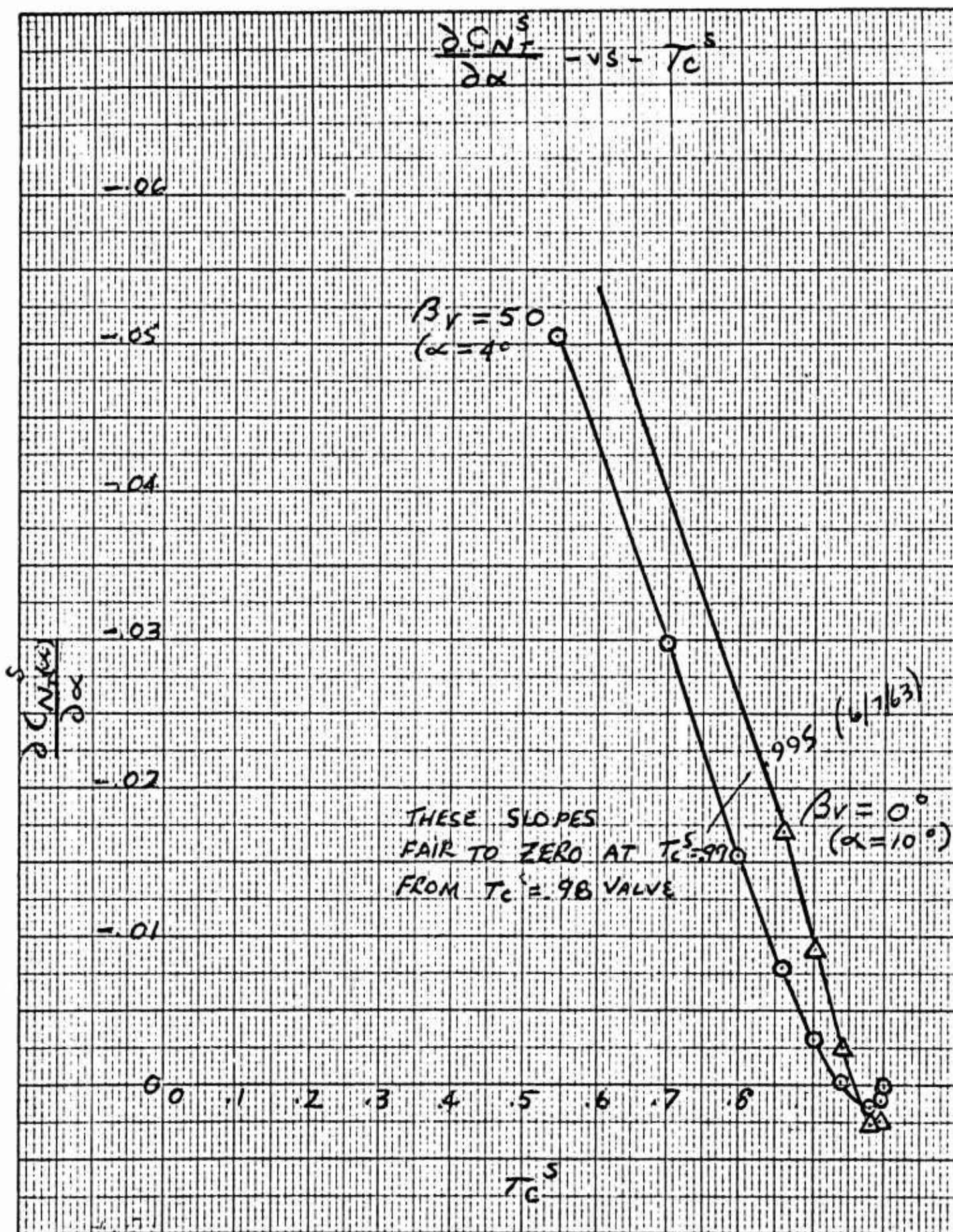
Figure 45   Variation of Normal Force Coefficient Slope with
Angle of Attack Due to Fan Thrust with T_c^s

The functions finally generated are the $\beta_V = 0$ slope, and the difference between the $\beta_V = 0$ slope and the $\beta_V = 50°$ slope. The difference is multiplied by $\beta_V/50$ which is then added to the $\beta_V = 0$ curve. This procedure in effect affords linear interpolations between the $\beta_V = 0$ and the $\beta_V = 50°$ data for $C_{N_\alpha}^S$ variations with T_C^S.

The functions as generated are given in Figure 46.

5N: This term corresponds to term 3N and is identical in all respects, except left wing parameters are used where shown.

6N: This term corresponds to term 4N and is identical in all respects, except left wing parameters are used where shown.

7N: This term represents the static lift contribution of the nose fan. The fan loading portion of the term is explained in the section on fan parameter generation.

The nose fan effectiveness portion of this term is a function of thrust reverser door position and is taken from the power curves as presented in Figure 39 of the presented aerodynamic functions.

8N: This term represents the variation of normal force with vertical velocity of the nose fan. It is computed on the basis of ram drag considerations (nominal nose fan mass flow is 4.38 slugs/sec.).

This term has no replacement term at higher transition speeds and therefore remains in the summation from hover to conversion.

9N: This term represents the normal force due to pitch rate and the rate of variation of the angle of attack. For this study, both portions of the term were approximated as constants and pitch rate was assumed equal to rate of variation of angle of attack.

The coefficients as approximated are shown in Figures 13 and 15 of the presented aerodynamic coefficients.

10N: This term represents the normal force generated by the horizontal tail. Its generation is based on the following auxiliary equations
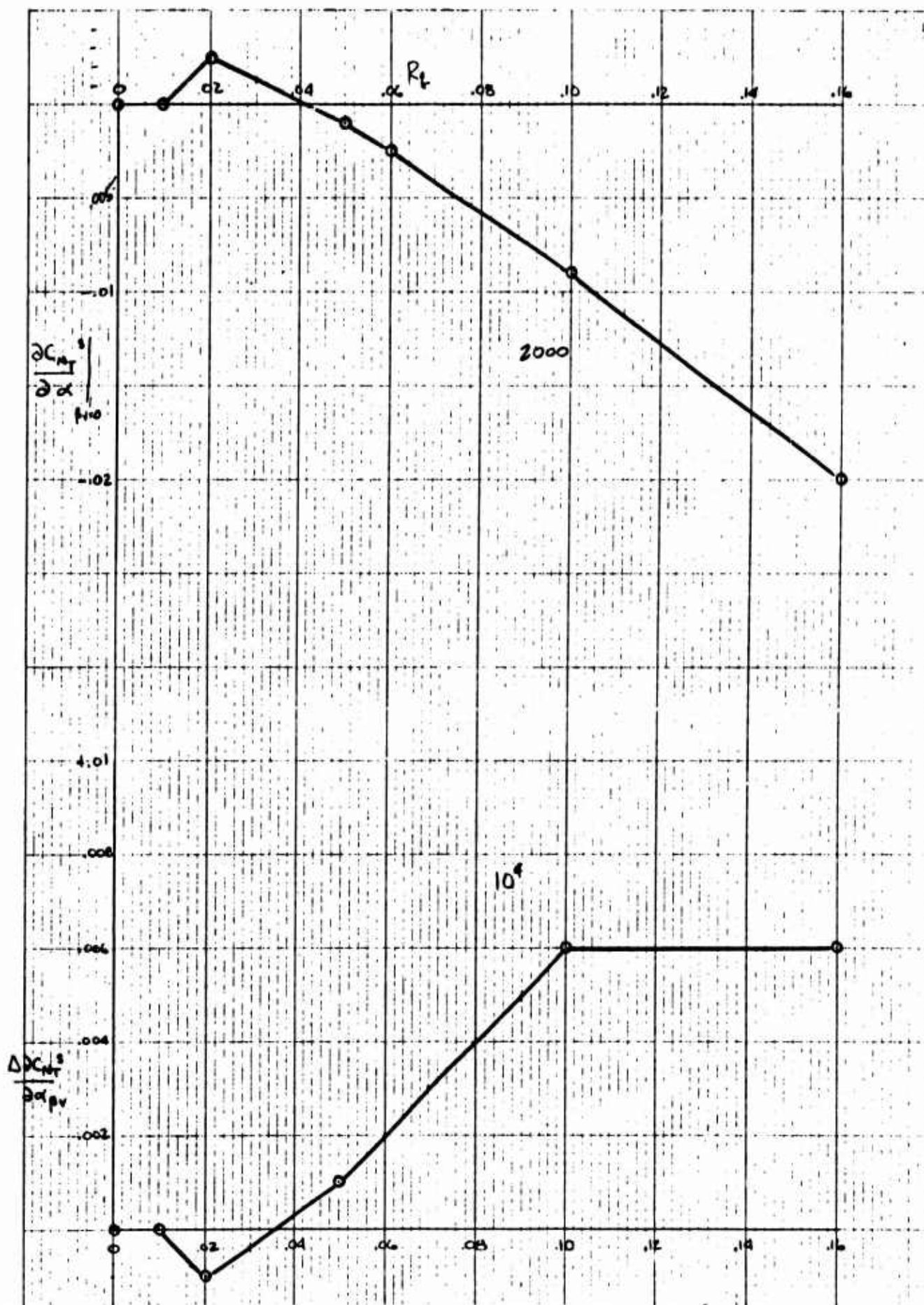
Figure 46 Final Configuration of Functions Used to Generate the Curve Family of
Figure 45. The upper curve is given the title "CNTSA," and the lower
curve is given the title "CNTSAB" in the simulation.

$$C_{N_t} = \left(C_{L_t} - C_{D_t} \sin \epsilon\right) \frac{S_t}{S_w} \left(\cos \alpha_{LIM}\right)$$

$$+ \left(C_{D_t} + C_{L_t} \sin \epsilon\right) \frac{S_t}{S_w} \left(\sin \alpha_{LIM}\right)$$

where:

$$C_{D_t} = C_{D_{o_t}} + K_i \left(C_{L_t}\right)^2$$

$$C_{L_t} = C_{L_{\alpha_t}} (\alpha + i_t - \epsilon) + C_{L_{\delta_e}} \cdot \delta_e$$

Generation of the term from these equations uses coefficients as presented in the tabulated data.

Downwash angle, ϵ, is generated as a function of average R_q and is valid for vehicle angles of attack of 20 degrees or less.

The downwash angle of this term is generated as presented in Figure 11 of the presented aerodynamic coefficients.

At low speeds, near hover, the angle of attack of the tail can be ±90°. In this simulation, the maximum angle of attack used in calculation C_{L_t} is 20°, and this value can cause the tail C_L to overload. This can only occur at very low velocities, and the effect of high C_{L_t} at these velocities is negligible.

11N: This term represents the normal force due to thrust developed by the gas generator in conventional flight mode.

T_j is the thrust of the gas generator and is taken directly from the power information presented in Figure 42 of Paragraph 2.1.4.

K_{TS} represents the spoiling factor of the thrust and was assumed to be a linear function of thrust spoiler position, as shown in Figure 43 of Paragraph 2.1.4.
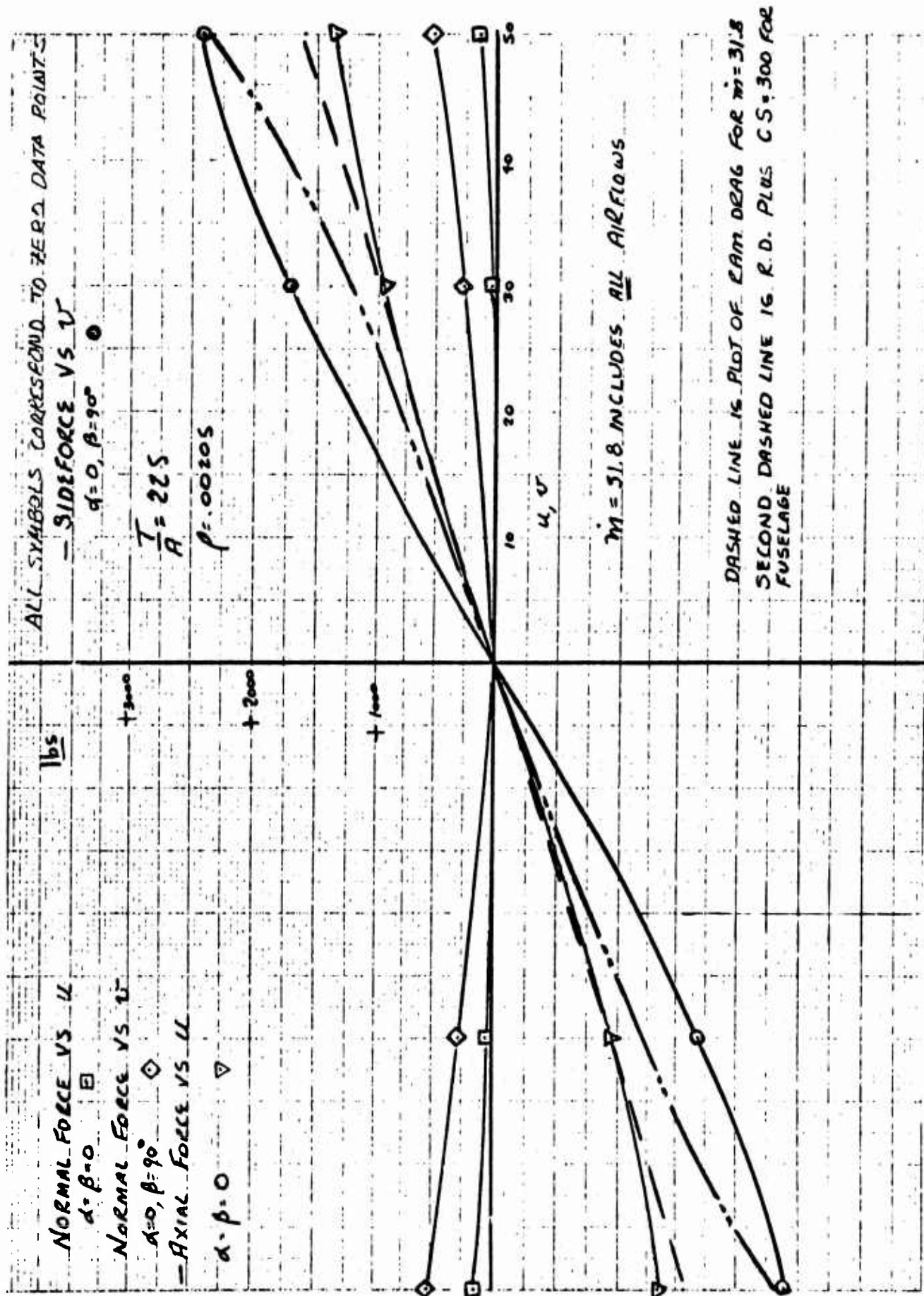
Figure 47 Plot of Low Speed Force vs Velocity for Velocity in the
Vehicle X-Y Plane
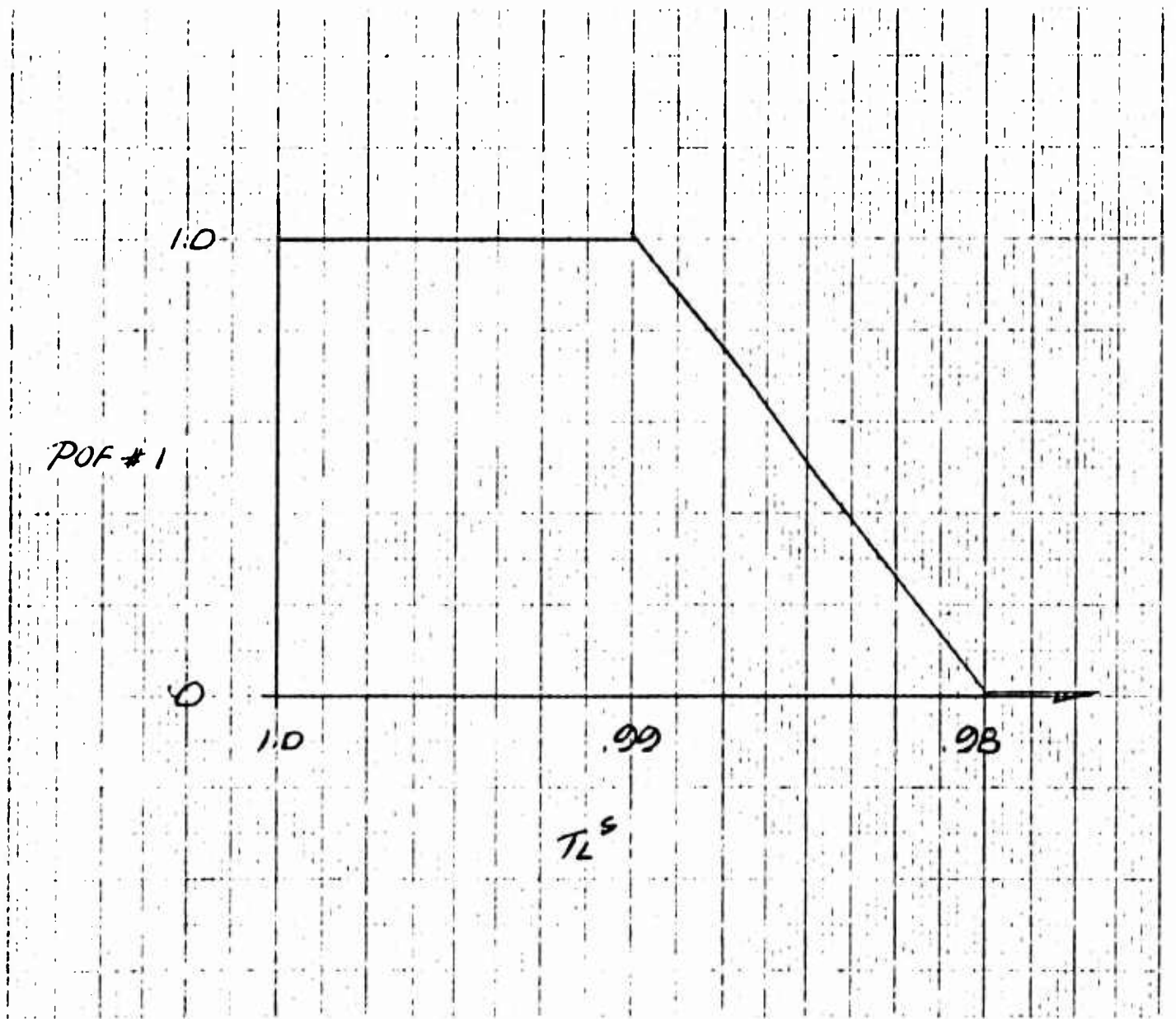
Figure 48 Phase Out Function No. 1

12N: This term is the low speed normal force variation due to u and v. This term was derived from Figure 47 which is a replot of Figures 10 and 26 of Paragraph 2.1.2 at their 90° points, plotted versus velocity instead of T_c^S, at a fan disc loading corresponding to 9200 lbs. total lift.

POF #1 is used in the generation of this term for the purpose of phasing it out for replacement by its corresponding high speed terms. Its use in subsequent terms is identical.

POF #1 is shown in Figure 48. It has a value of 1 from $T_c^S = 1.0$ to .99 and linearly decreases to zero from $T_c^S = .99$ to $T_c^S = .98$. At T_c^S values below .98, POF #1 remains at zero.

13N: This term represents variations in normal force with angle of attack near hover. It was derived from Figure 10 of the presented aerodynamic coefficients.

Since α near hover can vary from 0 to 360°, the information as presented was replotted versus sin α, w/V_T, as shown in Figure 49.

The information of Figure 49 in turn is approximated as shown for generation. Small errors must be accepted as a consequence of this approximation but not at the critical points of ±90°.

POF #2 is used in the function for two purposes. Reference to Figure 50 showing POF #2 shows that as T_c^S progresses from T_c^S's below .98 to $T_c^S = .98$, POF #2 is zero. For T_c^S's from .98 to .99; POF #2 progresses from 0 to 1 linearly, and from $T_c^S = .99$ to $T_c^S = 1.00$, POF #2 goes to zero. The purpose of POF #2 from $T_c^S = .98$ to $T_c^S = .99$ is to phase in this term; from $T_c^S = .99$ to $T_c^S = 1.00$, POF #2 scales the term as shown in the input aero functions for various T_c^S's. The use of POF #2 in all other instances is identical to its use here.

1X: This term is the high speed, power off, variation of drag with angle of attack. At low speeds its function is taken over by term 10X.

This term is based on fan area rather than wing area and is taken directly from the presented aerodynamic coefficients. (Refer to Figure 22.)

2X: This term represents the basic fan drag for both fans at $\beta_s = \beta_v = 0$. It is phased to zero starting at $T_c^S = .98$ and ending at $T_c^S = .98$, and replaced near hover by the corresponding ram drag term (10X).
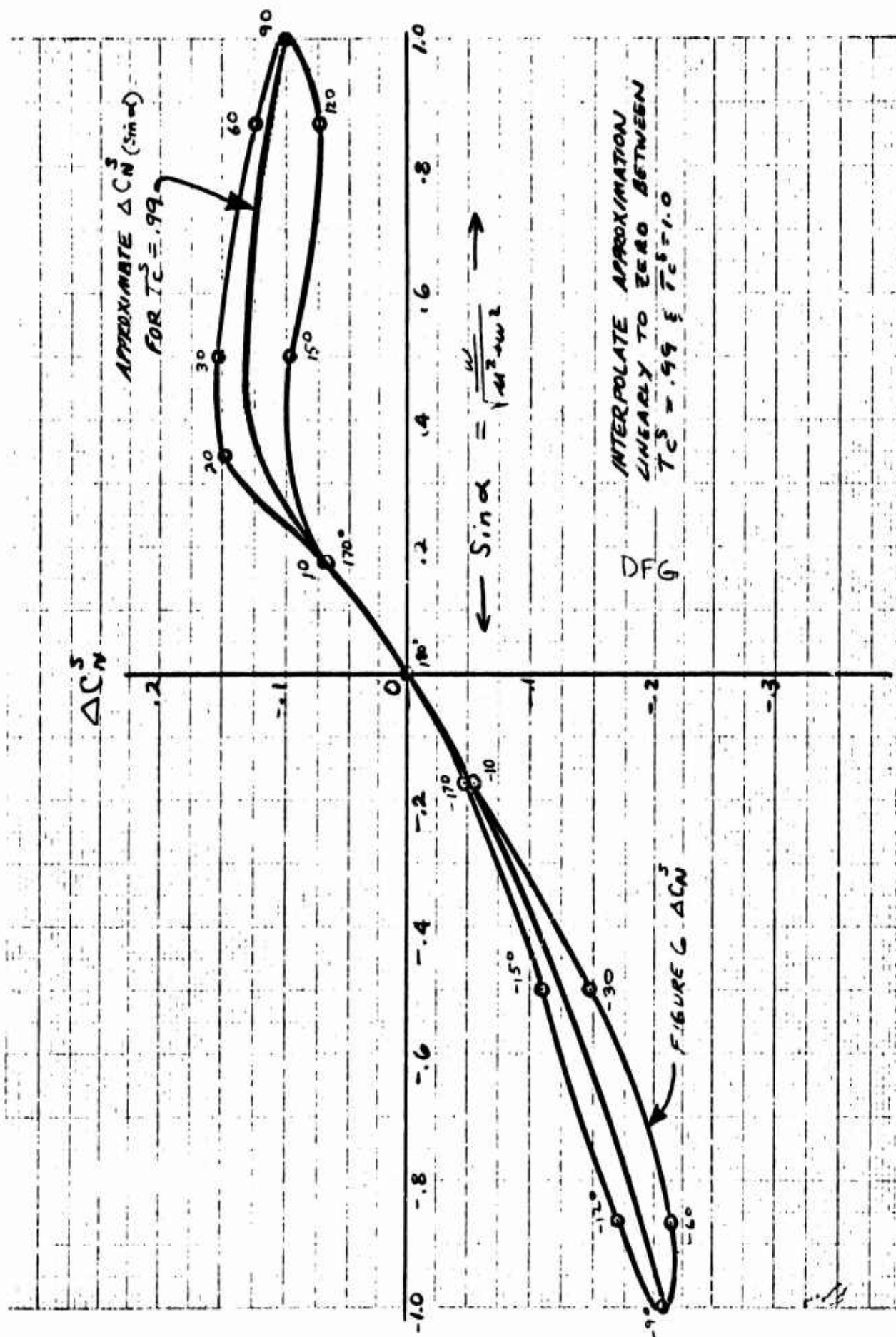
Figure 49 Curve of Figure 10 Plotted vs sin α, as Well as
Approximation Used to Fit the Data as Set Up on Diode
Function Generator F65
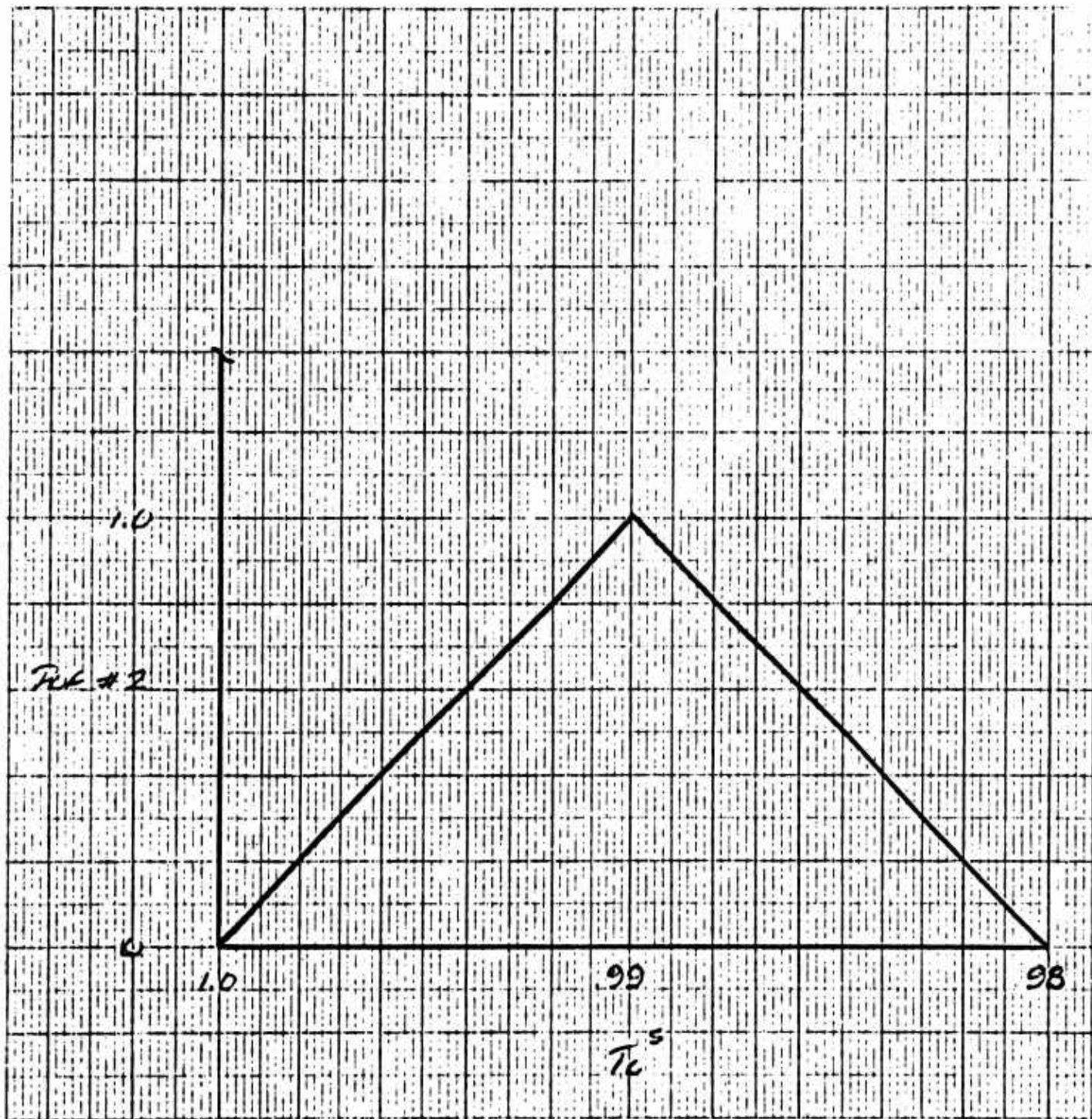
Figure 50 Phase Out Function No. 2

This term is handled in the same manner as Term 2N. An average value of $T_c{}^S$ is used as the independent variable in the generation of $C_{X_0}{}^S$, but the individual q^S values are used in generating the right and left axial force contributions of this term.

The coefficient of this term is taken from the aerodynamic coefficients as presented. (Refer to Figure 1.)

3X: This term represents the variations in axial force due to variations in the right fan exit louver positions from the positions corresponding to $\beta_V = \beta_S = 0$.

The first portion of the term accounts for variations due to stagger louver changes and the second position corresponds to variations due to vector louver changes.

Both $\Delta C_{X_{\beta_V}}{}^S$ and $\Delta C_{X_{\beta_S}}{}^S$ are generated as functions of the specific $T_c{}^S$ corresponding to the right wing.

This term is not shut off when the doors close. It sums with $C_{X_0}{}^S$ at $\beta_V = 50°$ (when the doors close) to provide the correct total $C_X{}^S$ after conversion.

The coefficients of this term are taken directly from Figures 2 and 3 of the presented aerodynamic coefficients.

4X: This term represents the variations in axial force with angle of attack that are due to the right wing fan. This term is shut off when the fan doors close.

The basic data for this term is presented in Figures 5, 7 and 22 of the input aerodynamic coefficients which show $C_X{}^S$ varying with α, $T_c{}^S$ and β_V.

This data is reduced for use from the presented form in the same manner as the data for term 4N.

The final result of the reduction is shown in Figure 51, and the functions finally generated are the $\beta_V = 0$ slope and the difference between the $\beta_V = 0$ and the $\beta_V = 50°$ slope, which are shown in Figure 52.
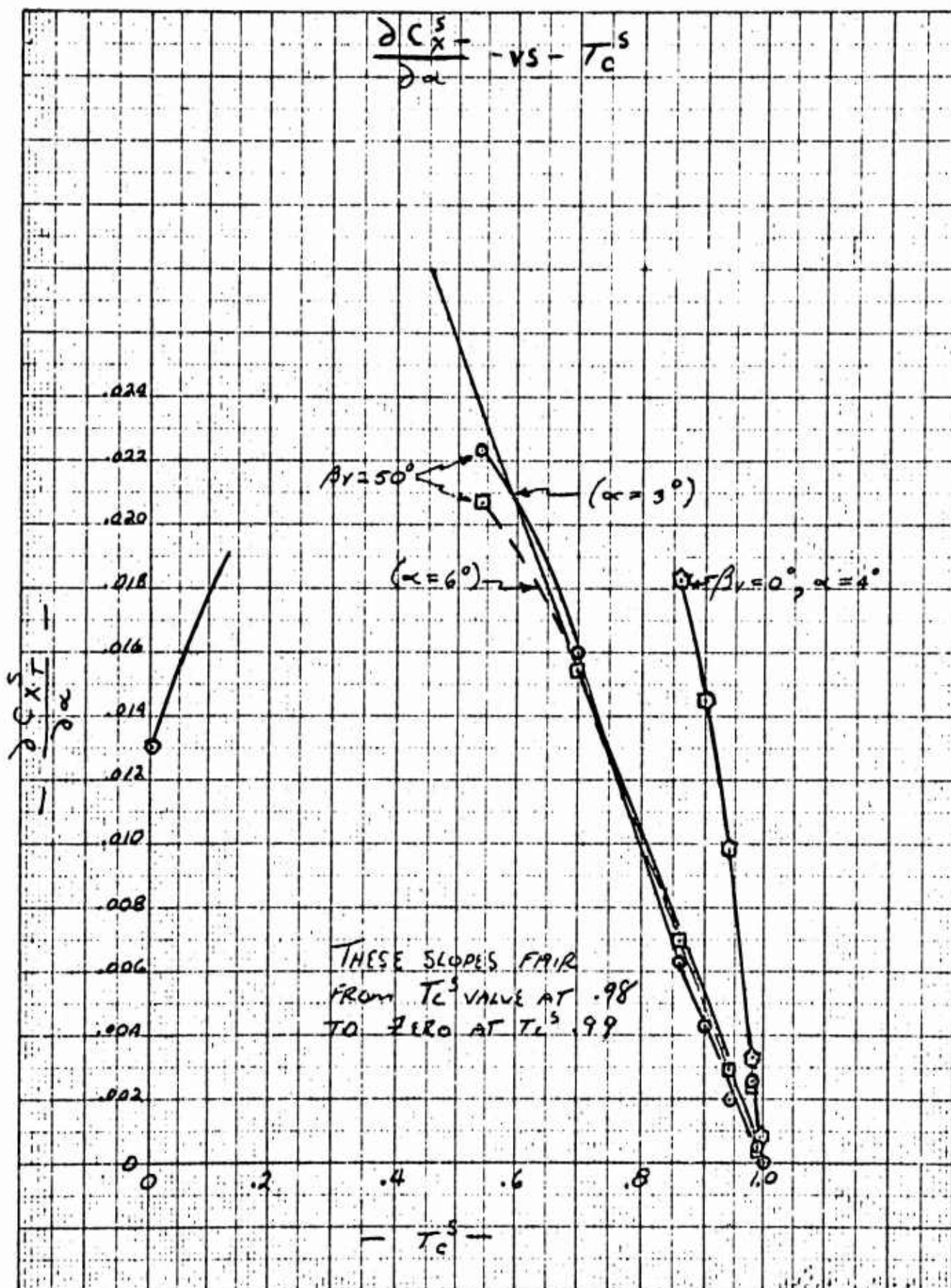
Figure 51 Variation of Axial Force Coefficient Slope with
Angle of Attack Due to Fan Thrust with T_c^s
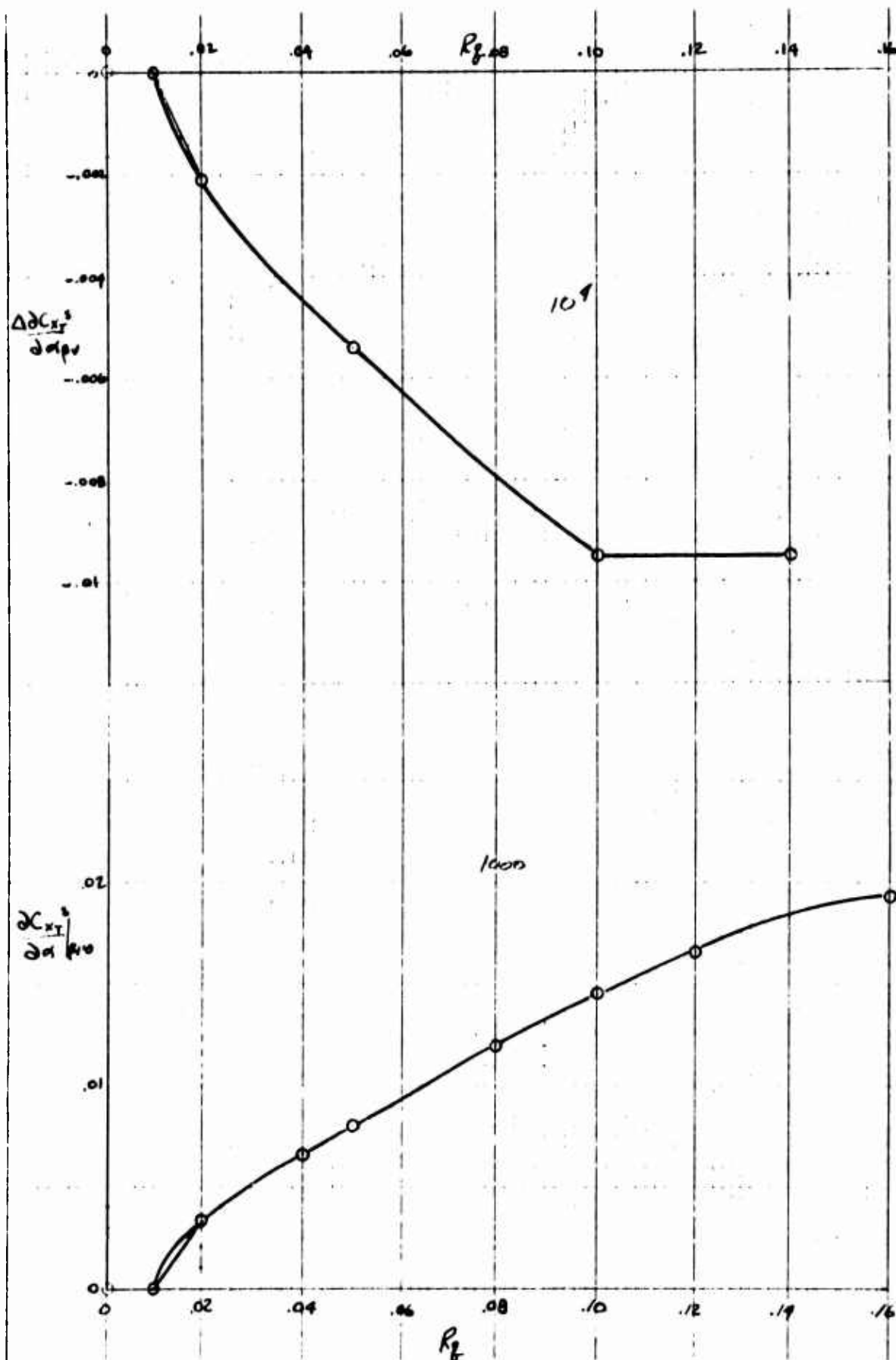
Figure 52 Final Configuration of Functions Used to Generate the
Curve Family of Figure 51. The upper curve is given
the title "CXTSA," and the lower curve is given the
title "CXTSAB."

5X: This term corresponds to the right wing term 3X. Its use and generation are identical except that all functions of $T_c{}^8$ are generated for the $T_c{}^8$ corresponding to the left wing.

6X: This term corresponds to the right wing term 4X. Its use and generation are identical except that all functions of $T_c{}^8$ are generated for $T_c{}^8$ corresponding to the left wing.

7X: This term represents the axial force due to tail drag. It is generated directly from the information presented in the tabulated aerodynamics in accordance with the following equations:

$$C_{X_t} = \left(C_{D_t} + C_{L_t} \sin \epsilon \right) \frac{S_t}{S_w} \cos \alpha_{LIM}$$

$$+ \left(C_{L_t} - C_{D_t} \sin \epsilon \right) \frac{S_t}{S_w} \sin \alpha_{LIM}$$

where:

$$C_{L_t} = C_{L_{\alpha_t}} (\alpha + i_t - \epsilon) + C_{L_{t \delta e}} \cdot \delta e$$

and

$$C_{D_t} = C_{D_{o_t}} + K_i C_{L_t}{}^2$$

Downwash angle, ϵ, is generated as a function of average R_q and is valid for angles of attack of 20 degrees of less.

8X: This term represents the gas generator thrust contribution to axial force. It is composed of two parts, T_j (refer to Figure 42 of the fan and engine input coefficients) which is the basic thrust of the engines as a function of N_g, and K_{TS} (refer to Figure 43 of the fan and engine input coefficients) the spoiler effectiveness, which is a function of spoiler position.

9X: This term represents the contribution to axial force by the nose fan.

It is based on ram drag considerations and is turned off after conversion when the nose fan inlet louvers close.

10X: This term represents the low speed variation of axial force with axial velocity due to the fans. This term was derived from the presented aerodynamic coefficients $C_{X_0}{}^S$ in Figure 1 near hover.

There is an error in the $C_{X_0}{}^S$ curve presented in Figure 1. $C_{X_0}{}^S$, as presented, is for $\beta_V = \beta_S = 0$. However, due to the camber of the exit louvers, a forward thrust exists at a louver tangent line angle of zero degrees, which amounts to about 4° turning of the fan thrust, which in turn results in a $C_{X_0}{}^S$ at $T_c{}^S = 1$ of about -.04. If the axial force resulting from $C_{X_0}{}^S$ near hover as presented in Figure 1 is plotted versus $T_c{}^S$ using the offset at $\beta_V = 0$, the axial force variation from the zero velocity point is almost exactly equal to the theoretical value of ram drag using momentum considerations.

Figure 53 shows the comparison of the actual and theoretical values using the offset at $\beta_V = 0$.

The two parts of term 10X then, are respectively, the thrust due to camber at zero velocity, and the momentum drag.

Multiplication of this term by POF #1 effects the replacement of this term at higher velocities by term 2X, which itself is phased to zero near hover in the process of its generation.

1 M : This term represents the variation in pitching moment with velocity. It is phased to zero near hover in the process of its generation, for replacement at low speeds by term 10 M explained below. It is taken from Figure 1 of the presented aerodynamic coefficients.

2 M : This term represents the variation in pitching moment with angle of attack. The term is phased to zero near hover in the process of its generation for replacement by term 11 M explained below.

Since the angle of attack cannot become large at the velocities where this term is in effect, the particular angle of attack used in this term is limited to ±20° for purposes of generation of the over-all term.
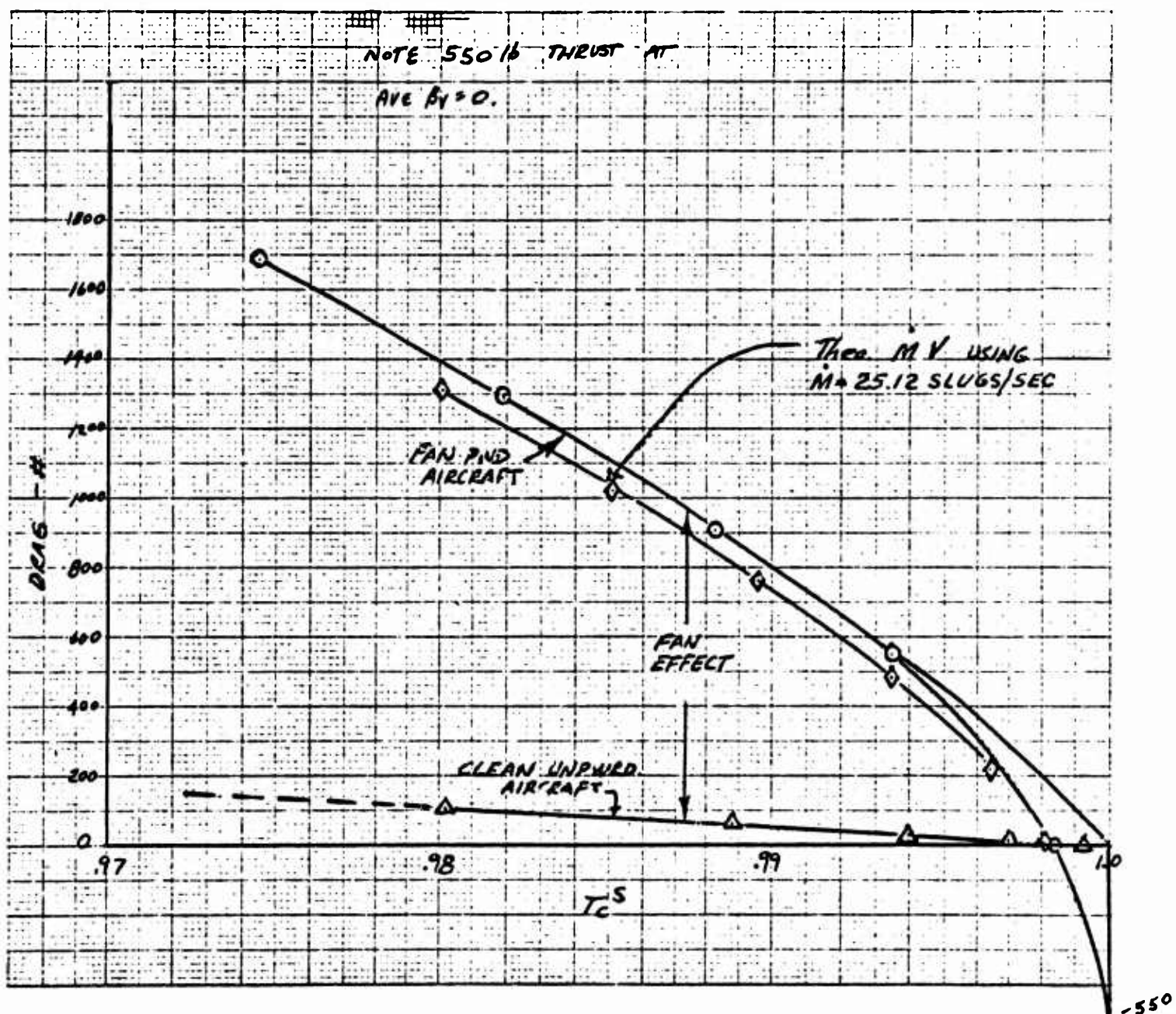
Figure 53 Drag at $\beta_v = 0, \alpha = 0$ versus T_c^s

The coefficient of the term is taken from Figure 9 of the presented aerodynamic coefficients.

$3\mathcal{M}$: This term represents the variation in pitching moment due to variations in the right fan exit louver positions.

The first portion of the term represents the variations due to louver stagger deflections, and the second, variations due to louver vector deflections.

Both $C_{m_{\beta_s}}$ and $C_{m_{\beta_v}}^{s}$ are generated as functions of the specific T_c^{s} generated for the right wing fan.

This term is not shut off when the doors close. It sums with $C_{m_o}^{s}$ at $\beta_v = 50°$ (when the doors close) to provide the correct total C_m^{s} after conversion.

The term coefficients are taken from Figures 2 and 4 of the presented aerodynamic coefficients.

$4\mathcal{M}$: This term is the left wing term corresponding to the right wing term $3\mathcal{M}$. Its use and generation are identical except that all functions of T_c^{s} are generated for the T_c^{s} corresponding to the left wing.

$5\mathcal{M}$: This term represents the variation in pitching moment with sideslip. Since it does not change sign with the sign of sideslip angle, the absolute value of sideslip angle is used to generate the term.

The sideslip angle used is limited to 20 degrees as no larger sideslip angles can be reached at velocity values large enough to make the term significant.

The coefficient $\dfrac{\partial C_m}{\partial |\beta|}$ is approximated as a constant as shown in Figure 17 of the presented aerodynamic coefficients.

$6\mathcal{M}$: This term represents the variation in pitching moment with variations in tail lift and drag.

The individual portions of the term are taken as generated for the axial and normal force summations, multiplied by the appropriate moment arm, and summed.

Refer to term explanations 10N and 7X for details.

7M: This term represents the pitching moment due to pitch rate and angle of attack rate of change.

For purposes of generation the coefficients required (presented aero coefficients, Figures 14 and 16) have been approximated as constants. Further, rate of change of angle of attack is assumed equal to pitch rate.

8M: This term represents the contributions to pitching moment of the nose fan.

The term is generated by multiplying the normal force of the nose fan as generated for the normal force summation by the appropriate moment arm.

For details refer to the explanation of term 7N.

9M: This term represents the variation in pitching moment of the nose fan with vertical velocity.

It was developed from ram drag considerations and is present throughout the transition velocity range. It is switched off after conversion when the doors close.

10M: This term represents the variation with forward velocity of pitching moment near hover.

Plotting pitching moment variation with velocity (refer to Figure 54) shows that the low speed pitching moment variation with velocity can be generated as a linear function of velocity and phased out by POF #1 at velocities about 50 feet per second.

For details on POF #1, see the term explanation 12N.

Note that the magnitude of the pitching moment variation with u is equal to the magnitude of the rolling moment variation with v. Using this fact as a basis, it was assumed that both moment variations with velocity were due to center of pressure shifts in the direction of the relative wind. This was the key to resolution of the low speed problem, where combinations of forward and side velocities occur.

11$\mathcal{M}$: This term represents the variation of pitching moment with angle of attack near hover. The term is phased in and out by POF #2. This term is equivalent to the moment coefficient data of Figure 10. The data of Figure 10 was plotted versus sin $(\alpha - 50°)$, and a correction factor, the "modified new function", MNF, was used to care of the hump in the curve of Figure 10 between $0°$ and $40°$ angle of attack. The resulting fit is accurate to within $\pm .04$ pitching moment coefficient over the entire angle of attack range.
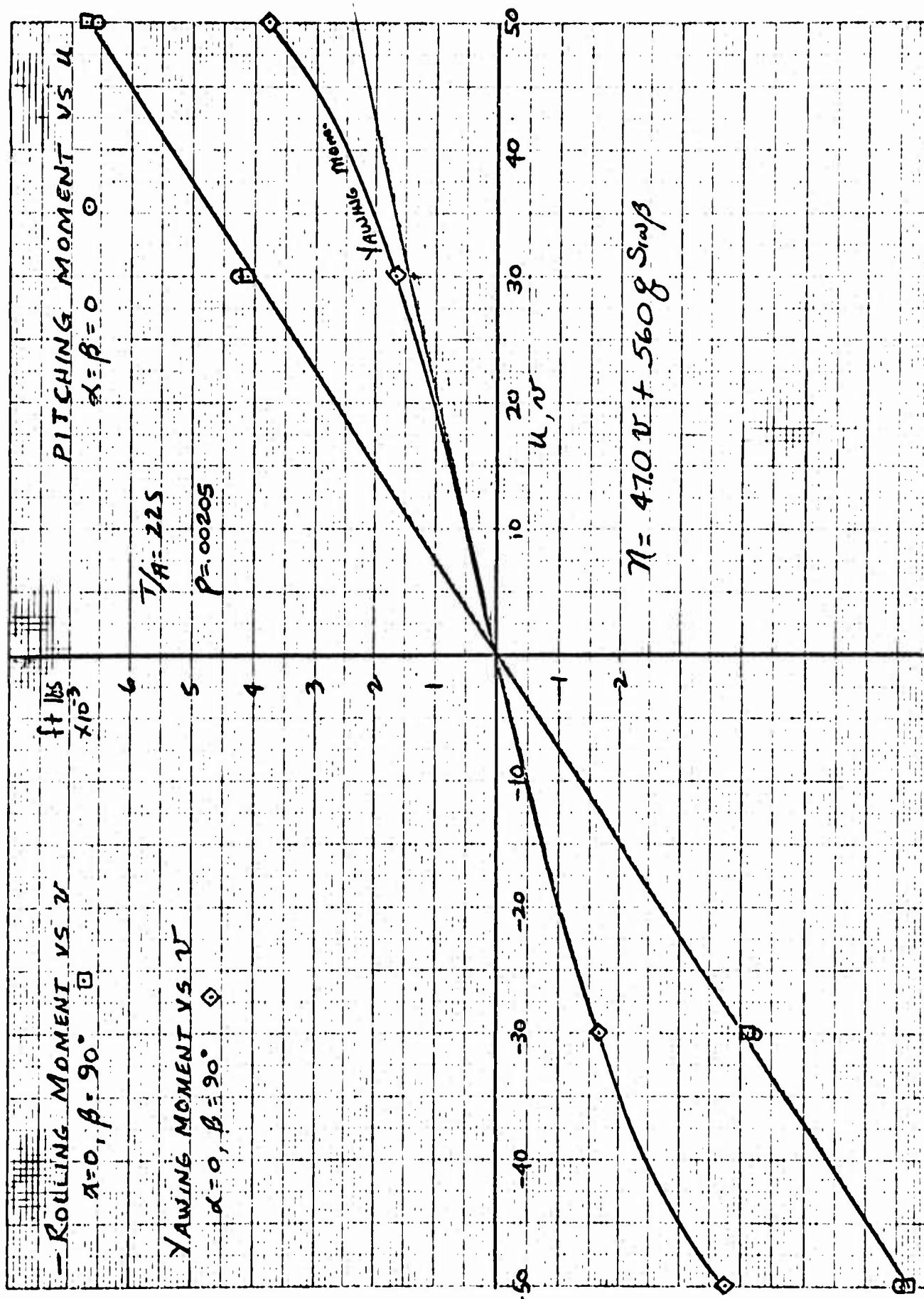
Figure 54 Variation of Rolling, Pitching and Yawing Moment vs
Velocity for Velocity in the Vehicle X-Y Plane

75

1Y: This term represents the side force due to sideslip at velocities above 50 feet per second. It is phased to zero near hover in the process of its generation for replacement by the corresponding low speed term 6Y.

The coefficient C_{Y_β} is used directly as presented and is generated as a function of average R_q.

The sideslip angle used in the generation of the term is limited to ± 20 degrees for convenience in generation. At velocities large enough to make the term significant, sideslip angles larger than 20 degrees are not attainable.

2Y: This term represents the contribution to sideforce of the ailerons.

The coefficient $C_{Y_{\delta_a}}$ is used as presented in the tabulated aerodynamic coefficients.

3Y: This term represents the contribution to side force of the rudder.

The coefficient $C_{Y_{\delta_r}}$ is used as presented in the tabulated aerodynamic coefficients.

4Y: This term represents the variation in side force due to yaw rate at velocities above 50 feet per second.

It is effectively phased to zero near hover by its diminishing velocity multiplier for replacement by the second portion of term 6Y.

The coefficient C_{Y_r} is approximated as a constant for use in generation. Refer to Figure 29 of the presented aero coefficients.

5Y: This term represents the total low speed aerodynamic and fan contribution to side force. It consists of three parts.

Part one is the variation with side velocity of the side force. This part of term 5Y was derived from Figure 47 showing side force plotted versus velocity corresponding closely to momentum theory.

Part two is the ram drag computed value of side force due to side velocity of the nose fan.

Part three is a conventional aerodynamic contribution to side force based on the profile flat plate area of the fuselage.

The entire term is phased in near hover by POF #1.

For detail on POF #1 refer to the explanation of term 12N.

1N: This term represents the variation in yawing moment with side velocity.

The coefficient $C_{n_\beta}^s$ is generated as a function of average R_q and phased to zero in the process of its generation for replacement by the corresponding part of term 9N which is based on ram drag considerations.

At velocities where this term becomes significant, sideslip angles larger than 20 degrees cannot be attained, so β is limited to 20 degrees for use in the generation of this term.

2N: This term represents the variation in yawing moment due to aileron deflection.

The coefficient of this term $C_{n_{\delta_a}}$ is used directly as presented in the tabulated aerodynamics.

3N: This term represents the variation in yawing moment with rudder deflection.

The coefficient of this term $C_{n_{\delta_r}}$ is presented in the tabulated aerodynamics as a constant plus a linear variation with T_c^s. This linear variation with T_c^s is neglected for use in generation of the term.

4N: This term represents the variation in yawing moment due to yaw rate.

The coefficient of this term C_{n_r} (refer to Figure 32 of the presented aerodynamic coefficients) is approximated as a constant for ease of generation.

5N: This term represents the variation in yawing moment due to roll rate.

The coefficient of this term C_{n_p} (refer to Figure 33 of the presented aerodynamic coefficients) is approximated as a straight line for ease of generation.

$6N/7N$: The difference of these terms represents the yawing moment due to differences in the axial forces developed by the right and left fans.

The axial force terms developed for the axial force summation are used as generated.

$9N$: This term represents the variations in yawing moment near hover due to aerodynamic and fan effects. It is made up of three parts.

Part One: This part is the yawing moment due to side velocity of the nose fan. It is derived from ram drag considerations.

Part Two: This part is due to the aerodynamic yawing moment developed by the fuselage in sideslip. It is based on the flat plate area of the fuselage profile and the estimated displacement distance of the profile center of pressure from the cg of the aircraft.

Part Three: This part represents the yawing moment which arises from yaw rates of the main fans. It is based on ram drag considerations.

The term is phased in near hover by POF #1. For further details on POF #1 refer to the explanation of term 12N.

1ℓ: This term represents the rolling moment variation with sideslip.

The coefficient of the term $C_{\ell_\beta}{}^S$ (refer to Figure 25 of the presented aerodynamic coefficients) is broken into two parts each of which is generated as a function of average R_q.

The first part is the variation of $C_{\ell_\beta}{}^S$ with R_q at a constant angle of attack of zero, while the second is the variation of $C_{\ell_\beta}{}^S$ with angle of attack, also generated as a function of R_q.

At velocities high enough to make this term significant, sideslip angle cannot exceed 20 degrees, so β in this term is limited to values of 20 degrees or less for generation of this term.

2ℓ: This term represents the rolling moment due to aileron deflection.

The coefficient of the term $C_{\ell_{\delta_a}}$ is taken directly from the tabulated aerodynamic coefficients.

3ℓ: This term represents the rolling moment due to rudder deflections.

The coefficient of this term is taken directly from the tabulated aerodynamics.

4ℓ: This term represents the rolling moment due to roll rate.

The coefficient of the term C_{ℓ_p} (see Figure 30 of the presented aerodynamic coefficients) is approximated as a constant for use in generation.

5ℓ: This term represents the rolling moment due to yaw rate.

The coefficient of the term C_{ℓ_r} (refer to Figure 31 of the presented aerodynamic coefficients), is approximated as a constant for use in generation.

$6\ell/7\ell$: The difference of these two terms represents the rolling moment due to differences in the normal force developed by each fan.

The terms are used as generated for the normal force summation.

8ℓ: This term represents the rolling moment due to low speed aero-dynamic effects of the fans. It consists of two parts.

Part One: This part represents the rolling moment due to sideslip. It is generated on the basis of ram drag considerations (see explanation of term 10M).

Part Two: The part represents the rolling moment due to roll rate of the main fans. It is generated strictly on the basis of ram drag considerations.

POF #1 is used to phase in this term near hover. For details on POF #1, see the explanation of term 12N.

2.2.3 Fan Equations

Main Fan Equation

$$\frac{T_{ooo}}{A_F} = (P_F)^{2/3} \times \frac{\rho^{1/3}}{A_F^{2/3}} \times \qquad\qquad \underline{1F}$$

$$\left(\cfrac{1}{\cfrac{C_{p}^{s}}{C_{p_o}^{s}} + \cfrac{\Delta C_{p_{\beta}}^{s}{}_{s}}{C_{p_o}^{s}}} \right)^{2/3}$$

$$\underline{2F} \qquad\qquad \underline{3F}$$

Nose Fan Equation

$$\frac{T_o}{A_{NF}} = (P_{NF})^{2/3} \times \left(\frac{\rho^{1/3}}{A_{NF}^{2/3}} \right) \times \qquad\qquad \underline{1NF}$$

$$\left(\frac{C_{p_{o}}^{s}{}_{NF}}{C_{p}^{s}{}_{NF}} \right)^{2/3} \qquad\qquad \underline{2NF}$$

2.2.4 Generation of Aerodynamic and Fan Parameters

Fan Parameters

All forces and moments developed by the aircraft, that are strongly influenced by the fans, are non-dimensionalized with respect to $T_c{}^s$ which is defined as:

$$T_c{}^s = \frac{T_{ooo}/A_F}{q^s}$$

where

$$q^s = \frac{\rho V_T{}^2}{2} + T_{ooo}/A_F \qquad \text{and}$$

T_{ooo} is the value of the fan thrust, if β_s, β_v and velocity were all suddenly reduced to zero. T_{ooo} is strictly a function of fan rpm and air density.

For use in generation, all coefficients that were non-dimensionalized with respect to $T_c{}^s$ as presented, are generated as functions of R_q which is defined as

$$R_q = 1 - T_c{}^s = \frac{\dfrac{\rho V_T{}^2}{2}}{q^s} = \frac{q}{q^s} \quad , \quad \text{the ratio of free-stream to slipstream q.}$$

The generation of R_q and correspondingly T_{ooo}/A_F involves the implicit solution of the following equation which relates T_{ooo}/A_F to its control parameters.

$$\frac{C_p{}^s}{C_{p_o}{}^s} = \frac{\left(P_F \rho^{1/2}\right)}{\left(T_{ooo}/A_F\right)^{2/3} A_F}$$

where

$$\frac{C_p^{\,s}}{C_{p_o}^{\,s}} = f\,(T_c^{\,s},\ \beta_v,\ \beta_s) \text{ and is the power coefficient ratio.}$$

$$P_F = f\,(N_g) \text{ and is the fan power.}$$

Generation of R_q, q^s and T_o/A_{NF} for the nose fan is carried out in the same way as for the main fans except the corresponding nose fan parameters are used. In this case, T_o is the thrust that would be generated by the nose fan at zero velocity.

Signals taken from various points within the closed loops performing the implicit solutions for T_{ooo}/A_F and T_o/A_{NF} provide all the required fan and combined fan and aerodynamic parameters.

Explanation of Terms

The terms required in the generation of the fan equations are explained below:

1F

The coefficient of this term P_F is the fan power. It is a direction function of gas generator rpm and an indirect function of atmospheric conditions, altitude and temperature (density).

This curve was generated as presented and then shifted up or down by an increment in fan power to represent changes in estimated gas generator characteristics. (Refer to Figure 34 of the fan and engine coefficients.)

2F

This term is the fan power coefficient ratio at zero louver stagger. It represents changes in T_{ooo}/A_F due to vector angle and velocity.

(Figure 35 of the fan and engine characteristics.)

3F

This term is the change in fan power coefficient ratio with stagger angle. (Figure 36 of the fan and engine coefficients.)

1NF

The coefficient of this term, P_{NF}, is the nose fan power. It is a direct function of gas generator rpm and an indirect function of atmospheric conditions, altitude and temperature (density).

The curve was generated as presented in Figure 37 of the fan and engine coefficients and then shifted by an increment in fan power to represent changes in estimated gas generator characteristics.

2NF

This term is the nose fan power coefficient ratio. It accounts for the changes in fan thrust due to forward velocity. (Figure 38 of the fan and engine characteristics.)

Aerodynamic Parameters

The aerodynamic parameters required are total velocity and the angles of sideslip and attack.

Total velocity is generated by taking the square root of the sum of the squares of the body axis velocities of the vehicle. Two separate total velocities are generated; one, V_T', based on the u and w velocities only, which is used to generate the angle of attack, and the other, V_T, based on u, v, and w which is used for all other purposes.

Both angle of attack and sideslip angle are generated as $\sin \alpha$ and $\sin \beta$ respectively. For small angles, the approximations are made $\sin \beta \simeq \beta$ and $\sin \alpha \simeq \alpha$, and all functions of these angles which require large angles have been generated in such a way as to use the sin of the required angle rather than the angle itself.

BLANK PAGE

2.3   FUNCTION GENERATION

2.3.1   Generation Methods

Two forms of function generation were used in the process of generating
the more complex functions in the XV-5A simulation. These are diode
function generation and pot padding function generation.

Pot padding function generation is done by modifying the characteristics
of the servo multiplier pots by adding or subtracting portions of the ref-
erence voltage to each of 17 taps equally spaced from top to bottom of the
pot.

Diode function generation utilizes biased diodes to provide variations in
output slope as a function of input voltage. As available in the Ryan Ana-
log Computer Laboratory, ten-twenty segment or twenty-ten segment
diode function generators are available.

Each form of function generation has its advantages. Diode function gen-
eration, since it does not depend on any mechanical elements, has a
much higher frequency response than pot padded function generation.
Diode function generation has been used in the generation of all functions
where the input variable varies rapidly, such as in the generation of
$K_{N_{NF}}$ where δ_p, a variable capable of extremely rapid change, is the
input.

Diode function generation is also easier to change. A diode function gen-
erator can be set up in 10 minutes or less, while set-up of the simplest
function on a pod-padded function generator takes from 45 minutes to an
hour for even the most well trained and nimble-fingered assistant.

Diode function generation has the third advantage that the starting points
for each segment can be spaced at will, which allows the user to place
the segments closer together where more accuracy is required (the func-
tion is changing slope rapidly) and use few slope changes where the func-
tion is changing slowly.

Pot padding function generation has two advantages over DFG. Pot pad-
ding function generation is cheaper and therefore much more of it is
available in the facility, and, since the reference for each cup is open,
multiplication by one variable is possible simultaneous with change in the
function due to change in the value of a second variable.

This possibility allows a function of two variables such as $C_p{}^s/C_{p_0}{}^s$ to be broken into three parts, each of which is padded on a separate pot:

1. A first part to represent the constant level of $C_p{}^s/C_{p_0}{}^s$ at any value of R_q, which is referenced to ± 100 volts.

2. A second part to represent the linear variation with β_v (slope) of $C_p{}^s/C_{p_0}$ at any value of R_q, which is referenced to a scale factor times $\pm \beta_v$.

3. A third part which represents the 2nd order variation with $\beta_v{}^2$ (curvature) of $C_p{}^s/C_{p_0}{}^s$ at any value of R_q, which is referenced to a scale factor times $\pm \beta_v{}^2$.

The sum of the outputs of these 3 padded cups represents the value of $C_p{}^s/C_{p_0}{}^s$ and will assume the correct value at any β_v due to changes in reference level for the 2nd and third pots, and the correct value for any R_q due to variations in the input voltage which moves the wiper arms to the correct positions for all the pots. In some cases functions of a single variable were required, and where possible these simple functions were generated using a polynomial curve fit with constant coefficients. As an example, function 3F was generated in this manner and was accurately fit as a constant multiplied by the value of stagger angle squared.

A detailed explanation of the use of padded-servo cup function generation is given in Appendix 12.

2.3.2 Summary of Functions as Generated

Each of the more complex nonlinear functions, then, was generated by either one or the other of the methods called out above.

Shown in the following pages are the functions which were generated by pot padding or diode function generation.

In the case of pod padded functions, the digital computer or manual resistor computation sheets are also given. These sheets provide voltage check levels at each of the 17 tap positions.

The functions generated are given labels identifying the function as well as the particular piece of equipment used which can be located by referring to the circuitry section, paragraph 2.6.

Figure 55 One Hundred Times the Linear Coefficient of the
Polynomial Fit to $C_{N_{\beta_s}^s}$, $C_{X_{\beta_s}^s}$ and $C_{m_{\beta_s}^s}$ Plotted vs

625 R_q for the Left Wing

Figure 56 One Hundred Times the Linear Coefficient of the
Polynomial Fit to $C_{N_{\beta_s}^s}$, $C_{X_{\beta_s}^s}$ and $C_{m_{\beta_s}^s}$ Plotted vs

625 R_q for the Right Wing

EN	RN	E	P	RS	CODE
-0.421000E 01	0.572426E 00	0.	0.500000E 00	0.100000E 01	8-16 B_1
-0.180000E 02	0.134045E 02	-0.100000E 03	0.100000E 01	0.130000E 02	8-16
-0.203200E 02	0.221006E 02	-0.100000E 03	0.500000E 00	0.220000E 02	8-16
-0.158800E 02	0.425357E 02	0.	0.500000E 00	0.430000E 02	8-16
-0.121400E 02	0.471273E 02	0.	0.500000E 00	0.470000E 02	8-16
-0.888300E 01	0.149244E 02	0.	0.500000E 00	0.150000E 02	8-16
-0.674200E 01	0.717438E 01	0.	0.500000E 00	0.750000E 01	8-16
-0.636300E 01	0.943921E 03	-0.100000E 03	0.500000E 00	0.910000E 03	8-16
-0.579800E 01	0.132804E 04	-0.100000E 03	0.500000E 00	0.130000E 04	8-16
-0.510000E 01	0.615701E 03	-0.100000E 03	0.500000E 00	0.620000E 03	8-16
-0.411300E 01	0.413306E 03	-0.100000E 03	0.500000E 00	0.430000E 03	8-16
-0.269100E 01	0.100913E 04	0.	0.500000E 00	0.100000E 04	8-16
-0.127400E 01	0.346195E 03	0.	0.500000E 00	0.360000E 03	8-16
0.136100E-00	0.302008E 05	0.100000E 03	0.500000E 00	0.300000E 05	8-16
0.154000E 01	0.376760E 05	0.100000E 03	0.500000E 00	0.390000E 05	8-16
0.293900E 01	0.259984E 05	0.100000E 03	0.500000E 00	0.270000E 05	8-16
0.433100E 01	0.128864E 03	0.100000E 03	0.500000E 00	0.130000E 03	8-16

OUTPUT $100\ C_{N_{\beta_{u_1}}}^{\delta}$ (SLOPE PORTION)

EN	RN	E	P	RS	CODE
-0.582300E 00	0.879997E 00	0.	0.500000E 00	0.100000E 01	33-40 B_1
-0.182300E 01	0.660724E 00	0.	0.500000E 00	0.100000E 01	33-40
-0.823700E 01	0.939681E 02	-0.100000E 03	0.500000E 00	0.910000E 02	33-40
-0.128200E 02	0.111731E 03	-0.100000E 03	0.500000E 00	0.110000E 03	33-40
-0.159400E 02	0.135873E 03	-0.100000E 03	0.500000E 00	0.130000E 03	33-40
-0.179000E 02	0.743659E 02	-0.100000E 03	0.500000E 00	0.750000E 02	33-40
-0.177900E 02	0.450713E 02	-0.100000E 03	0.500000E 00	0.470000E 02	33-40
-0.142600E 02	0.431250E 02	0.	0.500000E 00	0.430000E 02	33-40
-0.113500E 02	0.173159E 02	0.	0.500000E 00	0.180000E 02	33-40
-0.966900E 01	0.798651E 02	0.	0.500000E 00	0.820000E 02	33-40
-0.821500E 01	0.690723E 02	0.	0.500000E 00	0.680000E 02	33-40
-0.698400E 01	0.587220E 02	0.	0.500000E 00	0.560000E 02	33-40
-0.597600E 01	0.502466E 02	0.	0.500000E 00	0.510000E 02	33-40
-0.519100E 01	0.436463E 02	0.	0.500000E 00	0.430000E 02	33-40
-0.462900E 01	0.389210E 02	0.	0.500000E 00	0.390000E 02	33-40
-0.429000E 01	0.359096E 02	0.	0.500000E 00	0.360000E 02	33-40
-0.417500E 01	0.680706E 02	0.	0.500000E 00	0.680000E 02	33-40

OUTPUT $100\ C_{X_{\beta_{u_1}}}^{\delta}$ (SLOPE)

EN	RN	E	P	RS	CODE
-0.935500E-01	0.141874E 02	-0.100000E 03	0.100000E 01	0.150000E 02	50-57 B_1
0.131100E 02	0.196915E 02	0.100000E 03	0.500000E 00	0.200000E 02	50-57
0.180400E 02	0.175830E 02	0.100000E 03	0.500000E 00	0.180000E 02	50-57
0.142300E 02	0.266813E 04	0.	0.500000E 00	0.270000E 04	50-57
0.104300E 02	0.557952E 03	0.100000E 03	0.500000E 00	0.560000E 03	50-57
0.632900E 01	0.180074E 02	0.	0.500000E 00	0.180000E 02	50-57
0.288700E 01	0.717636E 01	0.	0.500000E 00	0.750000E 01	50-57
0.199300E-00	0.702756E 00	0.	0.500000E 00	0.100000E 01	50-57
-0.201100E 01	0.149580E 03	-0.100000E 03	0.500000E 00	0.150000E 03	50-57
-0.299300E 01	0.243995E 03	0.	0.500000E 00	0.240000E 03	50-57
-0.399800E 01	0.299851E 03	0.	0.500000E 00	0.300000E 03	50-57
-0.502800E 01	0.392014E 03	0.	0.500000E 00	0.390000E 03	50-57
-0.608200E 01	0.475155E 03	0.	0.500000E 00	0.470000E 03	50-57
-0.716000E 01	0.537003E 03	0.	0.500000E 00	0.560000E 03	50-57
-0.826300E 01	0.645542E 03	0.	0.500000E 00	0.620000E 03	50-57
-0.939000E 01	0.765497E 03	0.	0.500000E 00	0.750000E 03	50-57
-0.105400E 02	0.145859E 03	-0.100000E 03	0.500000E 00	0.150000E 03	50-57

OUTPUT $100\ C_{m_{\beta_s}}^{\delta}$ (SLOPE)

Figure 57 One Hundred Times the Second Degree Coefficient of the
Polynomial Fit to $C_{N_{\beta_s}^s}$, $C_{X_{\beta_s}^s}$ and $C_{m_{\beta_s}^s}$ Plotted vs
625 R_q for the Left Wing

Figure 58 One Hundred Times the Second Degree Coefficient of the
Polynomial Fit to $C_{N_{\beta_s}^s}$, $C_{X_{\beta_s}^s}$ and $C_{m_{\beta_s}^s}$ Plotted vs
625 R_q for the Right Wing

JOB NO. 1014 POT PADDER RESISTOR CALCULATION   6/7/63

EN		RN		E		P		RS		CODE	
-0.419400E	02	0.245186E	02	-0.100000E	03	0.500000E	00	0.240000E	02	8-16	B_2
-0.375000E	02	0.108843E	02	0.		0.500000E	00	0.110000E	02	8-16	
-0.395200E	02	0.398387E	02	0.		0.500000E	00	0.390000E	02	8-16	
-0.434000E	02	0.956081E	02	-0.100000E	03	0.500000E	00	0.100000E	03	8-16	
-0.461700E	02	0.224292E	03	-0.100000E	03	0.500000E	00	0.220000E	03	8-16	
-0.484900E	02	0.399096E	02	-0.100000E	03	0.500000E	00	0.390000E	02	8-16	
-0.483900E	02	0.252660E	02	-0.100000E	03	0.500000E	00	0.240000E	02	8-16	
-0.444600E	02	0.208406E	03	0.		0.500000E	00	0.200000E	03	8-16	
-0.409300E	02	0.144800E	03	0.		0.500000E	00	0.150000E	03	8-16	
-0.379300E	02	0.474126E	03	0.		0.500000E	00	0.470000E	03	8-16	
-0.350800E	02	0.160427E	03	0.		0.500000E	00	0.160000E	03	8-16	
-0.326400E	02	0.350833E	03	-0.100000E	03	0.500000E	00	0.360000E	03	8-16	
-0.298400E	02	0.375857E	03	-0.100000E	03	0.500000E	00	0.390000E	03	8-16	
-0.266900E	02	0.392732E	03	-0.100000E	03	0.500000E	00	0.390000E	03	8-16	
-0.231900E	02	0.400052E	03	-0.100000E	03	0.500000E	00	0.390000E	03	8-16	
-0.193300E	02	0.432160E	03	-0.100000E	03	0.500000E	00	0.430000E	03	8-16	
-0.151200E	02	0.673397E	01	0.		0.500000E	00	0.680000E	01	8-16	

OUTPUT $100 \ C_{N_{\beta_{a_2}}^{6}}$ (CURVATURE)

JOB NO. 1014 POT PADDER RESISTOR CALCULATION   6/7/63

EN		RN		E		P		RS		CODE	
0.229800E	01	0.108926E	02	0.100000E	03	0.100000E	01	0.110000E	02	33-40	B_2
-0.145200E	02	0.907149E	01	-0.100000E	03	0.100000E	01	0.910000E	01	33-40	
-0.136700E	02	0.692737E	02	0.		0.500000E	00	0.680000E	02	33-40	
-0.131900E	02	0.266834E	03	-0.100000E	03	0.500000E	00	0.270000E	03	33-40	
-0.121000E	02	0.798897E	02	-0.100000E	03	0.500000E	00	0.820000E	02	33-40	
-0.894700E	01	0.738689E	01	0.		0.500000E	00	0.750000E	01	33-40	
-0.806500E	01	0.399310E	01	0.		0.500000E	00	0.390000E	01	33-40	
-0.109700E	02	0.215395E	03	-0.100000E	03	0.500000E	00	0.220000E	03	33-40	
-0.131000E	02	0.975674E	02	-0.100000E	03	0.500000E	00	0.100000E	03	33-40	
-0.135600E	02	0.900416E	03	-0.100000E	03	0.500000E	00	0.910000E	03	33-40	
-0.138400E	02	0.100969E	04	-0.100000E	03	0.500000E	00	0.100000E	04	33-40	
-0.139600E	02	0.948970E	03	-0.100000E	03	0.500000E	00	0.910000E	03	33-40	
-0.139100E	02	0.949522E	03	-0.100000E	03	0.500000E	00	0.910000E	03	33-40	
-0.136900E	02	0.101144E	04	-0.100000E	03	0.500000E	00	0.100000E	04	33-40	
-0.133100E	02	0.903020E	03	-0.100000E	03	0.500000E	00	0.910000E	03	33-40	
-0.127500E	02	0.102246E	04	-0.100000E	03	0.500000E	00	0.100000E	04	33-40	
-0.120300E	02	0.313281E	02	0.		0.500000E	00	0.300000E	02	33-40	

OUTPUT $100 \ C_{X_{\beta_{a_2}}^{6}}$ (CURVATURE)

JOB NO. 1014 POT PADDER RESISTOR CALCULATION   6/7/63

EN		RN		E		P		RS		CODE	
0.879000E	01	0.914099E	01	0.100000E	03	0.100000E	01	0.910000E	01	50-57	B_2
-0.991900E	01	0.205277E	02	-0.100000E	03	0.500000E	00	0.200000E	02	50-57	
-0.204000E	02	0.119870E	02	-0.100000E	03	0.100000E	01	0.120000E	02	50-57	
-0.184300E	02	0.373034E	03	-0.100000E	03	0.500000E	00	0.360000E	03	50-57	
-0.160500E	02	0.187388E	03	-0.100000E	03	0.500000E	00	0.180000E	03	50-57	
-0.128300E	02	0.511835E	02	0.		0.500000E	00	0.510000E	02	50-57	
-0.100800E	02	0.462103E	02	0.		0.500000E	00	0.470000E	02	50-57	
-0.773900E	01	0.237879E	02	0.		0.500000E	00	0.240000E	02	50-57	
-0.600800E	01	0.636081E	01	0.		0.500000E	00	0.620000E	01	50-57	
-0.604800E	01	0.109416E	04	-0.100000E	03	0.500000E	00	0.110000E	04	50-57	
-0.592700E	01	0.109557E	04	-0.100000E	03	0.500000E	00	0.110000E	04	50-57	
-0.564500E	01	0.109885E	04	-0.100000E	03	0.500000E	00	0.110000E	04	50-57	
-0.520200E	01	0.109720E	04	-0.100000E	03	0.500000E	00	0.110000E	04	50-57	
-0.459700E	01	0.111106E	04	-0.100000E	03	0.500000E	00	0.110000E	04	50-57	
-0.383100E	01	0.111307E	04	-0.100000E	03	0.500000E	00	0.110000E	04	50-57	
-0.290300E	01	0.113786E	04	-0.100000E	03	0.500000E	00	0.110000E	04	50-57	
-0.181500E	01	0.312787E	01	0.		0.500000E	00	0.300000E	01	50-57	

OUTPUT $100 \ C_{m_{\beta_{a_2}}^{6}}$ (CURVATURE)

Figure 59 One Hundred Times the Linear Coefficient of the
Polynomial Fit to $C_{N_{\beta_v}}^s$, $C_{X_{\beta_v}}^s$ and $C_{m_{\beta_v}}^s$ Plotted vs
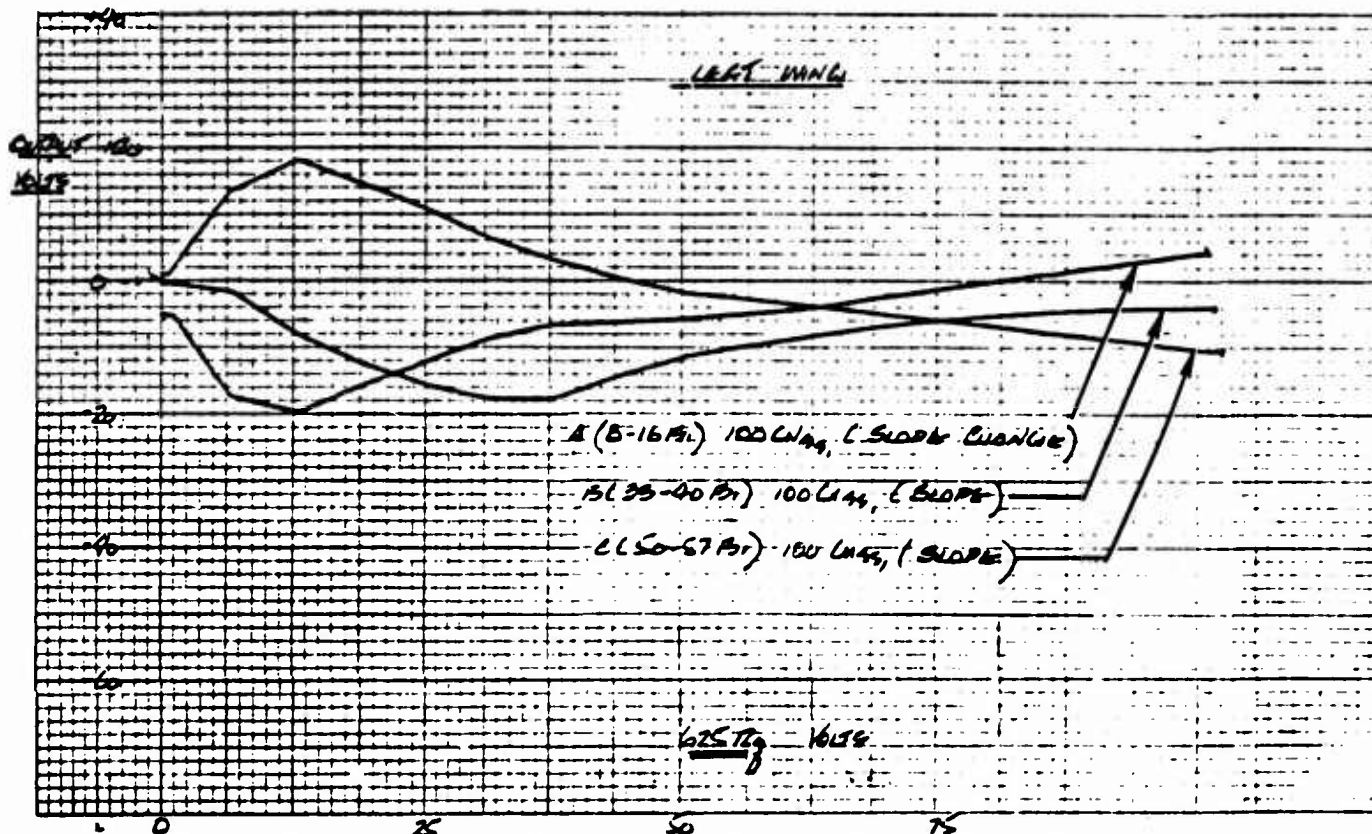625 R_q for the Left Wing
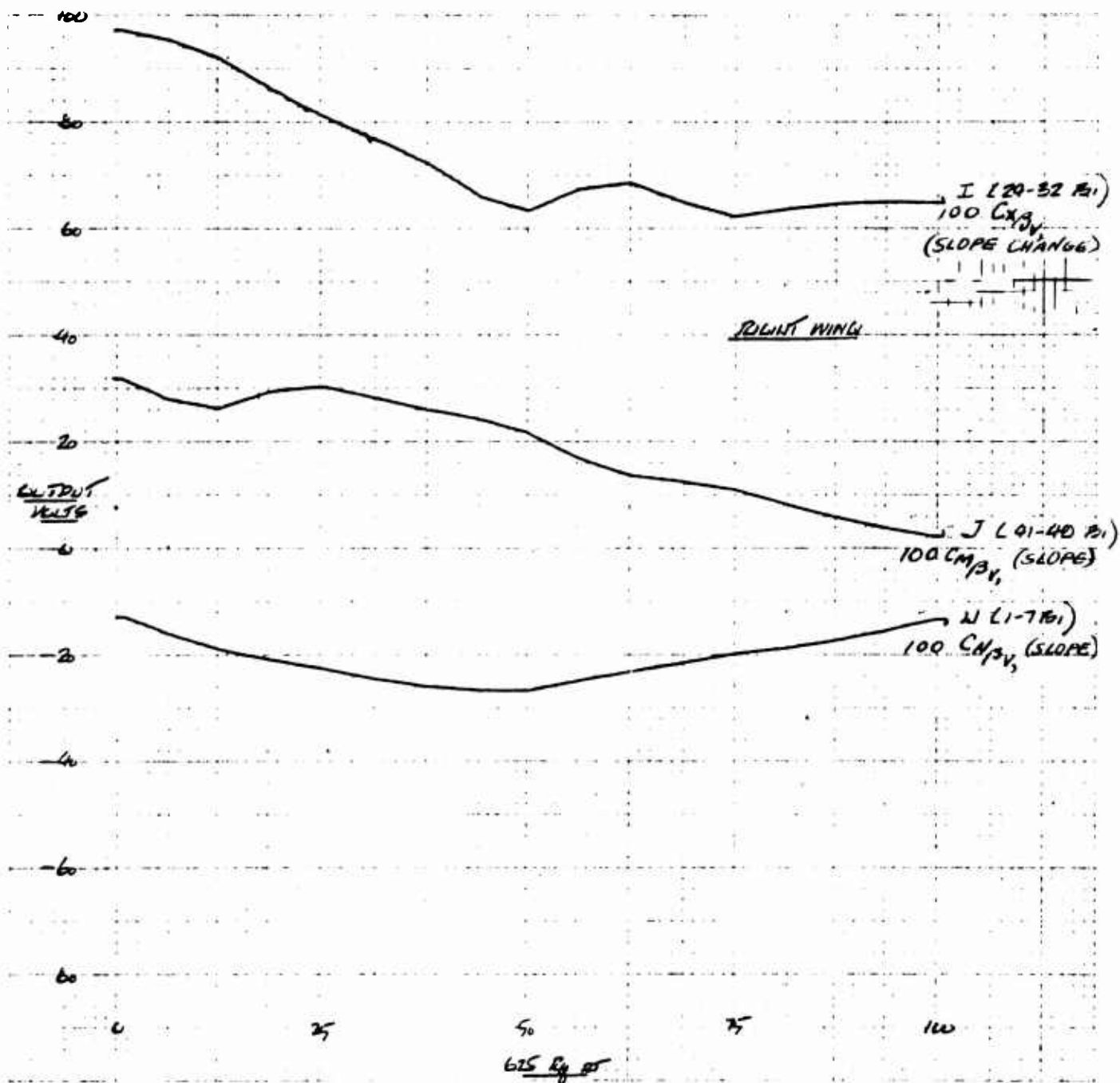
Figure 60 One Hundred Times the Linear Coefficient of the
Polynomial Fit to $C_{N\beta_v}^8$, $C_{X\beta_v}^8$ and $C_{m\beta_v}^8$ Plotted vs
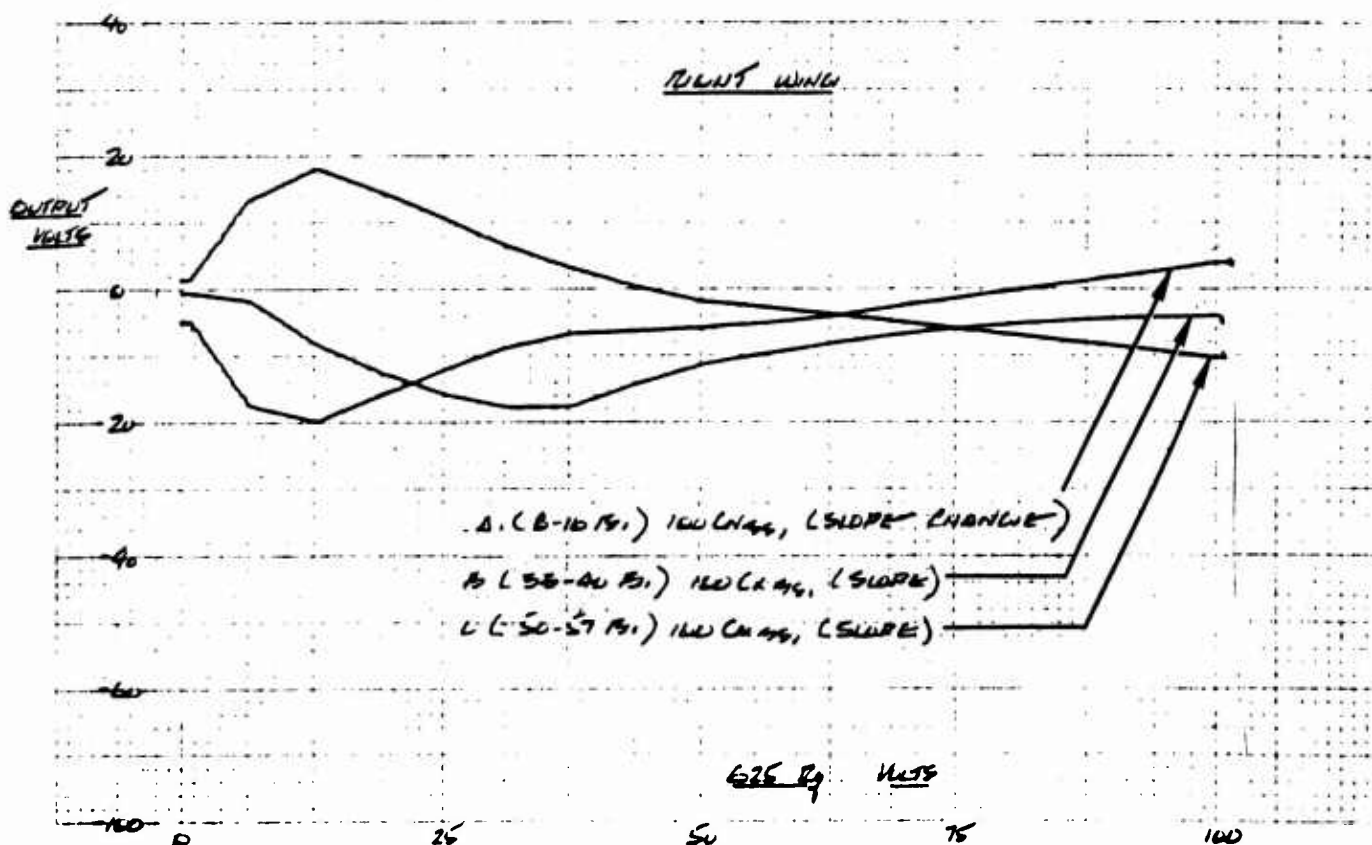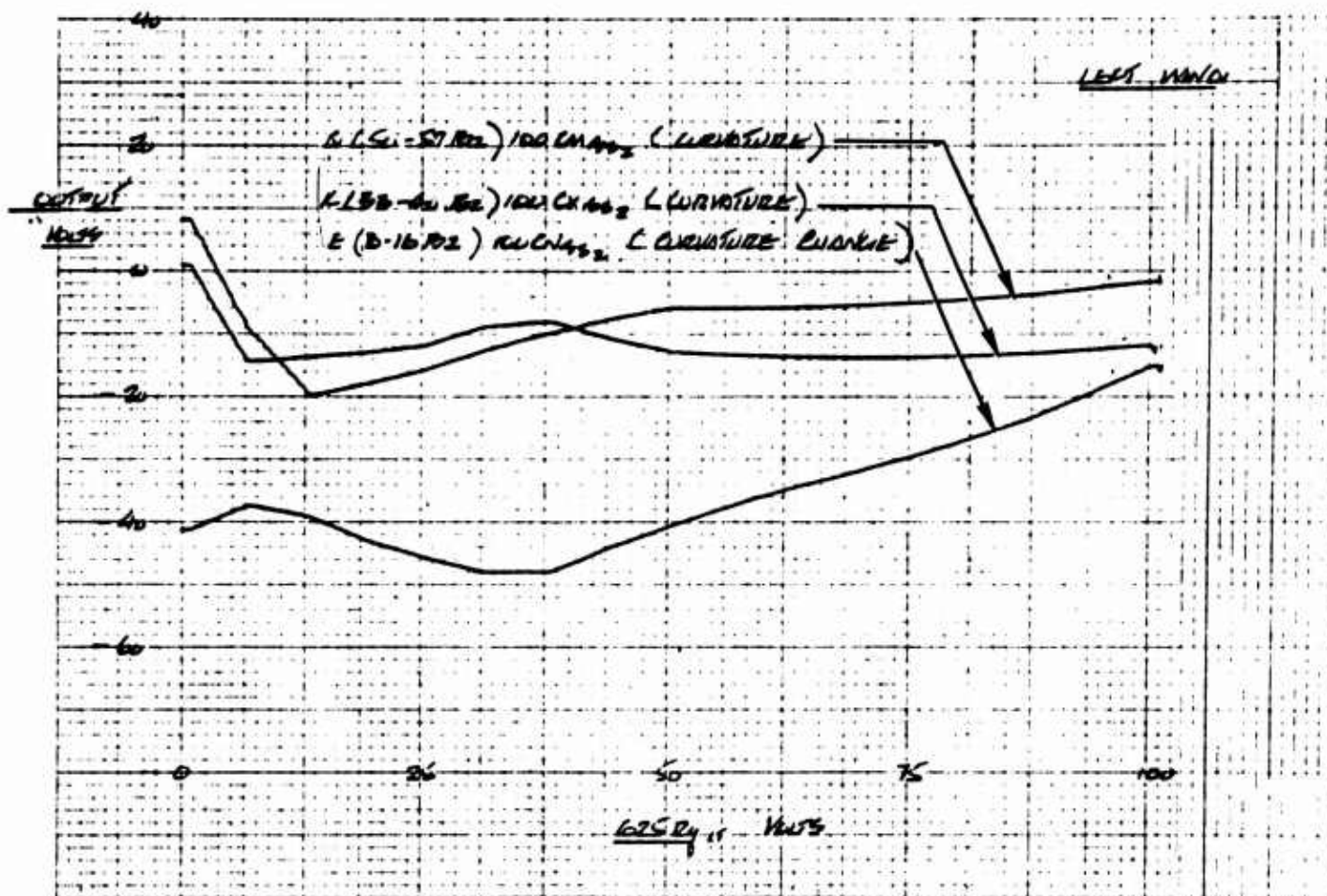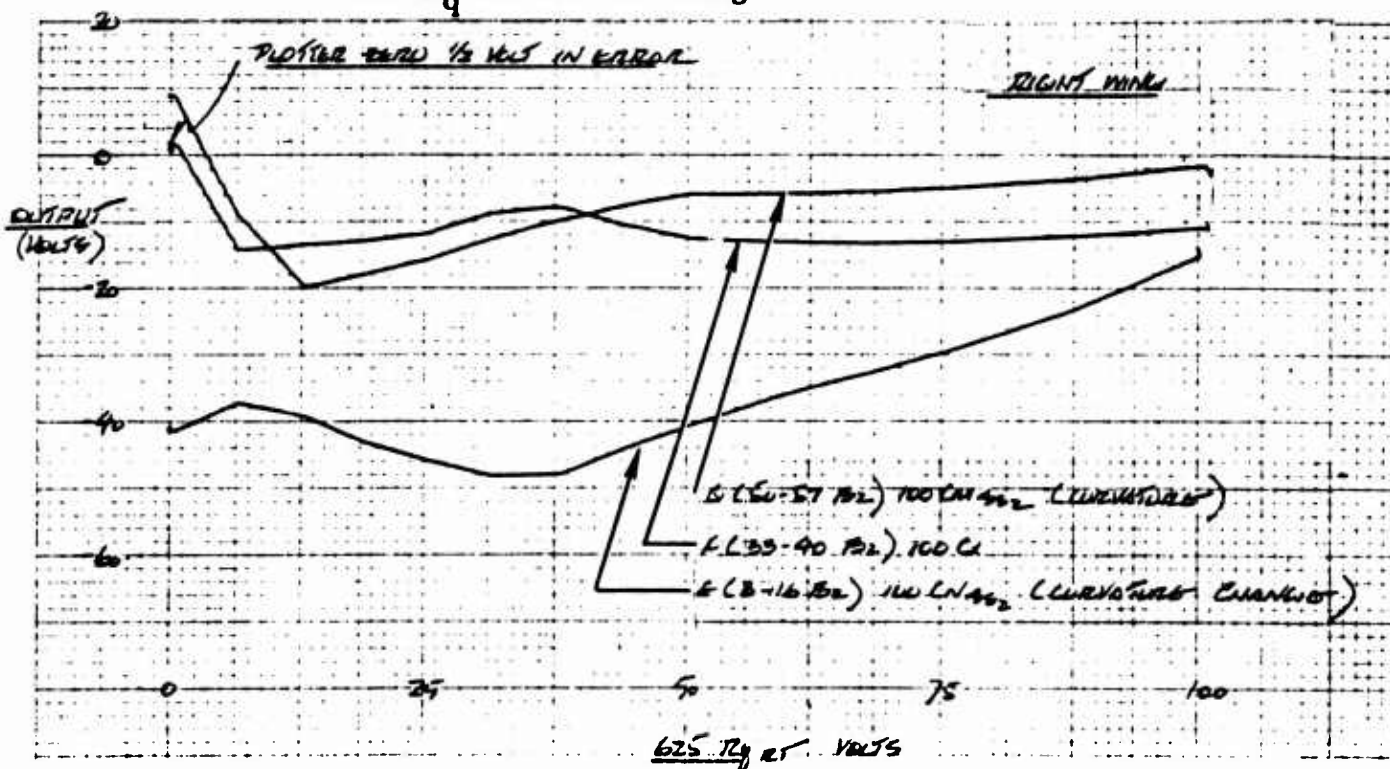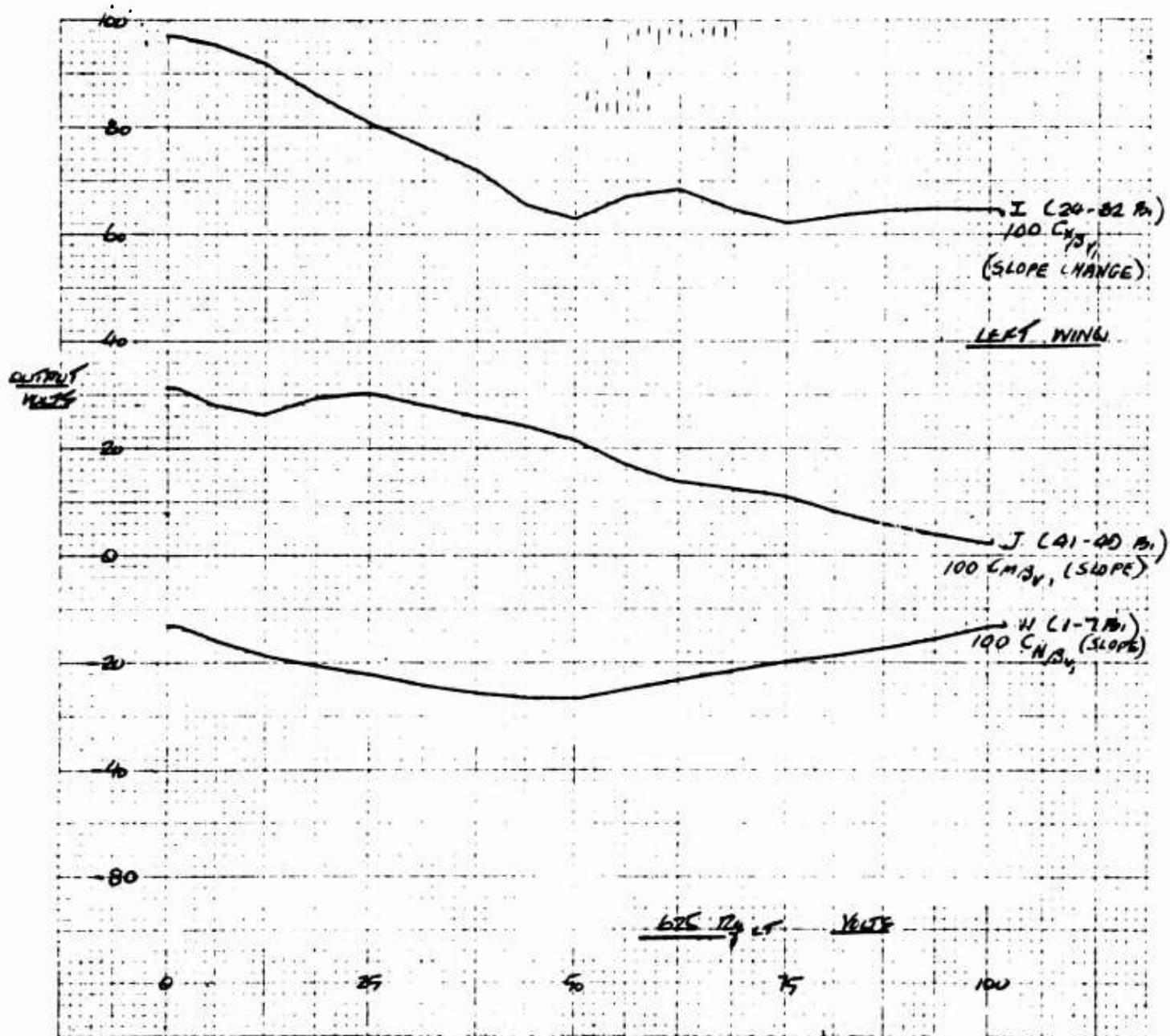625 R_q for the Left Wing

JOB NO. 1014 POT PADDER RESISTOR CALCULATION 6/6/63

EN	RN	E	P	RS	CODE
-0.126600E 02	0.645041E 01	0.	0.500000E 00	0.620000E 01	1-7 B₁
-0.163400E 02	0.206398E 03	-0.100000E 03	0.500000E 00	0.200000E 03	1-7
-0.192600E 02	0.142818E 03	-0.100000E 03	0.500000E 00	0.150000E 03	1-7
-0.211200E 02	0.704286E 03	-0.100000E 03	0.500000E 00	0.680000E 03	1-7
-0.227700E 02	0.837133E 02	0.	0.500000E 00	0.820000E 02	1-7
-0.249300E 02	0.195495E 03	-0.100000E 0?	0.500000E 00	0.200000E 03	1-7
-0.263700E 02	0.191745E 03	-0.100000E 03	0.500000E 00	0.200000E 03	1-7
-0.270900E 02	0.187269E 03	-0.00000E 03	0.500000E 00	0.180000E 03	1-7
-0.270800E 02	0.739054E 02	-0.100000E 03	0.500000E 00	0.750000E 02	1-7
-0.252200E 02	0.157624E 04	0.	0.500000E 00	0.160000E 04	1-7
-0.233900E 02	0.109641E 04	0.	0.500000E 00	0.110000E 04	1-7
-0.216000E 02	0.101250E 04	0.	0.500000E 00	0.100000E 04	1-7
-0.198500E 02	0.547335E 02	0.	0.500000E 00	0.560000E 02	1-7
-0.187800E 02	0.400756E 03	-0.100000E 03	0.500000E 00	0.390000E 03	1-7
-0.173300E 02	0.387516E 03	-0.100000E 03	0.500000E 00	0.390000E 03	1-7
-0.154800E 02	0.406346E 03	-0.100000E 03	0.500000E 00	0.390000E 03	1-7
-0.132400E 02	0.110826E 02	0.	0.500000E 00	0.110000E 02	1-7

OUTPUT $100\ C_{N_{\beta_{v_1}}}^{\delta}$ (SLOPE)

JOB NO. 1014 POT PADDER RESISTOR CALCULATION 6/6/63

EN	RN	E	P	RS	CODE
0.975400E 02	0.240234E 01	0.100000E 03	0.500000E 00	0.240000E 01	24-32 B₁
0.956200E 02	0.582447E 01	0.100000E 03	0.500000E 00	0.560000E 01	24-32
0.922900E 02	0.612553E 01	0.100000E 03	0.500000E 00	0.620000E 01	24-32
0.866000E 02	0.345479E 03	0.	0.500000E 00	0.360000E 03	24-32
0.813800E 02	0.203450E 03	0.	0.500000E 00	0.200000E 03	24-32
0.769100E 02	0.618468E 03	0.100000E 03	0.500000E 00	0.620000E 03	24-32
0.723700E 02	0.268426E 02	0.100000E 03	0.500000E 00	0.270000E 02	24-32
0.659000E 02	0.334858E 02	0.	0.500000E 00	0.330000E 02	24-32
0.631200E 02	0.167872E 02	0.	0.500000E 00	0.160000E 02	24-32
0.673900E 02	0.205180E 02	0.100000E 03	0.500000E 00	0.200000E 02	24-32
0.686800E 02	0.114697E 02	0.100000E 03	0.500000E 00	0.110000E 02	24-32
0.648500E 02	0.935337E 02	0.	0.500000E 00	0.910000E 02	24-32
0.623200E 02	0.285697E 02	0.	0.500000E 00	0.300000E 02	24-32
0.638800E 02	0.123136E 03	0.100000E 03	0.500000E 00	0.120000E 03	24-32
0.648900E 02	0.121910E 03	0.100000E 03	0.500000E 00	0.120000E 03	24-32
0.653600E 02	0.115982E 03	0.100000E 03	0.500000E 00	0.120000E 03	24-32
0.652700E 02	0.135979E 04	0.	0.500000E 00	0.130000E 04	24-32

OUTPUT $100\ C_{X_{\beta_{v_1}}}^{\delta}$ (SLOPE)

JOB NO. 1014 POT PADDER RESISTOR CALCULATION 6/7/63

EN	RN	E	P	RS	CODE
0.323500E 02	0.292267E 02	0.100000E 03	0.500000E 00	0.300000E 02	41-49 B₁
0.280100E 02	0.201995E 02	0.	0.500000E 00	0.200000E 02	41-49
0.262700E 02	0.979250E 01	0.	0.500000E 00	0.100000E 02	41-49
0.295600E 02	0.597624E 02	0.100000E 03	0.500000E 00	0.620000E 02	41-49
0.306400E 02	0.392000E 02	0.100000E 03	0.500000E 00	0.390000E 02	41-49
0.284100E 02	0.999999E 36	0.	0.	0.999999E 36	41-49
0.261800E 02	0.100179E 03	0.	0.500000E 00	0.100000E 03	41-49
0.244400E 02	0.153995E 03	0.100000E 03	0.500000E 00	0.150000E 03	41-49
0.217800E 02	0.711954E 02	0.100000E 03	0.500000E 00	0.680000E 02	41-49
0.170600E 02	0.238713E 02	0.	0.500000E 00	0.240000E 02	41-49
0.136800E 02	0.118750E 02	0.	0.500000E 00	0.120000E 02	41-49
0.124600E 02	0.586205E 03	0.100000E 03	0.500000E 00	0.560000E 03	41-49
0.109600E 02	0.129318E 03	0.100000E 03	0.500000E 00	0.130000E 03	41-49
0.816900E 01	0.392741E 02	0.	0.500000E 00	0.390000E 02	41-49
0.576800E 01	0.275893E 02	0.	0.500000E 00	0.270000E 02	41-49
0.375900E 01	0.180259E 02	0.	0.500000E 00	0.180000E 02	41-49
0.214100E 01	0.248107E 01	0.	0.500000E 00	0.240000E 01	41-49

OUTPUT $100\ C_{m_{\beta_{v_1}}}^{\delta}$ (SLOPE)
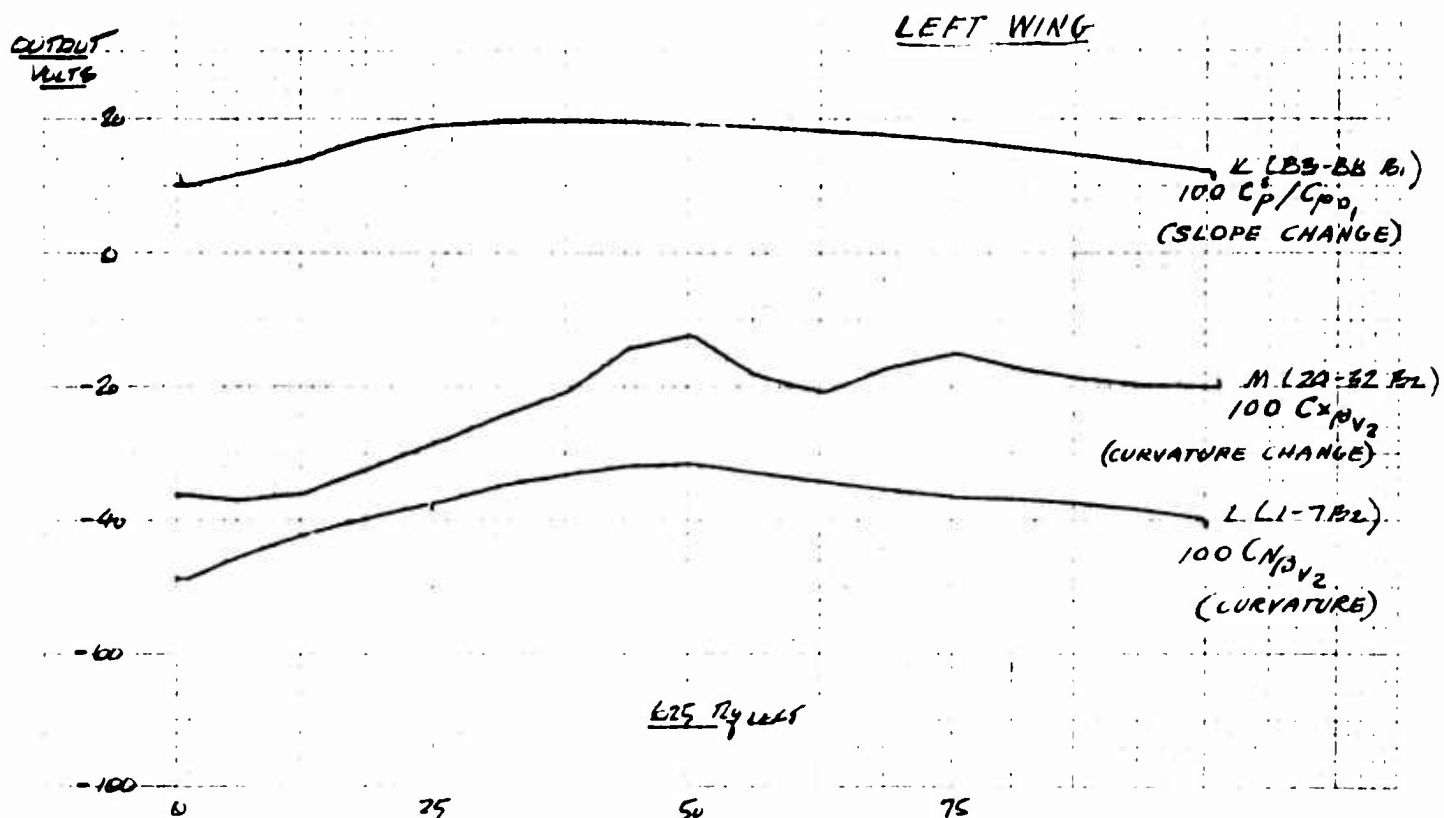
Figure 61 One Hundred Times the Linear Coefficient of the
Polynomial Fit to the Fan Power Coefficient Ratio,
And One Hundred Times the Second Degree Coefficient
Of the Polynomial Fit to $C_{X^S_{\beta_v}}$ and $C_{N^S_{\beta_v}}$ Plotted vs
625 R_q for the Left Wing

Figure 62 One Hundred Times the Linear Coefficient of the Polynomial Fit to the Fan
Power Coefficient Ratio, And One Hundred Times the Second Degree
Coefficient Of the Polynomial Fit to $C_{X^S_{\beta_v}}$ and $C_{N^S_{\beta_v}}$ Plotted vs
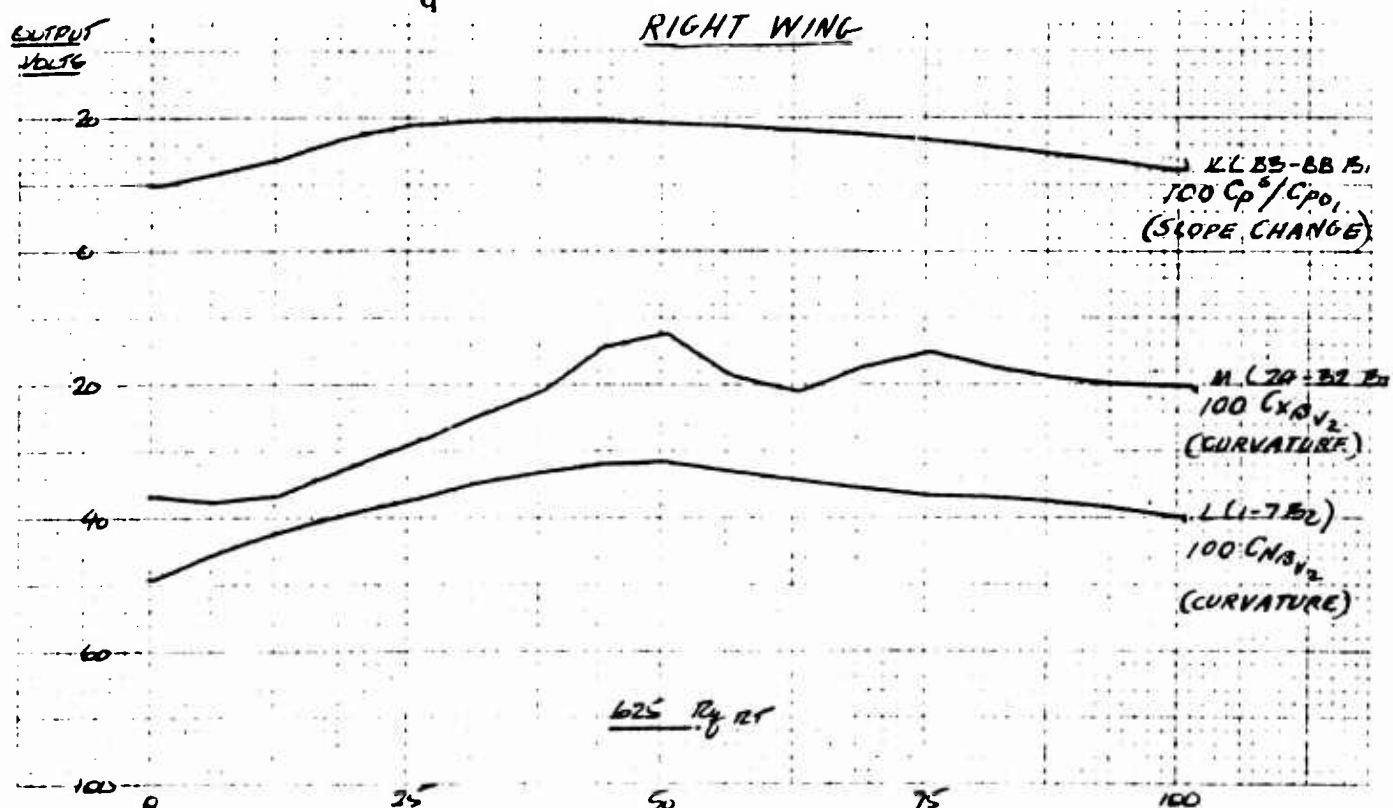625 R_q for the Right Wing

94

EN	RN	E	P	RS	CODE	
-0.498500E 02	0.239876E 02	-0.100000E 03	0.500000E 00	0.240000E 02	1-7	B_2
-0.459300E 02	0.156579E 03	0.	0.500000E 00	0.160000E 03	1-7	
-0.425600E 02	0.119105E 03	0.	0.500000E 00	0.120000E 03	1-7	
-0.398600E 02	0.219816E 03	0.	0.500000E 00	0.220000E 03	1-7	
-0.375000E 02	0.616775E 03	-0.100000E 03	0.500000E 00	0.620000E 03	1-7	
-0.349500E 02	0.922975E 02	0.	0.500000E 00	0.910000E 02	1-7	
-0.331100E 02	0.874384E 02	0.	0.500000E 00	0.910000E 02	1-7	
-0.319800E 02	0.856608E 02	0.	0.500000E 00	0.820000E 02	1-7	
-0.315500E 02	0.306509E 02	0.	0.500000E 00	0.300000E 02	1-7	
-0.330500E 02	0.125531E 04	-0.100000E 03	0.500000E 00	0.130000E 04	1-7	
-0.344500E 02	0.102421E 04	-0.100000E 03	0.500000E 00	0.100000E 04	1-7	
-0.357300E 02	0.109551E 04	-0.100000E 03	0.500000E 00	0.110000E 04	1-7	
-0.369000E 02	0.132935E 03	-0.100000E 03	0.500000E 00	0.130000E 03	1-7	
-0.371800E 02	0.170031E 03	0.	0.500000E 00	0.180000E 03	1-7	
-0.378700E 02	0.173186E 03	0.	0.500000E 00	0.180000E 03	1-7	
-0.389700E 02	0.178217E 03	0.	0.500000E 00	0.180000E 03	1-7	
-0.404800E 02	0.739073E 02	-0.100000E 03	0.500000E 00	0.750000E 02	1-7	

OUTPUT $\qquad$ $100\, C_{N_{\beta_{v_2}}}^{\beta}$ (CURVATURE)

EN	RN	E	P	RS	CODE	
-0.370500E 02	0.771875E 02	0.	0.500000E 00	0.750000E 02	24-32	B_2
-0.379500E 02	0.596634E 02	-0.100000E 03	0.500000E 00	0.620000E 02	24-32	
-0.369000E 02	0.410807E 02	-0.100000E 03	0.500000E 00	0.430000E 02	24-32	
-0.329700E 02	0.628392E 04	-0.100000E 03	0.500000E 00	0.620000E 04	24-32	
-0.290200E 02	0.108826E 04	0.	0.500000E 00	0.110000E 04	24-32	
-0.251200E 02	0.935999E 03	-0.100000E 03	0.500000E 00	0.910000E 03	24-32	
-0.210700E 02	0.616641E 02	-0.100000E 03	0.500000E 00	0.620000E 02	24-32	
-0.146200E 02	0.633083E 01	0.	0.500000E 00	0.620000E 01	24-32	
-0.125000E 02	0.280018E 01	0.	0.500000E 00	0.270000E 01	24-32	
-0.187500E 02	0.409526E 02	-0.100000E 03	0.500000E 00	0.390000E 02	24-32	
-0.212800E 02	0.233914E 02	-0.100000E 03	0.500000E 00	0.240000E 02	24-32	
-0.175000E 02	0.224743E 02	0.	0.500000E 00	0.220000E 02	24-32	
-0.151800E 02	0.616071E 01	0.	0.500000E 00	0.620000E 01	24-32	
-0.174800E 02	0.241758E 03	-0.100000E 03	0.500000E 00	0.240000E 03	24-32	
-0.191400E 02	0.236894E 03	-0.100000E 03	0.500000E 00	0.240000E 03	24-32	
-0.201600E 02	0.233906E 03	-0.100000E 03	0.500000E 00	0.240000E 03	24-32	
-0.205400E 02	0.392072E 03	-0.100000E 03	0.500000E 00	0.390000E 03	24-32	

OUTPUT $\qquad$ $100\, C_{X_{\beta_{v_2}}}^{\beta}$ (CURVATURE)

EN	RN	E	P	RS	CODE	
0.963400E 01	0.973262E 01	0.	0.500000E 00	0.100000E 02	83-88	B_1
0.114900E 02	0.591861E 02	0.	0.500000E 00	0.620000E 02	83-88	
0.137100E 02	0.227489E 02	0.	0.500000E 00	0.220000E 02	83-88	
0.170600E 02	0.130683E 03	0.100000E 03	0.500000E 00	0.130000E 03	83-88	
0.192200E 02	0.896228E 02	0.100000E 03	0.500000E 00	0.910000E 02	83-88	
0.196900E 02	0.627421E 03	0.100000E 03	0.500000E .0	0.620000E 03	83-88	
0.199200E 02	0.395131E 03	0.100000E 03	0.500000E 00	0.390000E 03	83-88	
0.197700E 02	0.100287E 04	0.100000E 03	0.500000E 00	0.100000E 04	83-88	
0.194700E 02	0.125828E 04	0.100000E 03	0.500000E 00	0.130000E 04	83-88	
0.190500E 02	0.101187E 04	0.100000E 03	0.500000E 00	0.100000E 04	83-88	
0.184800E 02	0.117577E 04	0.100000E 03	0.500000E 00	0.120000E 04	83-88	
0.177800E 02	0.110116E 04	0.100000E 03	0.500000E 00	0.110000E 04	83-88	
0.169400E 02	0.119798E 04	0.100000E 03	0.500000E 00	0.120000E 04	83-88	
0.159700E 02	0.112540E 04	0.100000E 03	0.500000E 00	0.110000E 04	83-88	
0.148600E 02	0.122798E 04	0.100000E 03	0.500000E 00	0.120000E 04	83-88	
0.136200E 02	0.115687E 04	0.100000E 03	0.500000E 00	0.120000E 04	83-88	
0.122400E 02	0.166304E 02	0.	0.500000E 00	0.160000E 02	83-88	

OUTPUT $\qquad$ $100\, C_{p}^{\beta}/C_{p_{0_i}}^{\beta}$ (SLOPE)

Figure 63   One Hundred Times the Constant of the Polynomial
           Fit to the Fan Power Coefficient Ratio, One Hundred
           Times the Second Degree Coefficient to the Polynomial
           Fit to the Fan Power Coefficient Ratio, and One Hundred
           Times the Second Degree Coefficient of the Polynomial
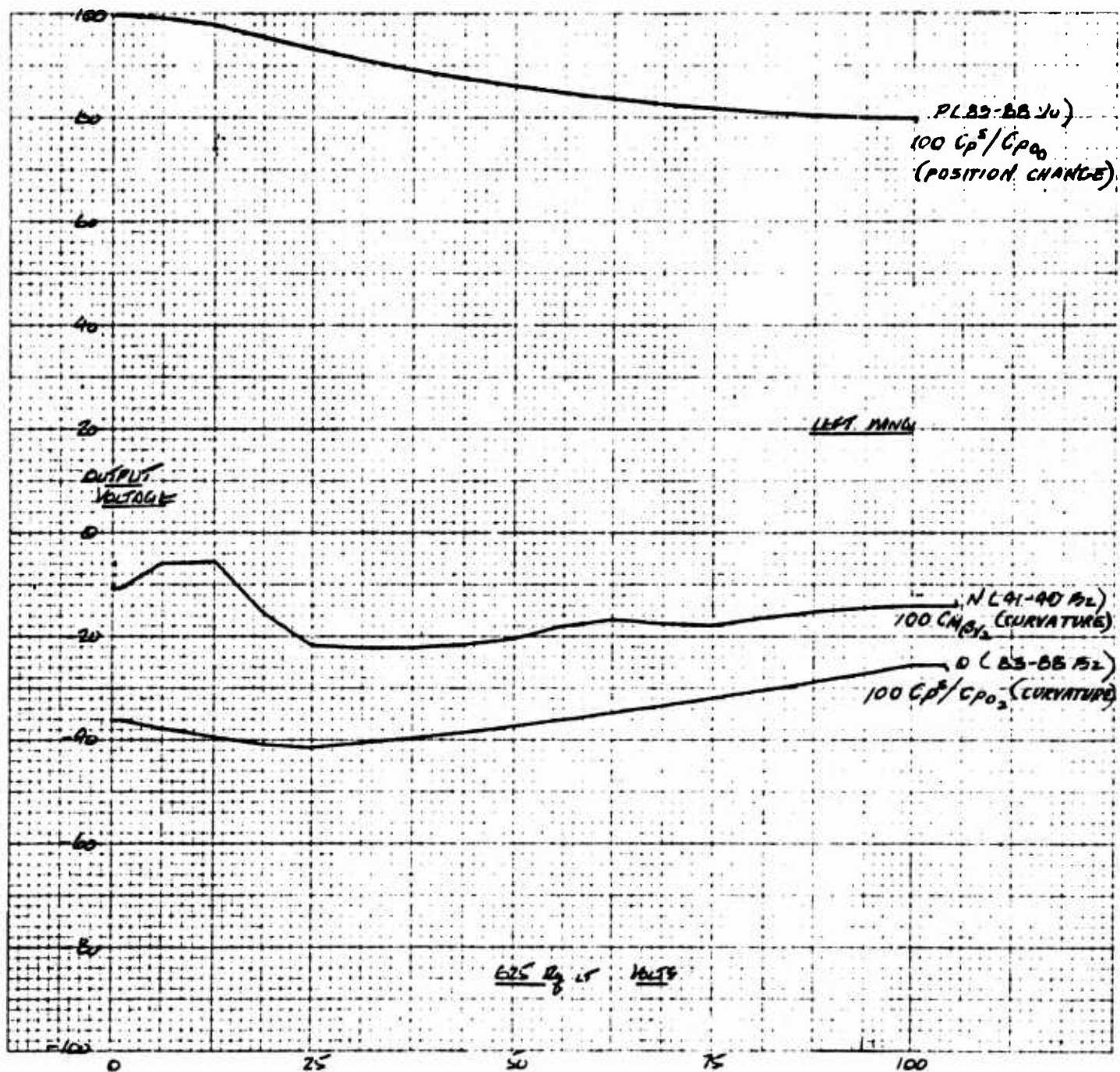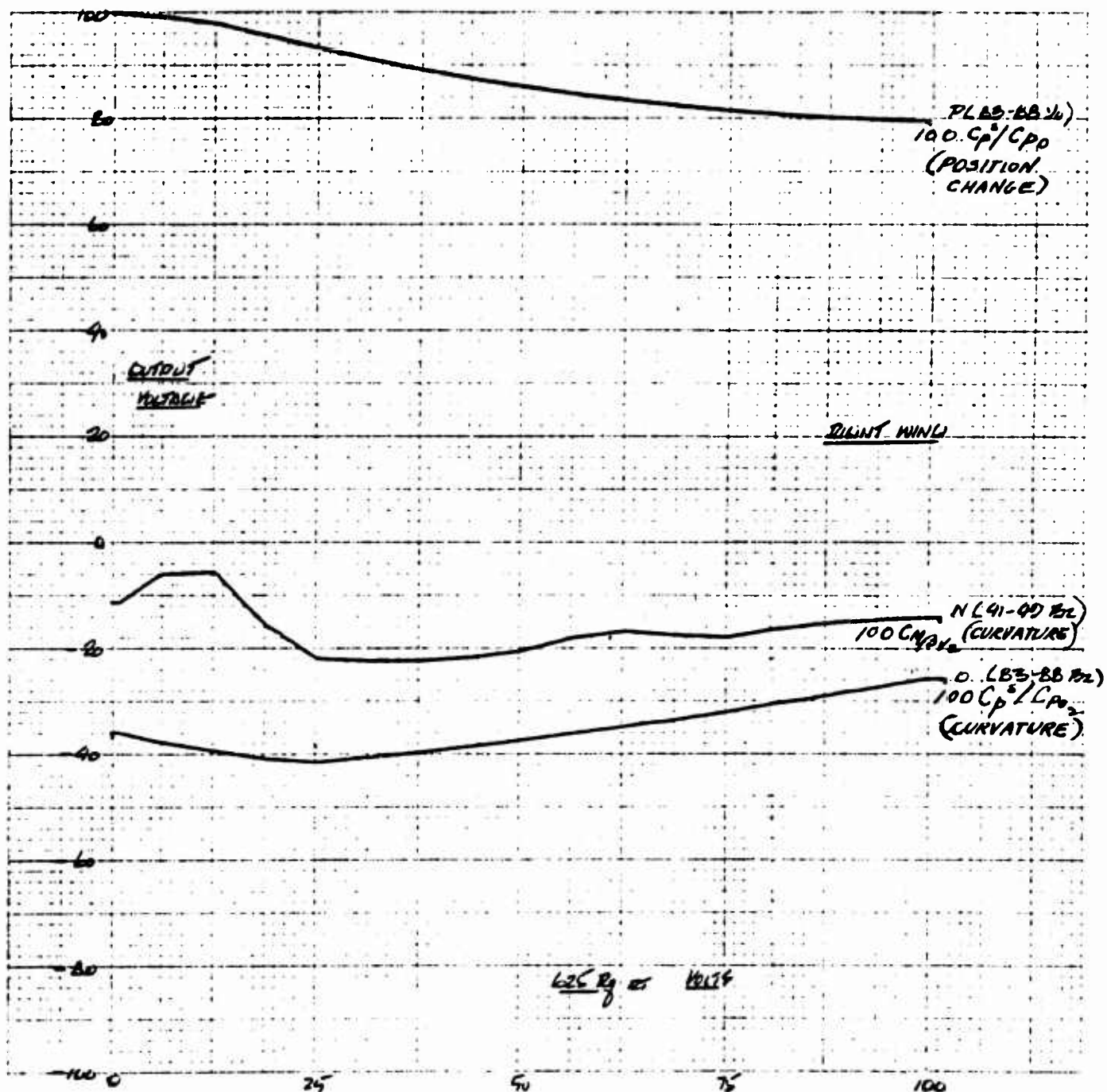   Fit to $C_{m}{}^{S}{}_{\beta_{v}}$ Plotted vs 625 R_q for the Left Wing

Figure 64   One Hundred Times the Constant of the Polynomial
Fit to the Fan Power Coefficient Ratio, One Hundred
Times the Second Degree Coefficient to the Polynomial
Fit to the Fan Power Coefficient Ratio, and One Hundred
Times the Second Degree Coefficient of the Polynomial
Fit to $C_{m_{\beta_v}}^s$ Plotted vs 625 R_q for the Right Wing

EN	RN	E	P	RS	CODE
0.100000E 03	0.	0.100000E 03	0.	0.	83-88 YO
0.993100E 02	0.208670E 01	0.100000E 03	0.500000E 00	0.200000E 01	83-88
0.980000E 02	0.374999E 01	0.100000E 03	0.500000E 00	0.360000E 01	83-88
0.956900E 02	0.149515E 04	0.	0.500000E 00	0.150000E 04	83-88
0.935000E 02	0.194795E 04	0.	0.500000E 00	0.200000E 04	83-88
0.914000E 02	0.856872E 03	0.	0.500000E 00	0.820000E 03	83-88
0.895000E 02	0.578666E 03	0.	0.500000E 00	0.560000E 03	83-88
0.878900E 02	0.102996E 04	0.	0.500000E 00	0.100000E 04	83-88
0.864400E 02	0.108050E 04	0.	0.500000E 00	0.110000E 04	83-88
0.851400E 02	0.997735E 03	0.	0.500000E 00	0.100000E 04	83-88
0.840000E 02	0.984388E 03	0.	0.500000E 00	0.100000E 04	83-88
0.830200E 02	0.103775E 04	0.	0.500000E 00	0.100000E 04	83-88
0.821900E 02	0.963165E 03	0.	0.500000E 00	0.100000E 04	83-88
0.815200E 02	0.101900E 04	0.	0.500000E 00	0.100000E 04	83-88
0.810000E 02	0.949231E 03	0.	0.500000E 00	0.910000E 03	83-88
0.806400E 02	0.945001E 03	0.	0.500000E 00	0.910000E 03	83-88
0.804400E 02	0.754129E 03	0.	0.500000E 00	0.750000E 03	83-88

OUTPUT $100\ C_p^B / C_{p_{0_0}}$ (INTERCEPT)

EN	RN	E	P	RS	CODE
-0.121600E 02	0.274637E 02	-0.100000E 03	0.500000E 00	0.270000E 02	41-49 B$_2$
-0.516300E 01	0.203983E 01	0.	0.500000E 00	0.200000E 01	41-49
-0.583100E 01	0.104214E 01	0.	0.500000E 00	0.100000E 01	41-49
-0.159900E 02	0.395875E 02	-0.100000E 03	0.500000E 00	0.390000E 02	41-49
-0.221700E 02	0.257374E 02	-0.100000E 03	0.500000E 00	0.270000E 02	41-49
-0.226800E 02	0.254342E 03	-0.100000E 03	0.500000E 00	0.240000E 03	41-49
-0.226200E 02	0.245911E 03	-0.100000E 03	0.500000E 00	0.240000E 03	41-49
-0.219700E 02	0.281358E 03	-0.100000E 03	0.500000E 00	0.270000E 03	41-49
-0.208000E 02	0.106071E 03	-0.100000E 03	0.500000E 00	0.110000E 03	41-49
-0.182300E 02	0.269144E 02	0.	0.500000E 00	0.270000E 02	41-49
-0.169300E 02	0.146285E 02	0.	0.500000E 00	0.150000E 02	41-49
-0.178000E 02	0.296394E 03	-0.100000E 03	0.500000E 00	0.300000E 03	41-49
-0.181500E 02	0.820689E 02	-0.100000E 03	0.500000E 00	0.820000E 02	41-49
-0.166300E 02	0.842737E 02	0.	0.500000E 00	0.820000E 02	41-49
-0.154800E 02	0.763816E 02	0.	0.500000E 00	0.750000E 02	41-49
-0.147100E 02	0.725823E 02	0.	0.500000E 00	0.750000E 02	41-49
-0.143200E 02	0.688462E 02	0.	0.500000E 00	0.680000E 02	41-49

OUTPUT $100\ C_m^B / \beta_{v_2}$ (CURVATURE)

EN	RN	E	P	RS	CODE
-0.362500E 02	0.338153E 02	0	0.500000E 00	0.330000E 02	83-88 B$_2$
-0.382600E 02	0.304638E 03	-0.100000E 03	0.500000E 00	0.300000E 03	83-88
-0.398900E 02	0.140881E 04	-0.100000E 03	0.500000E 00	0.150000E 04	83-88
-0.414400E 02	0.112041E 03	-0.100000E 03	0.500000E 00	0.110000E 03	83-88
-0.420100E 02	0.755078E 02	-0.100000E 03	0.500000E 00	0.750000E 02	83-88
-0.411400E 02	0.122625E 04	-0.100000E 03	0.500000E 00	0.120000E 04	83-88
-0.401800E 02	0.747747E 03	-0.100000E 03	0.500000E 00	0.750000E 03	83-88
-0.390700E 02	0.190405E 04	-0.100000E 03	0.500000E 00	0.200000E 04	83-88
-0.379000E 02	0.145547E 04	-0.100000E 03	0.500000E 00	0.150000E 04	83-88
-0.366500E 02	0.197967E 04	-0.100000E 03	0.500000E 00	0.200000E 04	83-88
-0.353400E 02	0.151547E 04	-0.100000E 03	0.500000E 00	0.150000E 04	83-88
-0.339500E 02	0.206405E 04	-0.100000E 03	0.500000E 00	0.200000E 04	83-88
-0.325000E 02	0.158201E 04	-0.100000E 03	0.500000E 00	0.160000E 04	83-88
-0.309700E 02	0.215719E 04	-0.100000E 03	0.500000E 00	0.220000E 04	83-88
-0.293800E 02	0.189160E 04	-0.100000E 03	0.500000E 00	0.180000E 04	83-88
-0.277200E 02	0.193607E 04	-0.100000E 03	0.500000E 00	0.200000E 04	83-88
-0.259900E 02	0.281684E 02	0.	0.500000E 00	0.270000E 02	83-88

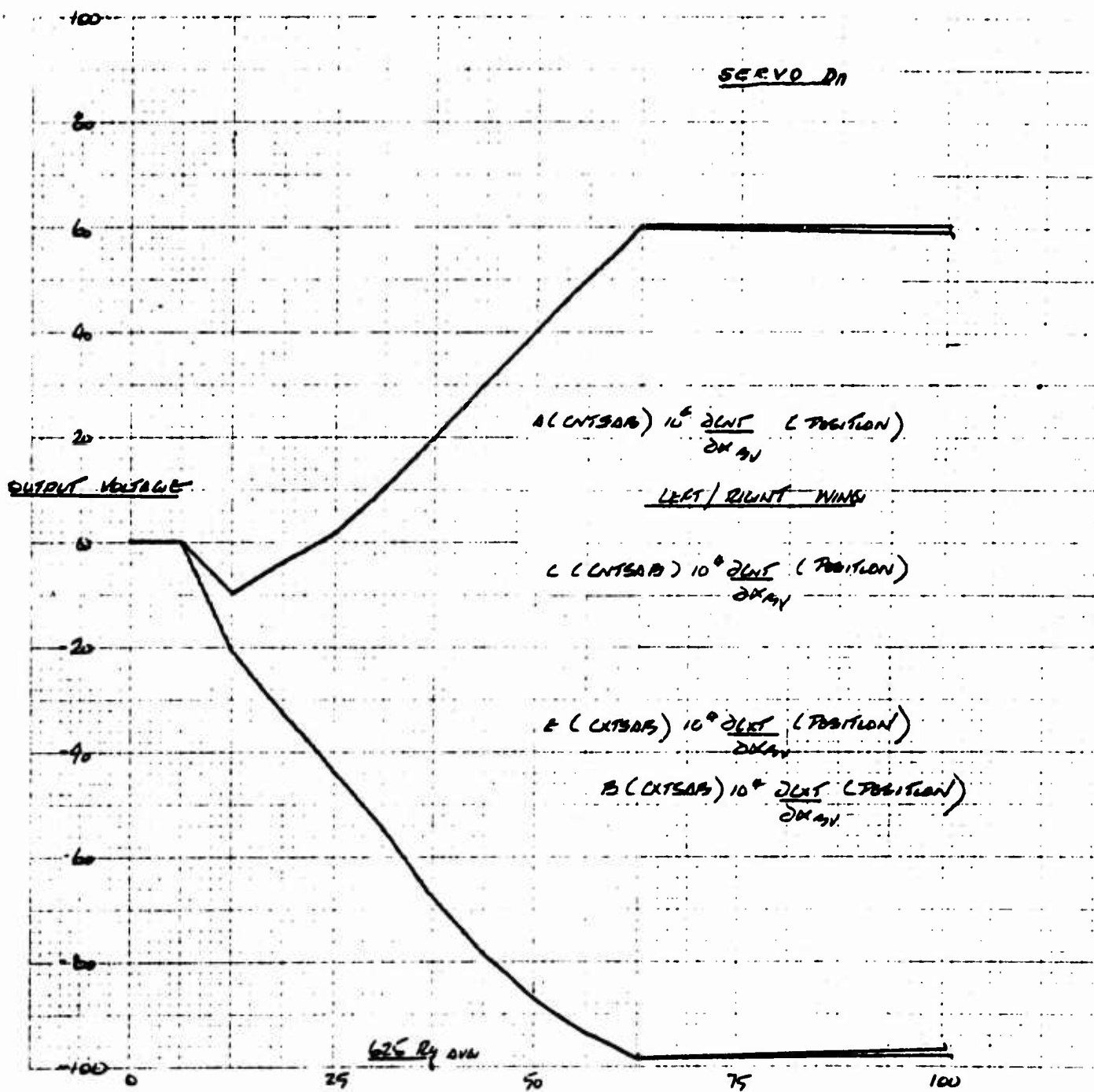OUTPUT $100\ C_p^B / C_{p_{0_2}}$ (CURVATURE)

Figure 65 Plot of 10^4 CNTSAB and 10^4 CXTSAB vs 625 R_q for Both Left and Right Wings (Plots Superimposed)

99

EN	RN	E	P	RS	CODE
0.	0.	0.	0.	0.	CXTSAB
0.	0.	0.	0.	0.	CXTSAB
-0.210000E 02	0.159274E 02	-0.100000E 03	0.500000E 00	0.160000E 02	CXTSAB
-0.327000E 02	0.180268E 03	-0.100000E 03	0.500000E 00	0.180000E 03	CXTSAB
-0.437000E 02	0.150804E 03	-0.100000E 03	0.500000E 00	0.150000E 03	CXTSAB
-0.540000E 02	0.390927E 02	0.	0.500000E 00	0.390000E 02	CXTSAB
-0.668900E 02	0.264175E 02	-0.100000E 03	0.500000E 00	0.270000E 02	CXTSAB
-0.774200E 02	0.180849E 02	-0.100000E 03	0.500000E 00	0.180000E 02	CXTSAB
-0.856300E 02	0.115144E 02	-0.100000E 03	0.500000E 00	0.120000E 02	CXTSAB
-0.914900E 02	0.678989E 01	-0.100000E 03	0.500000E 00	0.680000E 01	CXTSAB
-0.950000E 02	0.267094E 01	-0.100000E 03	0.500000E 00	0.270000E 01	CXTSAB
-0.950000E 02	0.999999E 36	0.	0.	0.999999E 36	CXTSAB
-0.950000E 02	0.999999E 36	0.	0.	0.999999E 36	CXTSAB
-0.950000E 02	0.999999E 36	0.	0.	0.999999E 36	CXTSAB
-0.950000E 02	0.999999E 36	0.	0.	0.999999E 36	CXTSAB
-0.950000E 02	0.999999E 36	0.	0.	0.999999E 36	CXTSAB
-0.950000E 02	0.999999E 36	0.	0.	0.999999E 36	CXTSAB

OUTPUT

$$10^4 \frac{\partial c_{X_T}^s}{\partial \alpha_{\beta_v}}$$

POT PADDER RESISTOR CALCULATION

		(1) E_n	(2) $2E_n$	(3) $-(E_{n+1}+E_{n-1})$	(4) $(1)+(2)$	(5) E	(6) $E-E_n$	(7) 1.875×5	$(6)\div(3)$
E_0	0010	0	0		0				0
E_1	0011	0	0		0				0
E_2	0012	0	0	+10	−	Gnd.			0
E_3	0013	-10	-20	+4	-16	-100	-90	-169	10.6 K.
E_4	0014	-4	-8	+8.5	+.5	Gnd.	+4	+7.5	15 K.
E_5	0015	+1.5	+3	-6	-3	Gnd.	-1.5	-2.81	.936 K.
E_6	0016	+10	+20	-21.5	-1.5	Gnd.	-10	-18.75	+12.5
E_7	0017	+20	+40	-40	0				∞
E_8	0018	+30	+60	-60	0				∞
E_9	0019	+40	+80	-80	0				∞
E_{10}	0020	+50	+100	-100	0				∞
E_{11}	0021	+60	+120	-110	+10	+100	40	+75	7.5 K.
E_{12}	0022	+60	+120	-120	0				∞
E_{13}	0023	+60	+120	-120	0				
E_{14}	0024	+60	+120	-120	0				
E_{15}	0025	+60	+120		0				
E_{16}	0026	+60	+120		0				
E_{17}	0027	+60	+120		0				
E_{18}	0028	+60	+120		0				

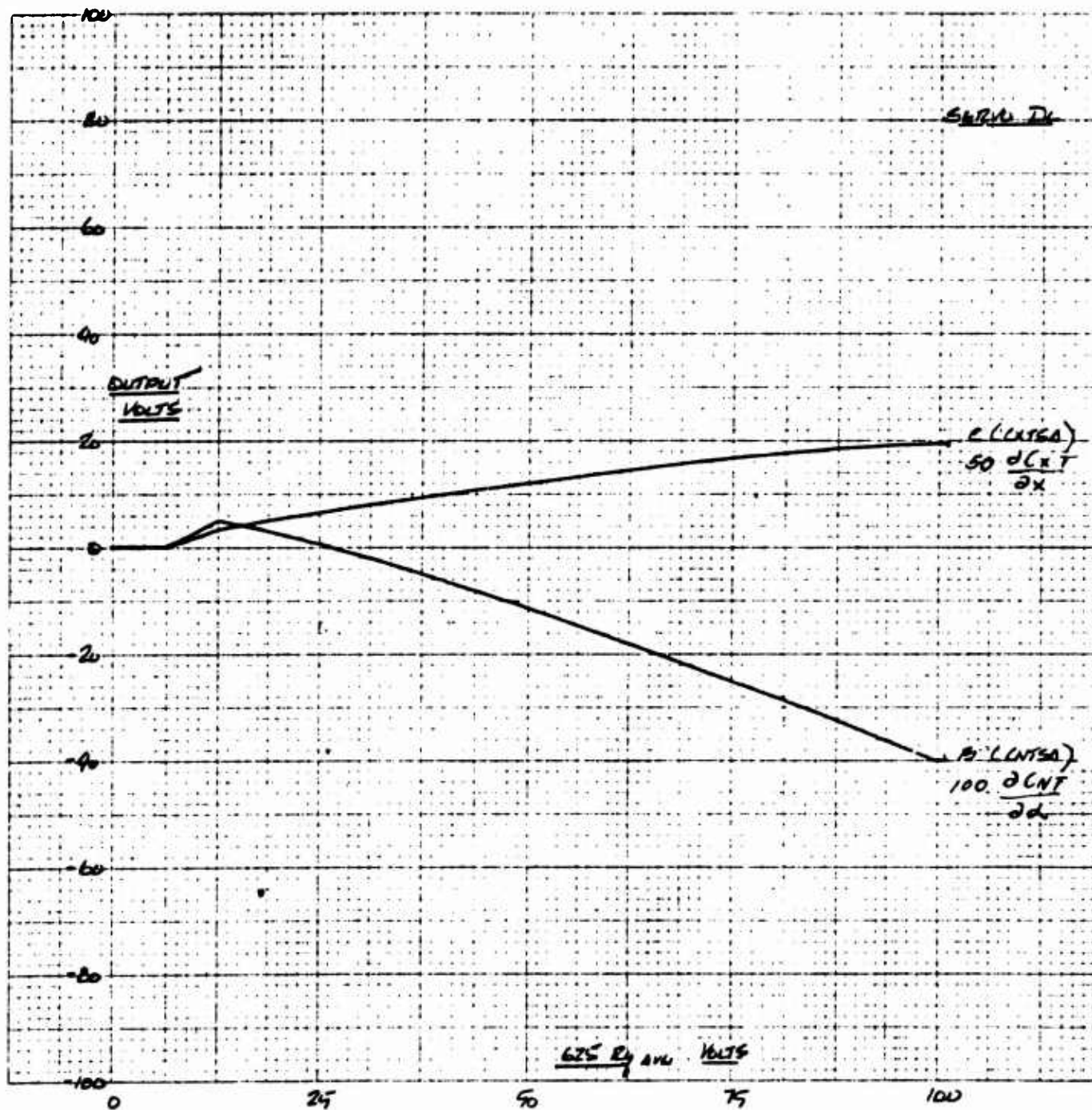$$\left(10^4 \cdot \frac{\partial c_{N_T}^s}{\partial \alpha_{\beta_v}}\right)$$

Figure 66 Plot of 50 CXTSA and 100 CNTSA vs 625 R_q (Both Wings Identical)

POT PADDER RESISTOR CALCULATION

		(1)	(2)	(3)	(1)+(2)	(4)	(5)	(6)	(7)
		E_n	$2E_n$	$-(E_{n+1}+E_{n-1})$		E	$E-E_n$	1.875×5	(6)-(3)
E_0	0010	0	0	0					
E_1	0011	0	0	0					
E_2	0012	0	0	-3.3		Gnd.	-	-	0
E_3	0013	3.3	6.6	-5	+1.6	+100	96.7	179	112K
E_4	0014	5	10	-9.8	+.2	+100	95	176	880
E_5	0015	6.5	13	-13	0	-	-		∞
E_6	0016	8	16	15.8	+0.2	+100	92	170	850
E_7	0017	9.3	18.6	-18.7	-.10	Gnd	-9.3	17.2	172
E_8	0018	10.7	2.4	-21.3	+.10	+100	89.3	165	165 M.
E_9	0019	12	24	-23.9	+.10	+100	88	163	1.63M.
E_{10}	0020	13.2	26.4	-26.5	-.10	Gnd.	-13.2	-24.4	2.44 K.
E_{11}	0021	14.5	29	-28.8	+.2	+100	85.5	160	800 K.
E_{12}	0022	15.6	31.2	-31.2	0				∞
E_{13}	0023	16.7	22.3	-33.2	+.2	+100	+83.3	155	775 K.
E_{14}	0024	17.6	35.2	-35.2	0				∞
E_{15}	0025	18.5	27.	-36.6	+.4	+100	81.5	151	378
E_{16}	0026	19.0	38	-37.8	+.20	+100	81	150	750 K.
E_{17}	0027	19.3	28.5	-38.3	+.30	+100	80.7	149	500 K.

$$\left(1000\ \frac{\partial^C X_T^s}{\partial \alpha}\right)$$

JOB NO. 1014 POT PADDER RESISTOR CALCULATION   01JUL63

EN	RN	E	P	RS	CODE
0.	0.	0.	0.	0.	CNTSA
0.	0.	0.	0.	0.	CNTSA
0.500000E 01	0.254464E 02	0.100000E 03	0.500000E 00	0.240000E 02	CNTSA
0.300000E 01	0.545679E 03	0.100000E 03	0.500000E 00	0.560000E 03	CNTSA
0.666700E 00	0.558638E 03	0.100000E 03	0.500000E 00	0.560000E 03	CNTSA
-0.200000E 01	0.112511E 02	0.	0.500000E 00	0.110000E 02	CNTSA
-0.500000E 01	0.750000E 02	0.	0.500000E 00	0.750000E 02	CNTSA
-0.812500E 01	0.190430E 03	0.	0.500000E 00	0.200000E 03	CNTSA
-0.113300E 02	0.249926E 03	0.	0.500000E 00	0.240000E 03	CNTSA
-0.146200E 02	0.304583E 03	0.	0.500000E 00	0.300000E 03	CNTSA
-0.180000E 02	0.421878E 03	0.	0.500000E 00	0.430000E 03	CNTSA
-0.214600E 02	0.502966E 03	0.	0.500000E 00	0.510000E 03	CNTSA
-0.250000E 02	0.585942E 03	0.	0.500000E 00	0.560000E 03	CNTSA
-0.286200E 02	0.596249E 03	0.	0.500000E 00	0.620000E 03	CNTSA
-0.323300E 02	0.757735E 03	0.	0.500000E 00	0.750000E 03	CNTSA
-0.361200E 02	0.752499E 03	0.	0.500000E 00	0.750000E 03	CNTSA
-0.400000E 02	0.289948E 02	-0.100000E 03	0.500000E 00	0.300000E 02	CNTSA

OUTPUT

$$2000\ \frac{\partial^C N_T}{\partial \alpha}$$
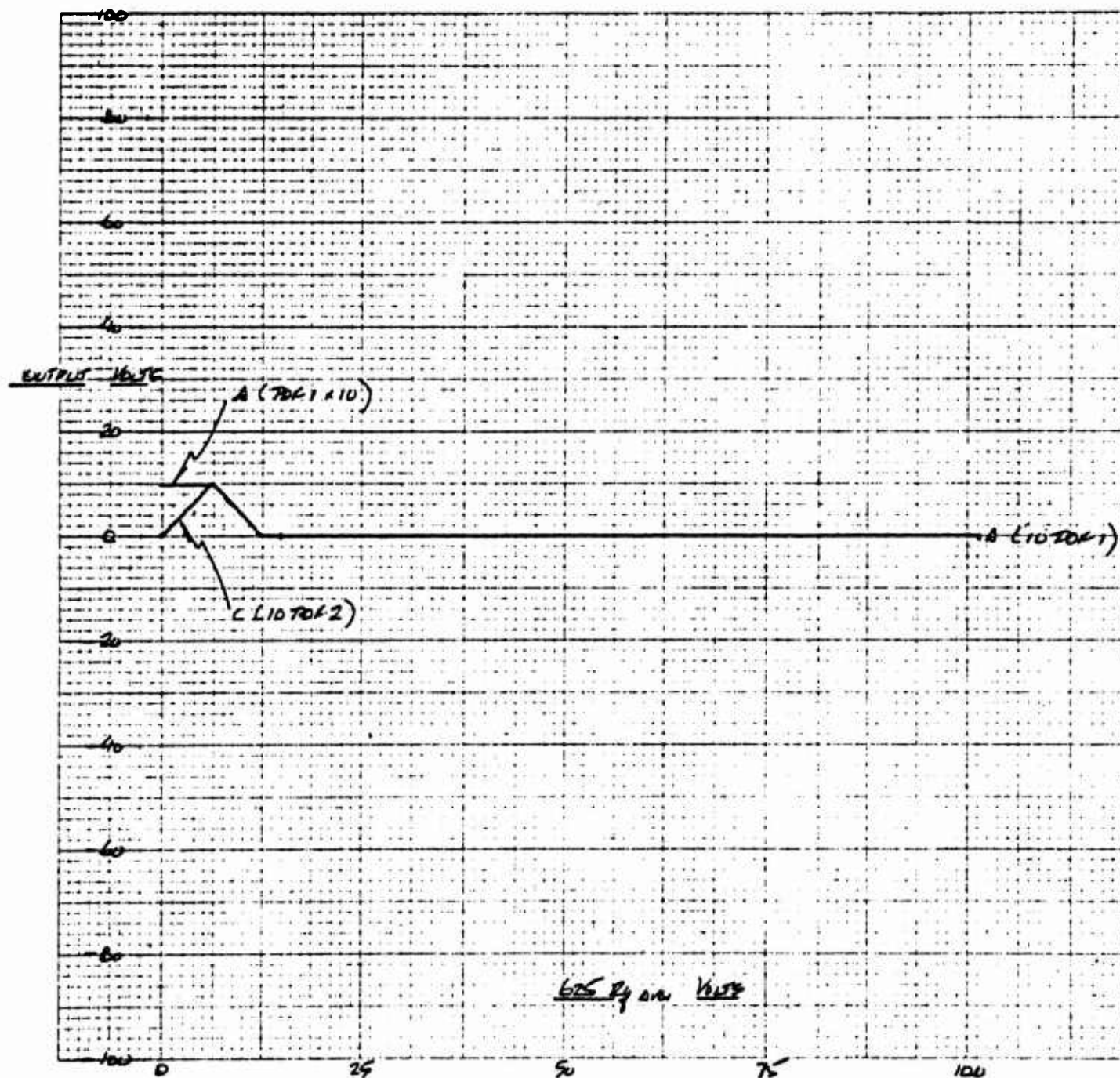
Figure 67 Plot of 10 POF No. 1 and 10 POF No. 2 vs 625 R_q

JOB NO. 1014 POT PADDER RESISTOR CALCULATION   01JUL63

EN	RN	E	P	RS	CODE
0.100000E 02	0.999999E 36	0.	0.	0.999999E 36	POF 1
0.100000E 02	0.168750E 02	0.100000E 03	0.500000E 00	0.160000E 02	POF 1
0.	0.	0.	0.	0.	POF 1
-0.	0.	0.	0.	0.	POF 1
-0.	0.	0.	0.	0.	POF 1
-0.	0.	0.	0.	0.	POF 1
-0.	0.	0.	0.	0.	POF 1
-0.	0.	0.	0.	0.	POF 1
-0.	0.	0.	0.	0.	POF 1
-0.	0.	0.	0.	0.	POF 1
-0.	0.	0.	0.	0.	POF 1
-0.	0.	0.	0.	0.	POF 1
-0.	0.	0.	0.	0.	POF 1
-0.	0.	0.	0.	0.	POF 1
-0.	0.	0.	0.	0.	POF 1
-0.	0.	0.	0.	0.	POF 1
-0.	0.	0.	0.	0.	POF 1

OUTPUT   10 POF 1

JOB NO. 1014 POT PADDER RESISTOR CALCULATION   01JUL63

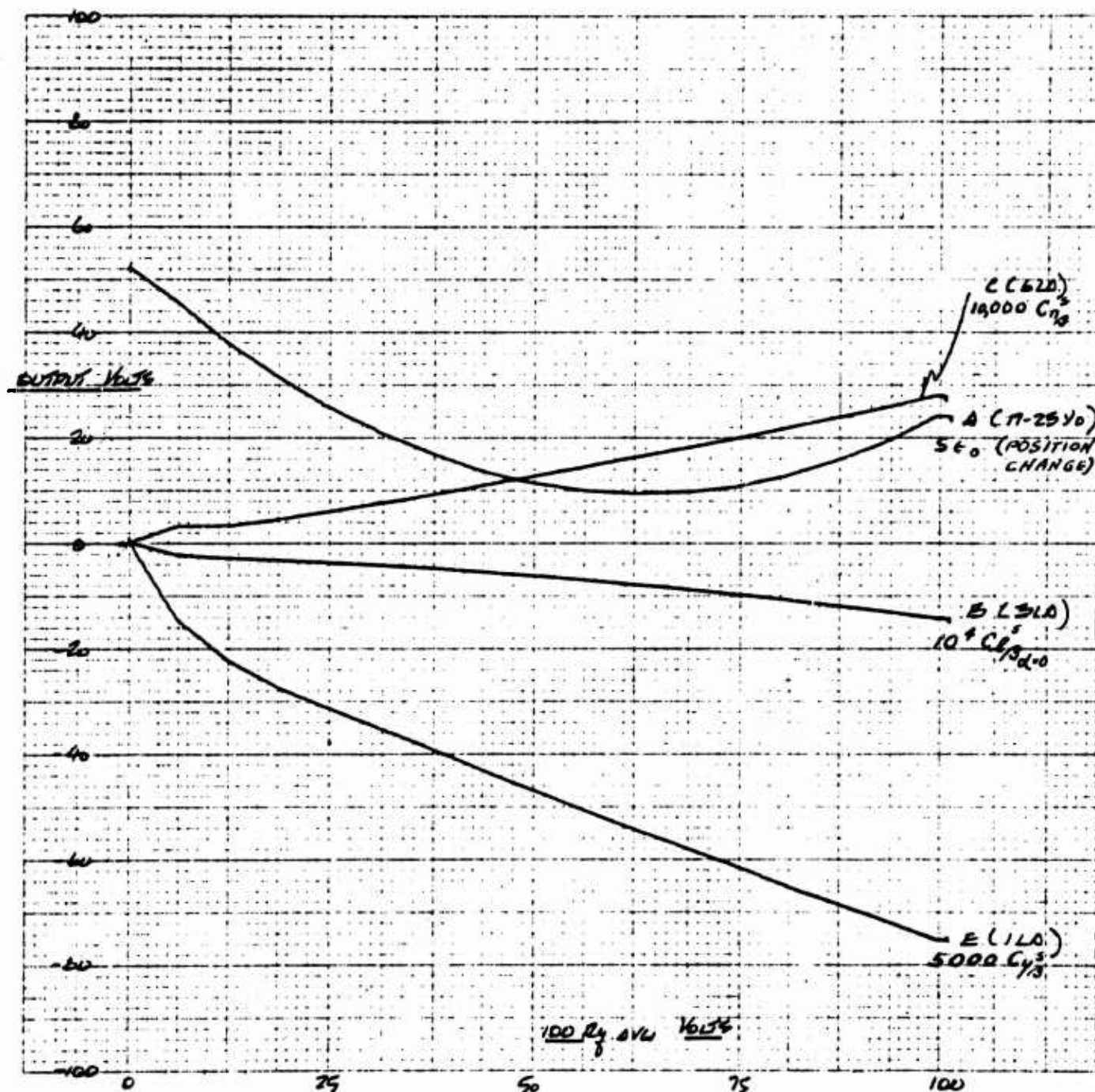| EN	RN	E	P	RS	CODE
0.	0.	0.	0.	0.	POF 2
0.100000E 02	0.843750E 01	0.100000E 03	0.100000E 01	0.820000E 01	POF 2
0.	0.	0.	0.	0.	POF 2
-0.866700E 01	0.128373E 03	-0.100000E 03	0.500000E 00	0.1300C0E 03	POF 2
-0.160000E 02	0.118155E 03	-0.100000E 03	0.500000E 00	0.120000E 03	POF 2
-0.220000E 02	0.109962E 03	-0.100000E 03	0.500000E 00	0.110000E 03	POF 2
-0.266700E 02	0.102607E 03	-0.100000E 03	0.500000E 00	0.100000E 03	POF 2
-0.300000E 02	0.986842E 02	-0.100000E 03	0.500000E 00	0.100000E 03	POF 2
-0.320000E 02	0.958646E 02	-0.100000E 03	0.500000E 00	0.100000E 03	POF 2
-0.326700E 02	0.942118E 02	-0.100000E 03	0.500000E 00	0.910000E 02	POF 2
-0.320000E 02	0.958646E 02	-0.100000E 03	0.500000E 00	0.100000E 03	POF 2
-0.300000E 02	0.986842E 02	-0.100000E 03	0.500000E 00	0.100000E 03	POF 2
-0.266700E 02	0.102607E 03	-0.100000E 03	0.500000E 00	0.100000E 03	POF 2
-0.220000E 02	0.109962E 03	-0.100000E 03	0.500000E 00	0.110000E 03	POF 2
-0.160000E 02	0.118155E 03	-0.100000E 03	0.500000E 00	0.120000E 03	POF 2
-0.866700E 01	0.128374E 03	-0.100000E 03	0.500000E 00	0.130000E 03	POF 2
-0.996900E-05	0.215667E-05	0.	0.500000E 00	-0.	POF 2

OUTPUT   10 POF 2

Figure 68 Plot of 5000 $C_{Y_\beta}^s$, $10^4 C_{l_\beta}^s$, (at $a = 0°$), 10,000 $C_{n_\beta}^s$ and The Constant Term of the Polynomial Fit to the Downwash Angle Plotted vs 100 R_q

EN	RN	E	P	RS	CODE
0.	0.	0.	0.	0.	
0.317500E 01	0.567157E 02	0.100000E 03	0.500000E 00	0.560000E 02	
0.314900E 01	0.494504E 01	0.	0.500000E 00	0.510000E 01	
0.431700E 01	0.204403E 02	0.	0.500000E 00	0.200000E 02	
0.588100E 01	0.262545E 03	0.	0.500000E 00	0.270000E 03	
0.748700E 01	0.319049E 03	0.	0.500000E 00	0.330000E 03	
0.913700E 01	0.398416E 03	0.	0.500000E 00	0.390000E 03	
0.108300E 02	0.432048E 03	0.	0.500000E 00	0.430000E 03	
0.125700E 02	0.785626E 03	0.	0.500000E 00	0.820000E 03	
0.143400E 02	0.448125E 03	0.	0.500000E 00	0.430000E 03	
0.161700E 02	0.101062E 04	0.	0.500000E 00	0.100000E 04	
0.180300E 02	0.676129E 03	0.	0.500000E 00	0.680000E 03	
0.199400E 02	0.934688E 03	0.	0.500000E 00	0.910000E 03	
0.218900E 02	0.102609E 04	0.	0.500000E 00	0.100000E 04	
0.238800E 02	0.895505E 03	0.	0.500000E 00	0.910000E 03	
0.259200E 02	0.121500E 04	0.	0.500000E 00	0.120000E 04	
0.280000E 02	0.649038E 02	0.100000E 03	0.500000E 00	0.620000E 02	

OUTPUT $10^4 C_{n_\beta}^s$

EN	RN	E	P	RS	CODE
0.520000E 02	0.132159E 02	0.100000E 03	0.500000E 00	0.130000E 02	17-23 Y$_o$
0.451900E 02	0.116763E 03	0.100000E 03	0.500000E 00	0.120000E 03	17-23
0.375000E 02	0.502233E 02	0.	0.500000E 00	0.510000E 02	17-23
0.312100E 02	0.100894E 03	0.	0.500000E 00	0.100000E 03	17-23
0.295000E 02	0.262500E 02	0.	0.500000E 00	0.560000E 02	17-23
0.204400E 02	0.450000E 02	0.	0.500000E 00	0.430000E 02	17-23
0.166400E 02	0.358621E 02	0.	0.500000E 00	0.360000E 02	17-23
0.135100E 02	0.298015E 02	0.	0.500000E 00	0.300000E 02	17-23
0.112300E 02	0.242863E 02	0.	0.500000E 00	0.240000E 02	17-23
0.981700E 01	0.214532E 02	0.	0.500000E 00	0.220000E 02	17-23
0.926200E 01	0.201699E 02	0.	0.500000E 00	0.200000E 02	17-23
0.956800E 01	0.209579E 02	0.	0.500000E 00	0.200000E 02	17-23
0.107300E 02	0.231783E 02	0.	0.500000E 00	0.240000E 02	17-23
0.127600E 02	0.278198E 02	0.	0.500000E 00	0.270000E 02	17-23
0.156500E 02	0.345221E 02	0.	0.500000E 00	0.360000E 02	17-23
0.193900E 02	0.417808E 02	0.	0.500000E 00	0.430000E 02	17-23
0.240000E 02	0.309111E 02	0.100000E 03	0.500000E 00	0.300000E 02	17-23

OUTPUT β_{ϵ_0}

JOB NO. 1014 POT PADDER RESISTOR CALCULATION   5/27/63

EN	RN	E	P	RS	CODE
0.	0.	0.	0.	0.	
-0.250600E 01	0.908555E 02	-0.100000E 03	0.500000E 00	0.910000E 02	
-0.300000E 01	0.142090E 04	-0.100000E 03	0.500000E 00	0.150000E 04	
-0.336600E 01	0.928126E 02	0.	0.500000E 00	0.910000E 02	
-0.380000E 01	0.104779E 03	0.	0.500000E 00	0.100000E 03	
-0.430200E 01	0.120392E 03	0.	0.500000E 00	0.120000E 03	
-0.487100E 01	0.132364E 03	0.	0.500000E 00	0.130000E 03	
-0.550900E 01	0.154170E 03	0.	0.500000E 00	0.150000E 03	
-0.621400E 01	0.171342E 03	0.	0.500000E 00	0.180000E 03	
-0.698700E 01	0.189864E 03	0.	0.500000E 00	0.180000E 03	
-0.782900E 01	0.222415E 03	0.	0.500000E 00	0.220000E 03	
-0.873700E 01	0.237418E 03	0.	0.500000E 00	0.240000E 03	
-0.971400E 01	0.263967E 03	0.	0.500000E 00	0.270000E 03	
-0.107600E 02	0.315235E 03	0.	0.500000E 00	0.330000E 03	
-0.118700E 02	0.317946E 03	0.	0.500000E 00	0.330000E 03	
-0.130500E 02	0.349554E 03	0.	0.500000E 00	0.360000E 03	
-0.143000E 02	0.128550E 03	-0.100000E 03	0.500000E 00	0.130000E 03	

OUTPUT $10^4\,C_{l_\beta}^{s}$

JOB NO. 1014 POT PADDER RESISTOR CALCULATION   5/27/63

EN	RN	E	P	RS	CODE
0.	0.	0.	0.	0.	
-0.150600E 02	0.215803E 02	-0.100000E 03	0.500000E 00	0.220000E 02	
-0.227400E 02	0.538522E 02	-0.100000E 03	0.500000E 00	0.560000E 02	
-0.277300E 02	0.134165E 03	-0.100000E 03	0.500000E 00	0.130000E 03	
-0.317100E 02	0.213405E 04	-0.100000E 03	0.500000E 00	0.220000E 04	
-0.356300E 02	0.201155E 04	-0.100000E 03	0.500000E 00	0.200000E 04	
-0.394900E 02	0.189092E 04	-0.100000E 03	0.500000E 00	0.180000E 04	
-0.432900E 02	0.212662E 04	-0.100000E 03	0.500000E 00	0.220000E 04	
-0.470400E 02	0.165499E 04	-0.100000E 03	0.500000E 00	0.160000E 04	
-0.507300E 02	0.184765E 04	-0.100000E 03	0.500000E 00	0.180000E 04	
-0.543700E 02	0.142593E 04	-0.100000E 03	0.500000E 00	0.150000E 04	
-0.579500E 02	0.131405E 04	-0.100000E 03	0.500000E 00	0.130000E 04	
-0.614700E 02	0.144487E 04	-0.100000E 03	0.500000E 00	0.150000E 04	
-0.649400E 02	0.109560E 04	-0.100000E 03	0.500000E 00	0.110000E 04	
-0.683500E 02	0.989071E 03	-0.100000E 03	0.500000E 00	0.100000E 04	
-0.717000E 02	0.106123E 04	-0.100000E 03	0.500000E 00	0.110000E 04	
-0.750000E 02	0.142045E 02	-0.100000E 03	0.500000E 00	0.150000E 02	

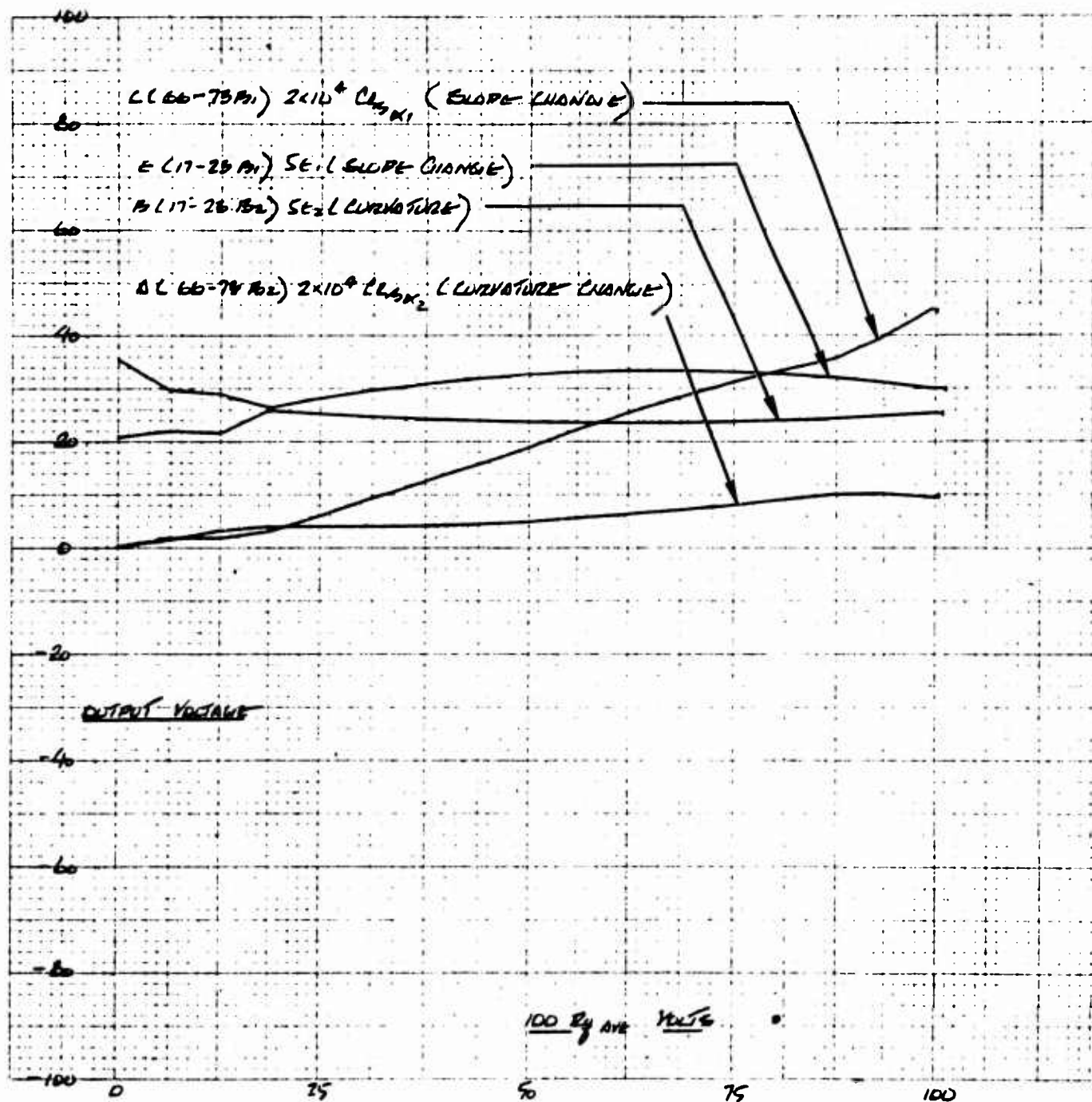OUTPUT $5000\,C_{Y_\beta}^{s}$

Figure 69 Plot of Twenty Thousand Times the Linear Coefficient
Of the Polynomial Fit to $C_{l_\beta}{}^S$, Five Times the Linear
Coefficient of the Polynomial Fit to ϵ, Five Times the
Second Degree Coefficient of the Polynomial Fit to ϵ, and
Twenty Thousand Times the Second Degree Coefficient of
The Polynomial Fit to $C_{l_\beta}{}^S$, Plotted vs 100 R_q

EN	RN	E	P	RS	CODE
0.	0.	0.	0.	0.	66-73 B_1
0.166400E 01	0.109881E 03	0.100000E 03	0.500000E 00	0.110000E 03	66-73
0.165000E 01	0.263074E 01	0.	0.500000E 00	0.270000E 01	66-73
0.281200E 01	0.286238E 01	0.	0.500000E 00	0.300000E 01	66-73
0.581600E 01	0.350643E 02	0.	0.500000E 00	0.360000E 02	66-73
0.913100E 01	0.304249E 04	0.100000E 03	0.500000E 00	0.300000E 04	66-73
0.123900E 02	0.335241E 04	0.100000E 03	0.500000E 00	0.330000E 04	66-73
0.156000E 02	0.263750E 04	0.100000E 03	0.500000E 00	0.270000E 04	66-73
0.187500E 02	0.152854E 03	0.	0.500000E 00	0.150000E 03	66-73
0.221300E 02	0.730032E 03	0.100000E 03	0.500000E 00	0.750000E 03	66-73
0.253100E 02	0.666875E 03	0.100000E 03	0.500000E 00	0.680000E 03	66-73
0.282800E 02	0.672374E 03	0.100000E 03	0.500000E 00	0.680000E 03	66-73
0.310500E 02	0.275066E 03	0.100000E 03	0.500000E 00	0.270000E 03	66-73
0.333500E 02	0.104140E 04	0.100000E 03	0.500000E 00	0.100000E 04	66-73
0.355300E 02	0.391875E 02	0.	0.500000E 00	0.390000E 02	66-73
0.394100E 02	0.432127E 02	0.	0.500000E 00	0.430000E 02	66-73
0.450000E 02	0.184481E 02	0.100000E 03	0.500000E 00	0.180000E 02	66-73

OUTPUT $\qquad$ $2 \times 10^4 \, C_{l_{\beta_{\alpha_1}}}$ (SLOPE CHANGE)

EN	RN	E	P	RS	CODE
0.354400E 02	0.201750E 02	0.100000E 03	0.500000E 00	0.200000E 02	17-23 B_1
0.294400E 02	0.101284E 02	0.	0.500000E 00	0.100000E 02	17-23
0.288900E 02	0.724626E 02	0.100000E 03	0.500000E 00	0.750000E 02	17-23
0.265000E 02	0.122383E 02	0.	0.500000E 00	0.120000E 02	17-23
0.281700E 02	0.561172E 03	0.100000E 03	0.500000E 00	0.560000E 03	17-23
0.296000E 02	0.549979E 03	0.100000E 03	0.500000E 00	0.560000E 03	17-23
0.307900E 02	0.564212E 03	0.100000E 03	0.500000E 00	0.560000E 03	17-23
0.317500E 02	0.533203E 03	0.100000E 03	0.500000E 00	0.510000E 03	17-23
0.324700E 02	0.550515E 03	0.100000E 03	0.500000E 00	0.560000E 03	17-23
0.329600E 02	0.523750E 03	0.100000E 03	0.500000E 00	0.510000E 03	17-23
0.332100E 02	0.521797E 03	0.100000E 03	0.500000E 00	0.510000E 03	17-23
0.332200E 02	0.544491E 03	0.100000E 03	0.500000E 00	0.560000E 03	17-23
0.330000E 02	0.523436E 03	0.100000E 03	0.500000E 00	0.510000E 03	17-23
0.325400E 02	0.549944E 03	0.100000E 03	0.500000E 00	0.560000E 03	17-23
0.318500E 02	0.511125E 03	0.100000E 03	0.500000E 00	0.510000E 03	17-23
0.309100E 02	0.588836E 03	0.100000E 03	0.500000E 00	0.560000E 03	17-23
0.297500E 02	0.480873E 02	0.	0.500000E 00	0.470000E 02	17-23

OUTPUT $\qquad$ b_{ϵ_1} (SLOPE CHANGE)

EN	RN	L	P	RS	CODE	
0.207200E 02	0.329237E 02	0.	0.500000E 00	0.310000E 02	17-23	B₂
0.219000E 02	0.898389E 02	0.100000E 03	0.500000E 00	0.910000E 02	17-23	
0.214500E 02	0.857543E 01	0.	0.500000E 00	0.820000E 01	17-23	
0.256900E 02	0.286101E 02	0.100000E 03	0.500000E 00	0.300000E 02	17-23	
0.250600E 02	0.522085E 03	0.	0.500000E 00	0.510000E 03	17-23	
0.245200E 02	0.459750E 03	0.	0.500000E 00	0.470000E 03	17-23	
0.240800E 02	0.451500E 03	0.	0.500000E 00	0.470000E 03	17-23	
0.237400E 02	0.494582E 03	0.	0.500000E 00	0.510000E 03	17-23	
0.234900E 02	0.400397E 03	0.	0.500000E 00	0.390000E 03	17-23	
0.233500E 02	0.466460E 03	0.	0.500000E 00	0.470000E 03	17-23	
0.233000E 02	0.436875E 03	0.	0.500000E 00	0.430000E 03	17-23	
0.233500E 02	0.437813E 03	0.	0.500000E 00	0.430000E 03	17-23	
0.235000E 02	0.489585E 03	0.	0.500000E 00	0.470000E 03	17-23	
0.237400E 02	0.404659E 03	0.	0.500000E 00	0.390000E 03	17-23	
0.240900E 02	0.501877E 03	0.	0.500000E 00	0.510000E 03	17-23	
0.245300E 02	0.459938E 03	0.	0.500000E 00	0.470000E 03	17-23	
0.250700E 02	0.260174E 03	0.100000E 03	0.500000E 00	0.270000E 03	17-23	

OUTPUT δ_{ϵ_2} (CURVATURE)

EN	RN	E	P	RS	CODE	
0.	0.	0.	0.	0.	66-73	B₂
0.132800E 01	0.693593E 01	0.	0.500000E 00	0.680000E 01	66-73	
0.301500E 01	0.196591E 03	0.100000E 03	0.500000E 00	0.200000E 03	66-73	
0.377700E 01	0.250581E 03	0.100000E 03	0.500000E 00	0.240000E 03	66-73	
0.381900E 01	0.644069E 04	0.100000E 03	0.500000E 00	0.620000E 04	66-73	
0.383300E 01	0.532361E 02	0.	0.500000E 00	0.510000E 02	66-73	
0.398200E 01	0.548989E 02	0.	0.500000E 00	0.560000E 02	66-73	
0.426700E 01	0.588281E 02	0.	0.500000E 00	0.560000E 02	66-73	
0.468800E 01	0.296959E 02	0.	0.500000E 00	0.300000E 02	66-73	
0.540500E 01	0.198713E 03	0.	0.500000E 00	0.200000E 03	66-73	
0.617300E 01	0.226949E 03	0.	0.500000E 00	0.220000E 03	66-73	
0.699200E 01	0.262200E 03	0.	0.500000E 00	0.270000E 03	66-73	
0.786100E 01	0.788202E 02	0.	0.500000E 00	0.820000E 02	66-73	
0.891700E 01	0.139330E 04	0.	0.500000E 00	0.130000E 04	66-73	
0.998500E 01	0.184861E 03	0.100000E 03	0.500000E 00	0.180000E 03	66-73	
0.101400E 02	0.183139E 03	0.100000E 03	0.500000E 00	0.180000E 03	66-73	
0.937500E 01	0.229779E 02	0.	0.500000E 00	0.220000E 02	66-73	

OUTPUT $2 \times 10^4 \, C_{l_{\beta_{\alpha_2}}}$ (CURVATURE)
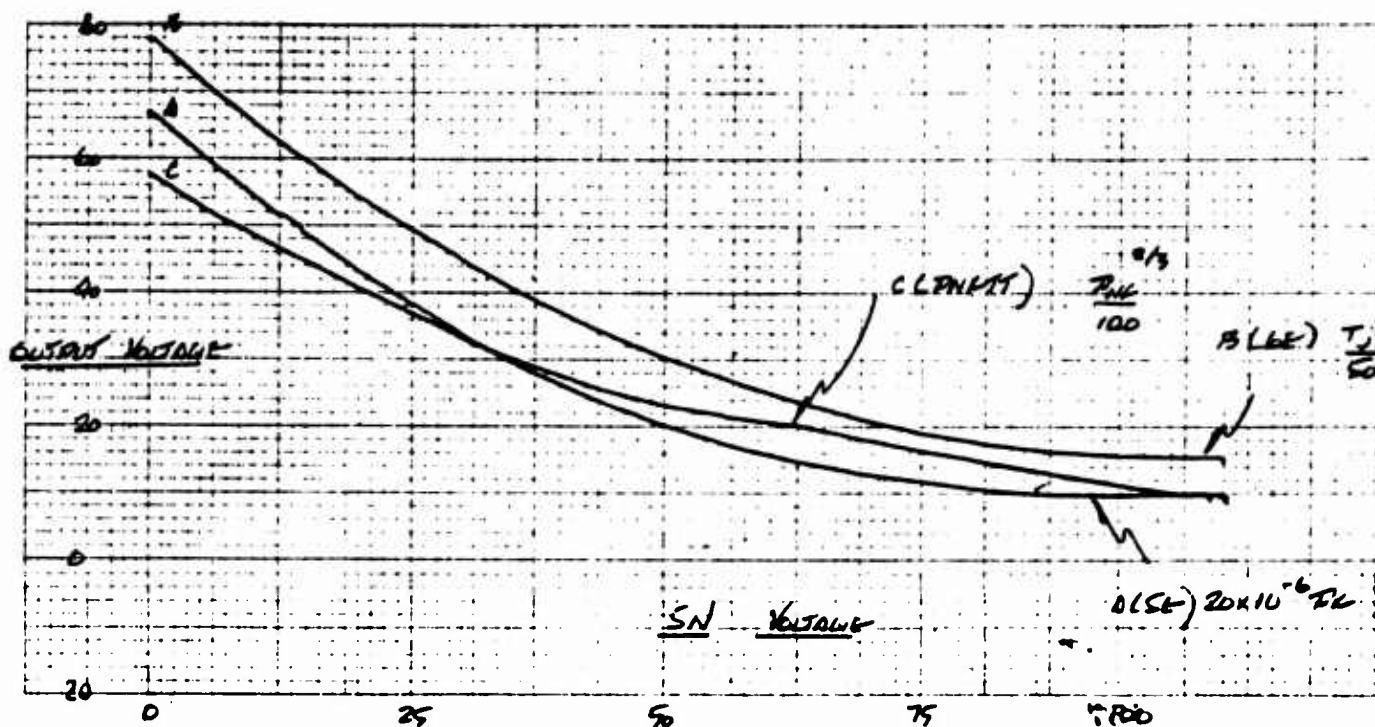
Figure 70 $(P_{NF})^{2/3}/100$, $T_J/50$ and $2 \times 10^{-5} P_F$ vs $5 N$

POT PADDER RESISTOR CALCULATION

		(1) E_n	(2) $-2 E_n$	(3) $+E_{n-1}+$ E_{n+1}	(4) $(2)+(3)$	E	(5) $E_n - E$	R_n	
E_0	0010	58	-116						
E_1	0011	58	-116	110	-6	+	-42	13.15	
E_2	0012	52	-104	105	+1	0	52	97.5	
E_3	0013	47	-94	94	0	0	47	Open	
E_4	0014	42	-84	84.25	+.25	0	42	315.0	$\left(\dfrac{P_{NF}}{100}\right)^{2/3}$
E_5	0015	37.25	-74.5	74.75	+.25	0	37.25	279.1	
E_6	0016	32.75	-65.5	66.5	+1	0	37.75	61.25	
E_7	0017	29.25	-58.5	58.75	+.25	0	29.25	219.5	
E_8	0018	26.00	-52	52.75	+.75	0	26	65	
E_9	0019	23.50	-47	47.7	+.70	0	23.5	63	
E_{10}	0020	21.70	-43.4	44	+.60	0	21.7	67.2	
E_{11}	0021	20.50	-41	40.2	-.80	+	-79.5	186	
E_{12}	0022	18.50	-37	37.25	+.25	0	18.5	139	
E_{13}	0023	16.75	-33.5	33.5	0	0	16.75	Open	
E_{14}	0024	15	-30	30.00	0	0	13.25	Open	
E_{15}	0025	13.25	-26.5	26.5	0	0	13.25	Open	
E_{16}	0026	11.50	-23	23.25	+.25	0	11.5	86.4	
E_{17}	0027	10	-20	21.50	+1.50	0	10	12.5 K.	
E_{18}	0028	10	-20						

EN	RN	E	P	RS	CODE
0.784000E 02	0.495716E 01	0.100000E 03	0.500000E 00	0.510000E 01	6E
0.702300E 02	0.215871E 03	0.	0.500000E 00	0.220000E 03	
0.626700E 02	0.192633E 03	0.	0.500000E 00	0.200000E 03	
0.557200E 02	0.121483E 03	0.	0.500000E 00	0.120000E 03	
0.496300E 02	0.163257E 03	0.	0.500000E 00	0.160000E 03	
0.441100E 02	0.168788E 03	0.	0.500000E 00	0.160000E 03	
0.390800E 02	0.152656E 03	0.	0.500000E 00	0.150000E 03	
0.345300E 02	0.132130E 03	0.	0.500000E 00	0.130000E 03	
0.304700E 02	0.114262E 03	0.	0.500000E 00	0.110000E 03	
0.269100E 02	0.105117E 03	0.	0.500000E 00	0.110000E 03	
0.238300E 02	0.930860E 02	0.	0.500000E 00	0.910000E 02	
0.212300E 02	0.796125E 02	0.	0.500000E 00	0.820000E 02	
0.191300E 02	0.732016E 02	0.	0.500000E 00	0.750000E 02	
0.175200E 02	0.684376E 02	0.	0.500000E 00	0.680000E 02	
0.163900E 02	0.627168E 02	0.	0.500000E 00	0.620000E 02	
0.157500E 02	0.602679E 02	0.	0.500000E 00	0.620000E 02	
0.156000E 02	0.195000E 03	0.	0.500000E 00	0.200000E 03	

OUTPUT $T_{1/50}$

EN	RN	E	P	RS	CODE
0.676000E 02	0.739051E 01	0.100000E 03	0.500000E 00	0.750000E 01	5E
0.593800E 02	0.176726E 03	0.	0.500000E 00	0.180000E 03	
0.517900E 02	0.149394E 03	0.	0.500000E 00	0.150000E 03	
0.448500E 02	0.133482E 03	0.	0.500000E 00	0.130000E 03	
0.385400E 02	0.112910E 03	0.	0.500000E 00	0.110000E 03	
0.328700E 02	0.733705E 02	0.	0.500000E 00	0.750000E 02	
0.280400E 02	0.834524E 02	0.	0.500000E 00	0.820000E 02	
0.238400E 02	0.859615E 02	0.	0.500000E 00	0.820000E 02	
0.201600E 02	0.687272E 02	0.	0.500000E 00	0.680000E 02	
0.170300E 02	0.614063E 02	0.	0.500000E 00	0.620000E 02	
0.144200E 02	0.500694E 02	0.	0.500000E 00	0.510000E 02	
0.123500E 02	0.436910E 02	0.	0.500000E 00	0.430000E 02	
0.108100E 02	0.376044E 02	0.	0.500000E 00	0.390000E 02	
0.980900E 01	0.346363E 02	0.	0.500000E 00	0.360000E 02	
0.933900E 01	0.327914E 02	0.	0.500000E 00	0.330000E 02	
0.940300E 01	0.330781E 02	0.	0.500000E 00	0.310000E 02	
0.100000E 02	0.282663E 03	0.100000E 03	0.500000E 00	0.270000E 03	

OUTPUT $20 \times 10^{-6}\ P_F$
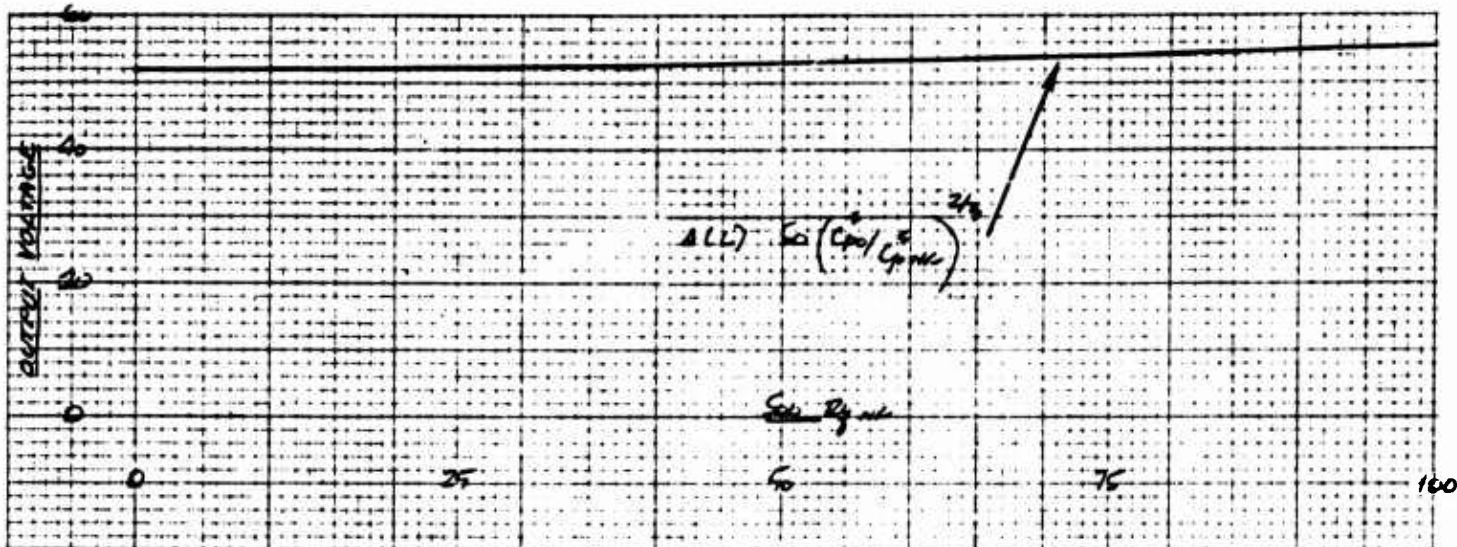
Figure 71 $50\left(\dfrac{Cp^s_{o_{NF}}}{Cp^s_{NF}}\right)^{2/3}$ vs $500\ R_{q_{NF}}$

POT PADDER RESISTOR CALCULATION

		(1) E_n	(2) $-2E_n$	(3) $+E_{n-1} + E_{n+1}$	(4) (2)+(3)	E	(5) $E_n - E$	R_n
E_0	0010	50	-100	-	-	-	-	-
E_1	0011	50	-100	100.115	+.115	0	50	815 K.
E_2	0012	50.115	-100.2	100.20	-.03	+	-49.885	3.118 M.
E_3	0013	50.2	-100.4	100.44	+.04	0	50.2	2.353 M.
E_4	0014	50.325	-100.65	100.625	-.025	+	-49.675	3.73 M.
E_5	0015	50.425	-100.85	100.90	+.050	0	50.425	1.89 M.
E_6	0016	50.575	-101.15	101.175	+.025	0	50.575	379 M.
E_7	0017	50.75	-101.50	101.475	-.025	+	-49.25	3.69 M.
E_8	0018	50.9	-101.81	101.875	+.075	0	50.9	1.27 M.
E_9	0019	51.125	-102.275	102.275	+.025	0	51.125	3.83 M.
E_{10}	0020	51.375	-102.75	102.775	+.025	0	51.375	3.85 M.
E_{11}	0021	51.65	-103.3	103.325	+.025	0	51.650	3.87 M.
E_{12}	0022	51.95	-103.9	103.850	-.050	+	-48.05	1.8 M.
E_{13}	0023	52.50	-104.4	104.55	+.150	0	52.2	653 K.
E_{14}	0024	52.60	-105.2	105.10	-.100	+	-47.40	894 K.
E_{15}	0025	52.90	-105.8	105.875	+.075	0	52.9	1.33 M.
E_{16}	0026	53.275	-106.55	106.50	-.050	+	-46.725	1.75 M.
E_{17}	0027	53.60	-107.2	106.875	-.325	+	-46.40	267 K.
E_{18}	0028	53.60	-107.2	-	-	-	-	-
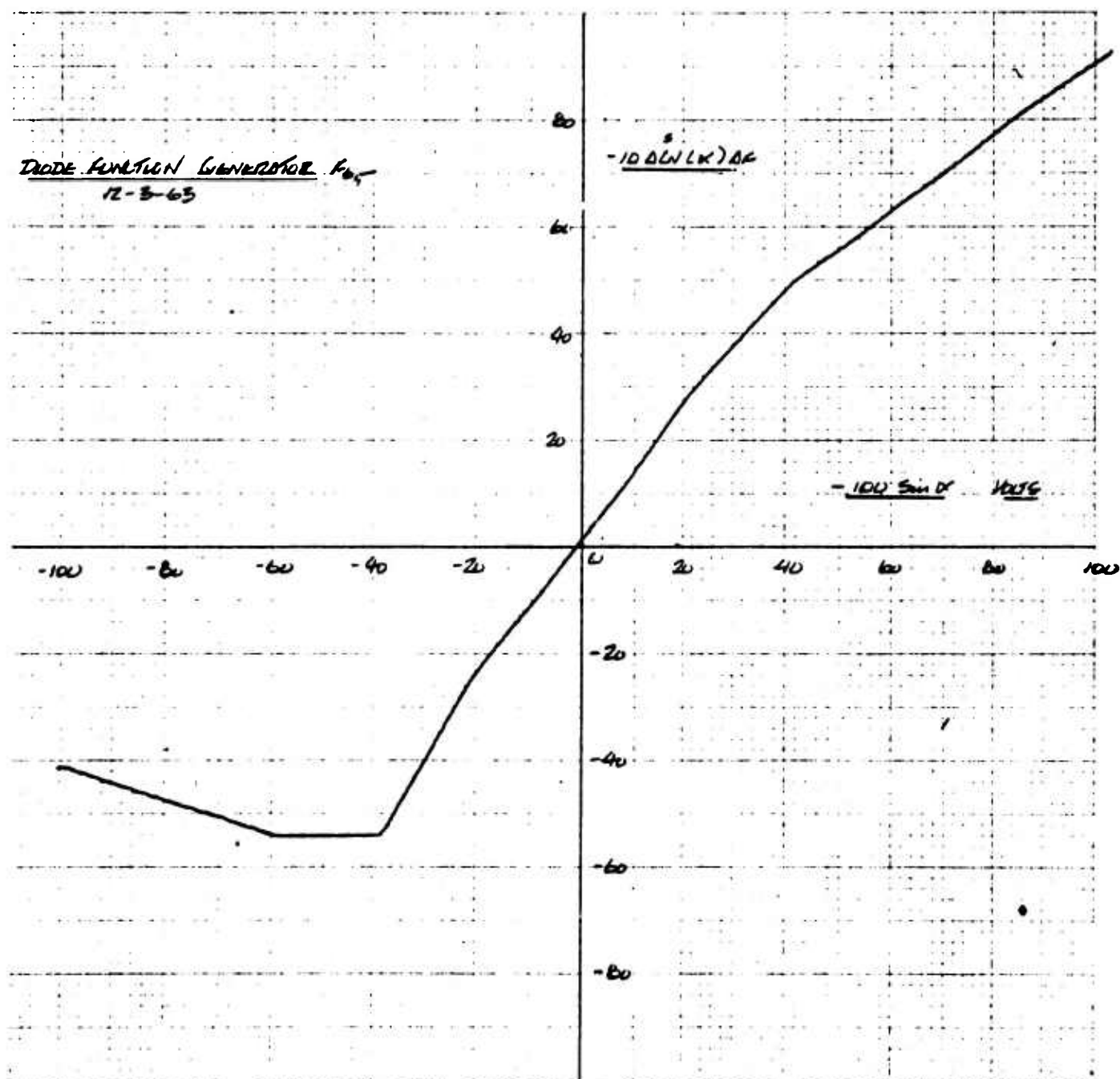
Figure 72 $-10\,C_N^s(a)A_F$ vs $-100\sin a$, as Set Up on Diode Function Generator F65. This is equivalent to Figure 49.
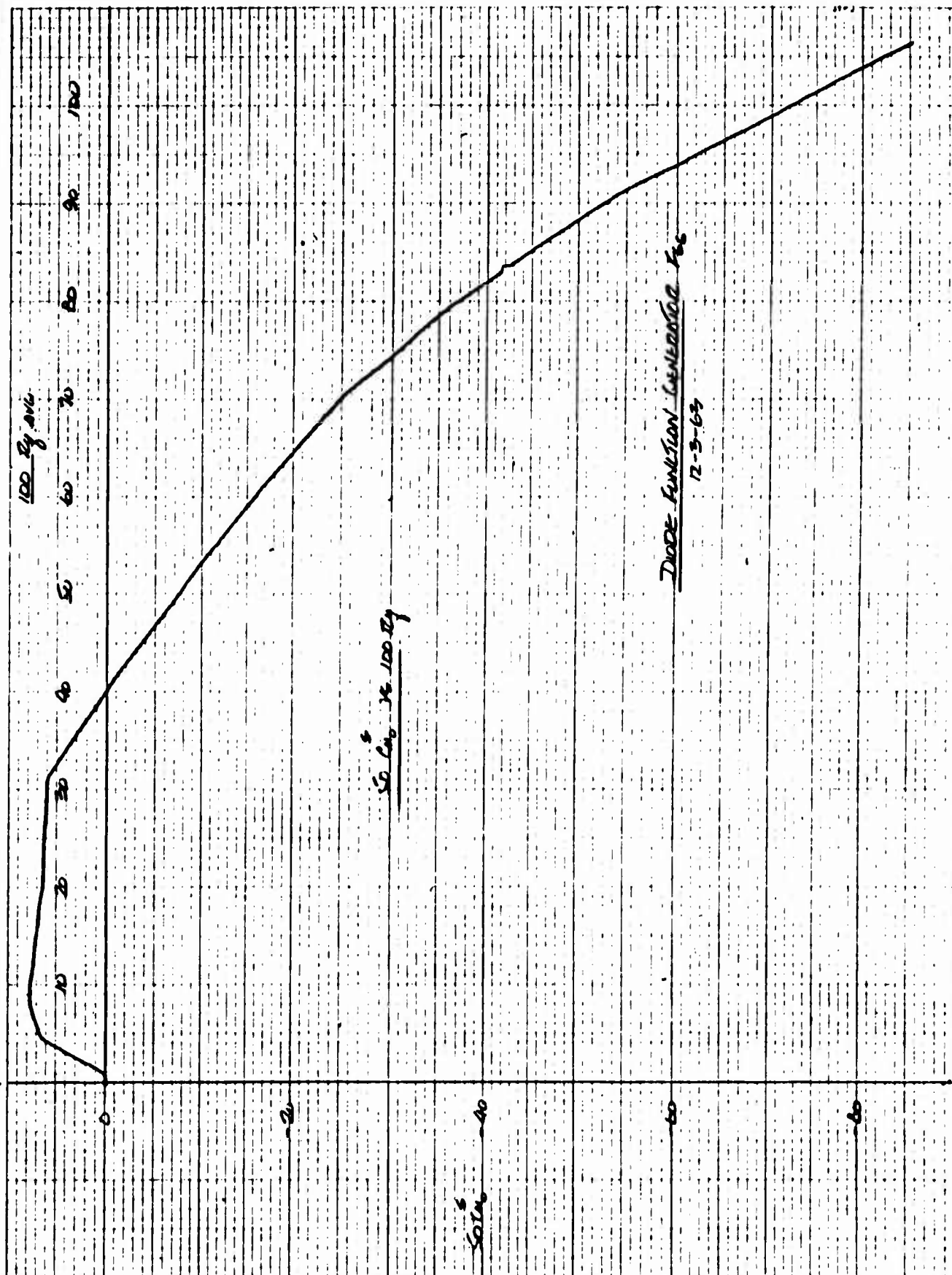
Figure 73 50 $C_{m_o}^s$ vs 100 R_q, as Set Up on Diode Function
Generator F66
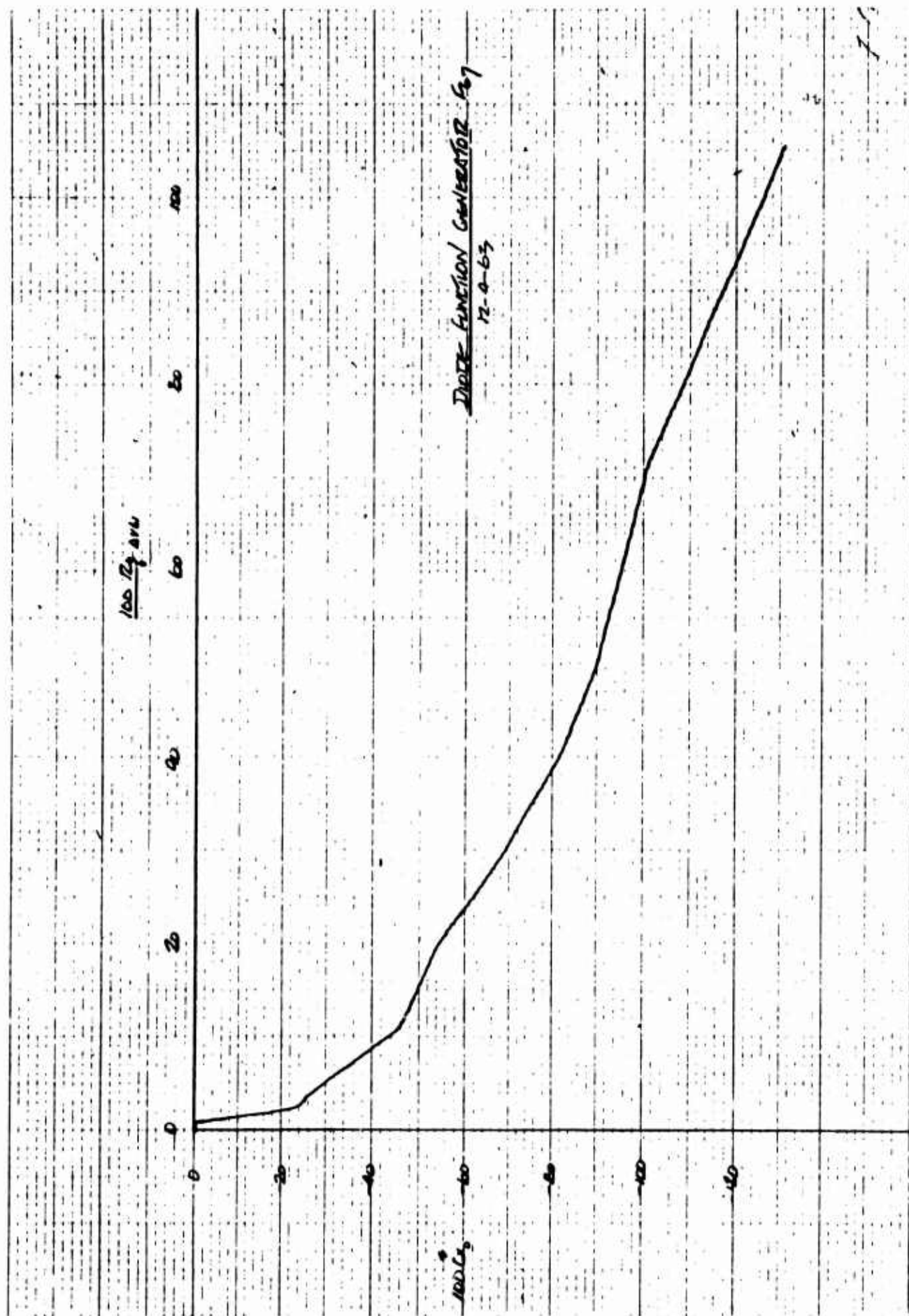
Figure 74 $100\,C_{X_0}^s$ vs $100\,R_q$, as Set Up on Diode Function Generator F67
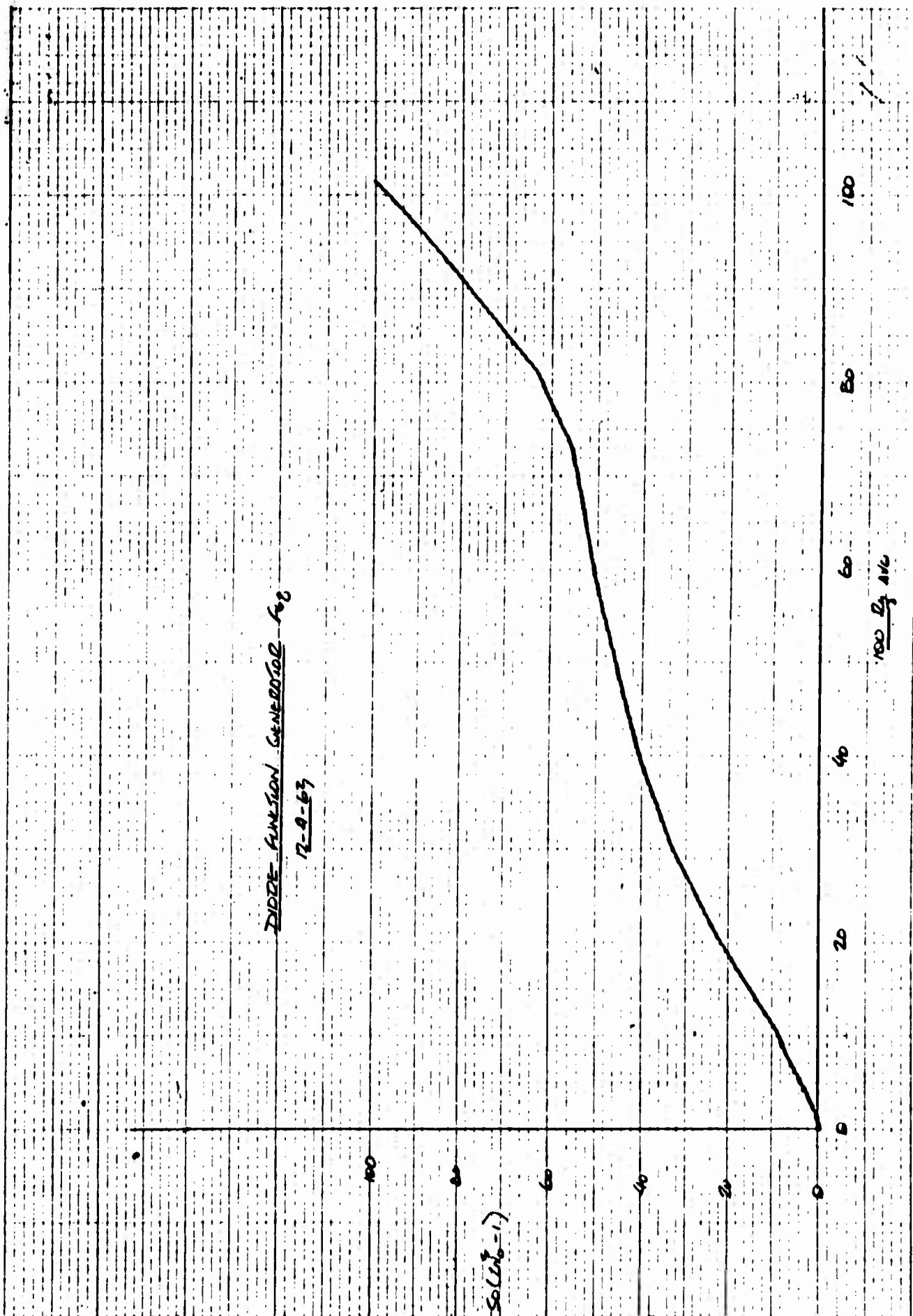
Figure 75 50 ($C_{N_O}^8 - 1$) vs 100 R_q, as Set Up on Diode Function
Generator F68

117
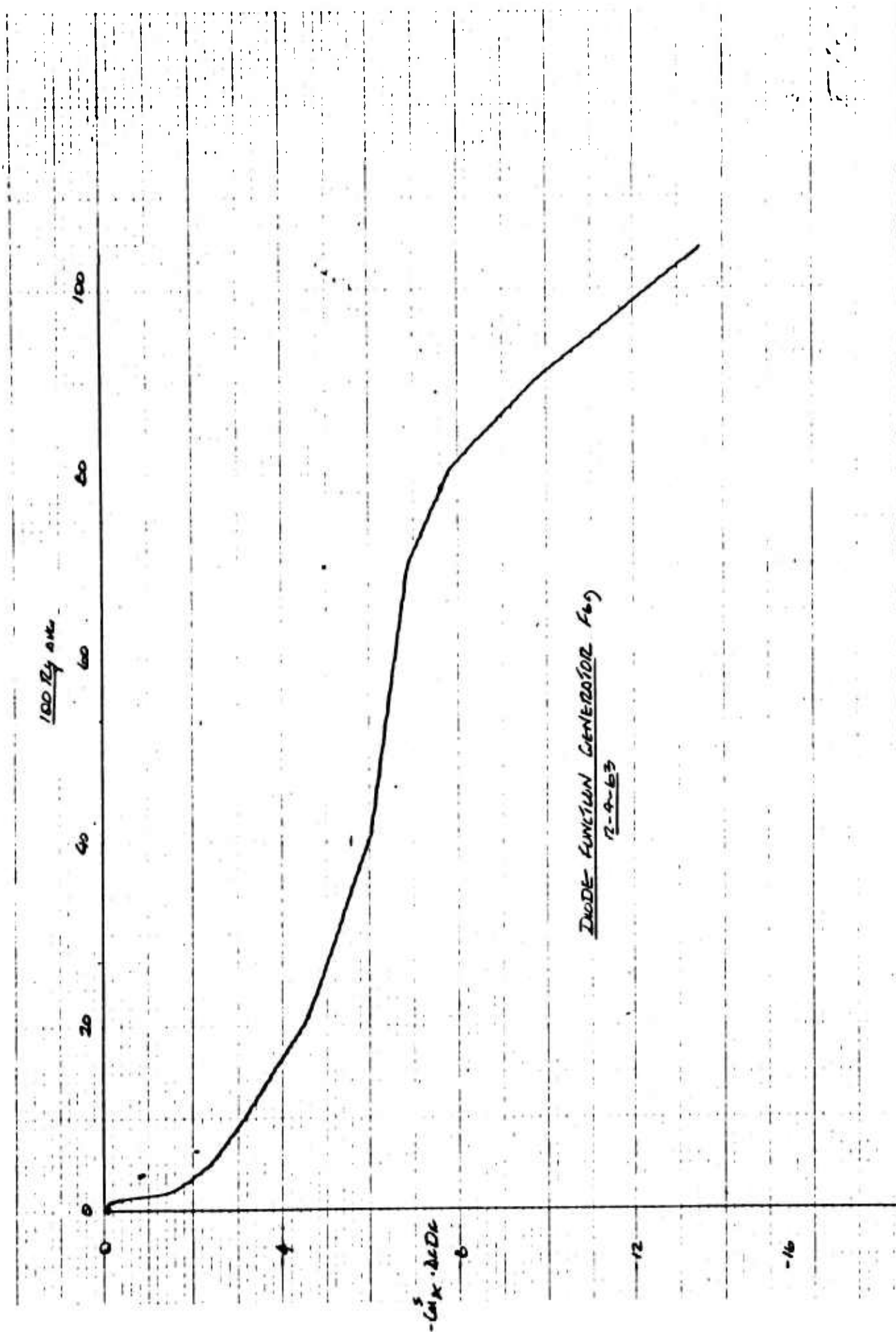
Figure 76 $-C_{m_\alpha}^s \, A_F \, D_F$ vs $100 \, R_q$, as Set Up on Diode Function
Generator F69
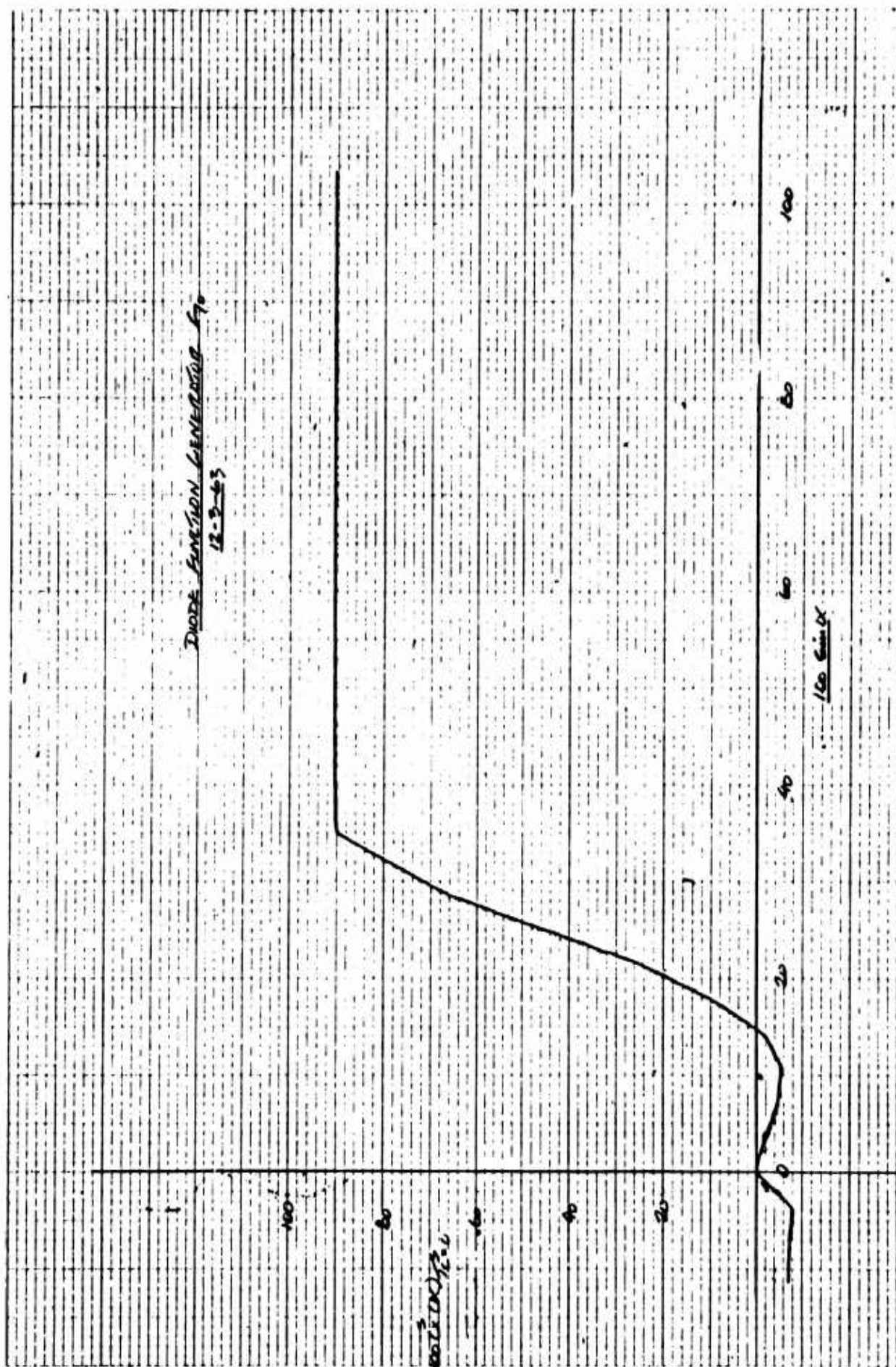
Figure 77 $100\,Cx^8(\alpha)$ at $T_c^8 = 0$ vs $100 \sin \alpha$, as Set Up on Diode Function Generator F70

119
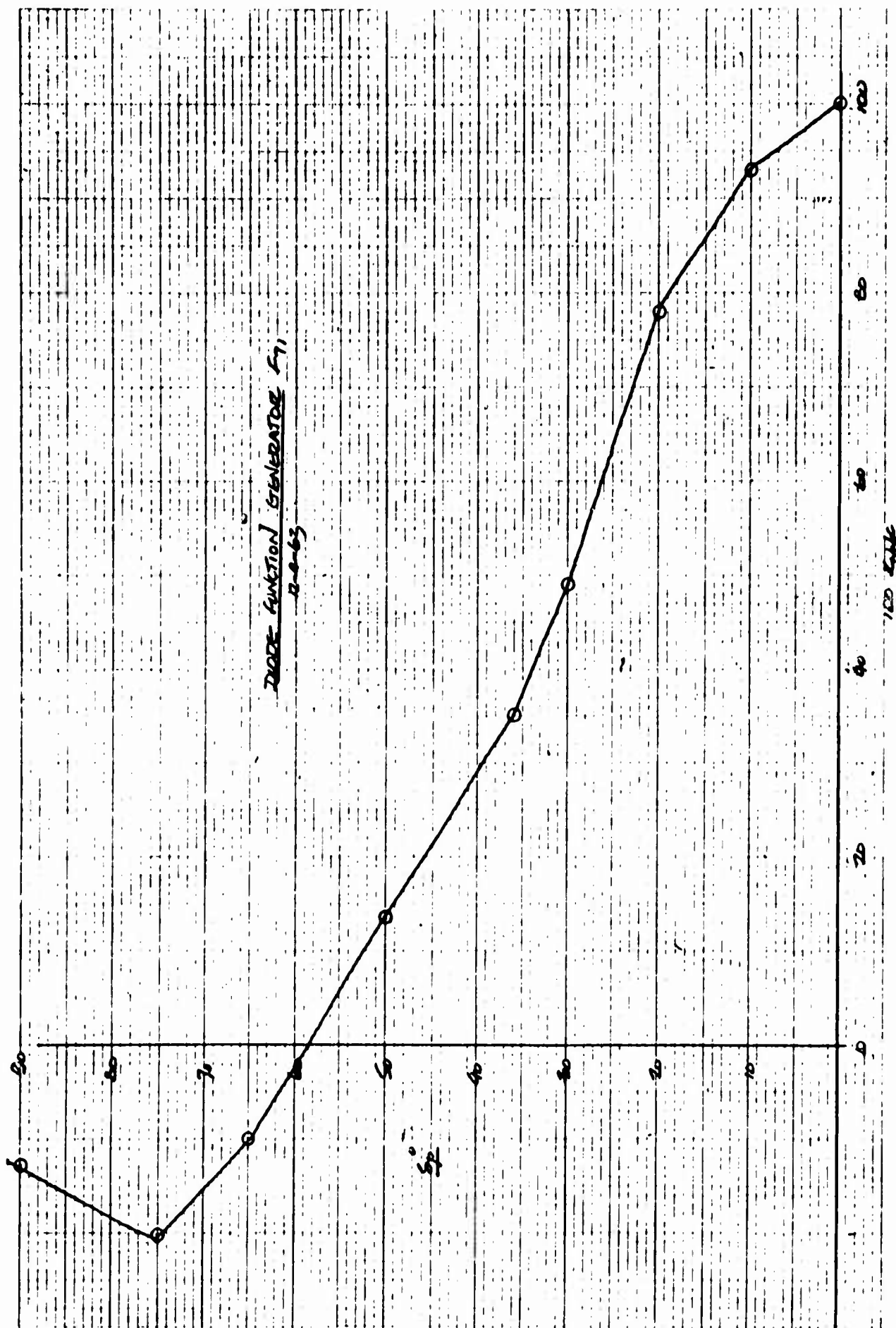
Figure 78 100 $K_{N_{NF}}$ vs δ_p^o, as Set Up on Diode Function Generator
F71
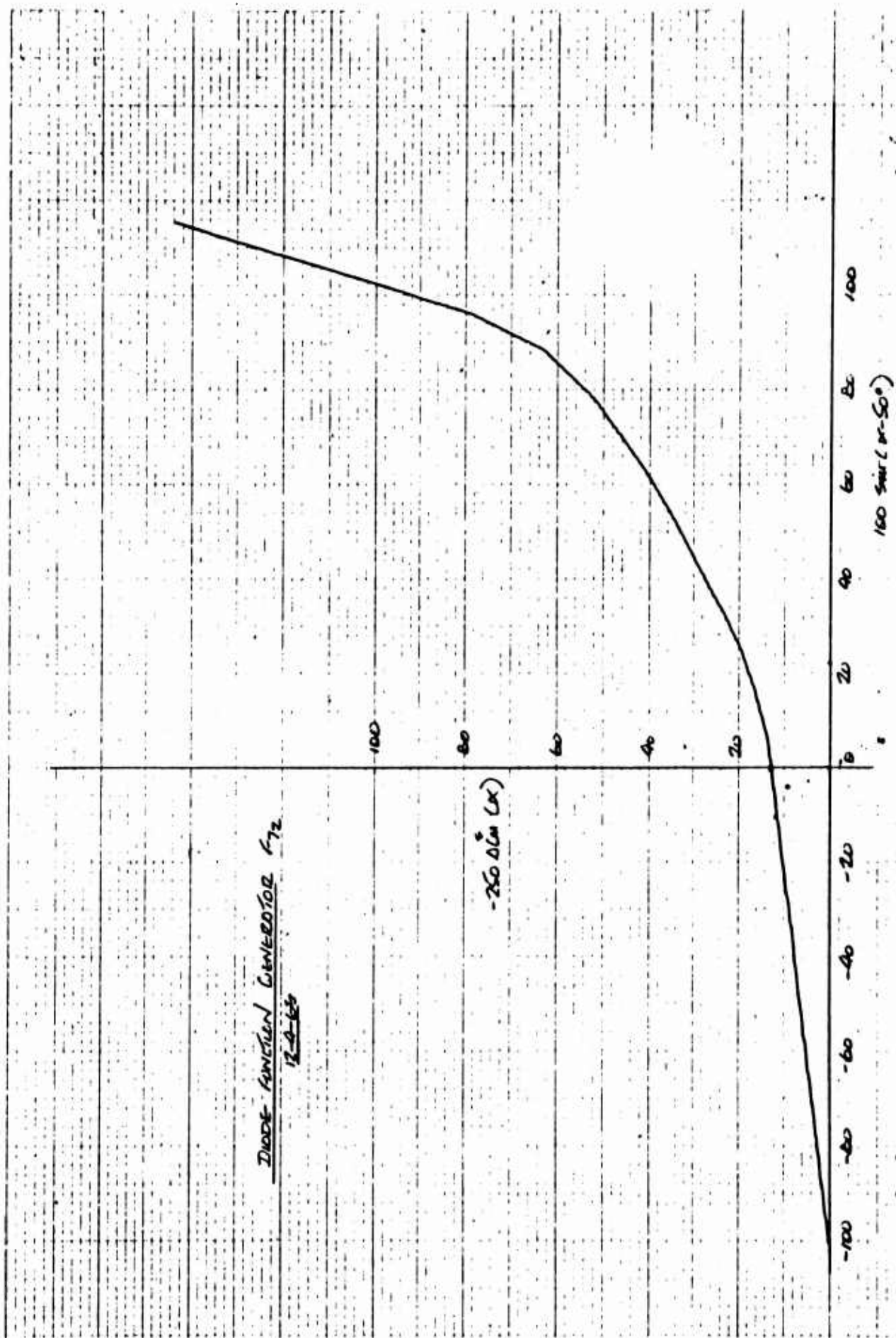
Figure 79 – 250 $\Delta C_m^s(\alpha)$ vs 100 sin $(\alpha - 50^\circ)$, as Set Up on Diode Function Generator F72
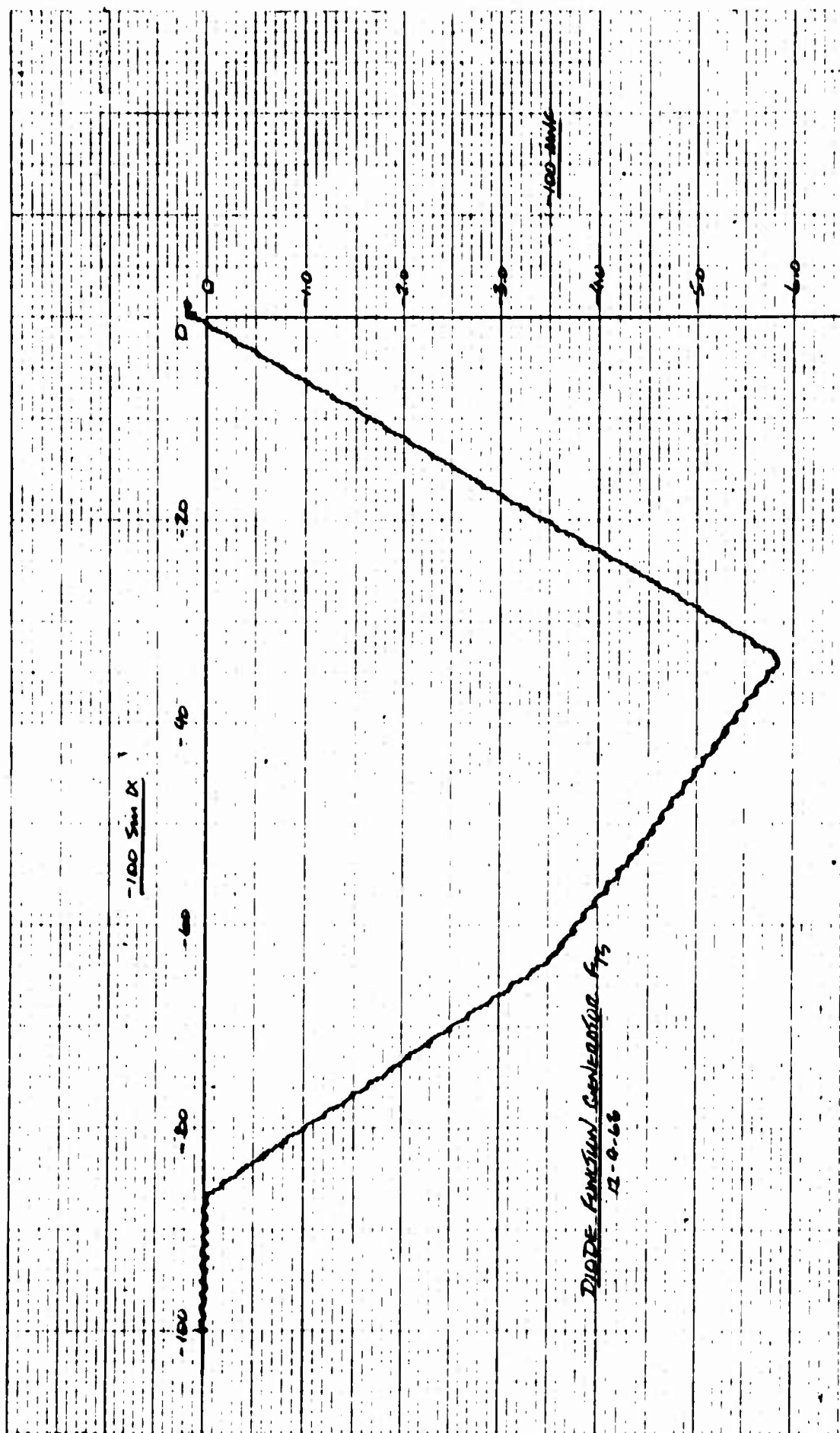
Figure 80 -100 MNF vs -100 sin *a* , as Set Up on Diode Function
Generator F73

122

2.4 EQUATIONS OF MOTION

The standard body axis six degree of freedom equations of motion were used for this simulation.

These equations are:

$$\dot{u} = rv - qw + g\ell_z + \frac{\Sigma F_x}{m} \qquad (1)$$

$$\dot{v} = pw - ru + gn_z + \frac{\Sigma F_y}{m} \qquad (2)$$

$$\dot{w} = qu - pv + gm_z + \frac{\Sigma F_z}{m} \qquad (3)$$

$$\dot{p} = \frac{I_{xz}}{I_x}(\dot{r} + pq) - \left(\frac{I_{z-y}}{I_x}\right)qr + \frac{qH_z - rH_y}{I_x} + \frac{\Sigma \ell}{I_x} \qquad (4)$$

$$\dot{q} = \frac{I_{xz}}{I_y}(r^2 - p^2) - \left(\frac{I_x - I_z}{I_y}\right)pr + \frac{rH_x - pH_z}{I_y} + \frac{\Sigma \mathcal{M}}{I_y} \qquad (5)$$

$$\dot{r} = \frac{I_{xz}}{I_z}(\dot{p} - qr) - \left(\frac{I_{y-x}}{I_z}\right)pq + \frac{pH_y - qH_z}{I_z} + \frac{\Sigma \mathcal{N}}{I_z} \qquad (6)$$

In the interests of conservation of computer equipment, certain of the angular acceleration terms were neglected. The maximum values of p, q and r were estimated to be .4, .3, and 1 rad/sec, which are the visual display limitations. Combining this data with the XV-5A inertia data, it can be seen that certain of the angular acceleration terms can be considered negligible. These are:

1.   The pq term in the $\dot{r}$ equation.

2.   The I_{xz}/I_y term in the $\dot{q}$ equation.

3.   The I_{xz}/I_z and pq terms in the $\dot{r}$ equation.

In addition, the angular momentum of the rotating fan and gas generator parts has been neglected. Hand analysis (Appendix 6) shows that at a flight condition where fu. roll control was required steady state (hover in a side wind), the gyroscopic coupling terms applied to an inertial body would result in a nutation oscillation with a period of around 35 seconds. Such a long period oscillation would be completely masked by shorter-term effects.

The modified equation of motion thus become:

$$\dot{u} = rv - qw + g\ell_z + \frac{\Sigma F_x}{m} \tag{7}$$

$$\dot{v} = pw - ru + gm_z + \frac{\Sigma F_y}{m} \tag{8}$$

$$\dot{w} = qu - pv + gn_z + \frac{\Sigma F_z}{m} \tag{9}$$

$$\dot{p} = \frac{I_{xz}}{I_x}\dot{r} - \left(\frac{I_z - I_y}{I_x}\right)qr + \frac{\Sigma \ell}{I_x} \tag{10}$$

$$\dot{q} = -pr\left(\frac{I_x - I_z}{I_y}\right) + \frac{\Sigma M}{I_y} \tag{11}$$

$$\dot{r} = \frac{\Sigma N}{I_z} \tag{12}$$

2.5   EULER/DISPLAY RELATIONS

As previously reported in Ryan Report 63B024, the Yaw, Roll, Pitch direction cosines and Euler angles are continuously calculated by developing the Euler angular rates as a function of the direction cosines, which are themselves functions of the Euler angles.

The relationships determining the Euler angular rates are:

$$\dot{\theta} = q + p\theta\varphi - r\varphi \tag{13}$$

$$\dot{\varphi} = p + r\theta \tag{14}$$

$$\dot{\Psi} = \frac{r - p\theta}{\cos\varphi} \tag{15}$$

Over the ranges of θ and ϕ used to drive the DeFlorez display, the approximation $\cos\theta = 1$, $\cos\varphi = 1 - \varphi^2/2$, $\sin\theta = \theta$, $\sin\varphi = \varphi$ were used. The relationships of the 9 direction cosines are given in equations 16 thru 24 in their approximate form.

$$\ell_x = \cos\Psi \tag{16}$$

$$m_x = -\cos\varphi \sin\Psi \tag{17}$$

$$n_x = \theta\cos\Psi + \varphi\sin\Psi \tag{18}$$

$$\ell_y = \sin\Psi \tag{19}$$

$$m_y = \cos\Psi \cos\varphi \tag{20}$$

$$n_y = \theta\sin\Psi - \varphi\cos\Psi \tag{21}$$

$$\ell_z = -\theta\cos\varphi \tag{22}$$

$$m_z = \varphi \tag{23}$$

$$n_z = \cos\varphi \tag{24}$$

The ground velocities can be computed from the direction cosines and body velocity components as follows:

$$\dot{S}_x = u\ell_x + vm_x + wn_x \tag{25}$$

$$\dot{S}_y = u\ell_y + vm_y + wn_y \tag{26}$$

$$\dot{S}_z = -\dot{h} = u\ell_z + vm_z + wn_z \tag{27}$$

2.6 ANALOG CIRCUITRY EMPLOYED

This section contains the complete analog schematic drawings for the hardware simulation.

To facilitate checkout and use of the simulation, circuits were broken up according to function, which resulted in some extra trunking between consoles but was very worthwhile in all other respects.

The figures following which show these sectionalized circuits are arranged in a sequence which runs from function generation to pilot displays and control commands.

An explanation of each figure is given below.

Figure 81: This figure shows the functions generated on each of the two multigluks (16 cup pot padders). The functions generated are all transition region fan functions. The numbers and letters given beside each cup (such as "8-16B1" for the "A" cup) correspond to functions similarly labeled in the preceding section.

Cups "H" and "K" show the absolute value of β_v being used as the cup excitation. This was done to increase the accuracy of the second order curve fits made to $\Delta C_{N_{\beta_v}}^s$ and $C_p^s/C_{p_o}^s$, due to negative vector angles occurring on a given wing when yaw control is applied near hover.

Figure 82: This figure shows the generation of some of the aerodynamic coefficients which varied nonlinearly with R_q.

Figure 83: This figure shows the generation of some of the aerodynamic coefficients which varied nonlinearly with R_q. Also shown is the generation of the phasing functions POF No. 1 and POF No. 2.
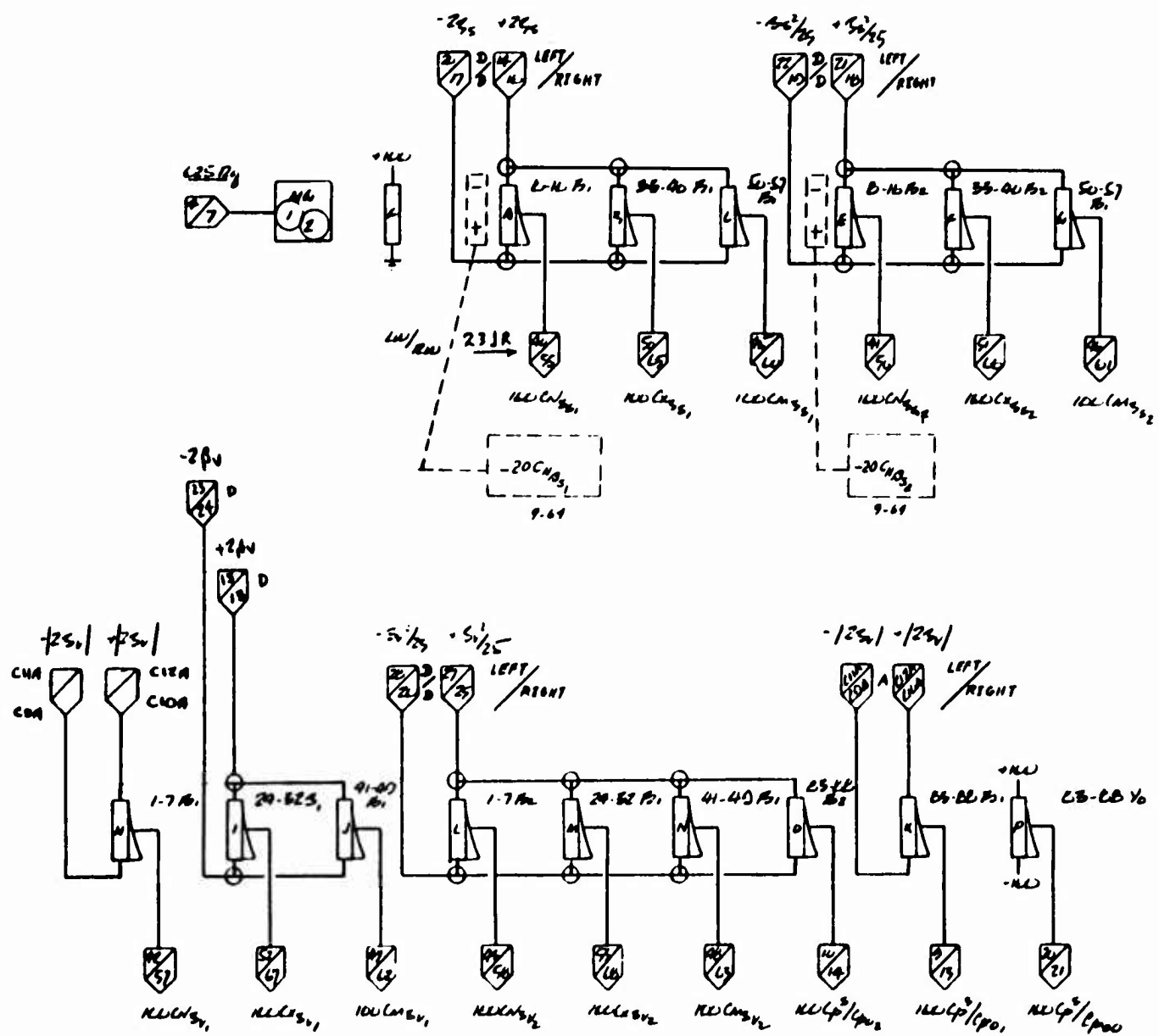
Figure 81 Pot Padding Function Generation - Central Patch Panel

129
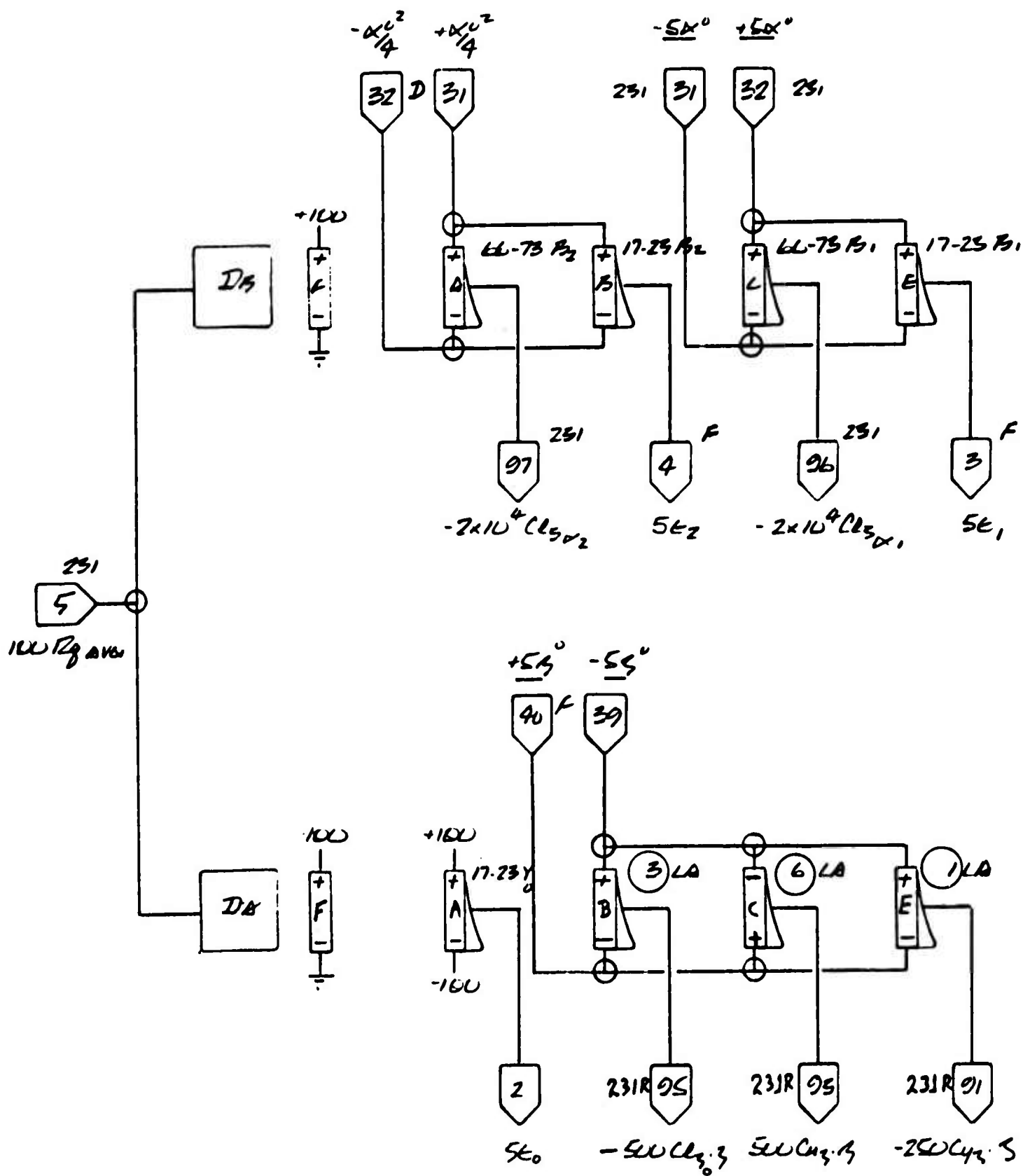
Figure 82 Pot Padding Function Generation – Central Patch Panel

131

Figure 83 Pot Padding Function Generation – Central Patch Panel

Figure 84: This figure shows the generation of some of the fan and engine parameters which varied nonlinearly with $R_{q_{NF}}$ or N.

Figure 85: This figure shows the generation of the required fan parameters for the right and left main fans and the nose fan. Also shown is the circuitry which generates the nose fan and main fan overspeed warnings.

The generation of 625 R_q includes limiters to keep the amplifiers from overloading after conversion, when R_q goes to 1.0.

Pots P12 and P13 are used to shift the fan power by a constant, to bring the gas generator output up to date.

Figure 86: This figure shows the generation of louver vector and stagger angles. The inputs for this circuit are pots located on the louver hardware of the simulation.

Figure 87: This figure shows the generation of the squares of the louver angles and the angle of attack. These squares are required in the second order fits to some of the aerodynamic and fan coefficients.
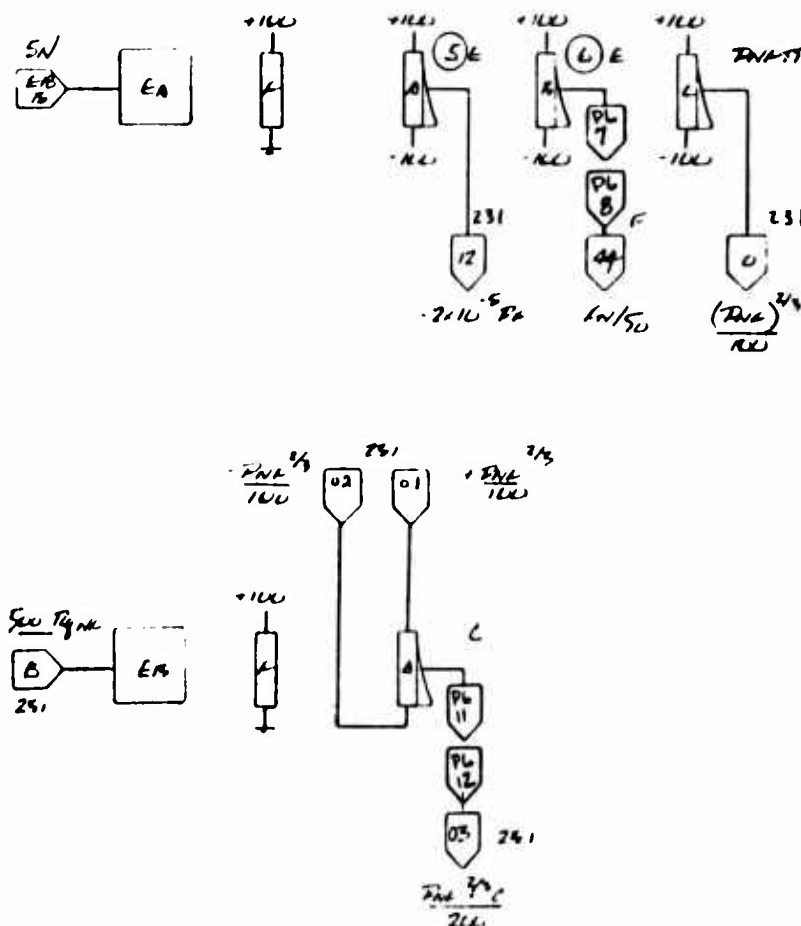
Figure 84 Pot Padding Function Generation - Central Patch Panel

LT FAN

(MG2-PX)
$+100\ Cp^s/Cp_{OO}$
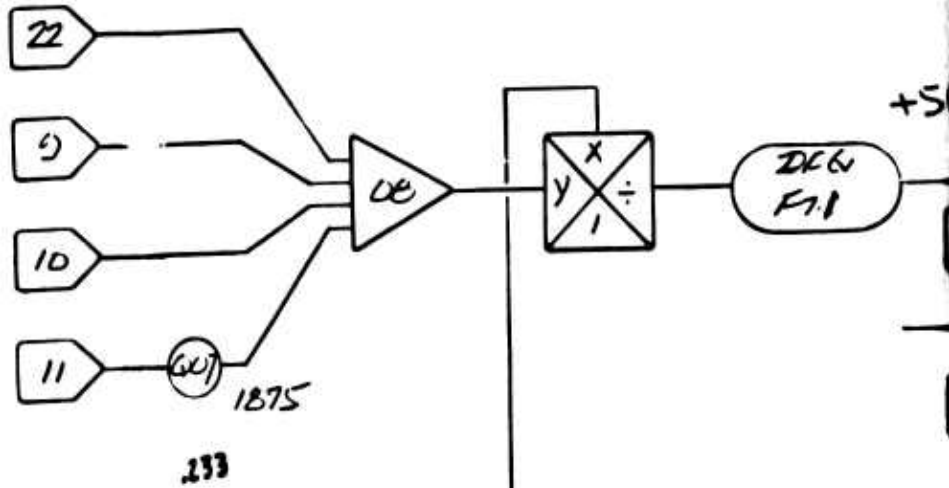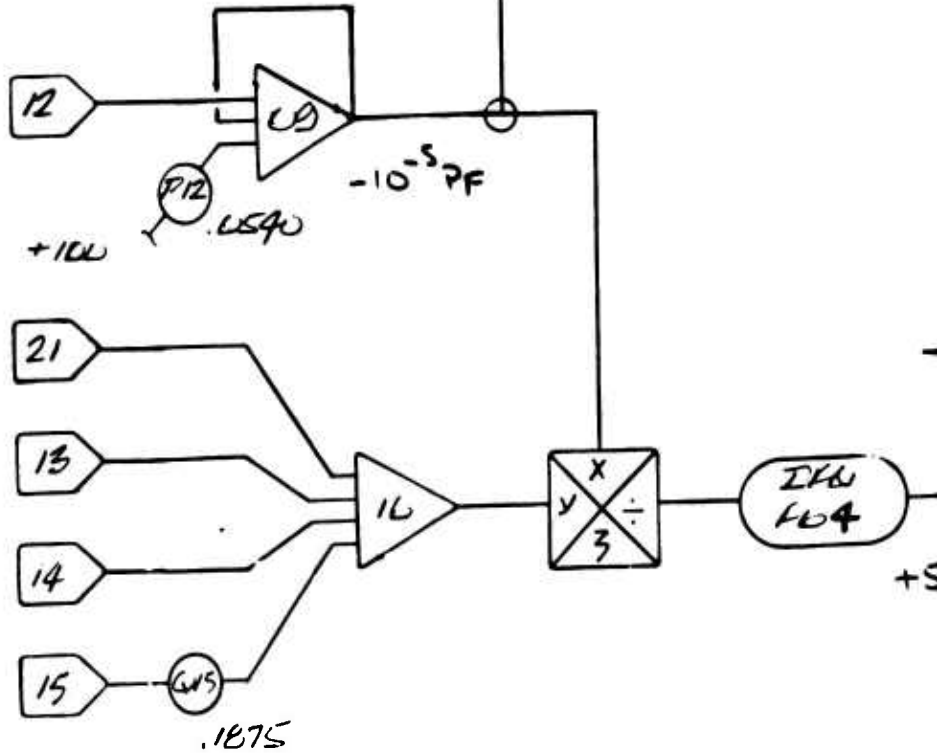
(MG1-KX)
$+100\ Cp^s/Cp_{O1}$

(MG1-OX)
$+100\ Cp^s/Cp_{O2}$

(D-22)
$-S_{81}^=/125$

22

9

10

11 (WO7) 1875

.133

DE

X·Y÷1

IFN F71 +S

(E_A-AX)
$+2\times10^{-5}\ I_C$

12

LD

(P12) .0540

$-10^{-5}\ PF$

$+100$

RT FAN

(MG1-PX)
$+100\ Cp^s/Cp_{OO}$

(MG2-KX)
$+100\ Cp^s/Cp_{O1}$

(MG2-OX)
$+100\ Cp^s/Cp_{O2}$

(D-19)
$-S_{5ET}^2/125$

21

13

14

15 (WO5) .1875

LC

X·Y÷3

IFN LO4 +S

NOSE FAN

(E_A-CX)
$(P_{NK})^{2/3}\div100$

LO .6650 $\frac{2}{13}$ $+100$

LU ⊖ OX (E_B-BA) DN $(P6-10)$ LB LS $\frac{P_{NK}^{2/3}\times L}{200}$ .4

L2 $(E_B-[-A])$

A

B

Figure 85   Fan System
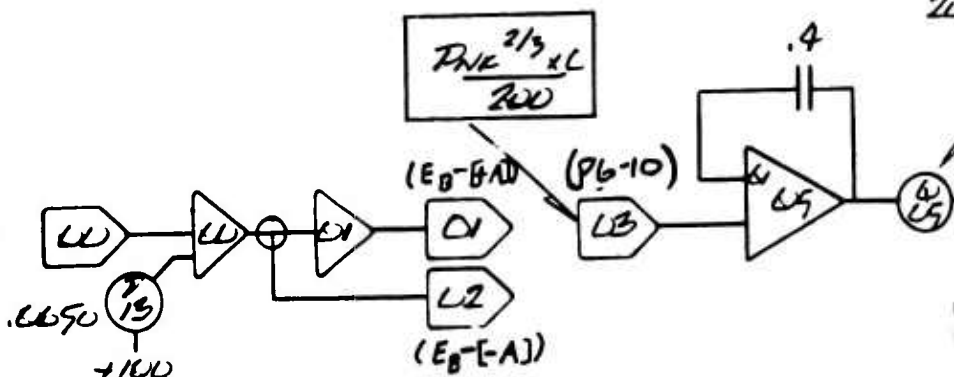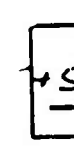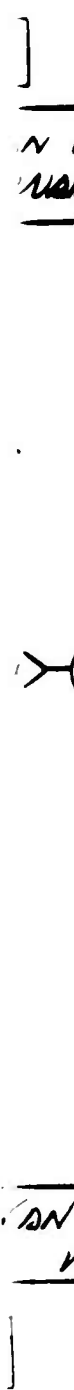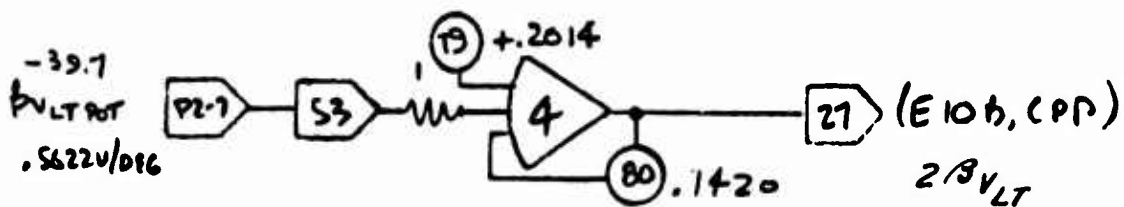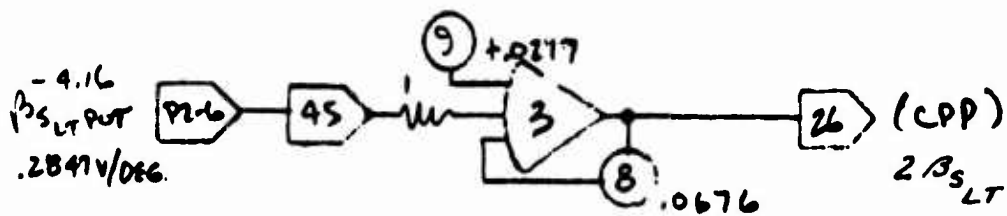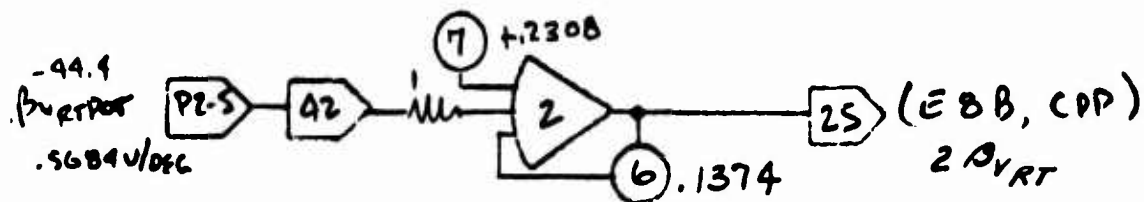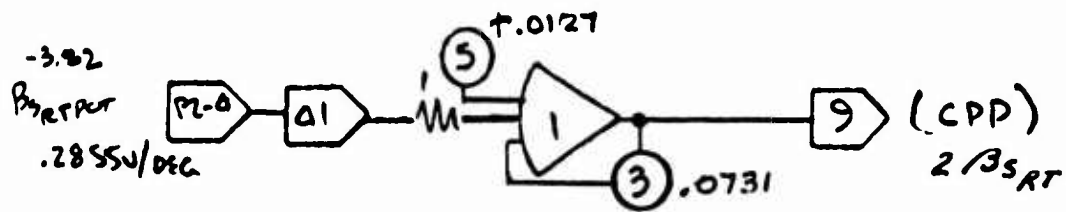
Figure 86 Development of β_V and β_S - Pace F
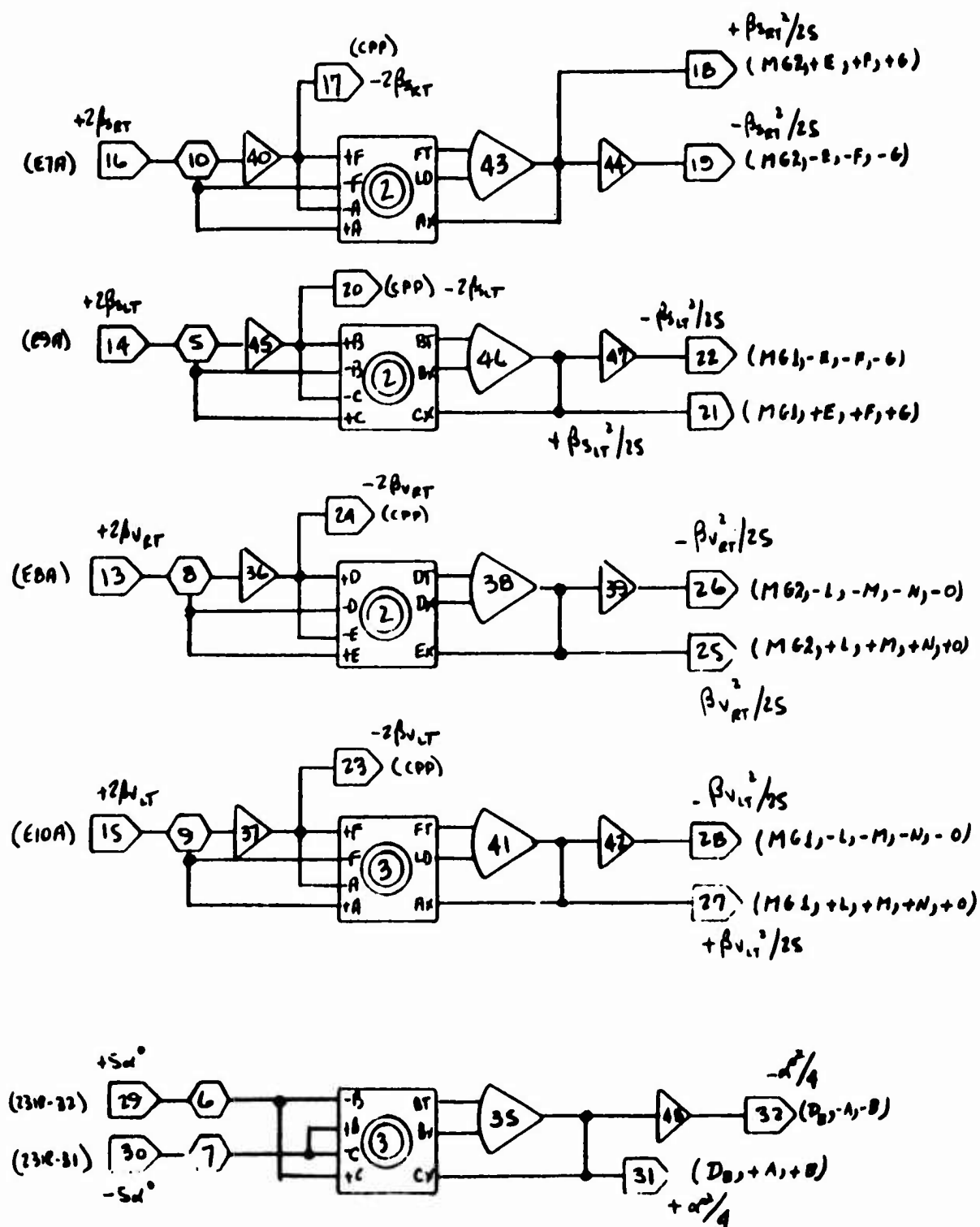
Figure 87 Development of Required Functions of β_V and β_S – Pace D

Figure 88: This figure shows the generation of the absolute value of the louver vector angle and the mixer vector angle, which differs from the louver vector angle by 2.5 degrees. At zero mixer vector, $\beta_V = -2.5$ degrees. The aircraft cockpit vector indicator reads mixer vector.

Figure 89: This figure shows the summation of the right fan normal force, axial force and pitching moment variations due to louver angle and R_q changes.

Figure 90: This figure shows the summation of the left fan normal force axial force and pitching moment variations due to louver angle and R_q changes.

Figure 91: This figure shows the generation of the normal and axial force variations for right and left fan due to angle of attack changes.

Figure 92: This figure shows the generation of angles of sideslip and attack, total velocity and dynamic pressure from the aerodynamic body axis velocities.
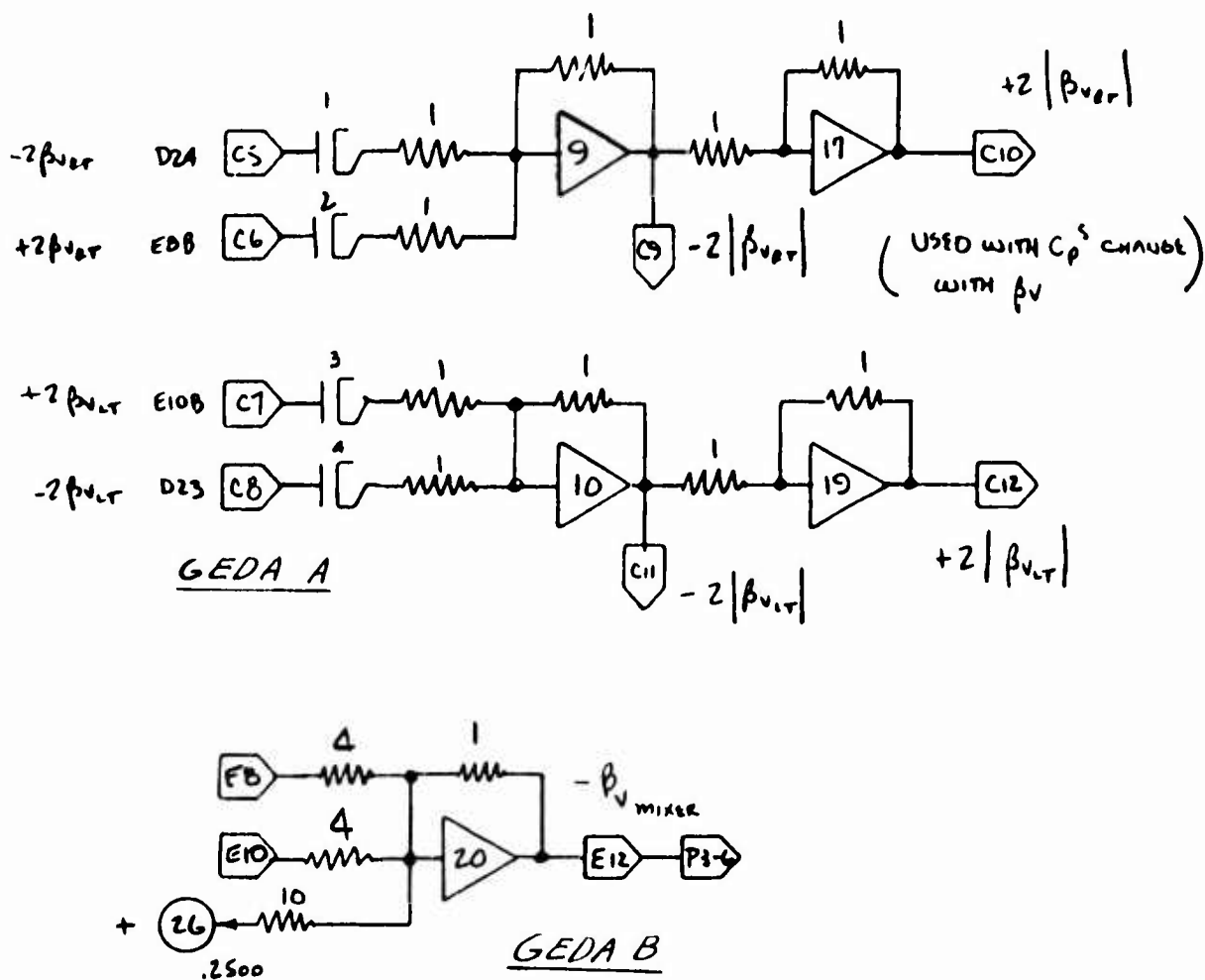
Figure 88 Development of Required Functions of β_V
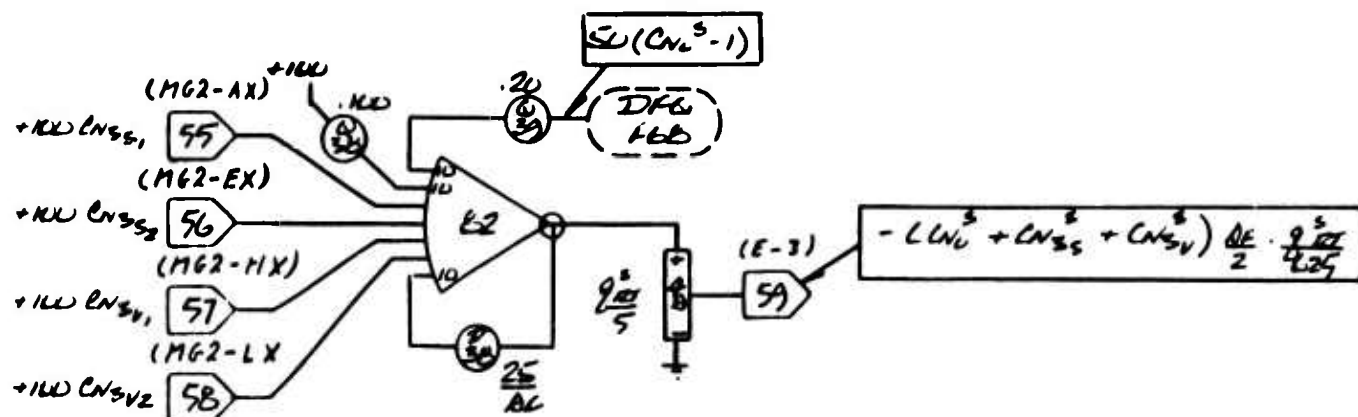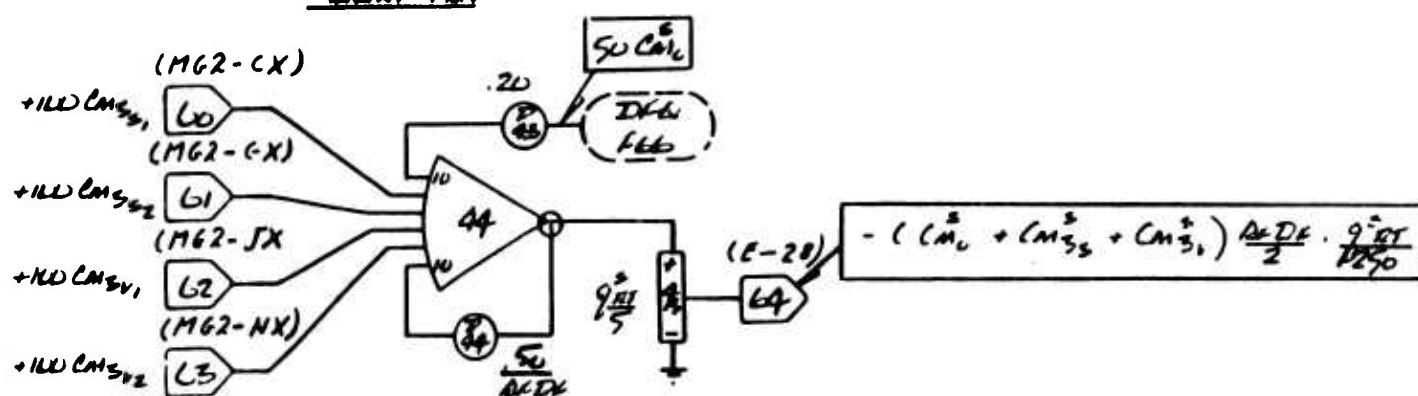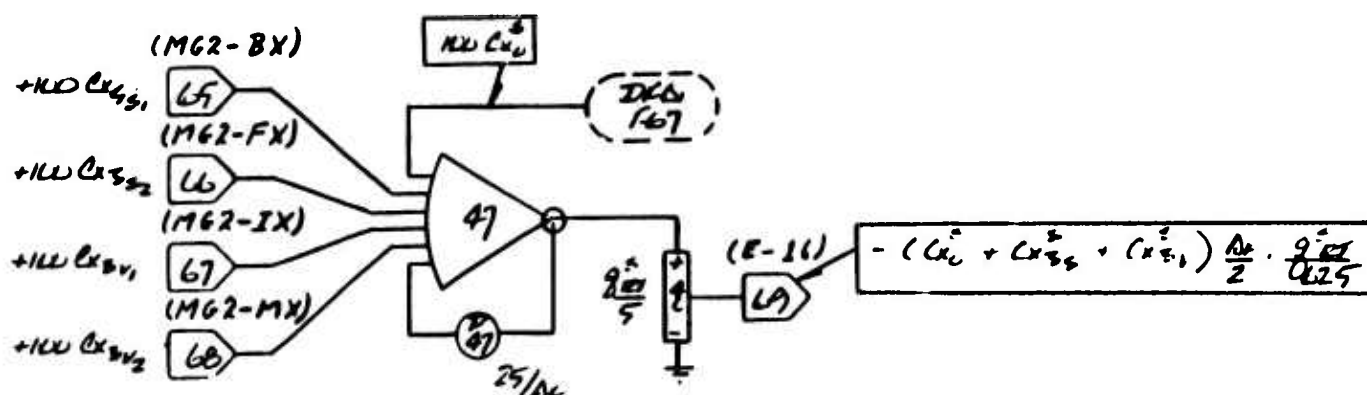
Figure 89 Generation of $C_N{}^8$, $C_m{}^8$ and $C_X{}^8$ For Right Fan
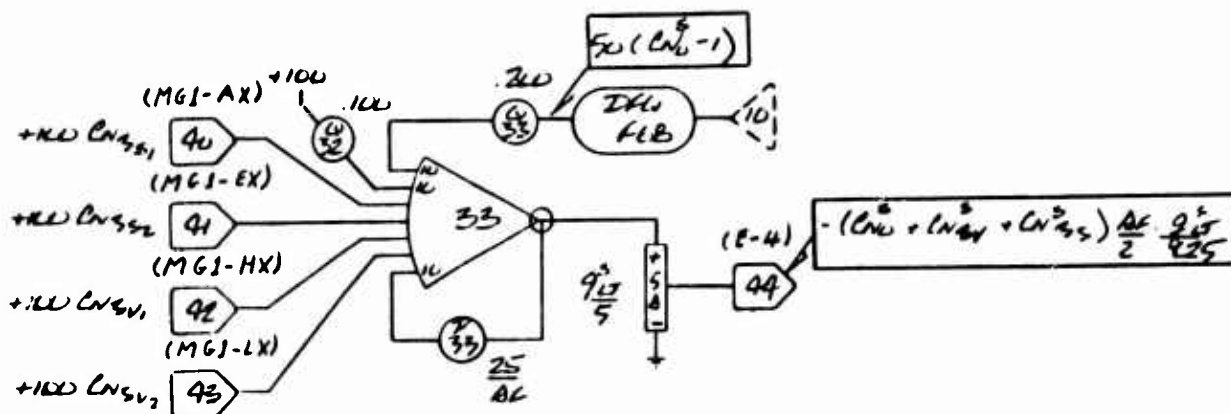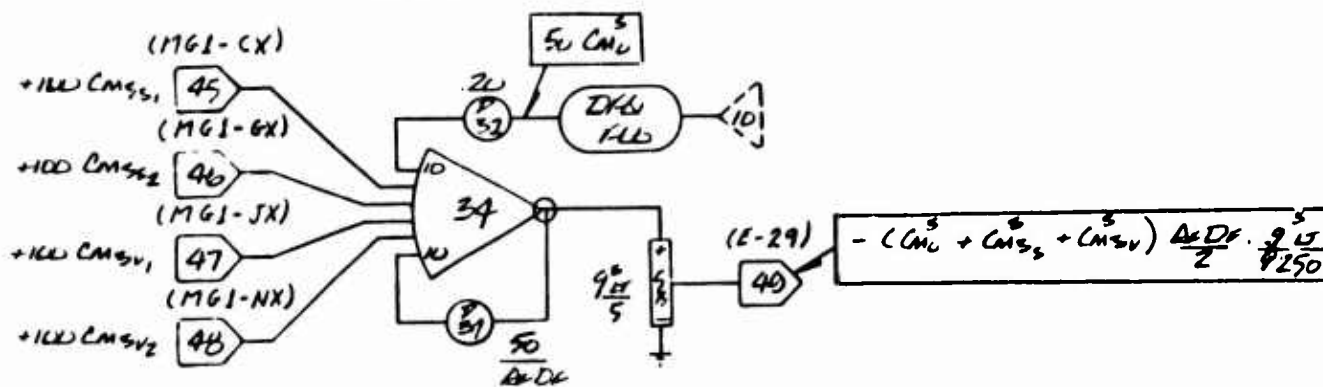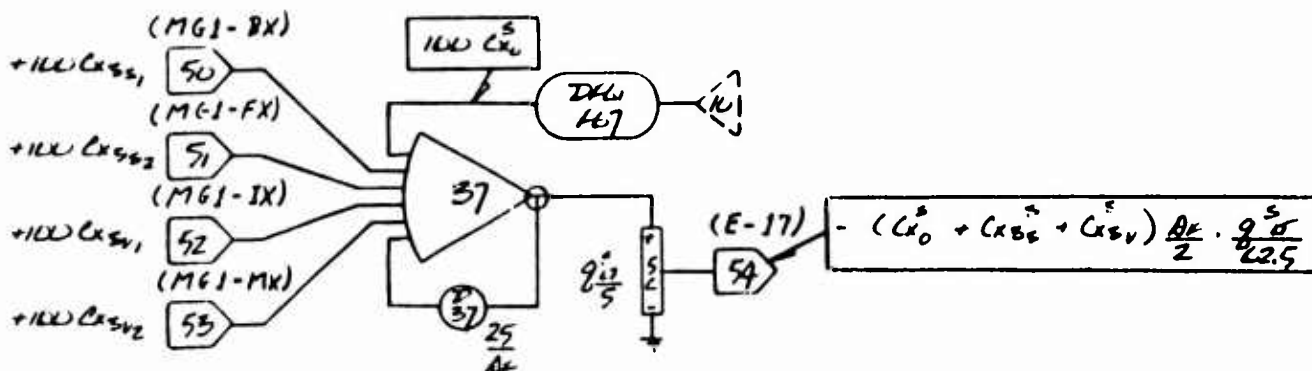
Figure 90 Generation of $C_N{}^8$, $C_m{}^8$ and $C_X{}^8$ For Left Fan
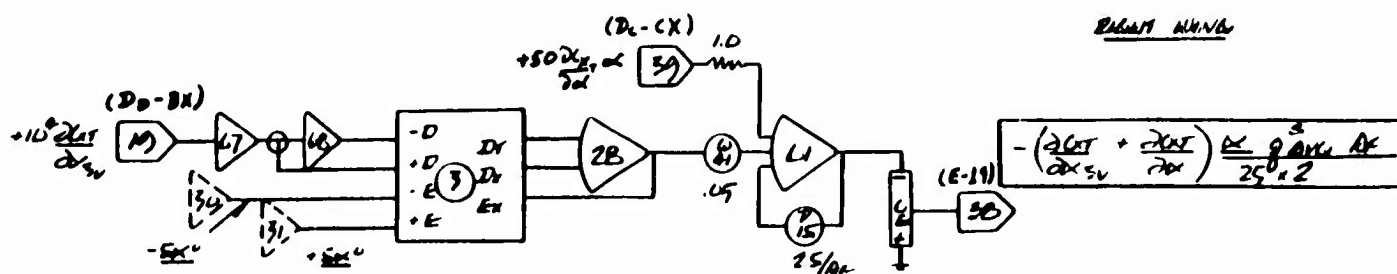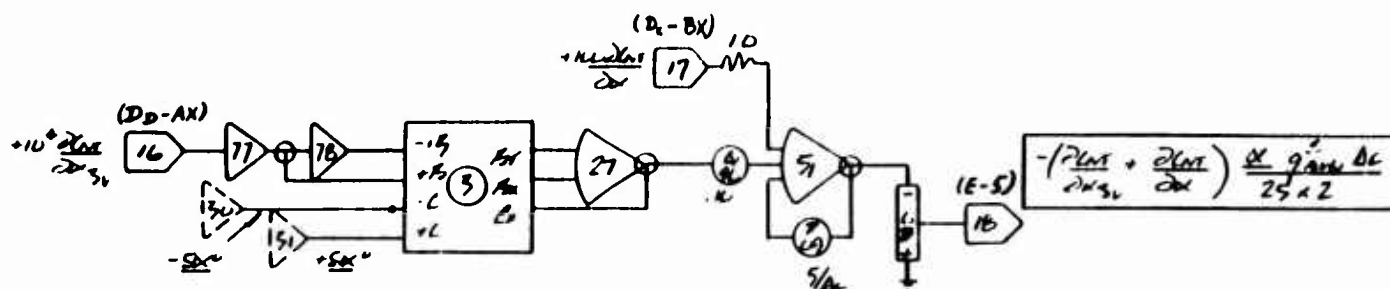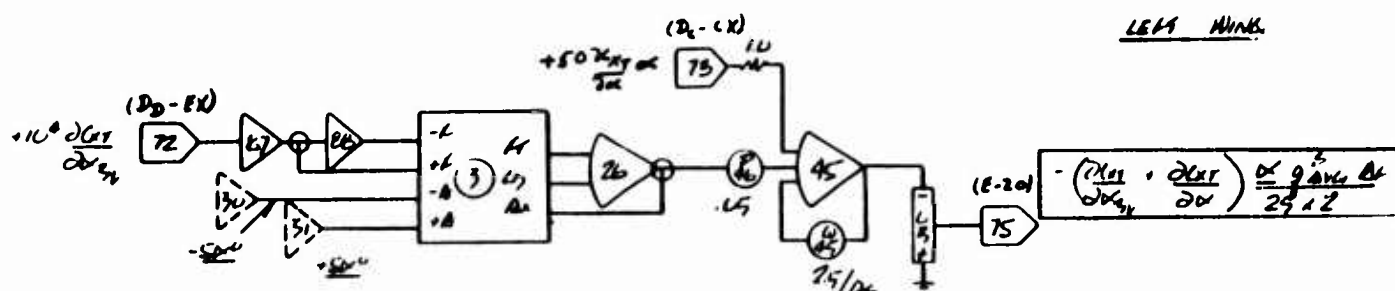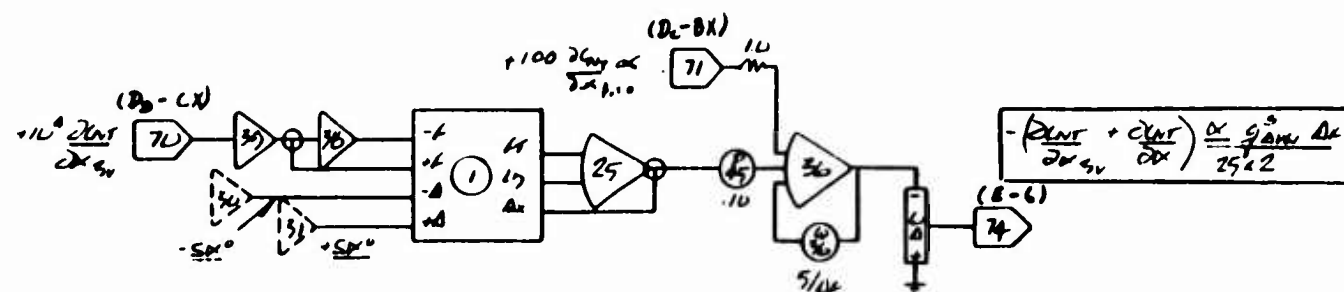
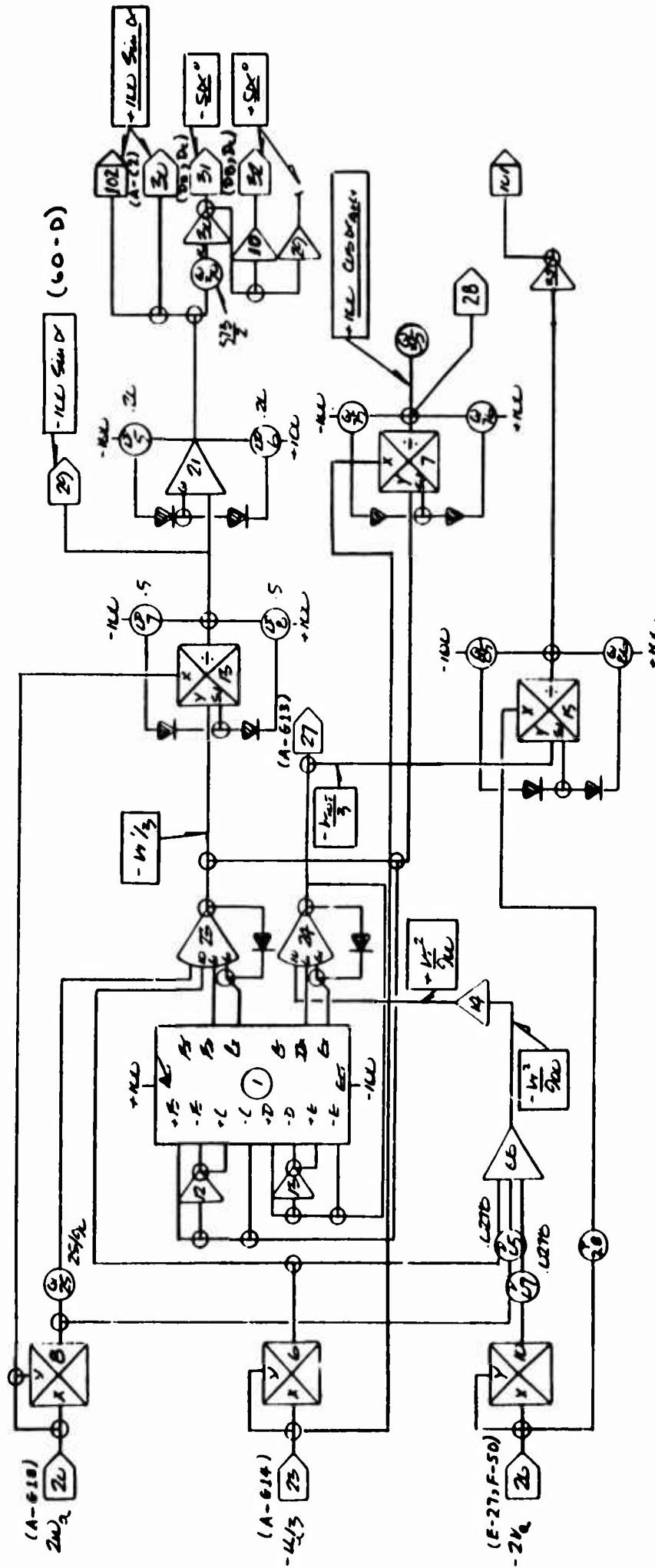Figure 91   Generation of "Fan Caused" Axial and Normal Force
Coefficient

Figure 92 Generation of Angle of Attack and Sideslip Angle

Figure 93: This figure shows the generation of the low speed (0 to 50 ft/sec) pitching moment, yawing moment, side force, and rolling moment.

Figure 94: This figure shows the generation of low speed (0 to 50 ft/sec) normal force, pitching moment from the nose fan, and axial force.

Figure 95: This figure shows the development of the aerodynamic control moments.

Figure 96: This figure shows the development of roll and yaw aerodynamic damping moments.

Figure 97: This figure shows the development of aerodynamic damping forces and moments in normal force, side force and pitching moment.

Figure 98: This figure shows the development of tail forces. The circuit also resolves these forces into the body axis coordinates.
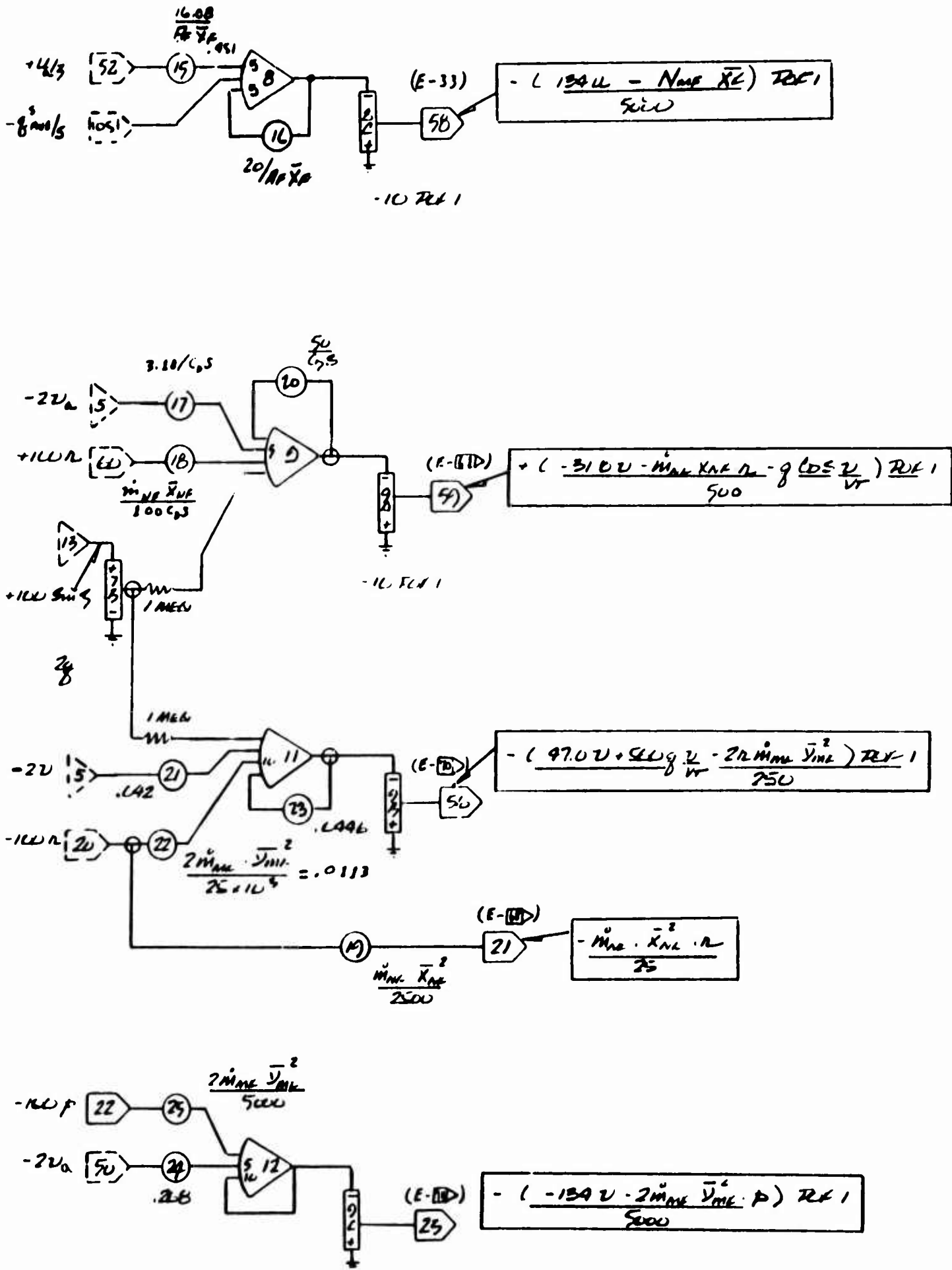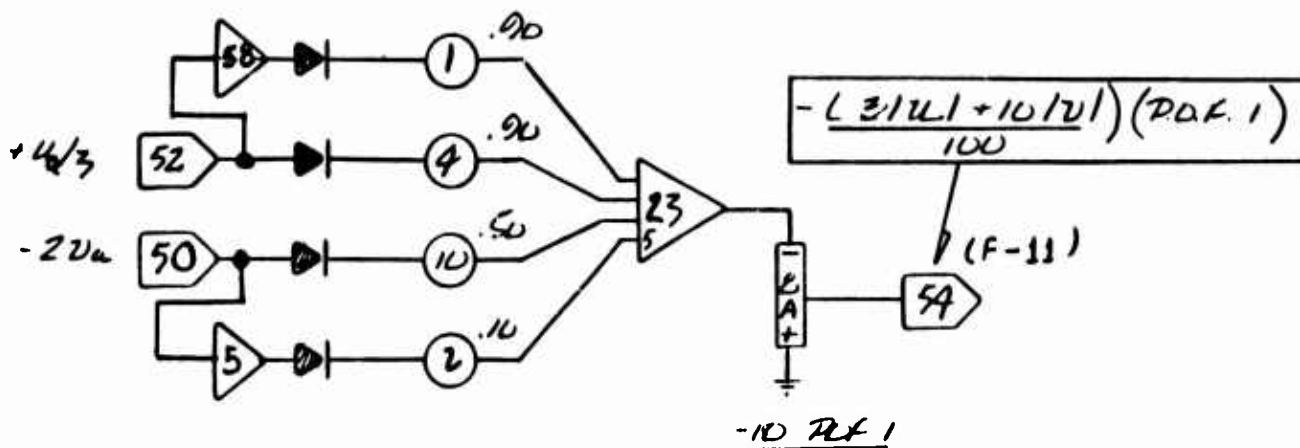
Figure 93 Low Speed Aerodynamics - Pace F

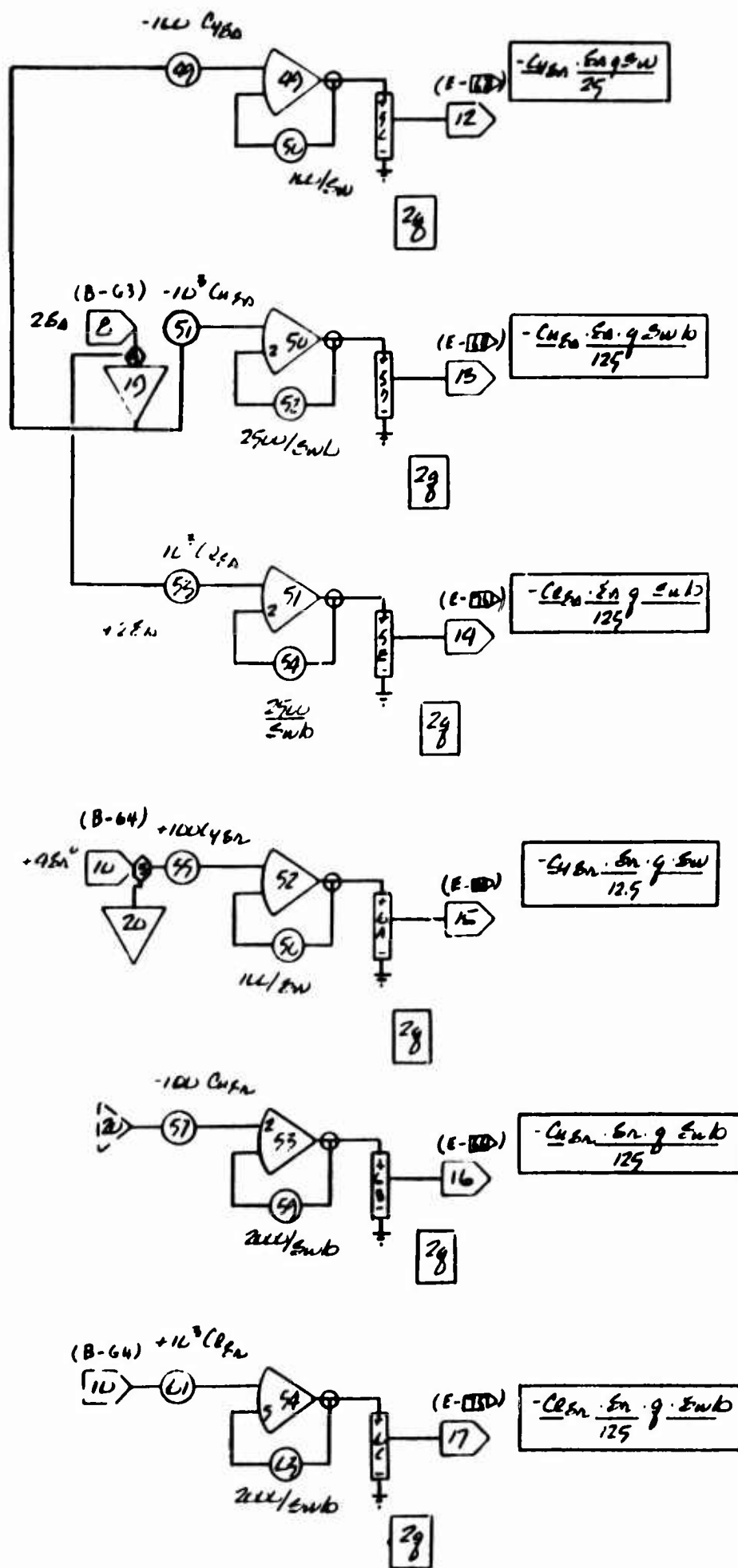145
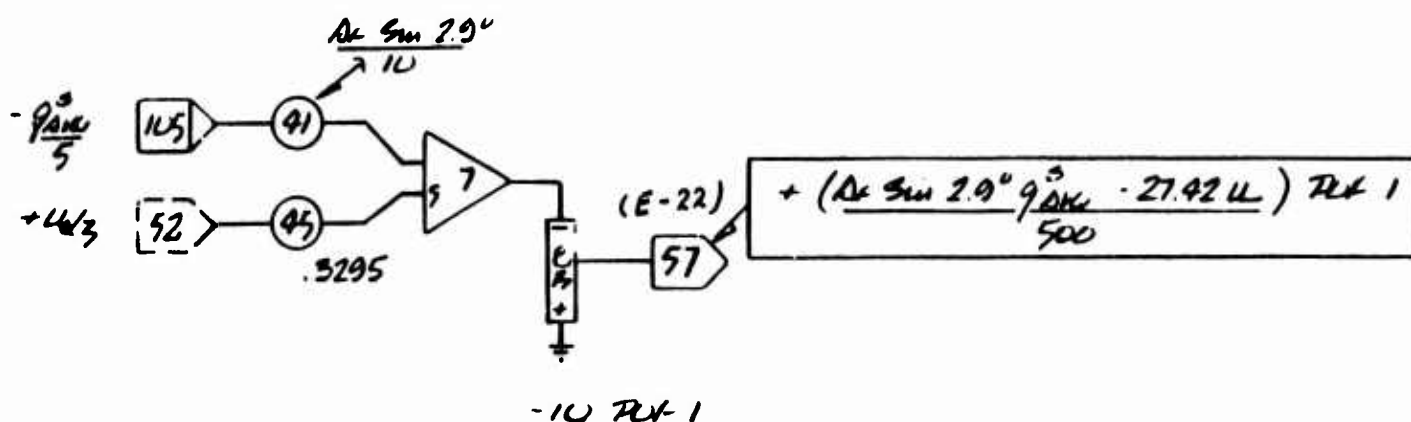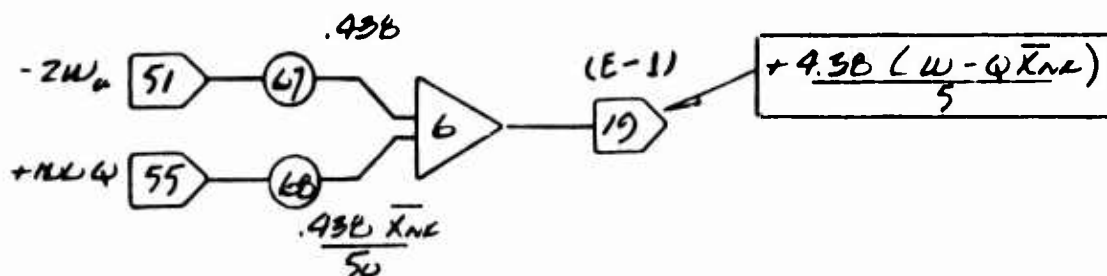
Figure 94 Low Speed Aerodynamics – Pace F

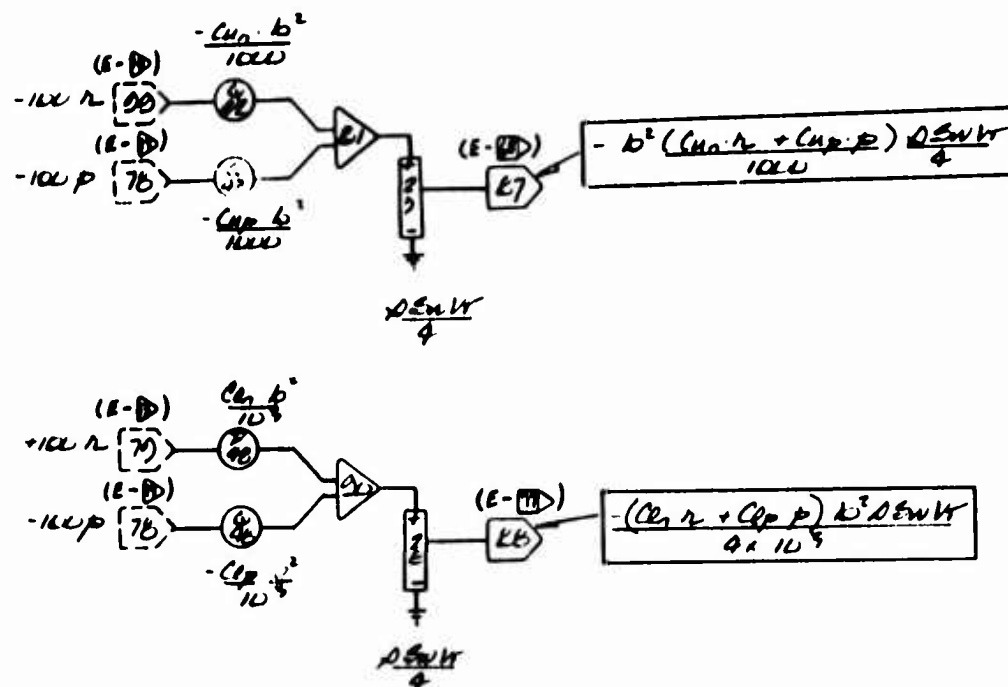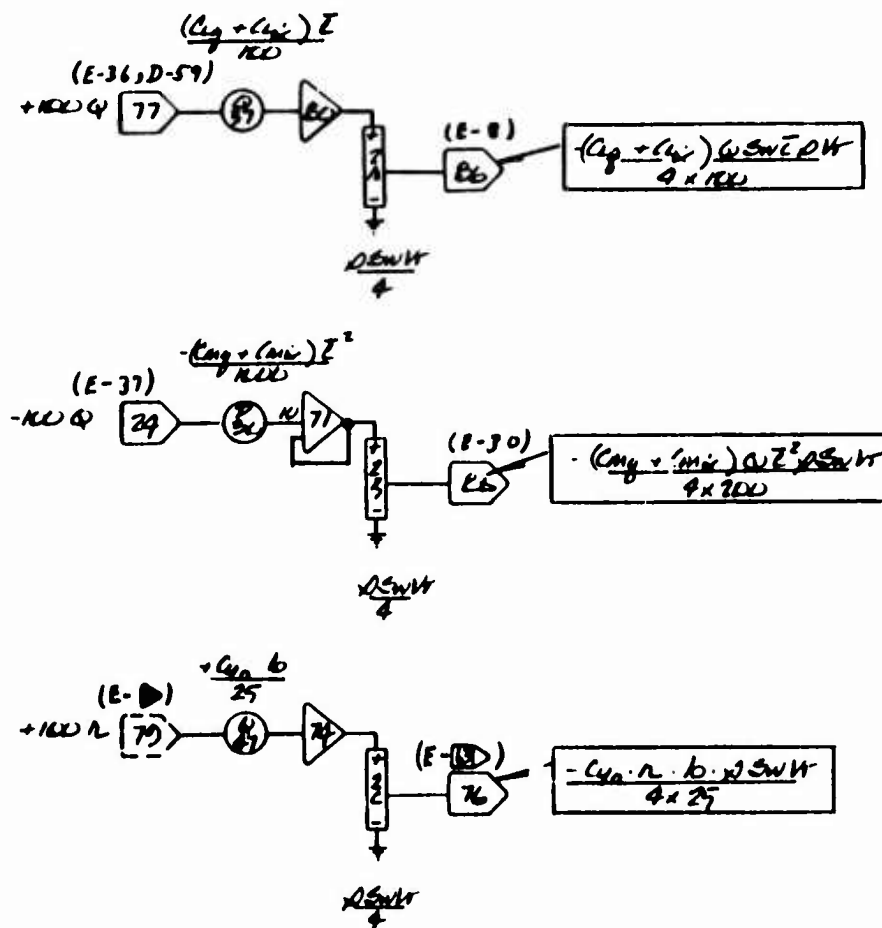Figure 95 Aerodynamic Control Forces and Moments - Pace F

Figure 96   Aerodynamic Damping - 231R
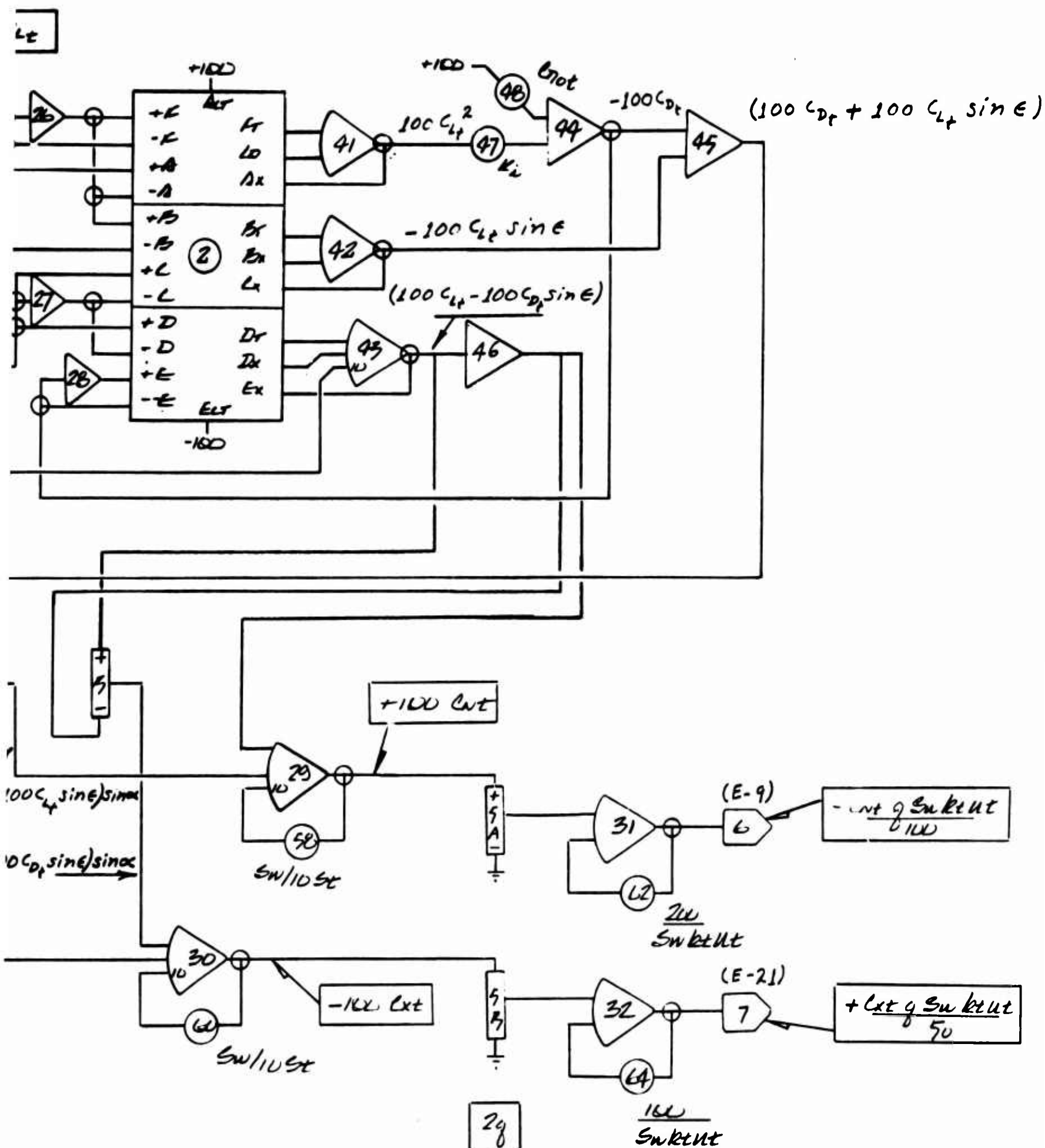

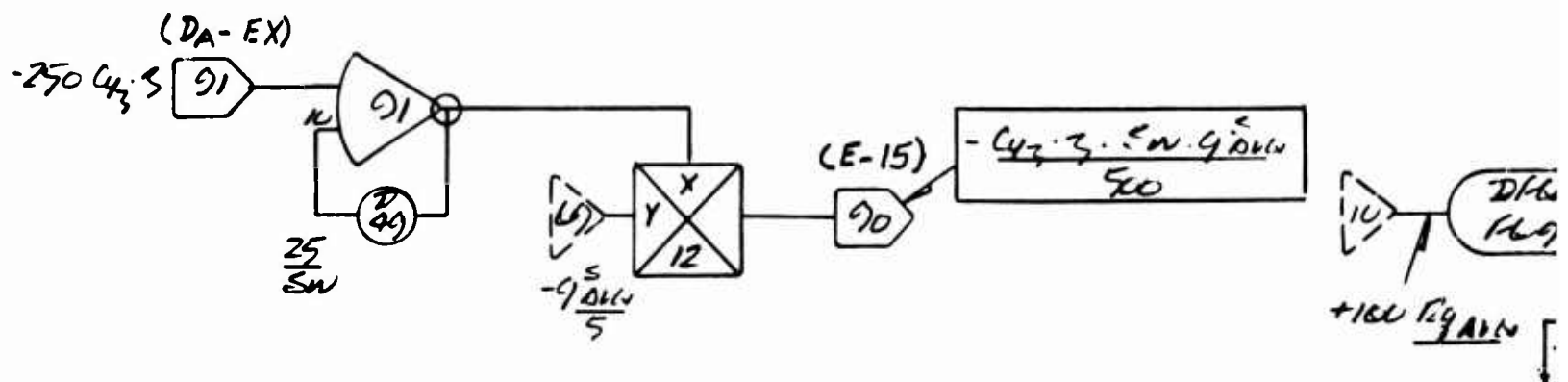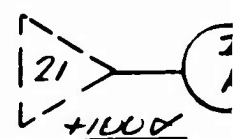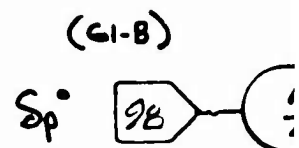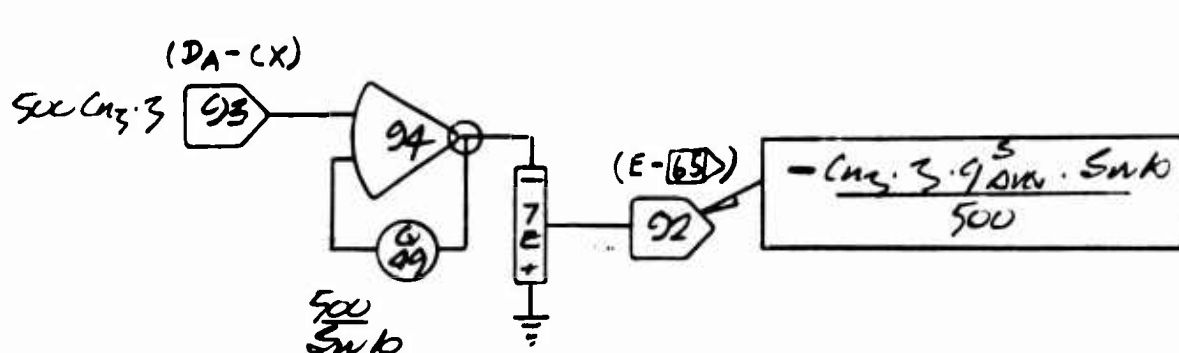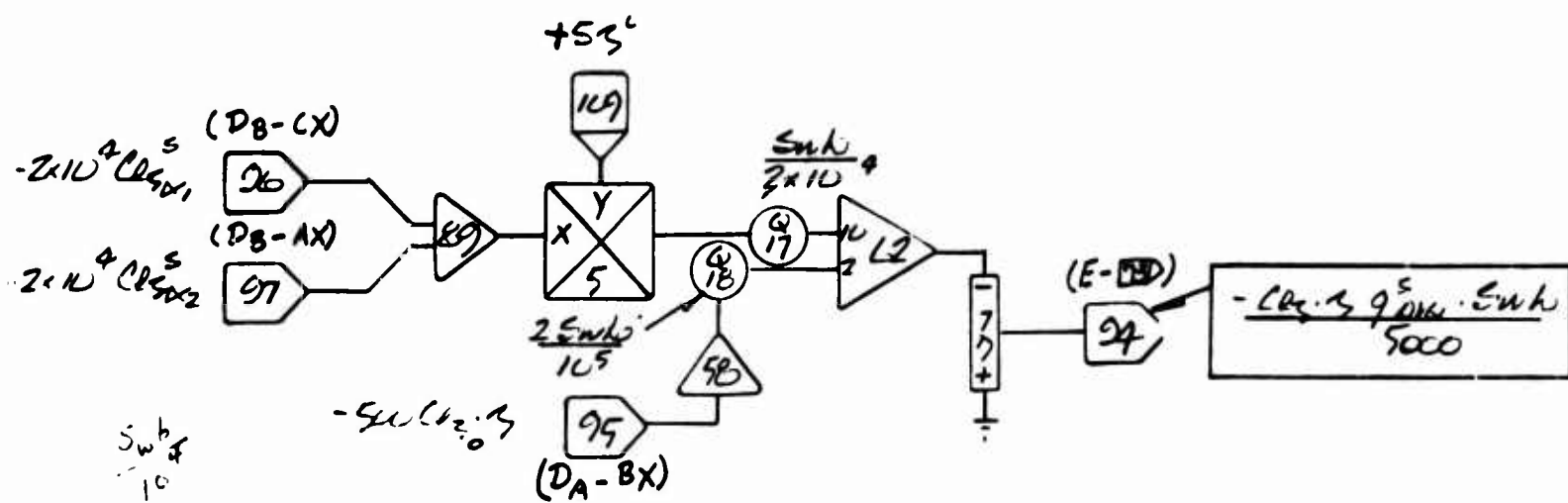Figure 97   Aerodynamic Damping - 231R

A

Figure 98 Tail Aerodynamics - Pace F

149

Figure 99: This figure shows the development of the lateral forces and moments due to sideslip as well as the pitching moment and normal force associated with the large angles of attack encountered near hover.

Some other assorted circuitry including the multiplier drives is also shown.

Figure 100: This figure shows the development of the limited sideslip angle required for generation of the sideslip functions, the circuitry developing thrust in the CTOL mode as modified by the thrust spoiler angle commanded by the pilot, and the multiplier drives of board F.

Figure 101: This figure shows the generation of pitching moment variation with angle of attack, and the thrust of the nose fan as a function of $K_{N_{NF}}$ which in turn is a function of δ_p.
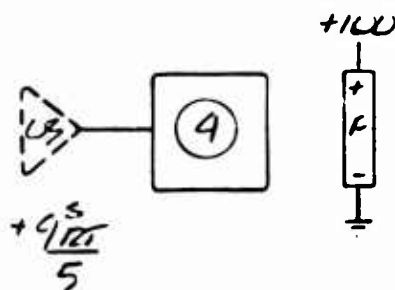
$-2\times10^{2}Cb_{SDX_1}^{S}$ (D_B-CX) | 20 |

$2\times10^{4}Cb_{SDX_2}^{S}$ (D_B-AX) | 97 |

$+53^{c}$ | 109 |

$\dfrac{Sin\phi}{2\times10^{4}}$

$\dfrac{2.Sin\phi}{10^{5}}$

$-Sin(h_{2}\cdot 3)$ | 95 | (D_A-BX)

$\dfrac{Sin\phi}{10^{4}}$

(E-□) | 94 | $\dfrac{-Cb_{3}\cdot g_{DOWN}^{S}\cdot Sin\phi}{5000}$

(D_A-CX) $Sin\,Cn_{3}\cdot 3$ | 93 |

$\dfrac{500}{Sin\phi}$

(E-65) | 92 | $\dfrac{-Cn_{3}\cdot 3\cdot g_{DOWN}^{S}\cdot Sin\phi}{500}$

(G-B) Sp° | 98 |

| 21 | $+1000$

(D_A-EX) $-250\,C_{H_3}\cdot 3$ | 91 |

$\dfrac{25}{Sin}$

$\dfrac{-g_{DOWN}^{S}}{5}$

(E-15) | 90 | $\dfrac{-C_{H_3}\cdot 3\cdot Sin\cdot g_{DOWN}^{S}}{500}$

| 10 | $+100\,Cg_{ADN}$

A
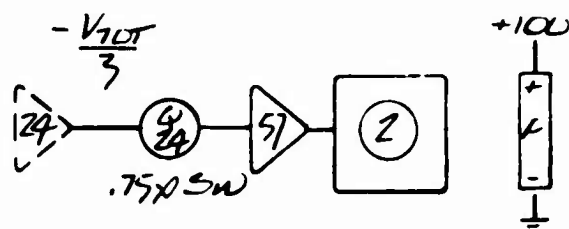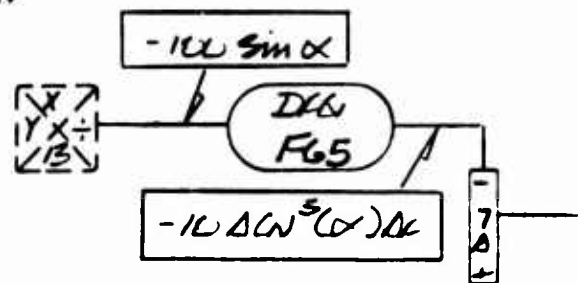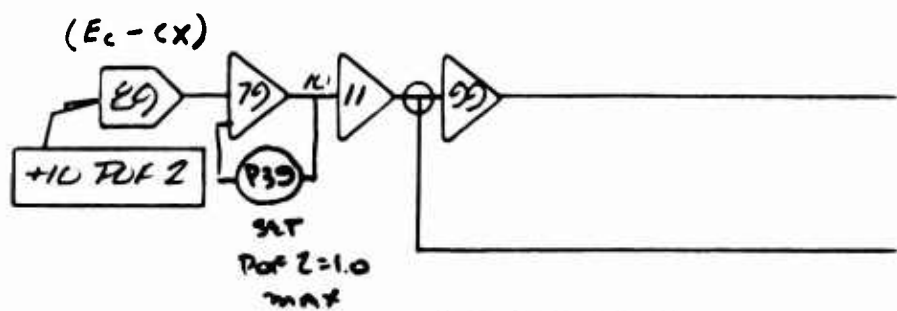
Figure 99 Aer

Figure 99 Aerodynamics - Miscellaneous Circuits - 231R

Figure 100 Miscellaneous Functions – Pace F

155

Figure 101 Miscellaneous Force and Moment Generation – Pace F

Figure 102: This figure shows the circuitry summing the components of the normal force and performing the integration required to obtain the body axis ver ical velocity.

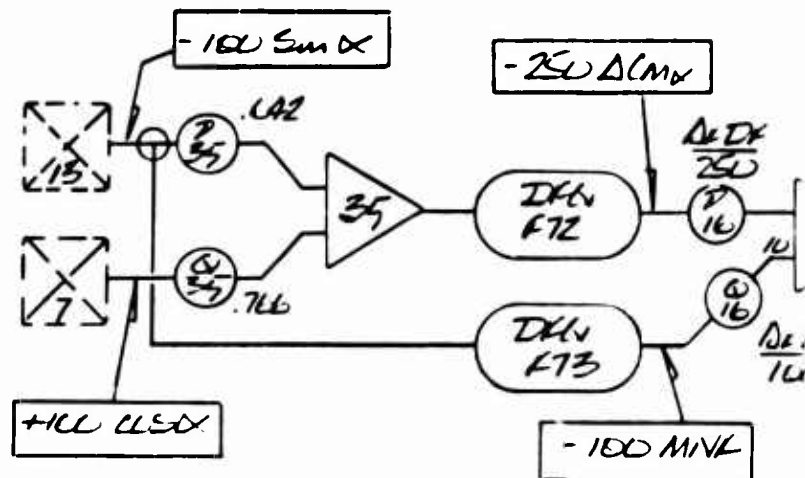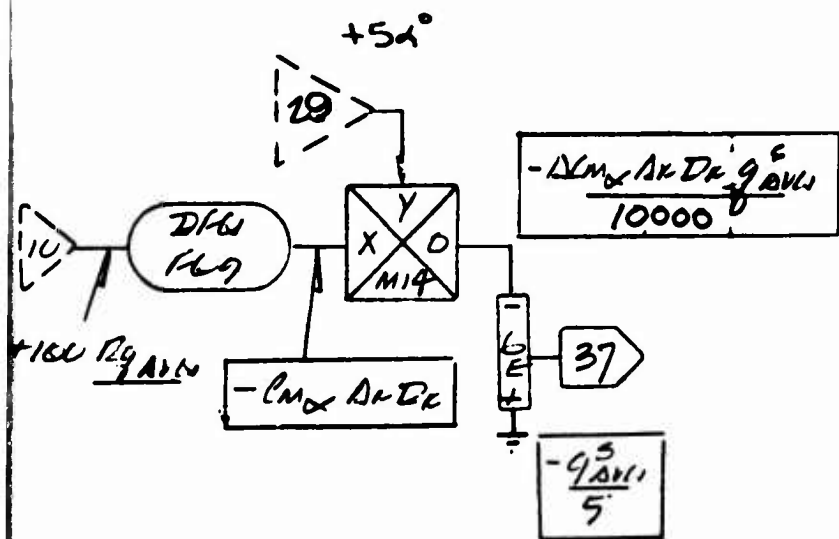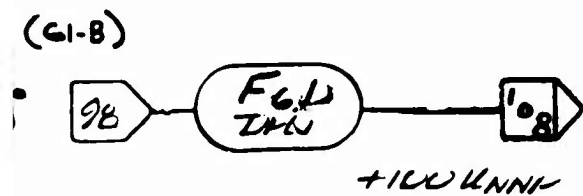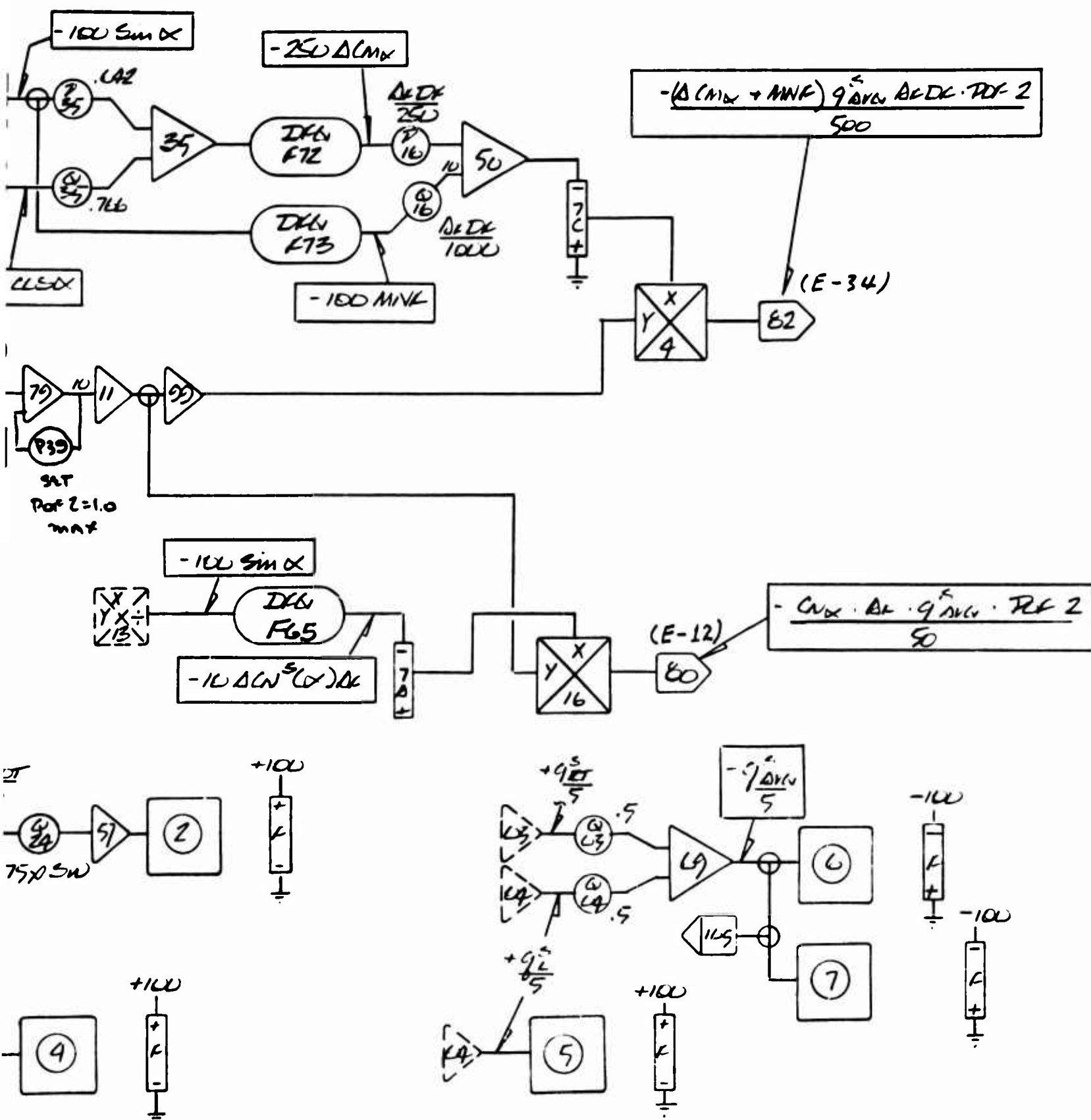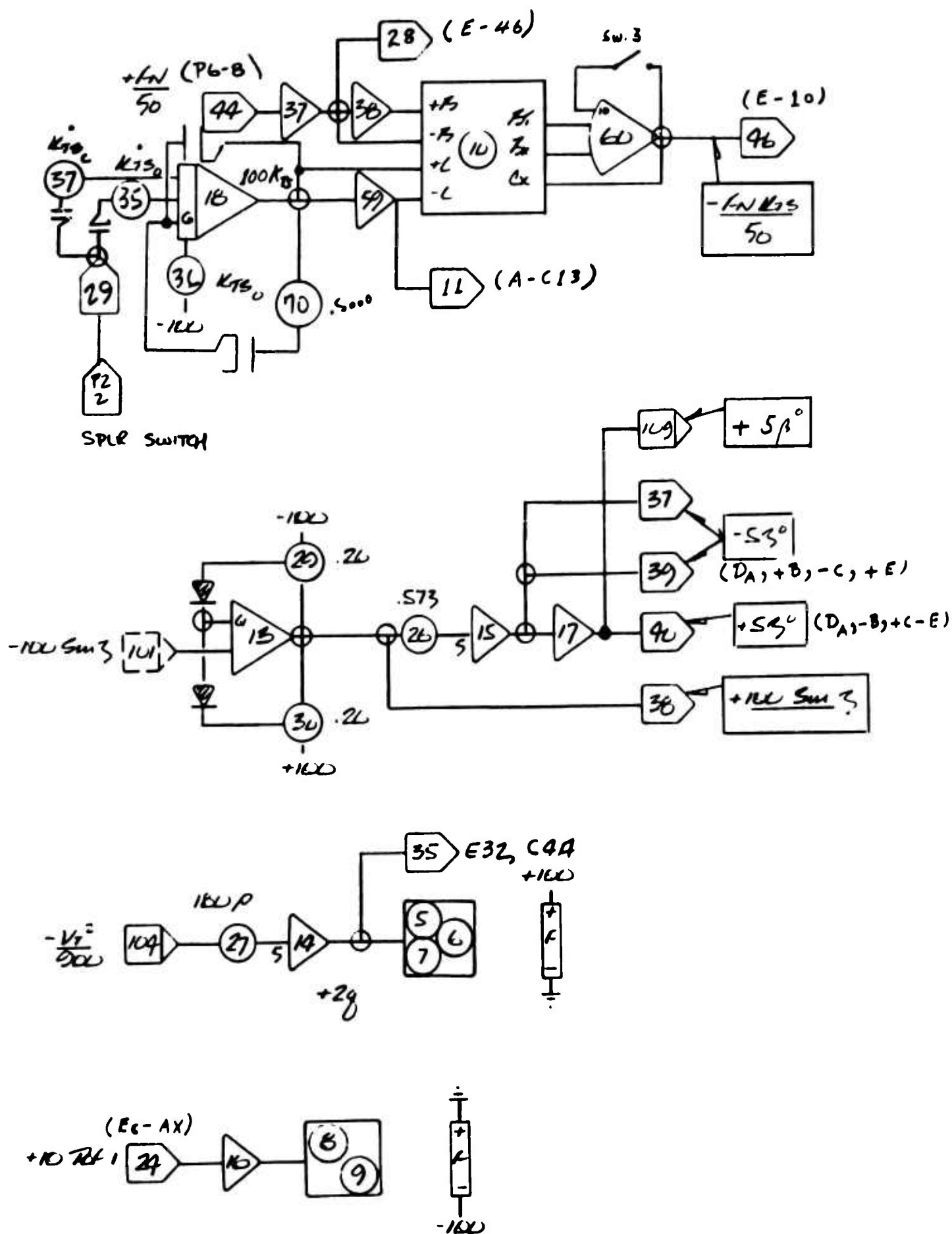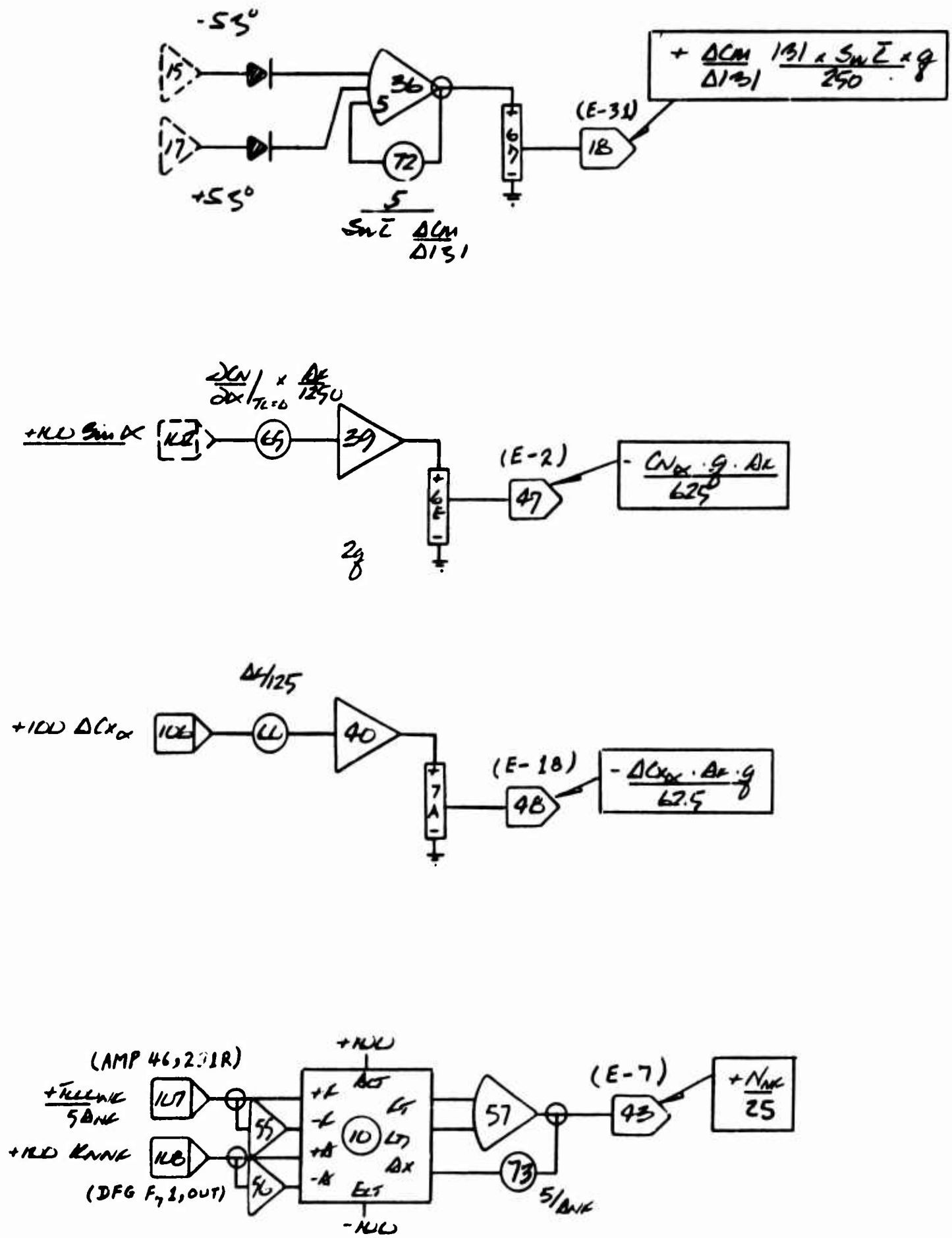This body axis velocity is summed with a gust velocity to give an airstream velocity for use in the generation of aerodynamic forces and moments.

Note the relay between pot 42 and amplifier 2. This relay opens this circuit when the doors close during the conversion sequence, which event causes the disappearance of the fan effects on the normal force.

Figure 103: This figure shows the summation of the force components making up the total axial force, and the integration of the resulting acceleration to obtain the body axis axial velocity.

This body velocity is summed with a gust velocity to obtain a total axial airstream velocity for use in the generation of forces and moments.

Note relay 4 between amplifiers 27 and 4. This relay shuts off the fan effects on the axial force upon the closing of the doors.

Relay 5 shown between pot 6 and amplifier 4, shuts off the ram drag term due to the nose fan upon the closing of the main fan doors.

Also shown in this figure is the circuitry which resolves the steady state and gust winds into the aircraft coordinates. Refer to the wind appendix (3) for an explanation of the method by which wind effects were added to the simulation.

Figure 104: This figure shows the summation of the moment components making up the total pitching moment.

To allow c.g. shifts, a pitching moment equal to the normal force multiplied by the c.g. shift from the nominal position of 246 inches is added to the pitching moment summation.
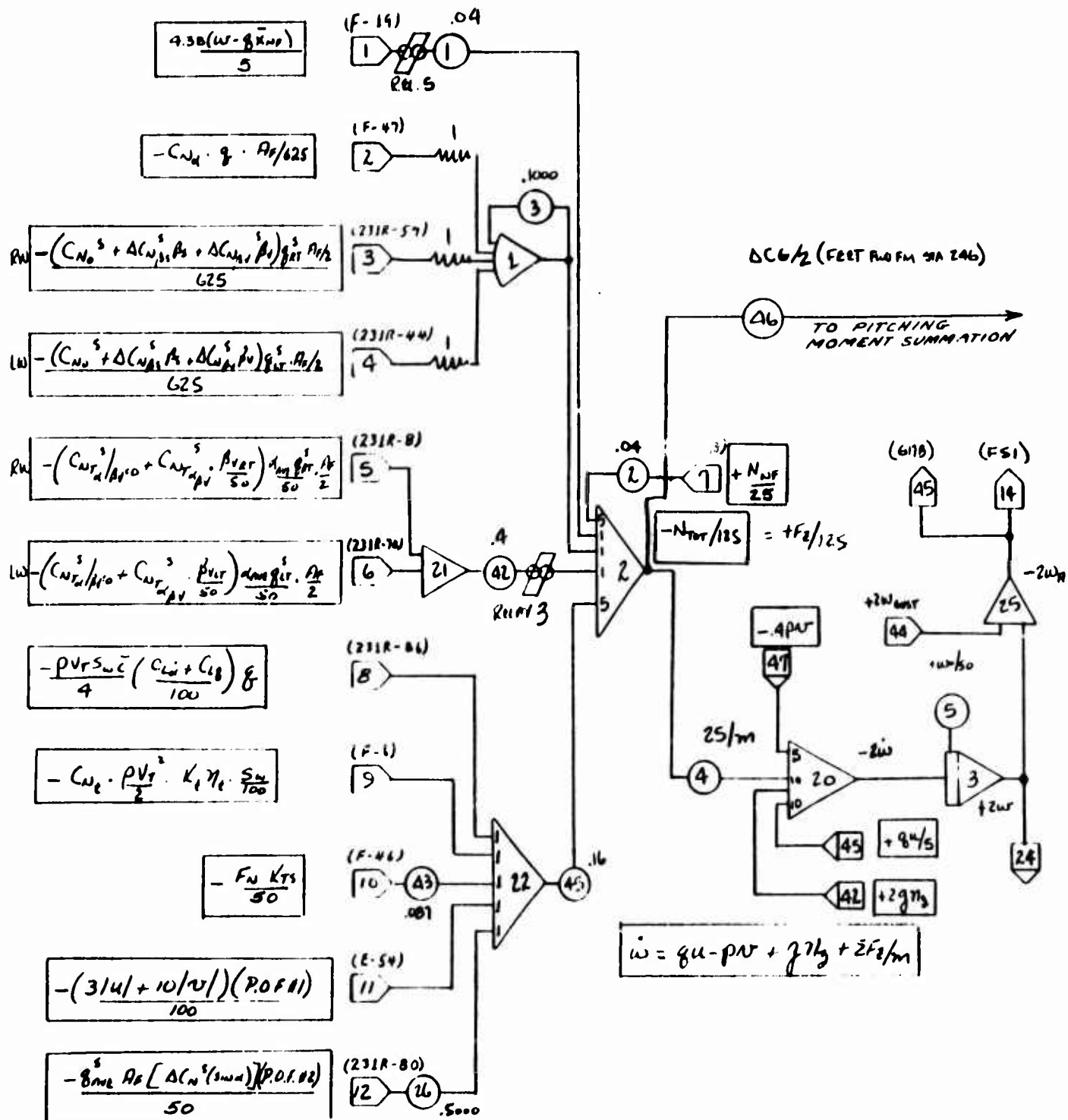
Figure 102 Z Force Summation - Pace E

$$RW \quad -\left(C_{x_o}{}^s + \Delta C_{x_{\beta\beta},\beta s} + \Delta C_{y_{\beta v},\delta v}\right)\frac{q_{RT}^s}{625} \cdot \frac{A_F}{2}$$

$$LW \quad -\left(C_{x_o}{}^s + \Delta C_{x_{\beta s},\beta s} + \Delta C_{y_{\beta v},\delta v}\right)\frac{q_{LT}^s}{625} \cdot \frac{A_F}{2}$$

$$-\left(C_{x_\alpha} \cdot \mathcal{E} \cdot \frac{A_F}{62.5}\right)$$

$$RW \quad -\left(C_{x_{T_\alpha}}{}^s\Big/_{\beta=0} + C_{x_{T_{\beta v}}}{}^s \cdot \frac{\beta v_{RT}}{50}\right)\alpha_{AVE} \cdot \frac{q_{RT}^s}{25} \cdot \frac{A_F}{2}$$

$$LW \quad -\left(C_{x_{T_\alpha}}{}^s\Big/_{\beta=0} + C_{x_{T_{\beta v}}}{}^s \cdot \frac{\beta v_{LT}}{50}\right)\alpha_{AVE} \cdot \frac{q_{LT}^s}{25} \cdot \frac{A_F}{2}$$

$$+ C_{x_t} \cdot K_t \cdot \eta_t \cdot \frac{\rho v_J^2}{2} \cdot \frac{S_w}{50}$$

$$+2g$$

$$+\frac{\left(q_{AVE}^s \, A_F \sin 2.9° - 27.424\right) POF \#1}{500}$$

$$-F_N \, k_{TS}/50$$

$(231R-69)_1$ 16

$(231R-54)_1$ 17

$(F-48)$ 18

26   .5000   52

$-2g\,l_3$ 37

$+\Delta q$ 36

$(231R-34)$ 19

$(231R-75)$ 20

Relay 4   27

$\frac{u_o}{300}$ 7

.0263   6

5

8   $\frac{100}{m}$

$(F-7)$ 21

$(F-35)$ 32 $C_0 S_{w\,HR}/500$ 15

$(F-57)$ 22

4

$-X_{TOTAL}/50$

24

28   29

56   .1000

$$\dot{u} = RV - qw + g$$

$(F-46)$ 10

Figure

Figure 103   X Force Summation Plus Wind Resolution Into X and
Y Components

$$\dot{u} = RN - qw + g\ell_3 + \Sigma F_x/m$$

159

$$\frac{4.38(\omega - q\bar{X}_{NF})}{5}$$

$$+\left(\frac{T_o}{A_{NF}}\right) \cdot \frac{A_{NF}}{25} \cdot K_{N_{NF}}$$

$$-\frac{\left(C_{M_o}^s + \Delta(C_{m_{\beta_v}}^s)\beta_v + \Delta(C_{m_{\beta_s}}^s)\beta_s\right)q_{RT}^s \cdot \frac{A_F D_F}{2}}{250}$$

$$-\frac{\left(C_{m_o}^s + \Delta C_{m_{\beta_v}}^s \beta_v + \Delta C_{m_{\beta_{s_1}}}^s \beta_s\right)q_{LT}^s \cdot \frac{A_F D_F}{2}}{250}$$

$$-\frac{\rho V_T S_w \bar{c}^2}{4} \cdot \left(C_{m_q} + C_{m_{\dot{\alpha}}}\right)\frac{q}{100}$$

$$\left(\frac{-N_{TOTAL}}{125} \times \frac{\Delta CG}{2}\right) \qquad + \frac{\rho V_T^2}{2} \cdot \frac{S_w \bar{c}}{250} C_{m_{|\beta|}}^s |\beta|_{LIM}$$

$$-\frac{\rho V_T^2}{2} \cdot \frac{S_w \bar{c}}{100} \cdot K_\ell \eta_\ell \cdot C_{N_\ell}$$

$$+\frac{\rho V_T^2}{2} \cdot \frac{S_w \bar{c}}{50} \cdot K_\ell \eta_\ell \cdot C_{X_\ell}$$

$$-\frac{\left(134\mathcal{U} - q_{AVE}^s A_I \bar{X}_F\right) POF \#1}{5000}$$

$$-\frac{q_{AVE}^s A_F D_F \left(\Delta C_m^s (\alpha \cdot 50°) + MNF\right) POF \#2}{500}$$

$$-\frac{\left(C_{m_\alpha}^s \alpha_{LIM} q_{AVE}^s A_F D_F\right)}{10000}$$

(F-14) $\bar{X}_{NF}/250$ [1]   RLS   (60)

(F-43) $\bar{X}_{NF}/100$ [7]   (61)

(231R-64)   [28]

(231R-49)   [29]   31   (36) .040

(231R-85)   .4   [30]   32   (6A)

(F-18)   [31]

(F-6)   [9]   (65) $\ell_t/25$

(F-7)   [21]   (67) $z_t/25$

(F-58)   [33]

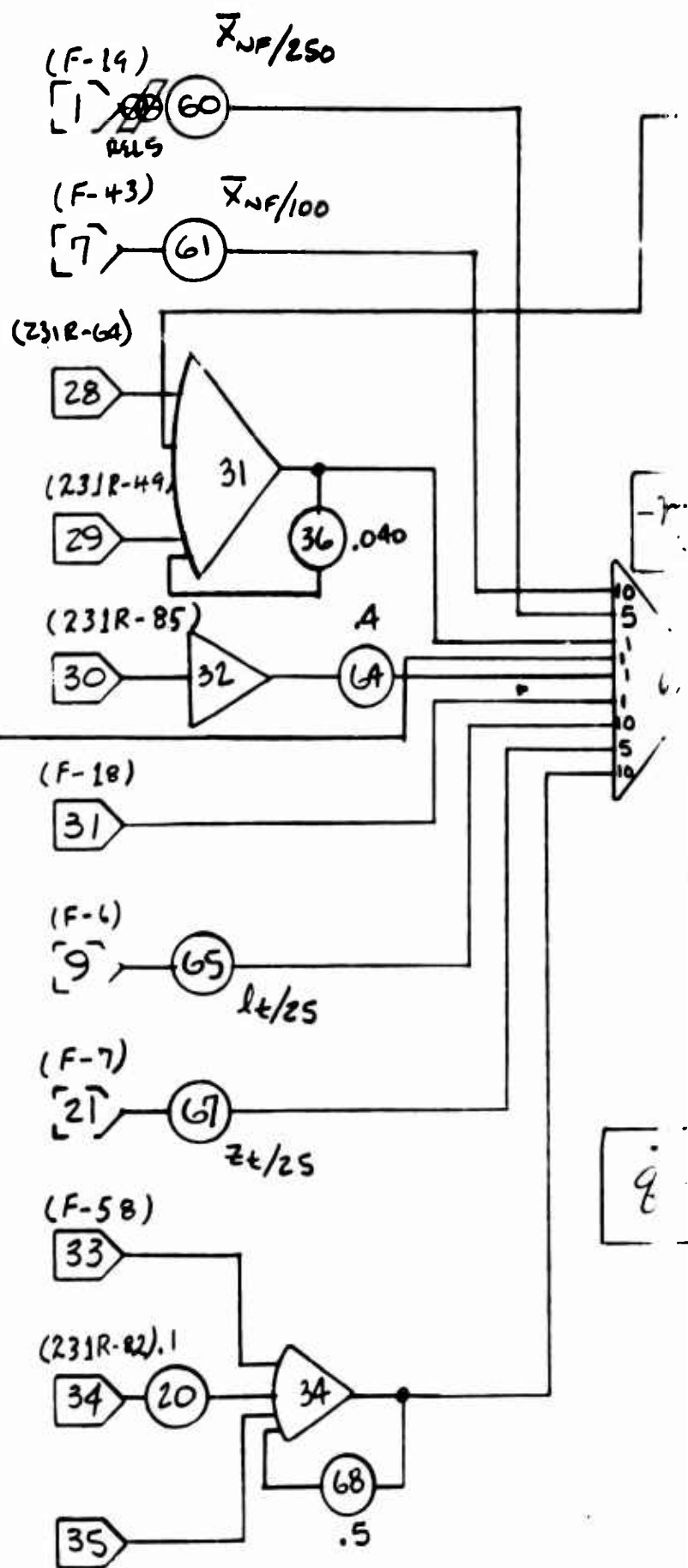(231R-82).1   [34]   (20)   34   (68) .5   [35]
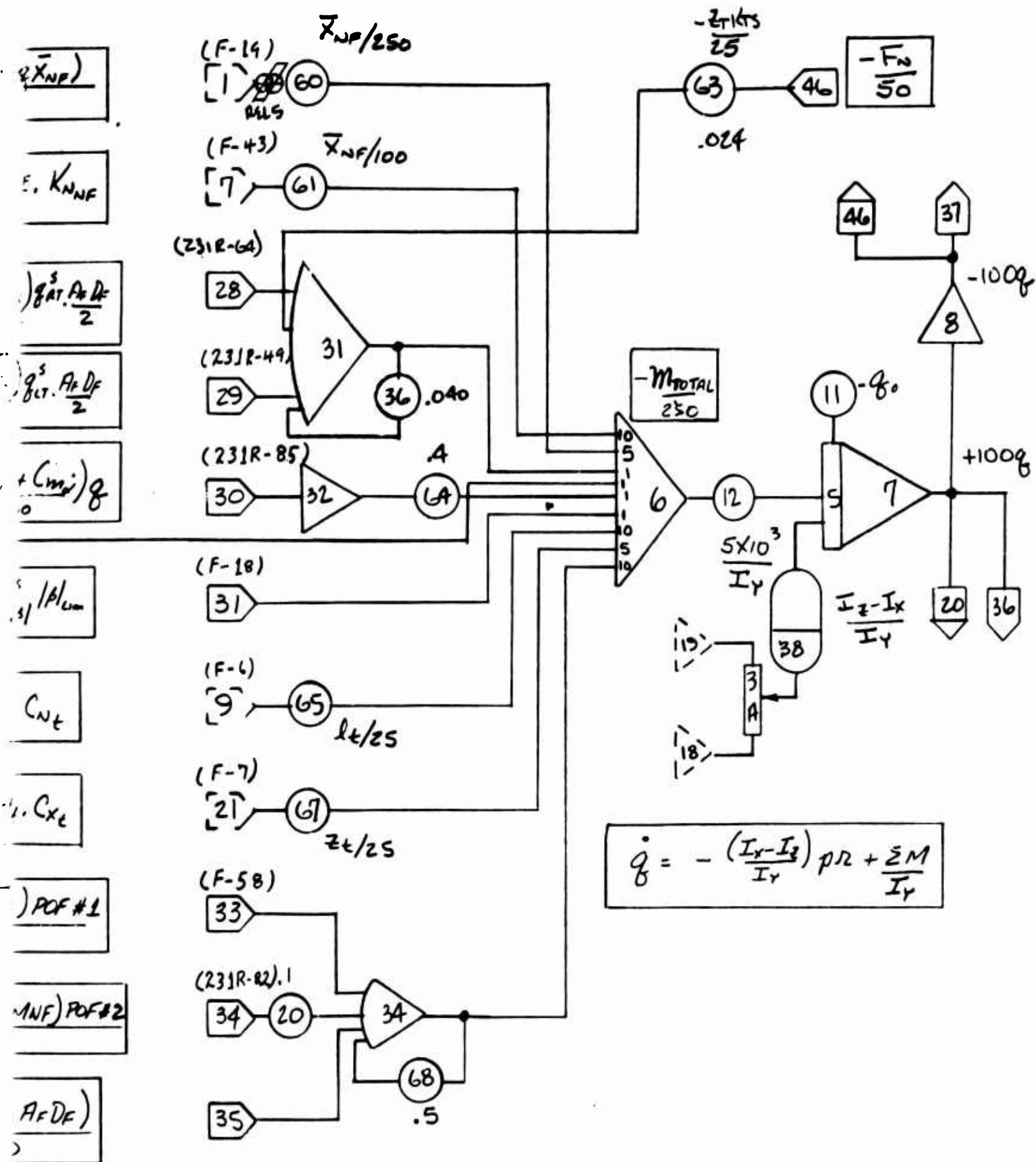
Figure 104 Pitching Mome

A

Figure 104 Pitching Moment Summation – Pace E

B

Figure 105: This figure shows the summation of the force components making up the total side force and the required integration to obtain the body axis side velocity.

The side velocity so obtained is added to a gust wind velocity (shown resolved in Figure 103) to obtain an airstream velocity for use in the generation of aerodynamic forces and moments.

Figure 106: This figure shows the summation of components making up the total yawing moment.

The resulting acceleration is integrated to obtain the body axis yaw rate.

Figure 107: This figure gives the summation of the components making up the total rolling moment.

The resulting acceleration with the appropriate cross coupling terms is integrated to obtain the rolling velocity.
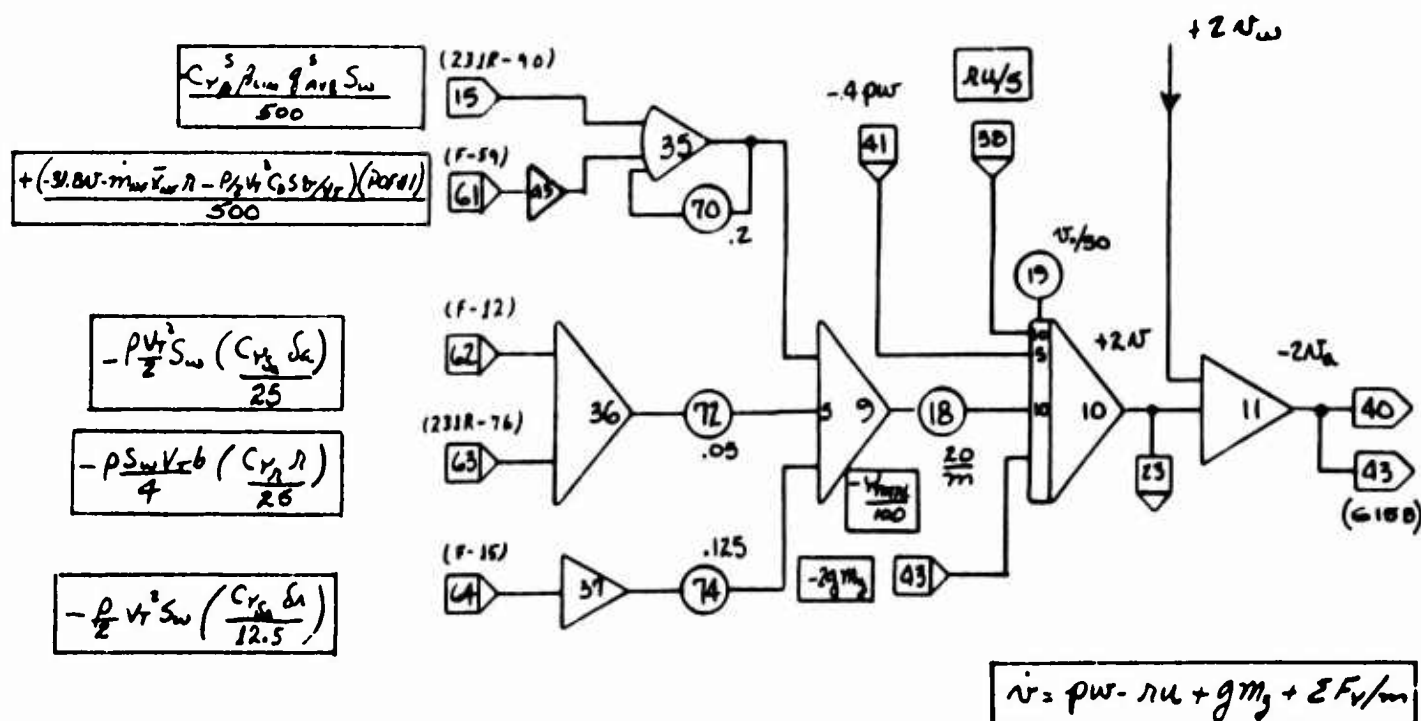

Figure 105 Side Force Summation - Pace E

$$-\frac{C_{n_p}{}^3\,\beta_{lin}{}^3\,q_{AVE}\,S_w\,b}{500}$$

$$-\frac{\rho}{2}V_T{}^2 S_w b\left(C_{n_{\delta a}}\frac{\delta a}{125}\right)$$

$$-\frac{\rho}{2}V_T{}^2 S_w b\left(C_{n_{\delta r}}\frac{\delta r}{125}\right)$$

$$-\frac{\frac{\rho}{4}V_T S_w b^2\left(C_{n_r}r+C_{n_p}p\right)}{1000}$$

$$-\left(C_{x_o}{}^3+\Delta(x_{\beta_V}{}^3)\beta_V+\Delta(x_{\beta_S}{}^3)\beta_S\right)\frac{q_{RT}{}^5}{62.5}\cdot\frac{A_F}{2}$$

$$-\left(C_{x_o}{}^3+\Delta(x_{\beta_V}{}^3)\beta_V+\Delta(x_{\beta_S}{}^3)\beta_S\right)\frac{q_{LT}{}^5}{62.5}\cdot\frac{A_F}{2}$$

$$-\frac{\dot{m}_{NF}\,\bar{x}_{NF}\,r}{25}$$

$$-\frac{\left(47r+560\frac{\rho}{2}V_T{}^2\cdot\frac{v}{V_T}-2\ell\dot{m}_{MF}\,\psi_{MF}{}^2\right)PoF\#1}{250}$$

(231R-92) 65 ▷ ▷38

(F-13) 66 ▷
(F-16) 67 ▷ ▷39 ⊙18 .125

(231R-87) 68 ▷ ▷40

(231R-69) 16 ▷—ⱳⱳ—▷41

(231R-54) 17 ▷—ⱳ—▷42 ⊙75 $Y_F/8$

(F-21) 68 ▷ ⊙76 .25

(F-56) 70 ▷ ▷45 ⊙77 .5000

TO
MON

Fig

Figure 106 Yawing Moment Summation - Pace E

$$\dot{n} = \frac{\Sigma \eta}{I_z}$$

$-\dfrac{n_{TOTAL}}{200}$

$\dfrac{2000}{I_z}$

$2\times10^{4} I_{xz}/I_x I_z$

TO ROLLING
MOMENT SUMMATION

231R-79

231R-99

$+100\Omega$

-100Ω

.125

.25

.5000

$Y_F/8$

A,B

B

$$-\left(\frac{C_{\ell_\beta}{}^S \, \beta_{trim} \, \bar{q}_{AVG}{}^S \, S_w b}{5000}\right)$$

$$-\left(\frac{-134N - 2\dot{m}_{MF} \, Y_{MF}{}^2 \, p}{5000}\right) POF\#1$$

$$-\frac{\rho}{2} V_T{}^2 S_w b \left(\frac{C_{\ell_{S_n}} \, \delta_n}{125}\right)$$

$$-\frac{\rho}{2} V_T{}^2 S_w b \left(\frac{C_{\ell_{S_a}} \, \delta_a}{125}\right)$$

$$-\left(\frac{C_{N_0}{}^S + \Delta(C_{N_{\beta s}})^S \beta_s + \Delta(C_{N_{\beta v}})^S \beta_v}{625}\right) \frac{q_{LT}{}^S \, A_F}{2}$$

$$-\left(\frac{C_{N_0}{}^S + \Delta(C_{N_{\beta s}})^S \beta_s + \Delta(C_{N_{\beta v}})^S \beta_v}{625}\right) \frac{q_{RT}{}^S \, A_F}{2}$$

$$-\frac{\rho}{4} V_T S_w b^2 \left(\frac{C_{\ell_p} p + C_{\ell_r} r}{1000}\right)$$

(231R-94) 13
(F-23) 14
46

(F-17) 15
(F-14) 16
47
.25
19

(231R-44) 4
28
.5000
15
30
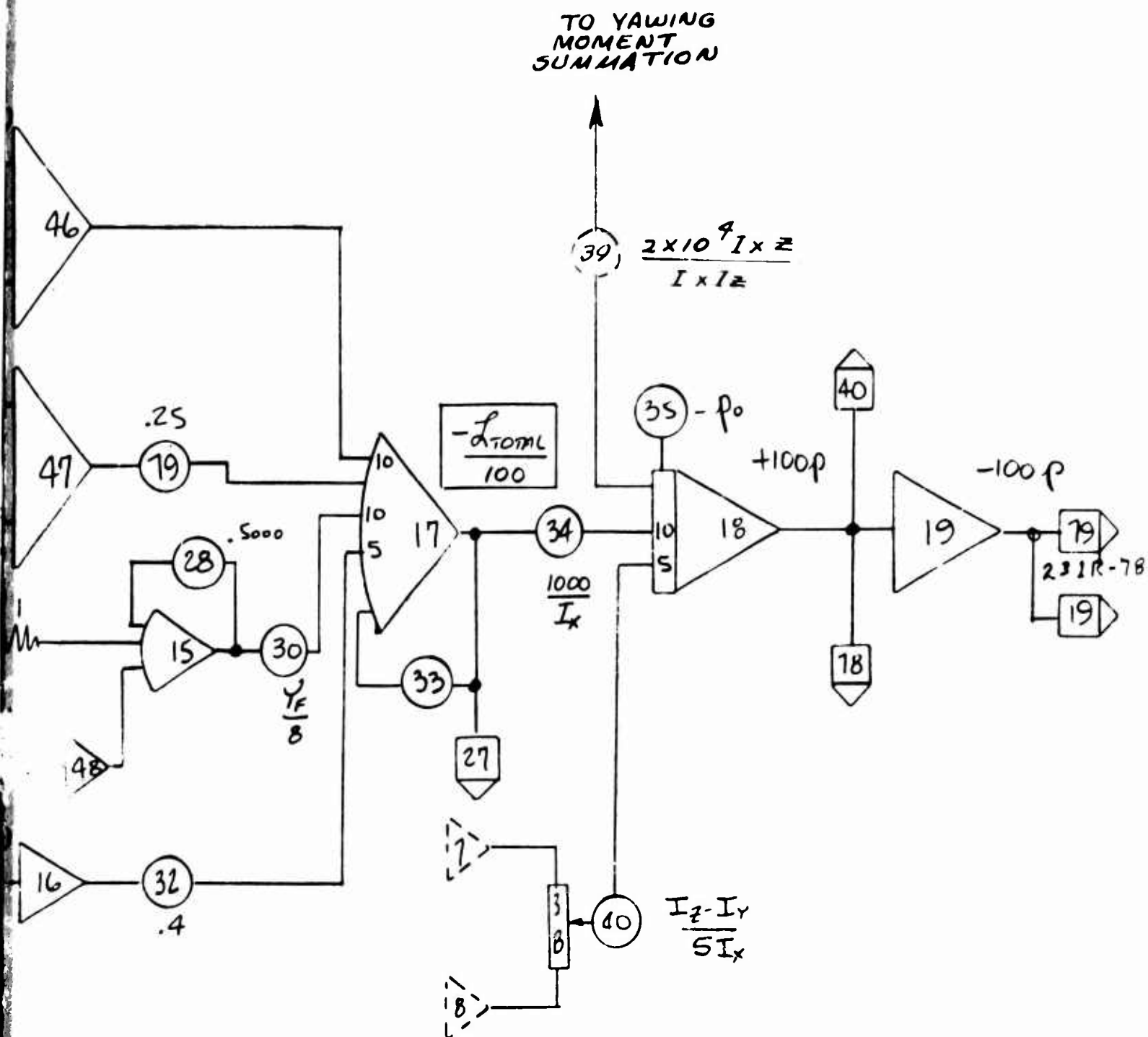$\frac{Y_F}{8}$

(231R-59) 3
48

(231R-88) 77
16
32
.4

A

Figure 107 Rolling Moment Summation - Pace E

Figure 108: This figure shows the resolution of the body axis rates into Euler angle rates and earth rates which drive the display.
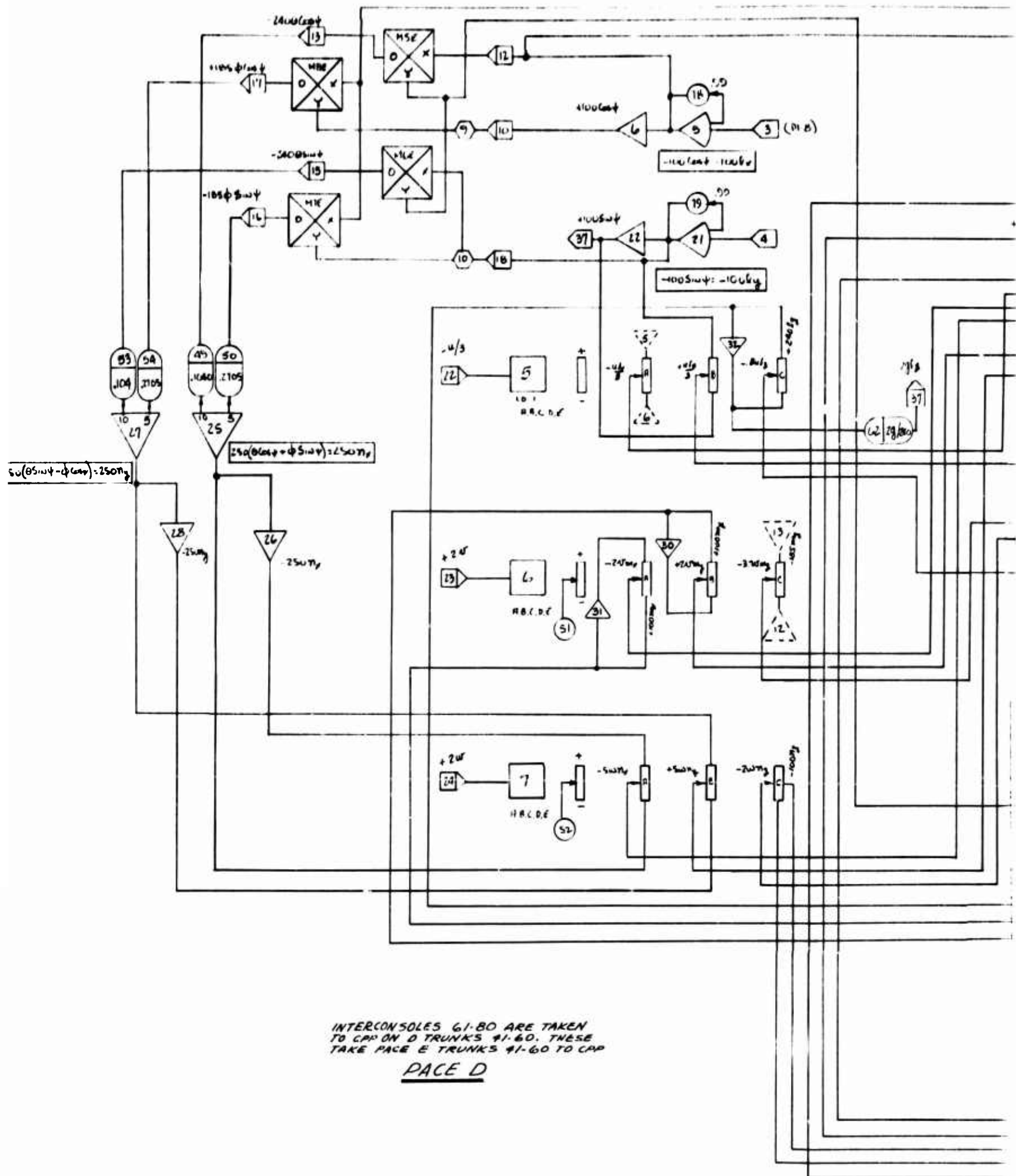
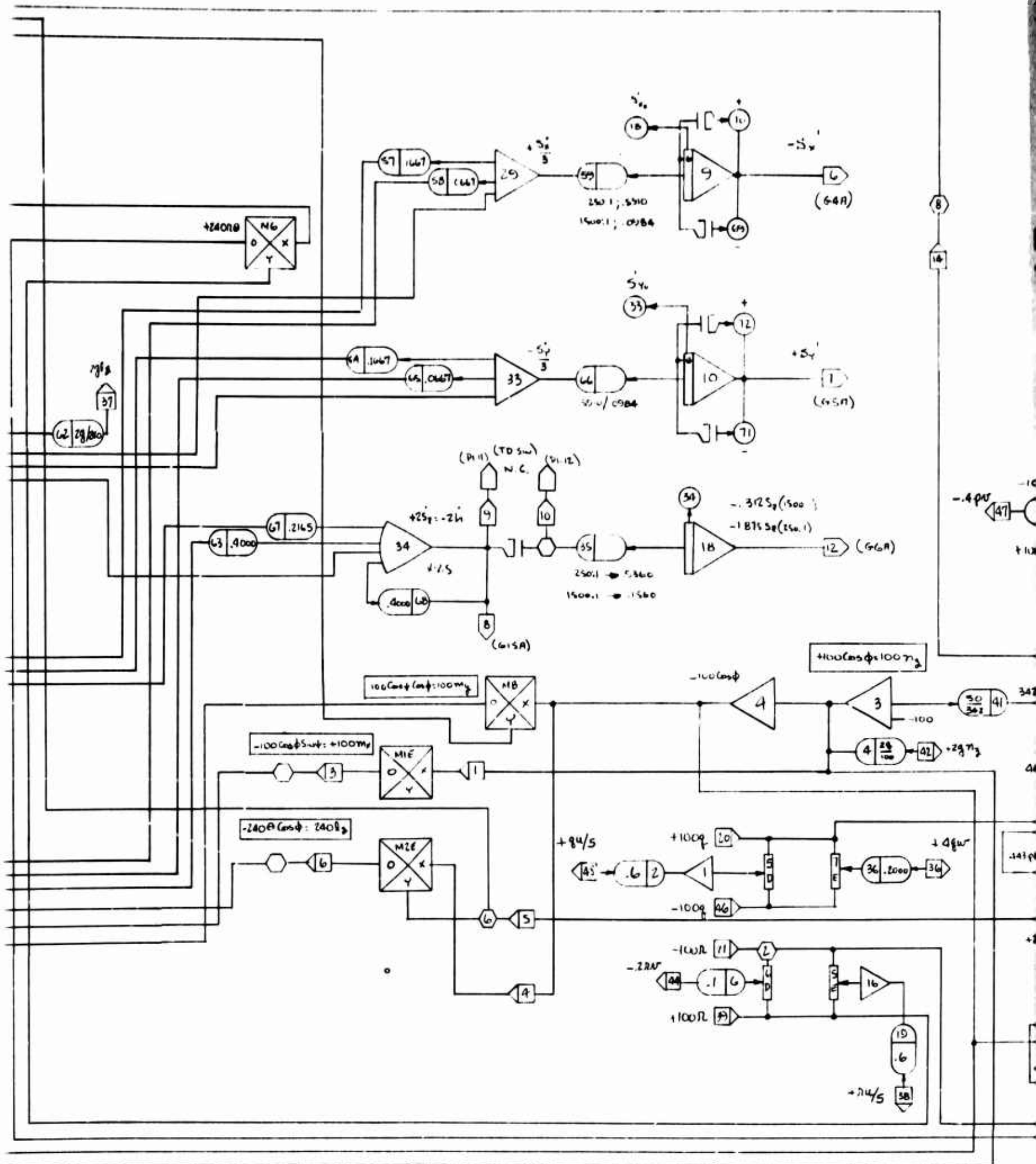Also shown are the following items:

- The scaling of the earth rates for the two transparencies used on the display (pots 59, 66 and 35).

- The limiting of the angular and x and y drives to the display.

- The relays triggering the cockpit display lights which tell the pilot he is at a pitch or roll display limit and therefore in danger of losing the true angular reference of his aircraft (relays 3 and 4).

- The function switch allowing α to be used as an initial condition for θ, forcing γ to be zero, for accomplishing trim of the aircraft (function switch 3).

- The touchdown switch which interrupts any downward display rates which would allow the aircraft to drive itself down through the ground level of the display.

Figure 109: This figure shows the display and aritficial horizon drives as scaled for input to these devices.

Also shown are the following:

- The scaling of the computer altitude for drive of the altimeter.

- The relay controls which allow the display to reset in yaw after the computer has gone to reset and the display has reset its altitude to the 2-1/2 inch level.

- Yaw reset is held off until the 2-1/2 inch condition has been met so that the rotation of the display will not cause the display projection lamp to come into contact with any of the three dimensional objects attached to the transparency.

INTERCONSOLES 61-80 ARE TAKEN
TO CPP ON D TRUNKS 41-60. THESE
TAKE PACE E TRUNKS 41-60 TO CAP

PACE D

A

B

Figure 108 Euler Angle Resolution – Pace D

171

Figure 110: This figure shows the simulation of the gas generator. A single gas generator was used, both generators being assumed to be locked together.

Relay (RY 1), shown, cuts back the gas generator rpm to 96% (or whatever is called for on pot 21) when opened by a signal from the fan overspeed circuitry.

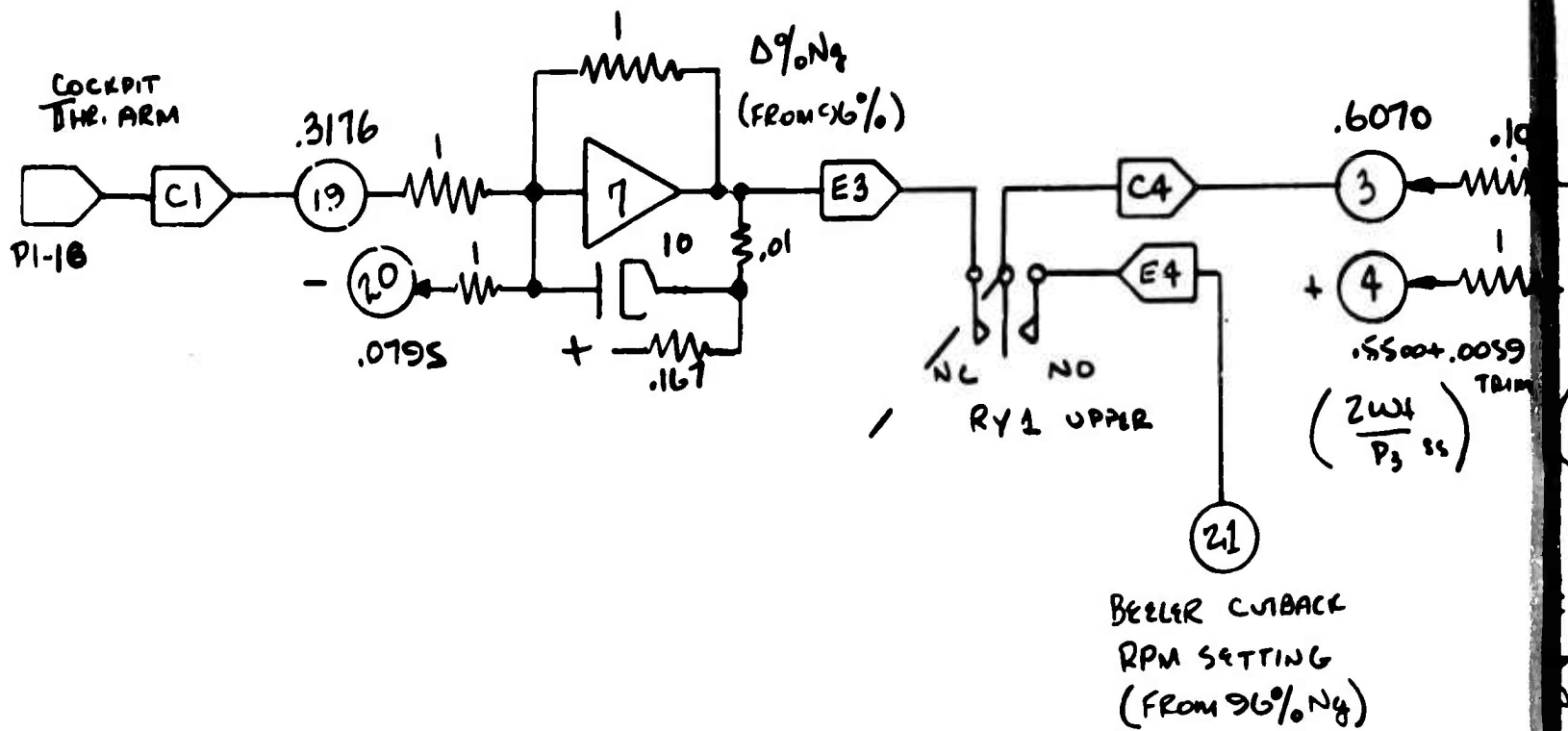Figure 111: This figure shows the fan overspeed circuitry (and the gas generator cutback).

Note Relay 2, which turns on the fan overspeed warning display on the cockpit panel prior to gas generator cutback.

Figure 112: This figure shows the fan door closing relays. This relay interrupts the circuits delivering fan effects to the force and moment summations.
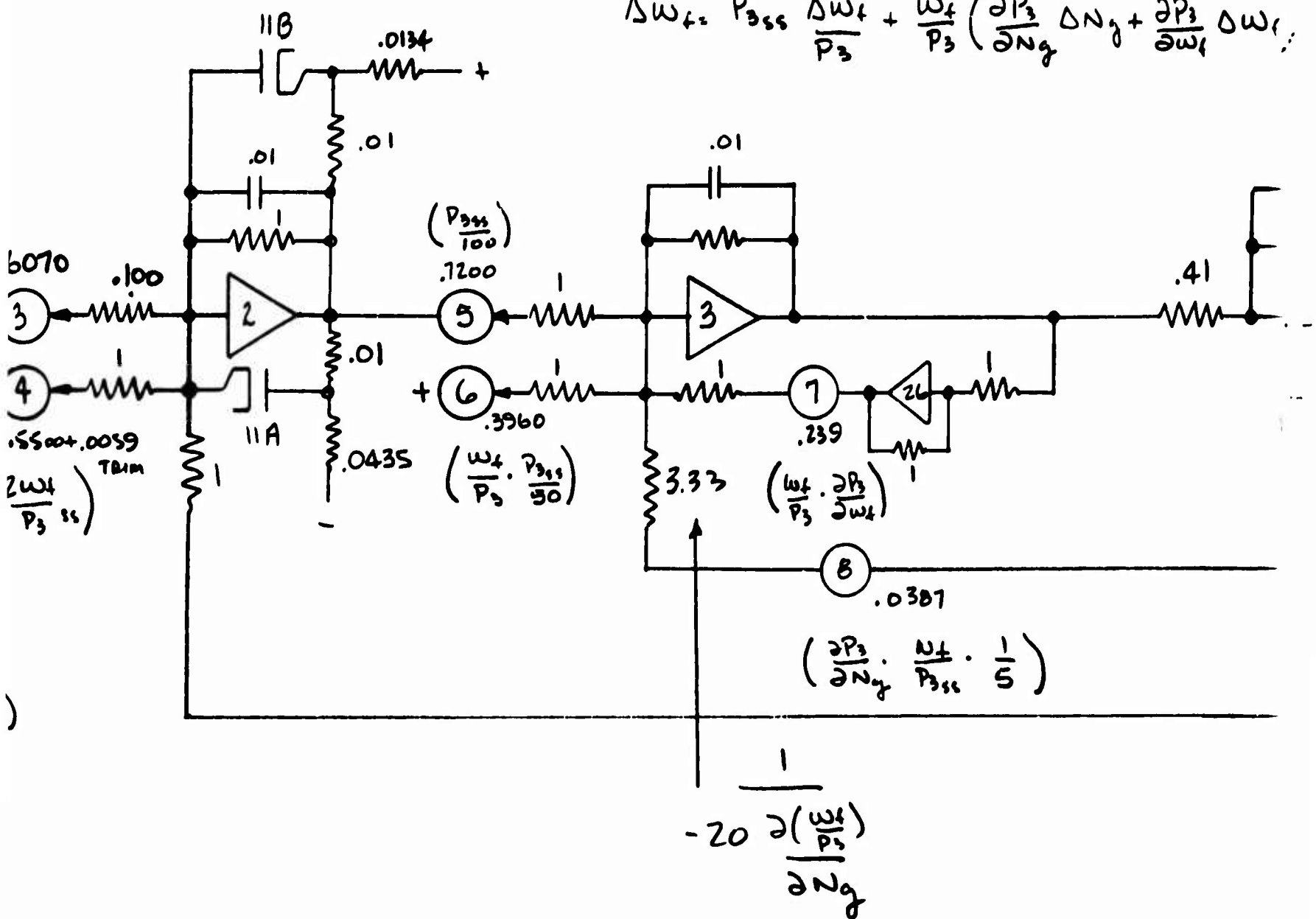
Figure 113: This figure shows the scaling of the body axis angular rates for delivery to the SA system modulators.

Bias pots were included in each circuit to zero out offsets in the modulator and SA system.

Figure 109 Display and Artificial Horizon Drives

COCKPIT
THR. ARM

.3176

PI-18

$\Delta\%N_g$
(FROM 96%)

.6070

E3

C4

3

E4

+ 4

.0795

.167

10 ⋛.01

NC   NO

RY1 UPPER

21

BEELER CUTBACK
RPM SETTING
(FROM 96% N_g)

.5500+.0059
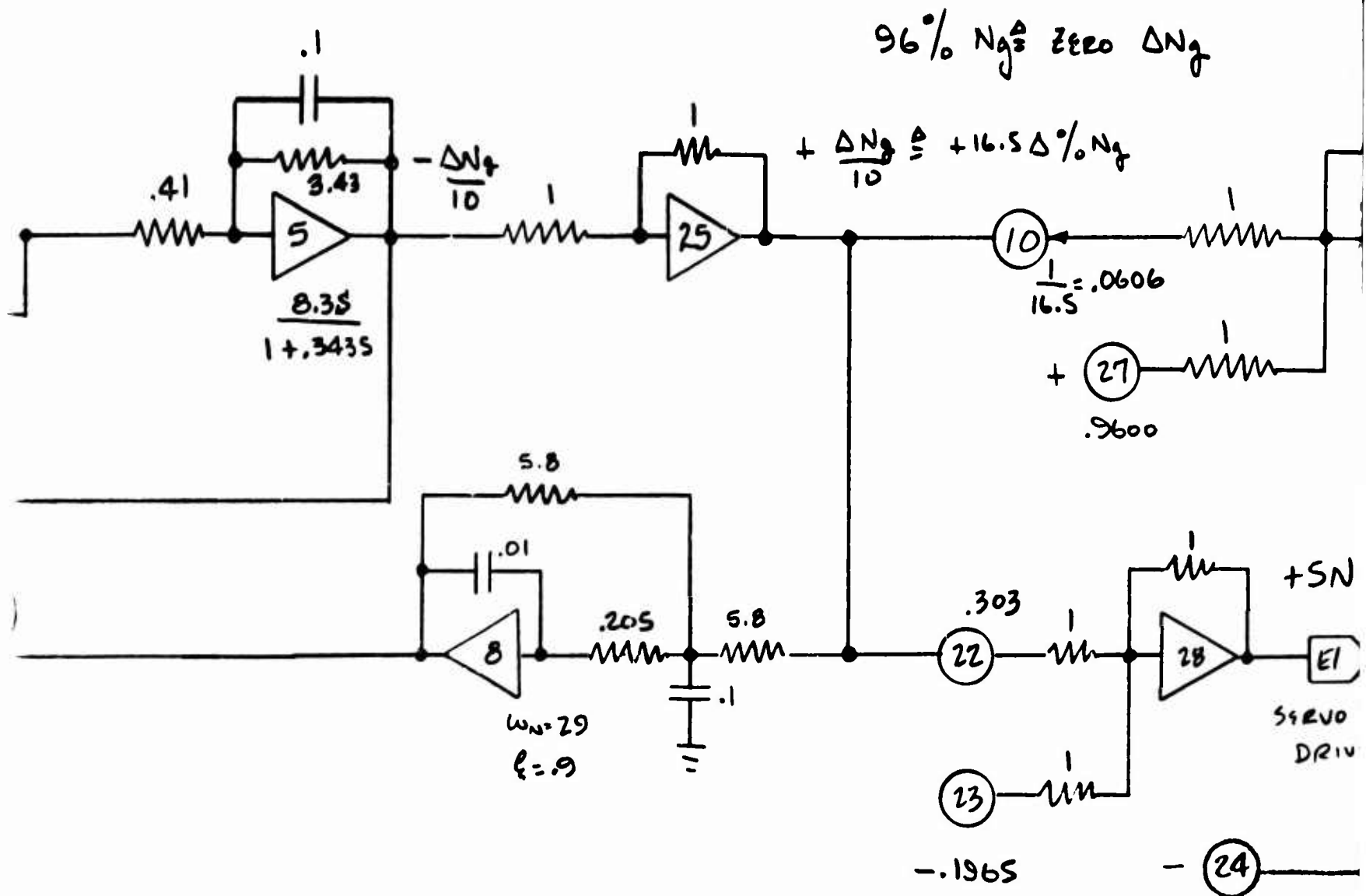TRIM

$$\left(\frac{2W_4}{P_3}\text{ }\text{ }s\right)$$

A

$$\Delta \omega_f = P_{3ss} \frac{\Delta \omega_f}{P_3} + \frac{\omega_f}{P_3}\left(\frac{\partial P_3}{\partial N_g}\Delta N_g + \frac{\partial P_3}{\partial \omega_f}\Delta \omega_f\right)$$

11B

.0134

+

.01

.01

6070

.100

.01

③

②

④

1

11A

.0435

$\left(\frac{P_{3ss}}{100}\right)$

.1200

⑤

1

③

.01

.41

.239

7 ⑦

2L

1

⑥ +

1

.3960

$\left(\frac{\omega_f}{P_3}\cdot\frac{P_{3ss}}{50}\right)$

3.33

$\left(\frac{\omega_f}{P_3}\cdot\frac{\partial P_3}{\partial \omega_f}\right)$

B

.0387

$\left(\frac{\partial P_3}{\partial N_g}\cdot\frac{N_f}{P_{3ss}}\cdot\frac{1}{5}\right)$

$.5500+.0059$

TRIM

$\left(\frac{2\omega_f}{P_3}ss\right)$

)

$$-20\ \frac{\partial\left(\frac{\omega_f}{P_3}\right)}{\partial N_g}$$

$$\Delta N_g + \frac{\partial P_3}{\partial \omega_f} \Delta \omega_f \Big)$$

$$96\% \, N_g \stackrel{\triangle}{=} ZERO \, \Delta N_g$$

.1

.41   3.43 $-\frac{\Delta N_f}{10}$ 1 $+\frac{\Delta N_g}{10} \stackrel{\triangle}{=} +16.5 \Delta \% N_g$

5

$$\frac{8.35}{1+.3435}$$

⑤   ㉕   ⑩ $\frac{1}{16.5} = .0606$

$+$ ㉗   .9600

5.8

.01   .205   5.8   .303 $+SN$

⑧   ㉒   ㉘ $\boxed{E1}$

$\omega_N = 29$ .1   SERVO DRIV

$\xi = .9$ ㉓

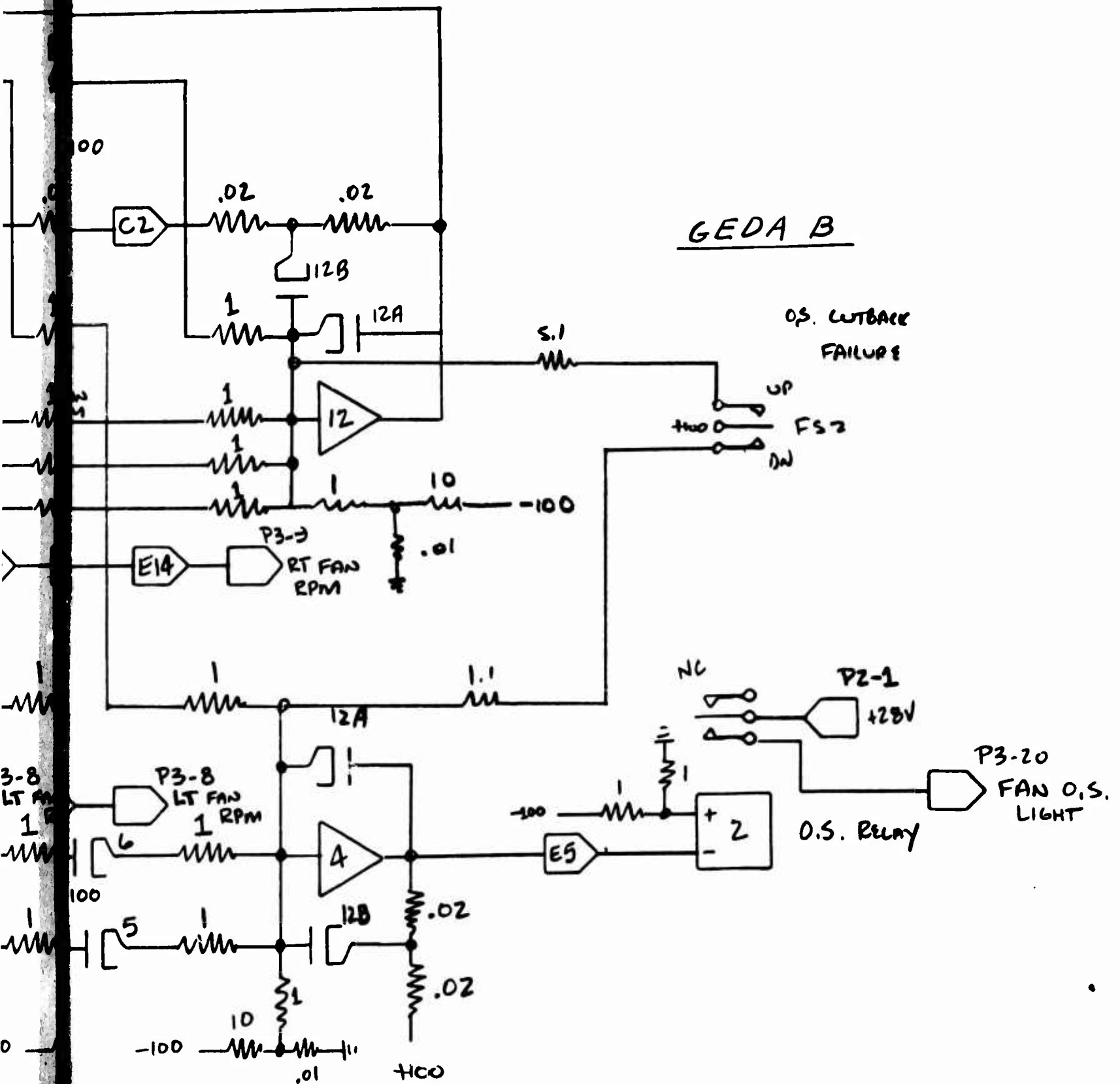$-.1965$ $-$ ㉔

)

C
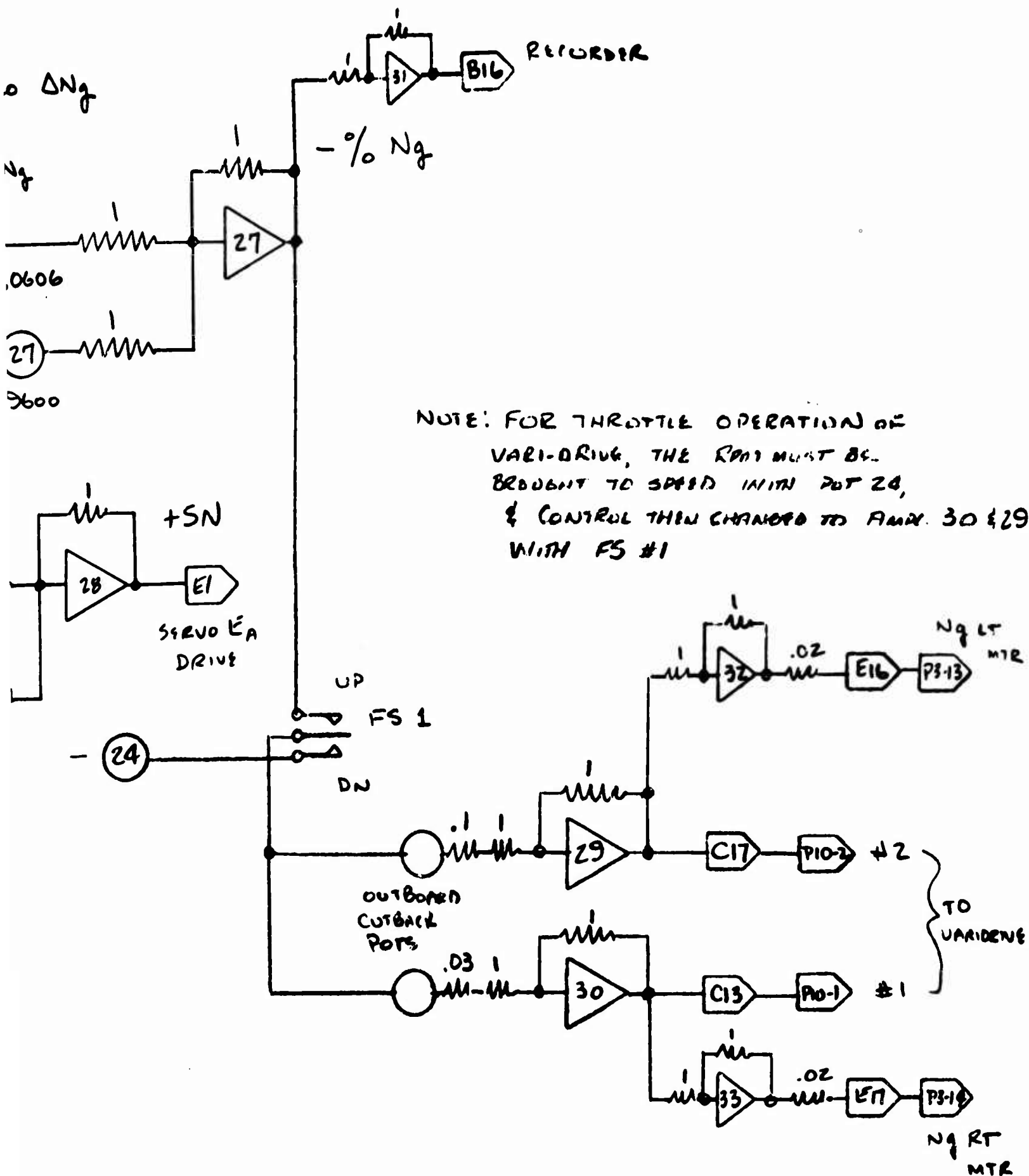
Figure 110 Gas Generator

175
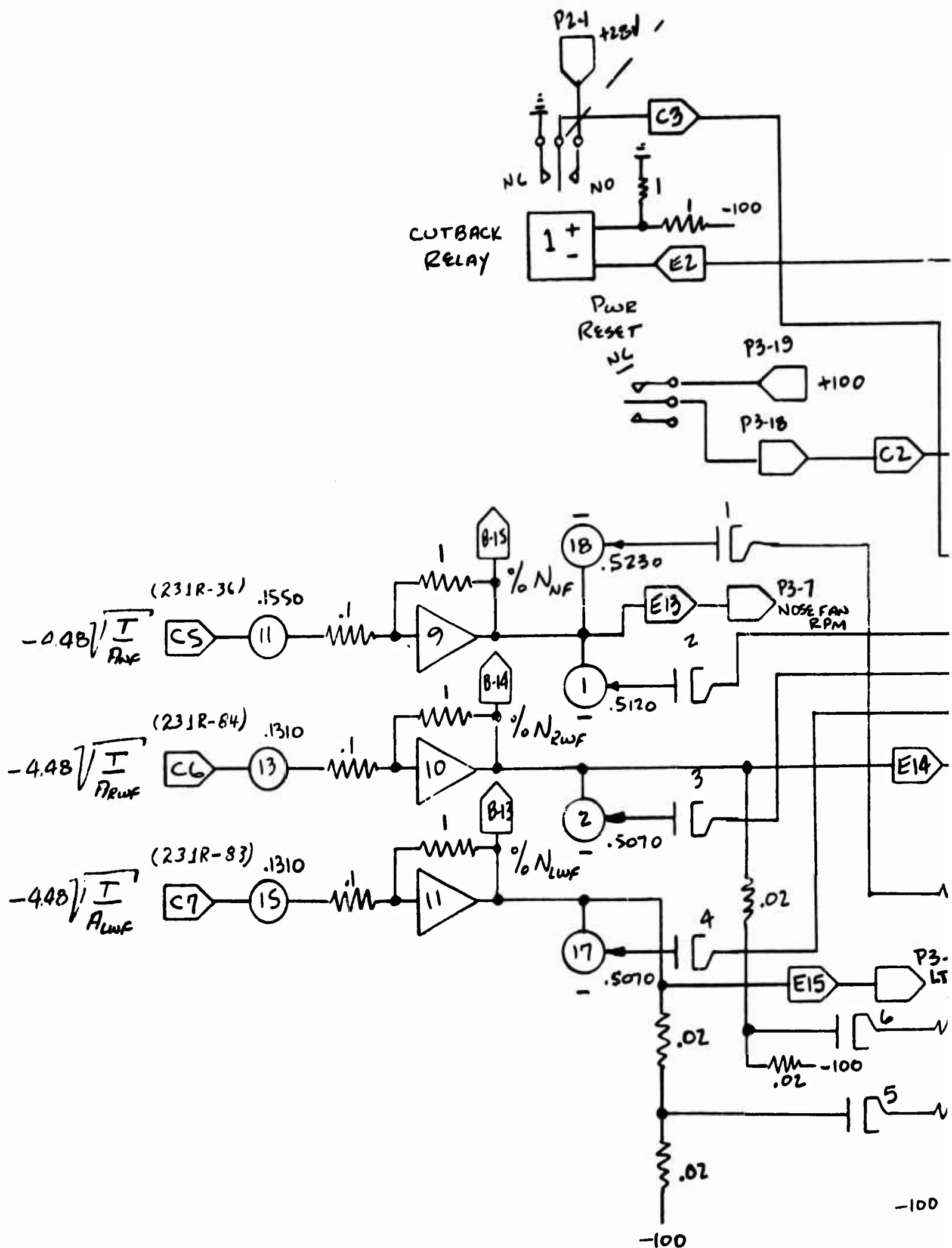
A

Figure 111 Fan Overspeed Circuitry

BLANK PAGE

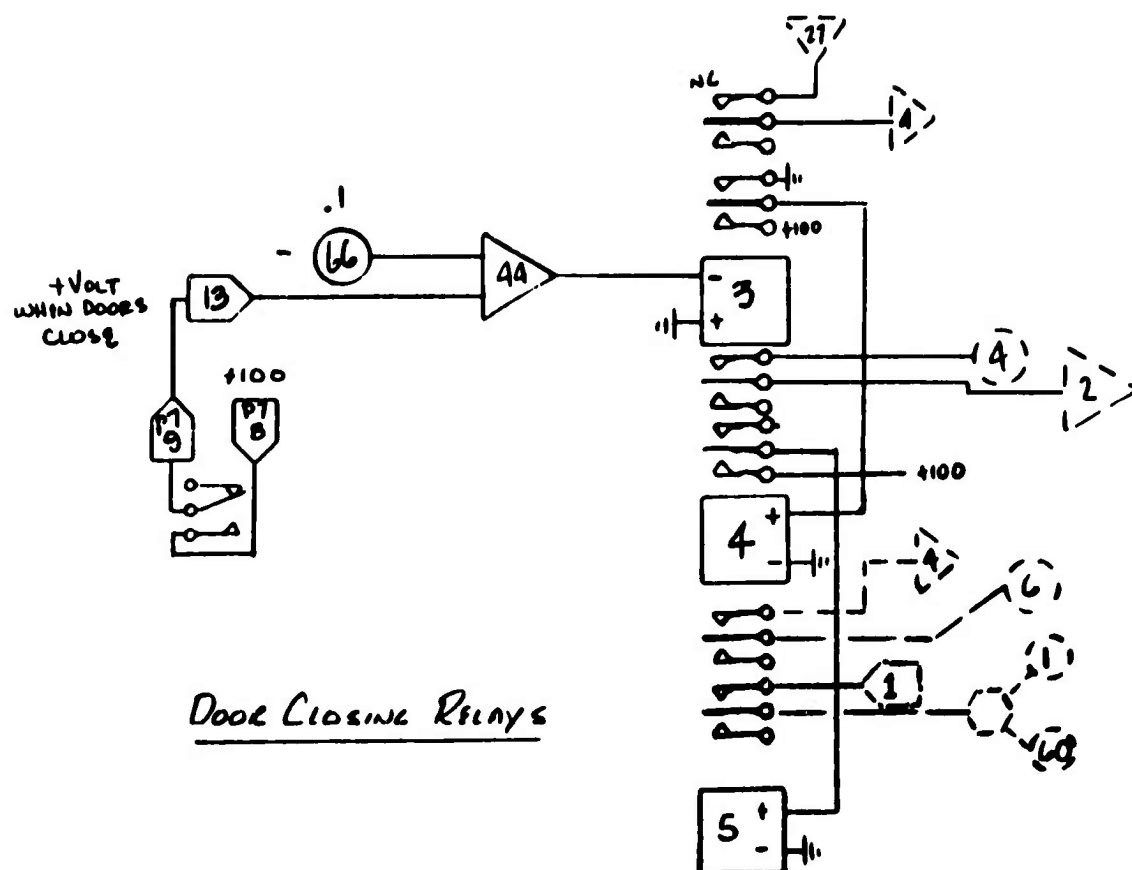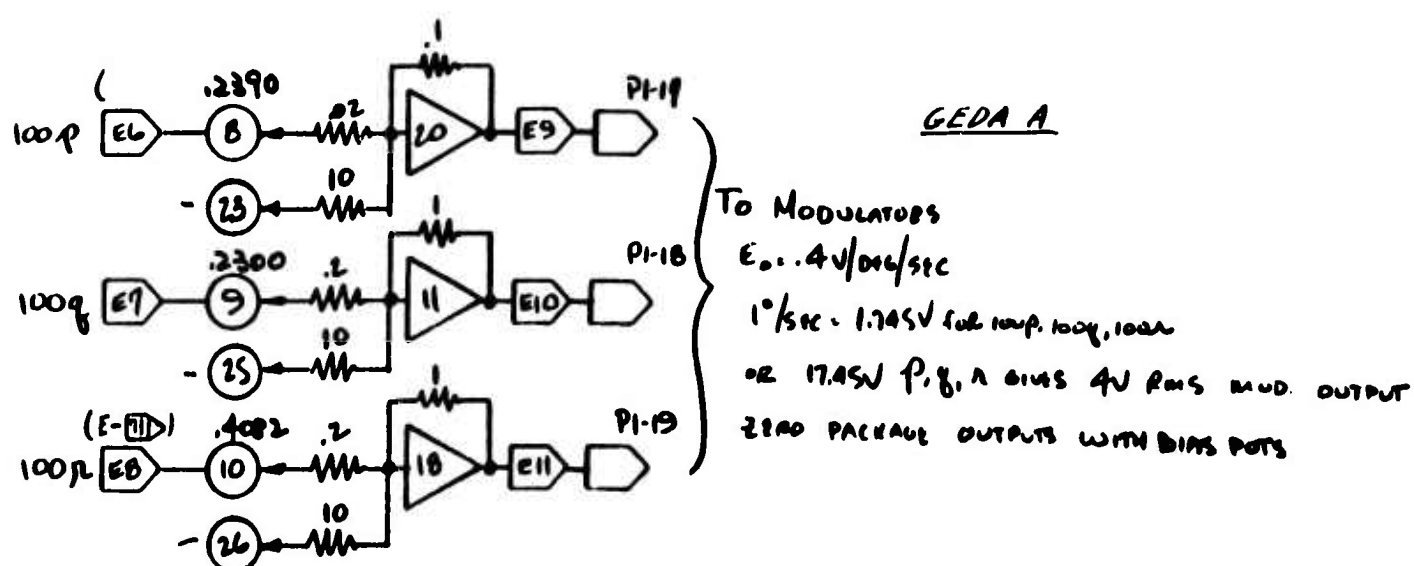Figure 112 Door Closing Relays - Pace E

Figure 113 Modulator Excitation Signals (Stability Augmentation System)

Figure 114: This figure shows the circuits delivering the artificial horizon drives to the arificial horizon and the signals indicating closing or opening of the diverter and fan doors to the diverter and door relays.

Figure 115: This figure shows the development of the cockpit instrument displays of sideslip angle, attack angle, tail incidence, and thrust spoiler position.

Figure 116: This figure shows the development of the signals required for cockpit indication of airspeed and rate of climb.

Figure 117: This figure shows the development of the signals monitoring the stick and collective positions.

Figure 118: This figure shows the circuits which scale the inputs to the computer from the control surface pots for use by the computer. Bias pots are included for the purposes of matching computer neutral control positions to indicated neutral positions, making corrections for possible pot slippage and for temperature variations in the high bay (hardware) area.

Figure 119: This figure shows the development of the "stick feel" transducer excitation. (See Appendix 13)

Figure 120: This figure shows the circuitry developing the wind for the simulation and the trunking of the total body axis wind velocities through inverters for use in the development of aerodynamic forces and moments.
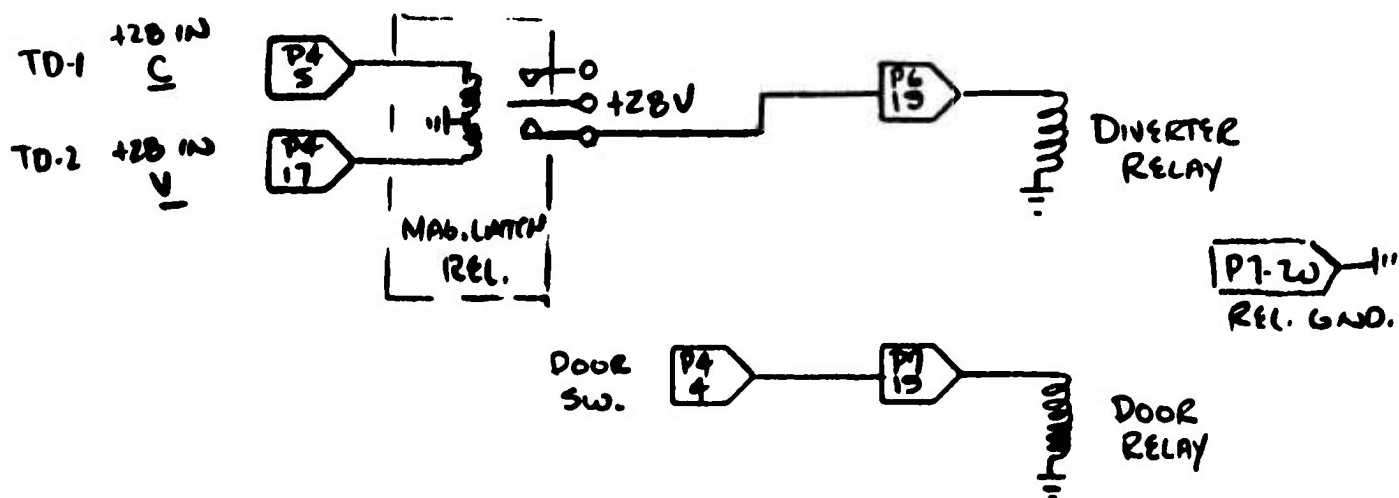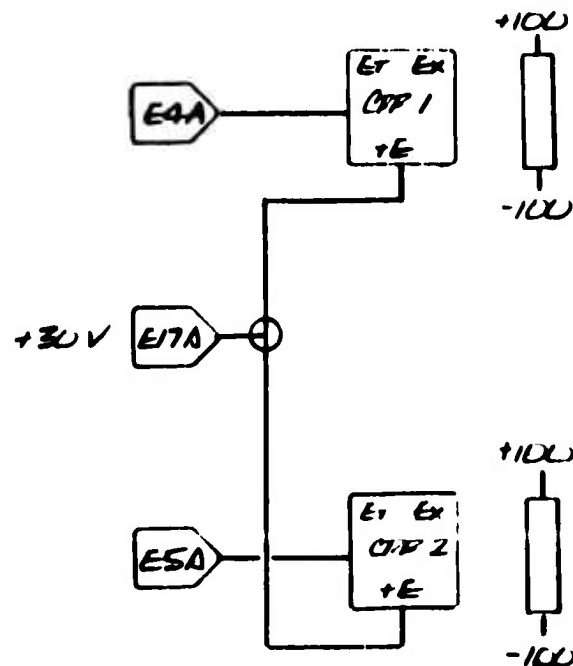
Figure 114 Artificial Horizon Drives, Diverter Valve Simulation,
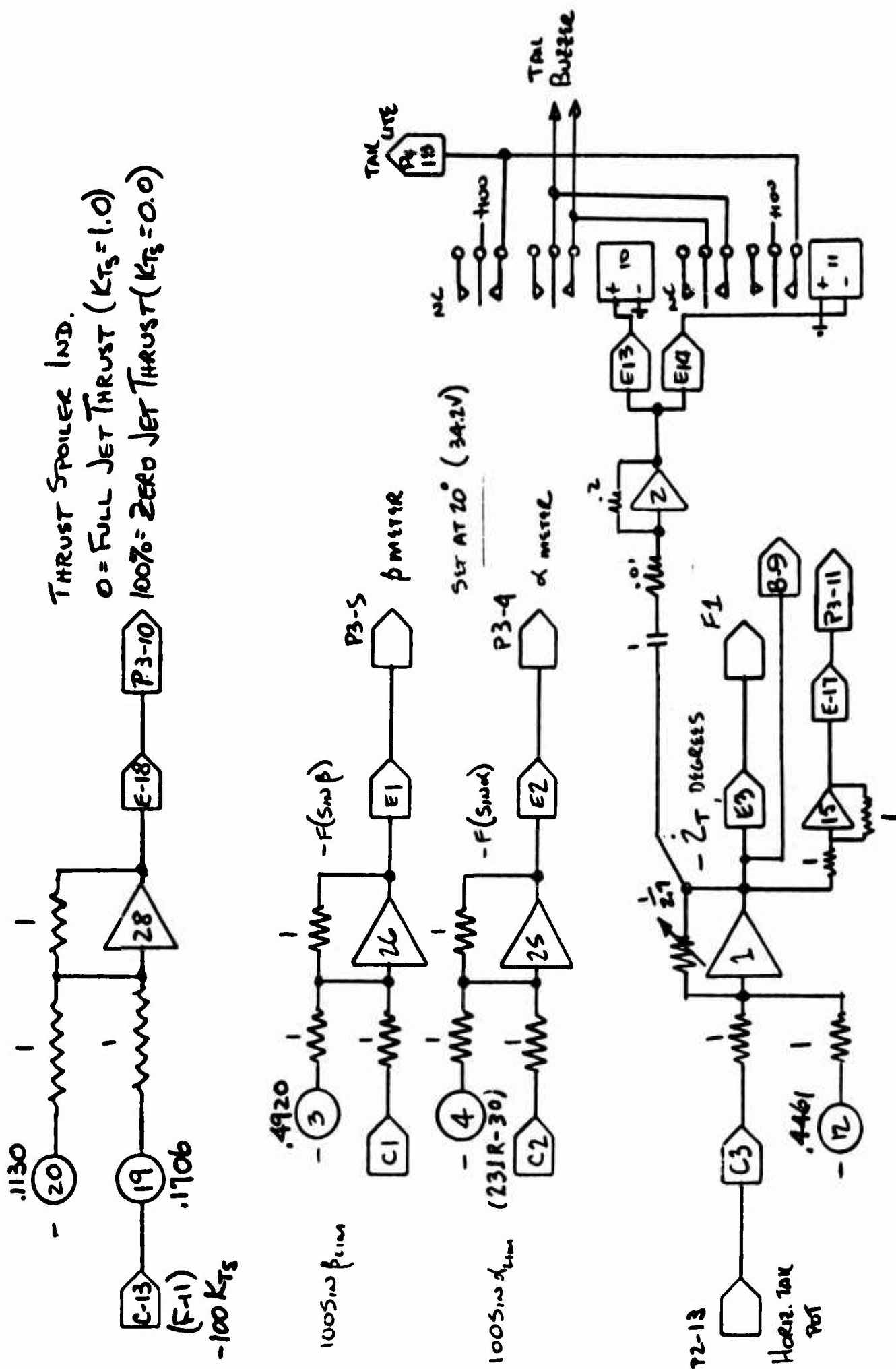And Wing Fan Closure Door Simulation

Figure 115 Cockpit Display Signals and Tail Incidence Measurement
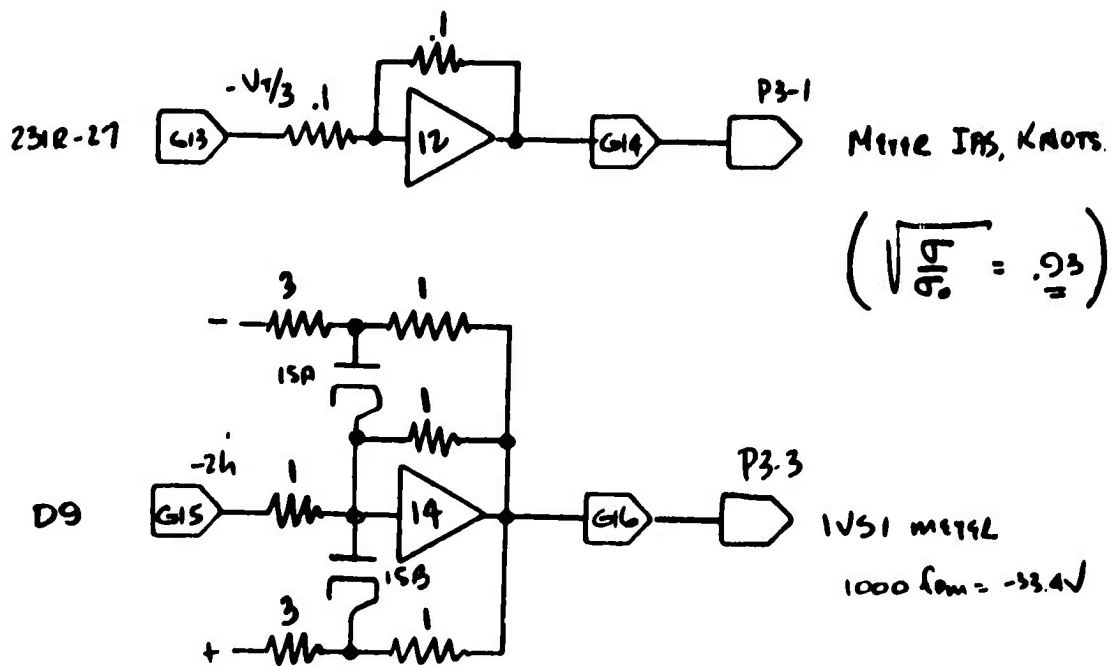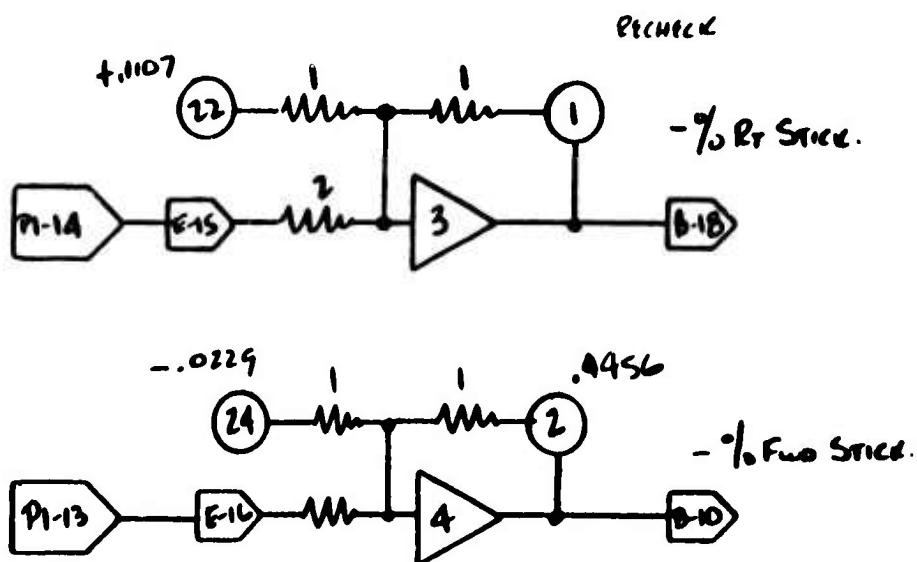
Figure 116 Cockpit Display Signals
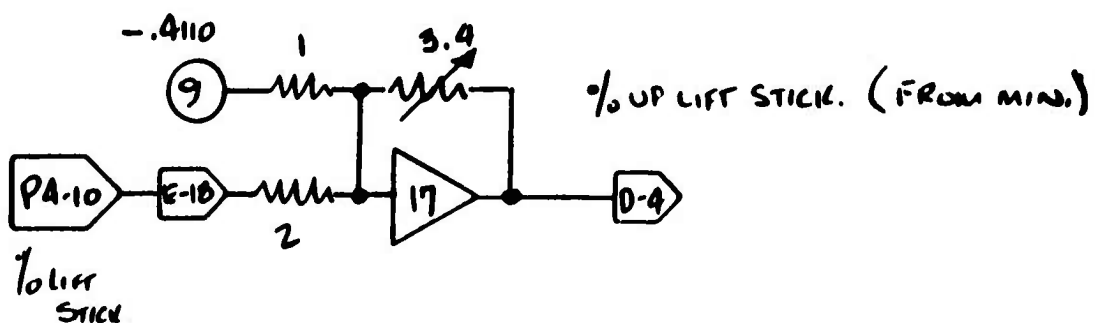
Figure 117 Control Deflection Monitors

183
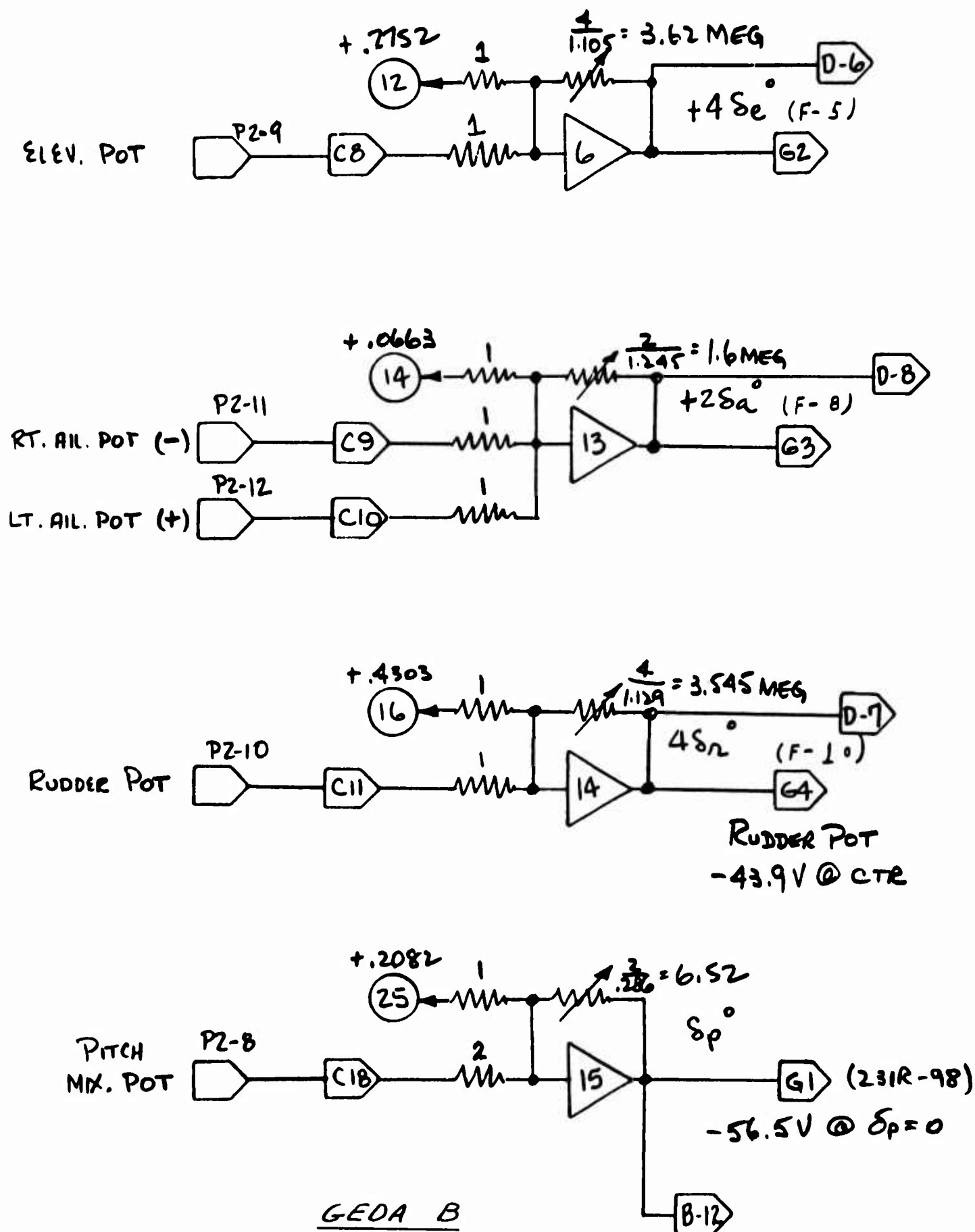
Figure 118 Control "Surface" Positions

TRANS EXCIT
-100V F39

SET .0291
+ (7)

Ail. Pot.
- $P_A/15$

C16

6

FS1 100PSI BACK PRESS.

$D_o = 116PSI$

3.47 PSI/LB/FT^2

C19

AIL. VALVE

.0438
(S)

(±2?)
F35

C4

.5330
(6)

.0967 (14)

Rud-Elev Pot
- $P_{R,E}/15$
1500 PSI=100V

C17

7

FS2

C15

RUD, ELEV. VALVE

16 PSI/LB/FT^2

$P_o = 145 PSI$
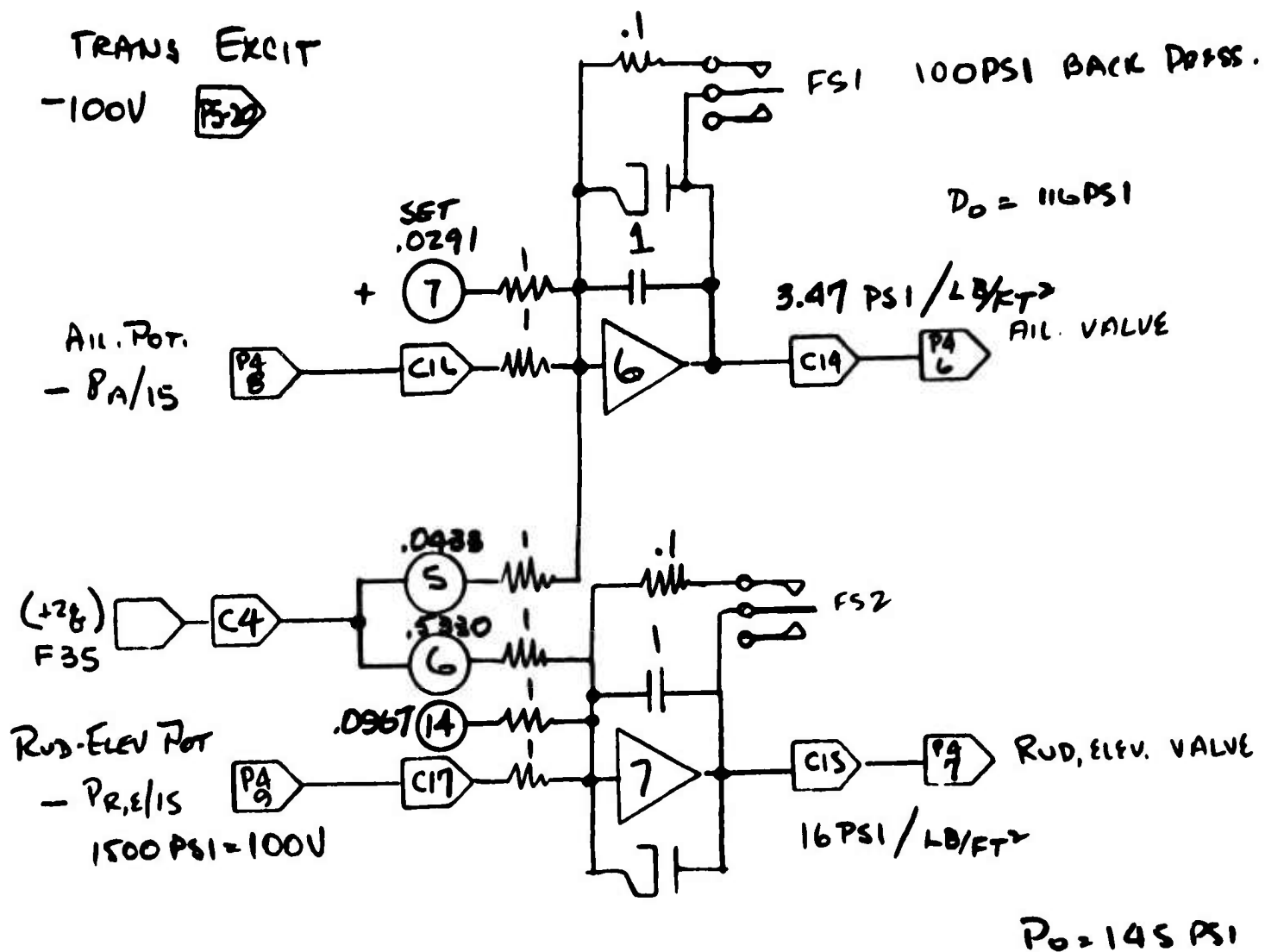
GEDA A

POT 14 .0363
POT 6 .2000
FB INP: .1
FOR P/40 POT
IN GEDA.

(SET 100PSIA FOR ZERO ?)
= 85 PSIG ON TAIL GAUGE
2-6-64
H.S.

Figure 119 "Stick Feel" Transducer Excitation

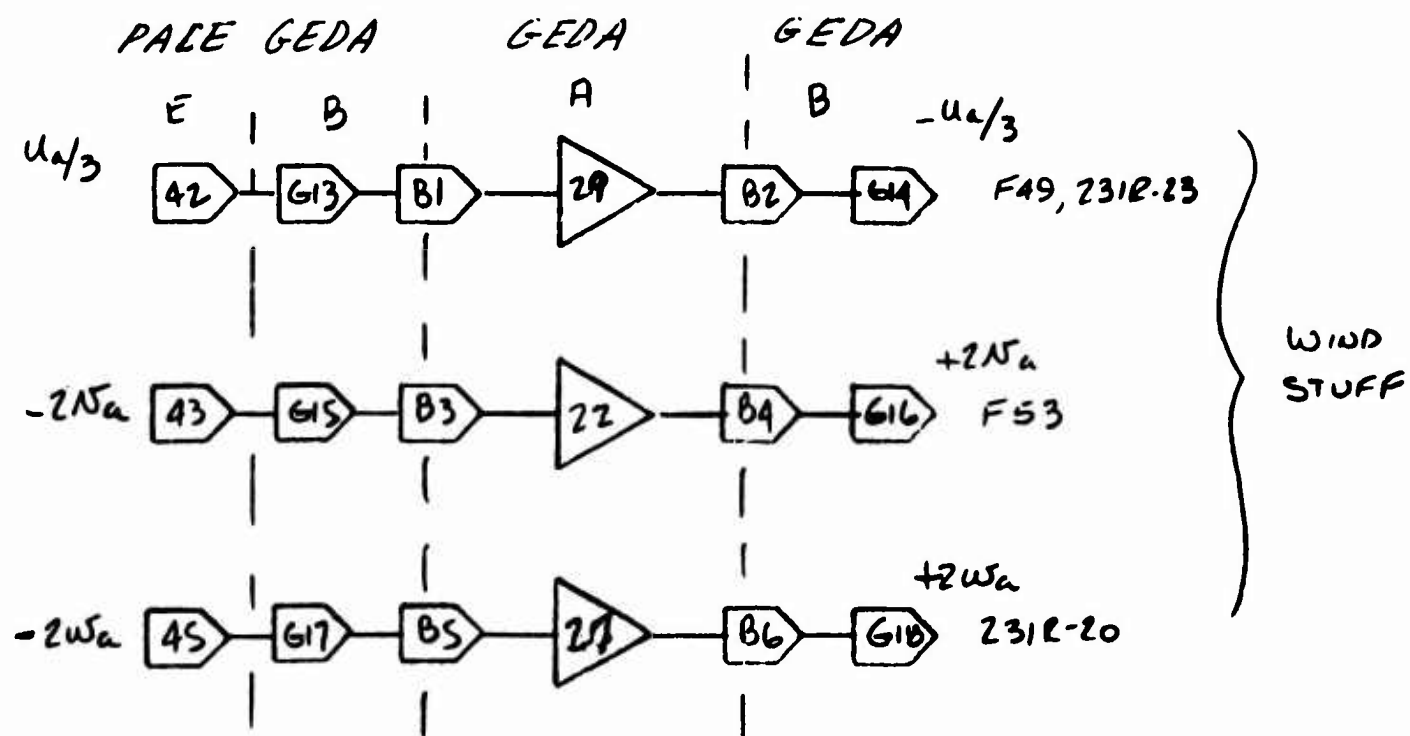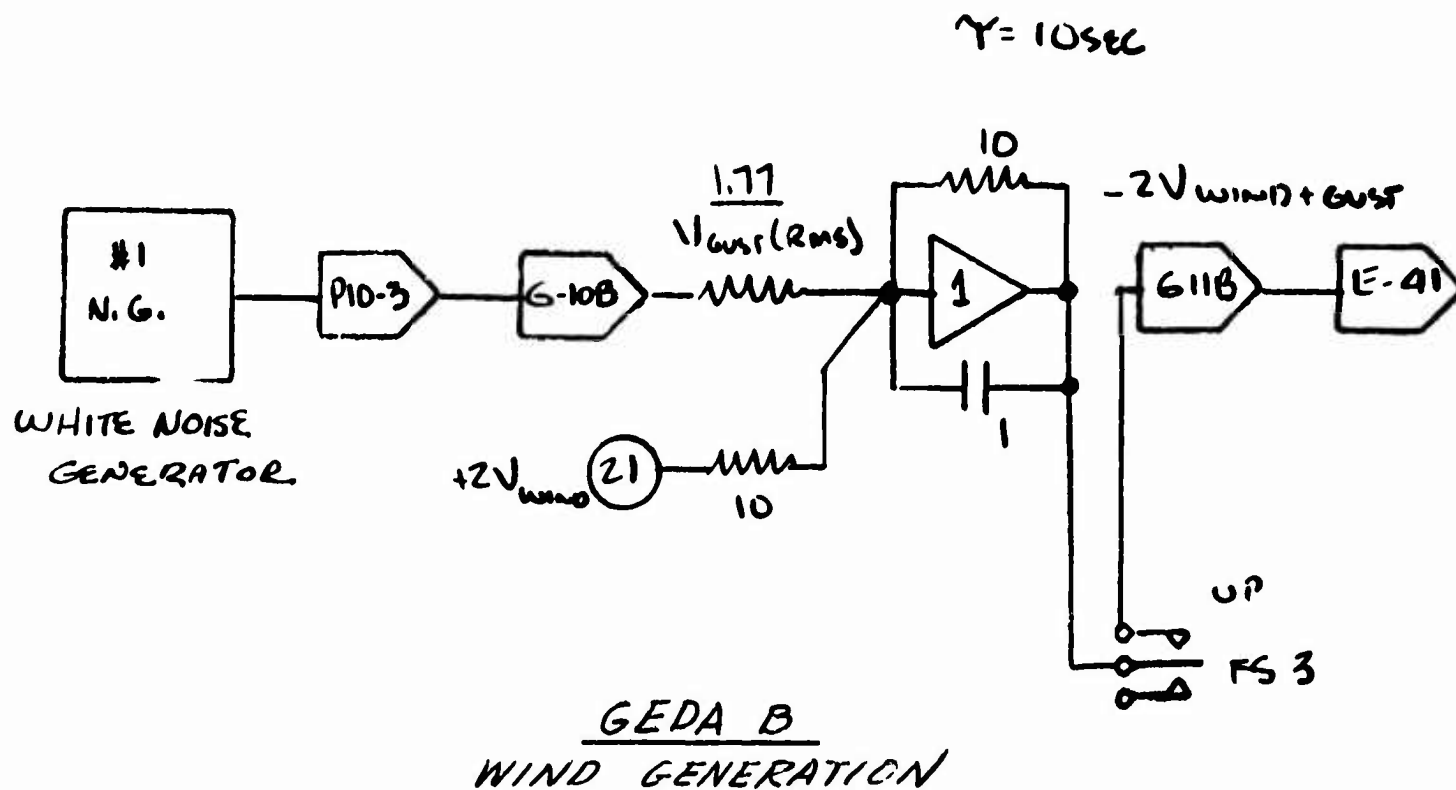Figure 120 Wind Generation and Wind Circuit Trunking

2.7   SIMULATION HARDWARE SUMMARY

Figure 121 is a photograph of the hydraulic simulator and six-degree-of-freedom fixed base display used for pilot evaluations.

The simulator was rigidly constructed to provide a solid mounting for the aircraft hardware, with the hardware located as far as possible in the correct relative positions, so that cable runs and tubing runs were identical.

There were two major deviations from this goal. They were:

1.   The nose-fan thrust reverser door hardware was relocated behind and under the cockpit so as to keep aircraft hydraulic components out of the display projection screen area.

2.   The hydraulic pumps and associated hardware were placed crosswise and under the simulator frame between the wing and the tail. This was necessary because of the orientation and location of the varidrive units which were used to simulate the engines.

The location of these two items can be seen in Figure 121.

This same figure shows the display hardware above the cockpit, as well as the curved projection screen.

Figure 121 Hydraulic Simulator
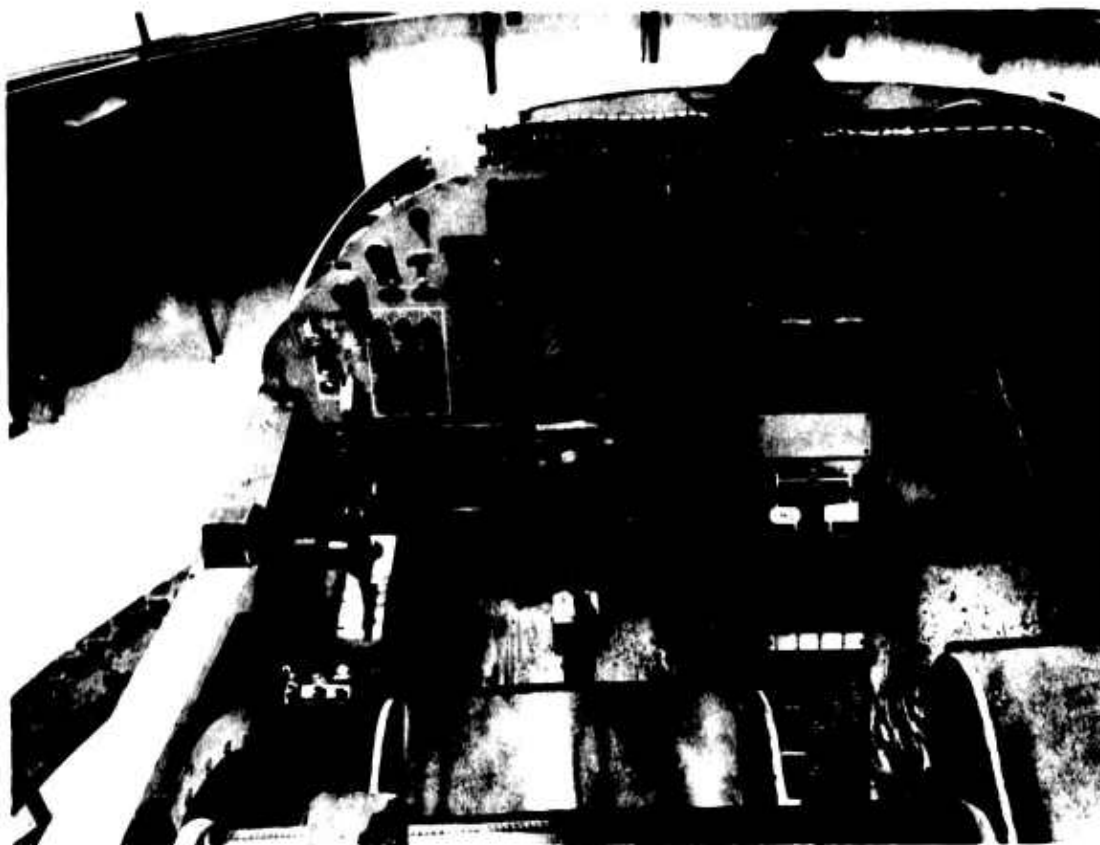
Figure 122 Simulator Cockpit

The layout of the simulator cockpit is shown in Figure 122 above.

Active cockpit instruments included:

1. Instantaneous Vertical Speed Indicator (IVSI)

2. 0-1000 ft. Altimeter

3. Indicated Airspeed, Knots

4. Thrust Spoiler Position

5. Louver Vector Angle

6. Left and Right Wing Fan

7. Nose Fan

8. Angle of Attack, $\pm 20^{\circ}$

9. Sideslip Angle, $\pm 20^{\circ}$

10. Horizontal Tail Position

11. Artificial Horizon

12. Right and Left Gas Generator RPM

13. Caution Lights and Annunciator Panel

14. Stability Augmentation, Primary-Standby Indication

15. Power Pilot Lamps and System Configuration Lamps

16. Tail Motion Warning Light and Audio Tone

In addition, two lights were provided to notify the pilot if the vehicle at any time exceeded the roll and pitch limitations of the display.

Active cockpit controls included:

1. Roll Stick and Pitch Stick

2. Rudder Pedals

3. Lift Stick

4. Gas Generator Throttle Control (left hand only - in this simulation there was no provision for independent engine throttle control)

5. Roll, Pitch and Yaw VTOL Trim

6. Horizontal Tail Trim

7. Flap Actuator Switch

8. Mode Selector Control

9. Fan Overspeed Power Reset Button

10. Pri-Standby Electrical Power Control

11. Louver vector actuator switch

12. Stability Augmentation, Primary-Standby Indication

13. Thrust Spoiler Switch

14. All Circuit Breakers

Control variables measured and fed to the computer were:

1. Elevator Position

2. Horizontal Tail Position

3. Rudder Position

4. Total Aileron Position

5. Nose Fan Thrust Reverser Door Position

6. Throttle Position

7.   Right Wing Louver Vector and Stagger Angles

8.   Left Wing Louver Vector and Stagger Angles

Output variables fed to the visual display were:

1.   Euler Roll and Pitch Angles

2.   Euler Yaw Rate

3.   Ground x, y and z coordinates

The nose fan door position as well as the right and left wing louver variables were measured by means of rotary potentiometers, since the large angles involved caused considerable nonlinearity using the original linear potentiometers.

In addition, a mechanism was developed to enable the direct measurement of louver vector and stagger angles. This was necessary both for the sake of accuracy and also to release computer equipment for other tasks.

The wing louver hardware was not installed on the simulator, so a means of introducing the effect of the fan louver stagger mechanical stops was required.

This same hardware with slight modification was used to enable the direct measurement of stagger and vector angles.

β_2 is defined as the angle aft from vertical of the tangent line of the 7th louver(counting from forward).

β_1 is defined as the angle aft from vertical of the tangent line of the 8th louver.

β_s, the stagger angle, is defined as $\beta_2 - \beta_1$.

β_V, the vector angle, is defined as $\dfrac{\beta_1 + \beta_2}{2}$.

The mechanism for stagger and vector measurement, then, had to take the sum and difference of the even and odd louver motions.

Figure 123 on the following page is a schematic of the mechanism.

Referring to Figure 123, it is seen that the two pot cases (β_s pot and β_V pot) are attached to Arm 1. The shaft of the stagger pot is attached to

Arm 2, and the shaft of the vector pot is attached to Arm 3. Thus, the stagger pot measures the difference in angle between Arm 1 and Arm 2, while the vector pot measures the difference in angle between Arm 1 and Arm 3.

If the fore and aft louvers both move in an increasing direction at the same rate, Arms 1 and 2 move together, and the stagger change is zero. However, Arm 3 rotates in the opposite direction of Arm 2, and the vector pot output will change.

Arm 3 is driven by the β_1 rotation reverser mechanism, which results in Arms 2 and 3 having equal and opposite motion.
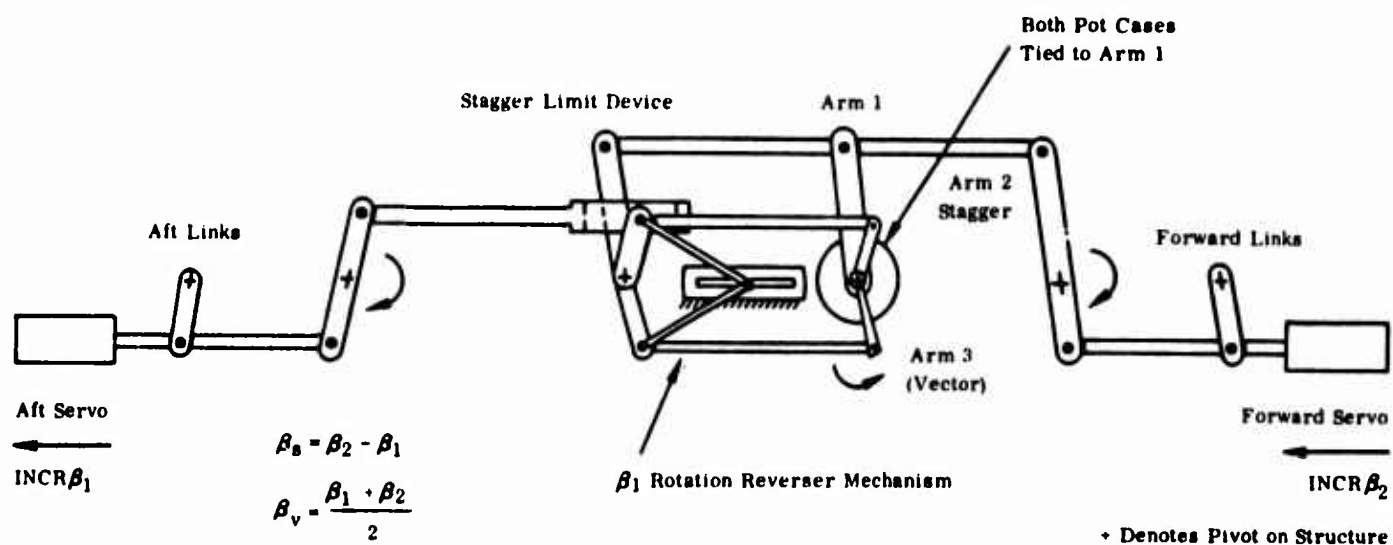

Figure 123 Schematic of Mechanism for Stagger and Vector Measurement

Figure 124 and 125 below are photographs of the stagger stops and vector measurement system.

The forward and aft links are designed to be identical in dimension to the links on the fan, and thus the louver mechanism geometry is reproduced.
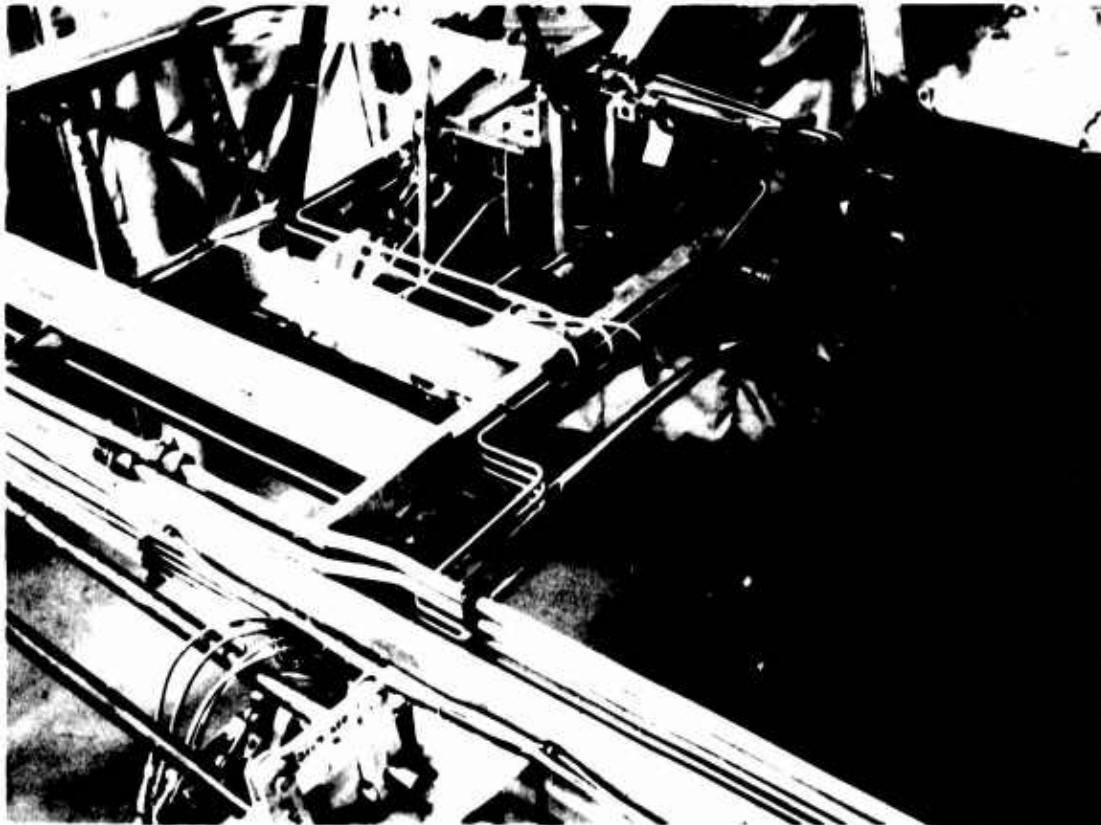

Figure 124 Stagger Stops

Figure 125 Vector Measurement System

The calibrations of the hardware potentiometers are given in Figures 130 through 135 of Paragraph 2.8.

Simulated hinge moment gradients were required to develop an adequate representation of control stick and pedal forces encountered throughout the flight regime.

The principle of the system used to attain these effects is shown in the following Figure 126.
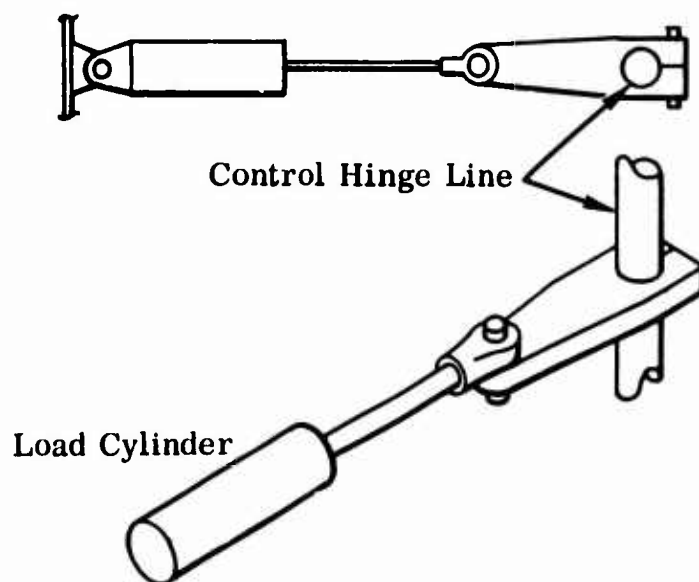

Control Hinge Line

Load Cylinder

Figure 126 Control Stick and Pedal Force

If a pressure is applied across the load cylinder so that it tends to retract, a tension will result between the cylinder and the hinge line. If a control torque is applied around the hinge line, the control will deflect, and the tension from the load cylinder will develop a moment around the control hinge line which will be proportional to the control deflection, at least for deflections sufficiently small.

For a given load system geometry, the hinge moment gradient as a function of dynamic pressure dictates the load cylinder differential pressure required as a function of dynamic pressure. At low Mach numbers, the load cylinder pressure is a linear function of dynamic pressure.

Figures 127 and 128 show the hardware used for the rudder and aileron load systems. Two sets of load cylinders at each control surface are in evidence. One set (the smaller cylinders) is used for low-speed flight, and the larger set is used for high speed flight.

In Figure 127, the rudder cables and quadrant can be seen. The rudder quadrant is attached to the simulated rudder torque tube, which has a protractor installed on the other end to measure rudder deflection. The arm which drives the rudder position pot is seen below the protractor.

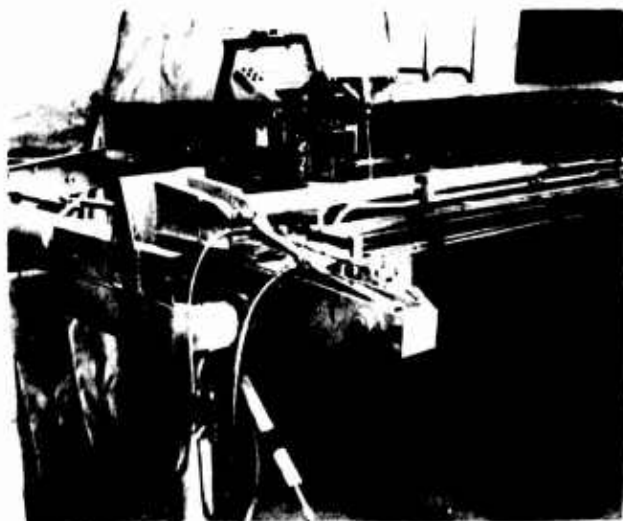Figure 127 Rudder Cables and Quadrant

Figure 128 is a photo of the left wing hardware with the left aileron system in the foreground. Since the aileron system is power-boosted, the load reflected to the stick is just the aileron tab hinge moment. This is quite small, and thus the load cylinder has a small area, as is seen the Figure.

Figure 128 Left Aileron System

The next requirement was to be able to provide a controlled hydraulic pressure differential across the load cylinders which was proportional to dynamic pressure.

This requirement was mechanized by using a manually-controlled pressure regulator valve to set the load cylinder extending pressure, and using an electrically-controlled pressure regulator valve to set the load cylinder retracting pressure.

The retracting pressure was controlled by a Denison "Electroilic" control valve. This valve has a large hysteresis loop which made open loop operation unfeasible.

The control valve nonlinearities were straightened out by using the valve along with a pressure transducer and an integrating amplifier in a closed loop such that the amplifier output adjusted itself to make the commanded and actual pressures equal.

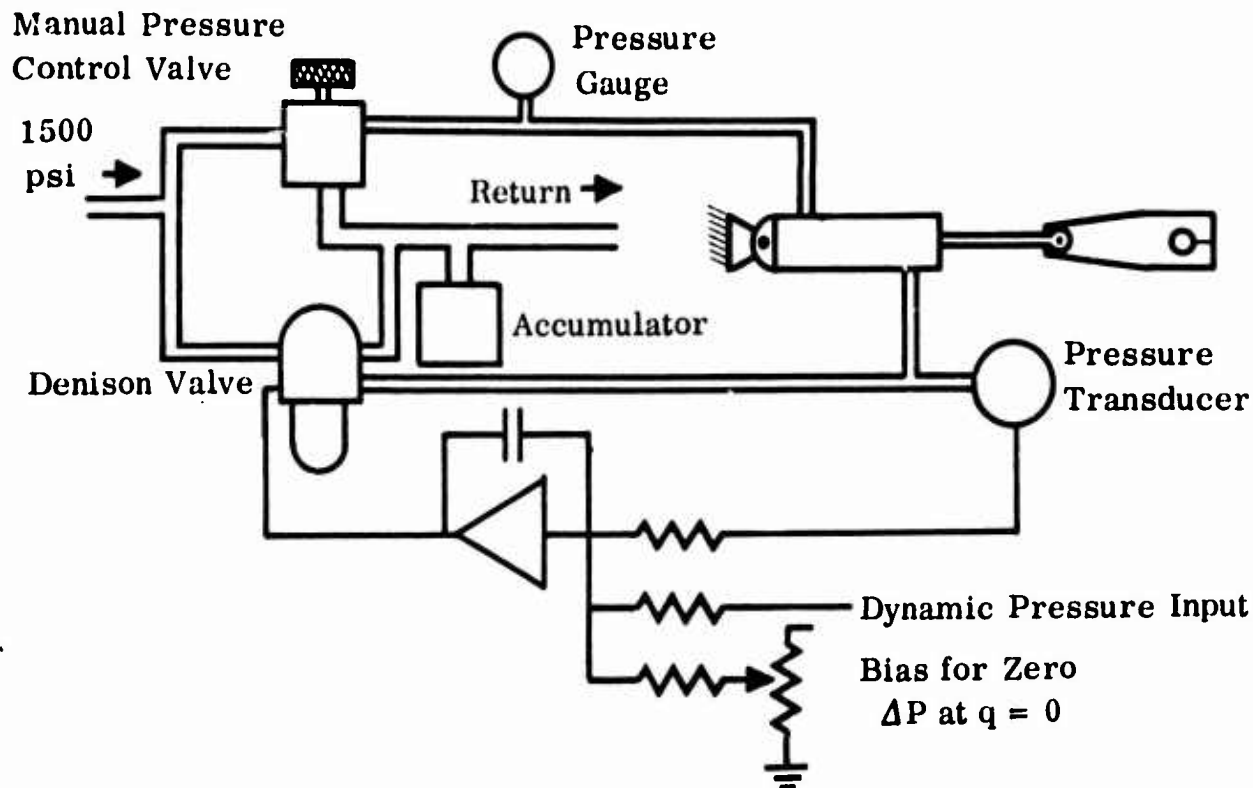A schematic of this system is shown in the following Figure 129.

Figure 129 Schematic of Airload Simulation System

The manual control valve is set to control the extending pressure at any desired level. This valve is necessary because the pressure output of the Denison valve is not zero at zero current input, and is, in fact, around 100 psi.

The back pressure was set so that the pressure commanded at zero dynamic pressure was around 125 psi.

Since the load cylinders used were single-ended, the area ratio was not unity, and this had to be taken into account in setting up the system for zero force at zero q, or dynamic pressure.

Also, since the aileron load requirements are much lower than those for the elevator and rudder, a different load cylinder was used for the aileron system, which had a different area ratio and thus required a separate pressure control loop. The same manual pressure regulator was used for both return systems.

As first mechanized, there was oscillation in the load system return line, but his problem was eliminated by the use of an accumulator at the return outlet of each Denison valve.

A further problem arose in the aileron system, because the load cylinders

originally chosen had considerable friction at zero differential pressure, which was reflected into higher roll stick breakout force.

Referring to Figure 128, the lower aileron load cylinder was the original unit, which was to be used for both low and high speed flight. As a result of the friction problems, the smaller cylinder shown connected was installed (one on each aileron) and the added system friction was then negligible.

A load cylinder is required on each aileron, because in the aileron drooped condition the individual aileron displacement is nonlinear with pilot input, even though the total aileron is nearly a linear function of stick position.

The gain of the load-feedback loop is set by varying the size of the capacitor in the integration amplifier. The capacitor is picked so that the system is stable but still responds rapidly enough to follow input dynamic pressure commands. These requirements proved to be feasible in this system.

2.8 SIMULATION HARDWARD CALIBRATION

The aircraft simulation described in this report in actuality consisted of two main segments. The first segment involved a mostly "analytical" simulation, where the actual servo actuators were not yet available, which made it necessary to approximate their estimated characteristics. This portion of the simulation utilized the cockpit control positions for aileron, elevator and rudder positions.

The mechanical louver (main) mixer and the pitch mixer were completed for these tests, and their respective outputs were used to derive louver vector, louver stagger and nose fan thrust reverser door position. The main mixer has as its output push-pull rods which position the four louver actuators in response to vectoring, roll, yaw, and collective lift inputs, as well as an output to the pitch mixer which programs the nose fan thrust reverser gain and center position with longitudinal control as a function of collective vector command.

The main mixer push-pull rods were instrumented with potentiometers which enabled the four louver command positions to be measured, which in turn enabled the computation of vector and stagger angles for both main fans.

This data was then applied to the airframe through first-order lags representing the approximate servo transfer functions. The complete flight regime of the vehicle was investigated using this mechanization of the hardware, and it was intended that when the hydraulic simulator was put into full operation the final phase of the simulation would be a check on the previous work in preparation for complete pilot evaluation of vehicle handling qualities for normal and emergency operations.

The simulation progressed according to this plan, and the hardware calibration data is presented in Figures 130 through 135 following.

The inclusion of the actual vehicle hardware presented no problems, and the previous systems development work was validated.
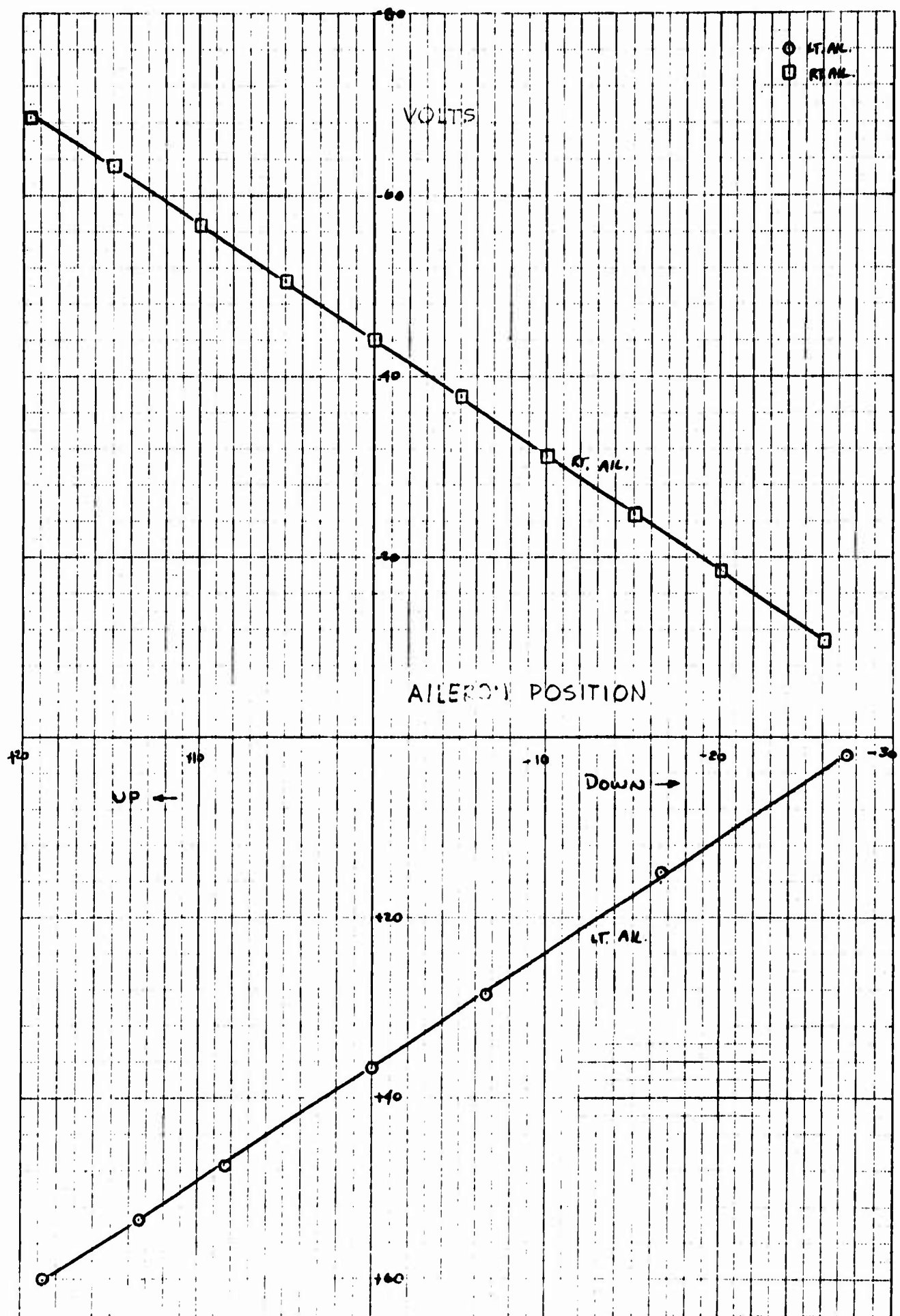
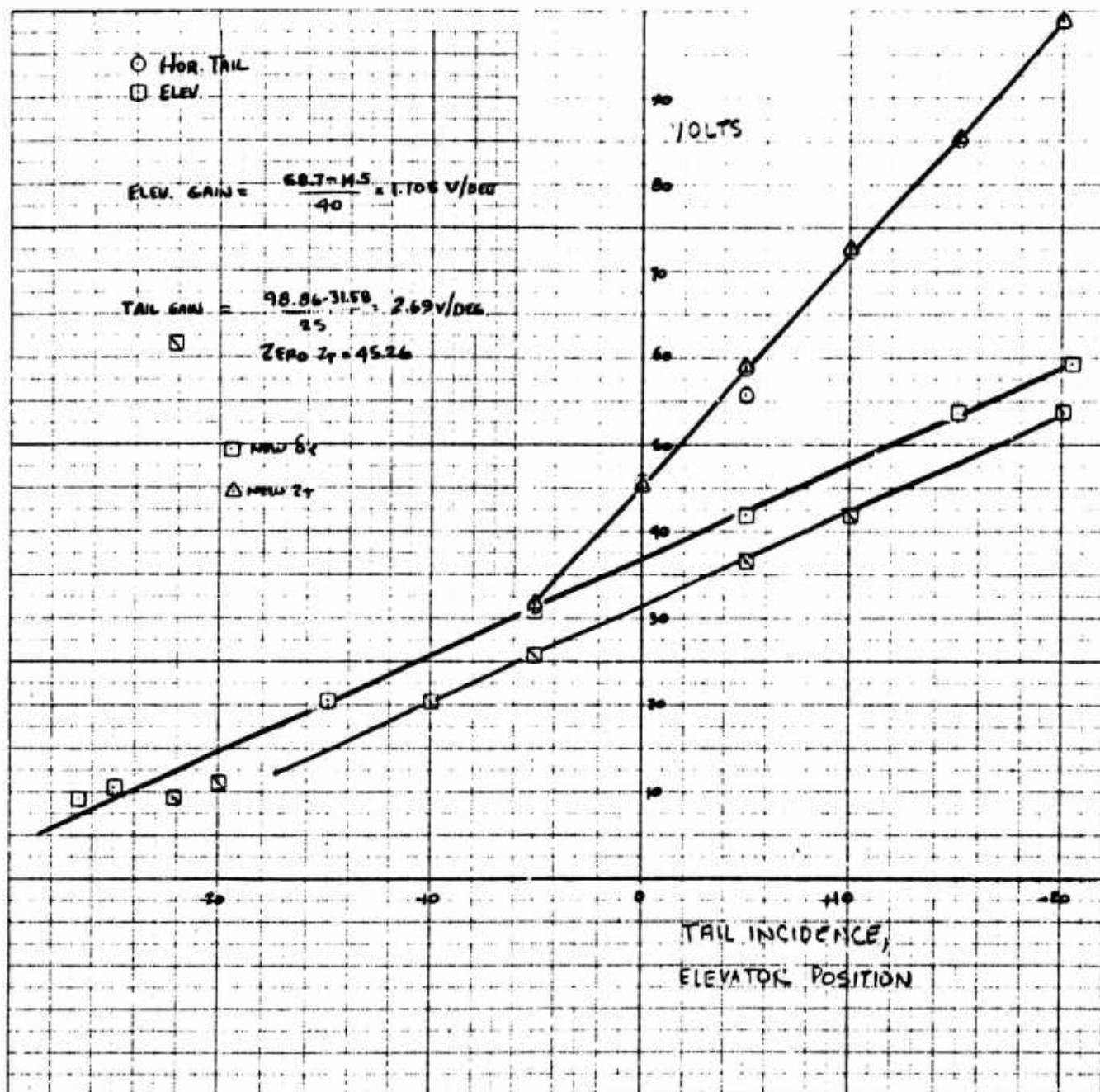Figure 130 Aileron Calibration

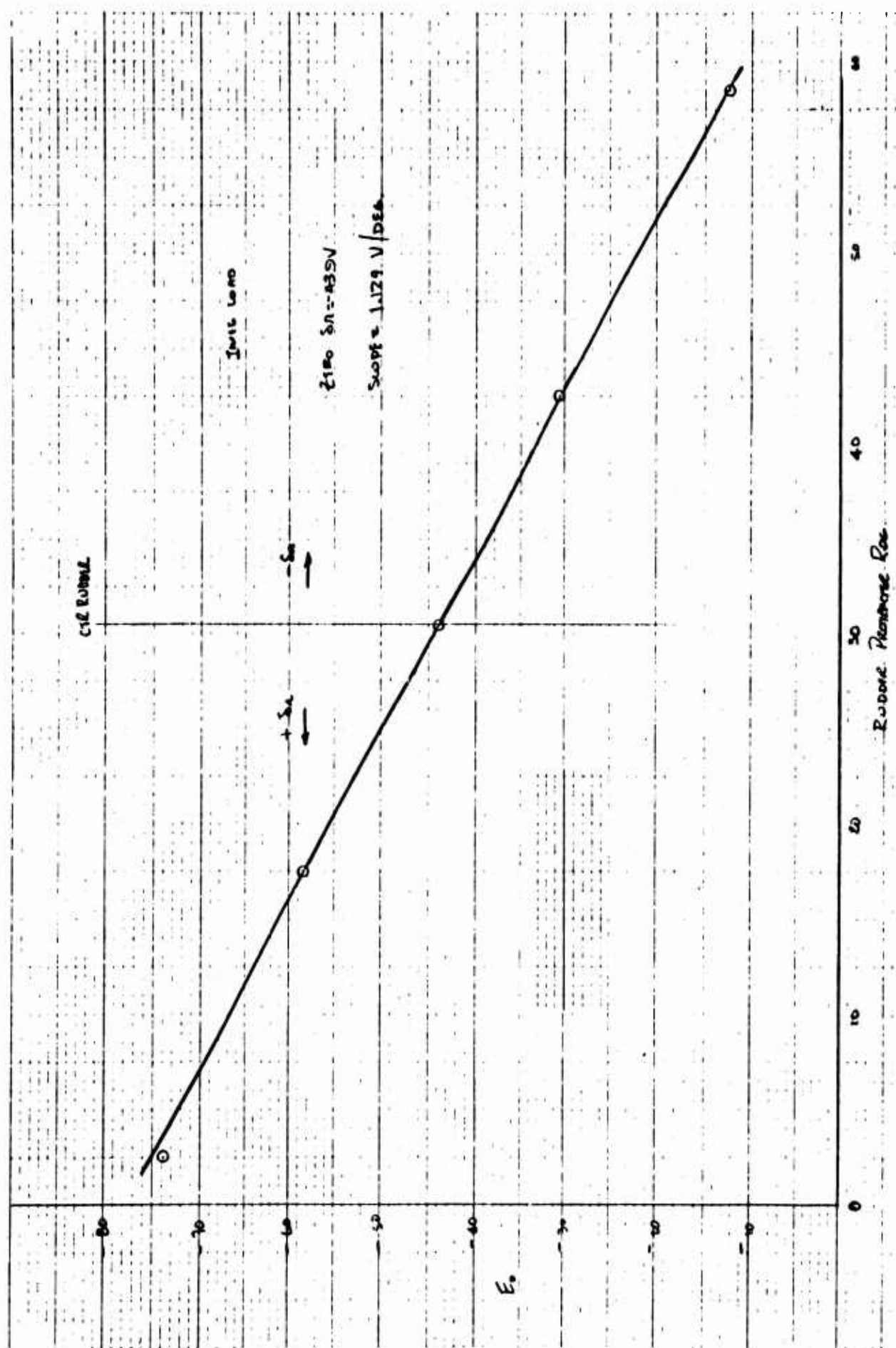Figure 131 Horizontal Tail and Elevator Calibration

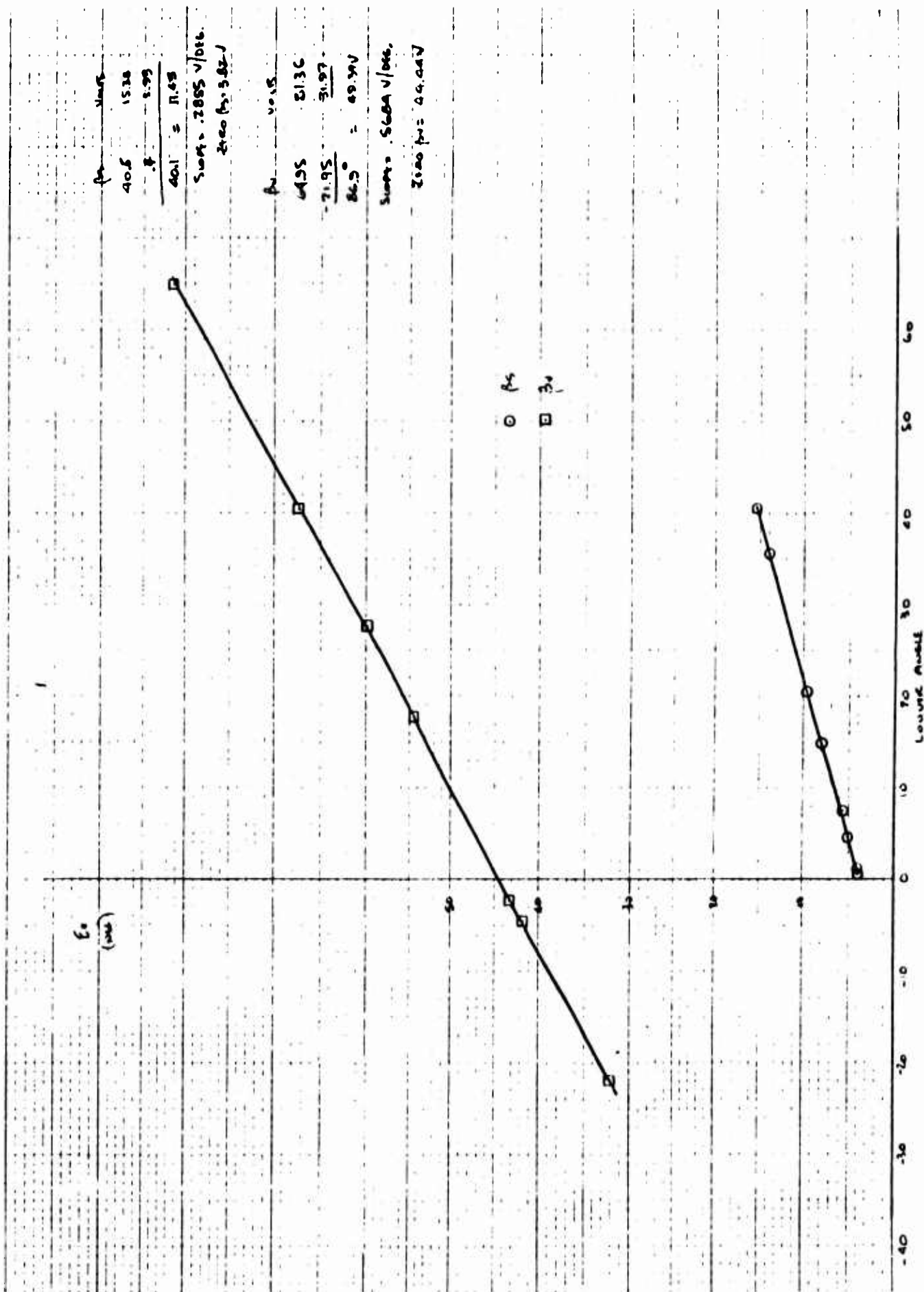Figure 132 Rudder Calibration

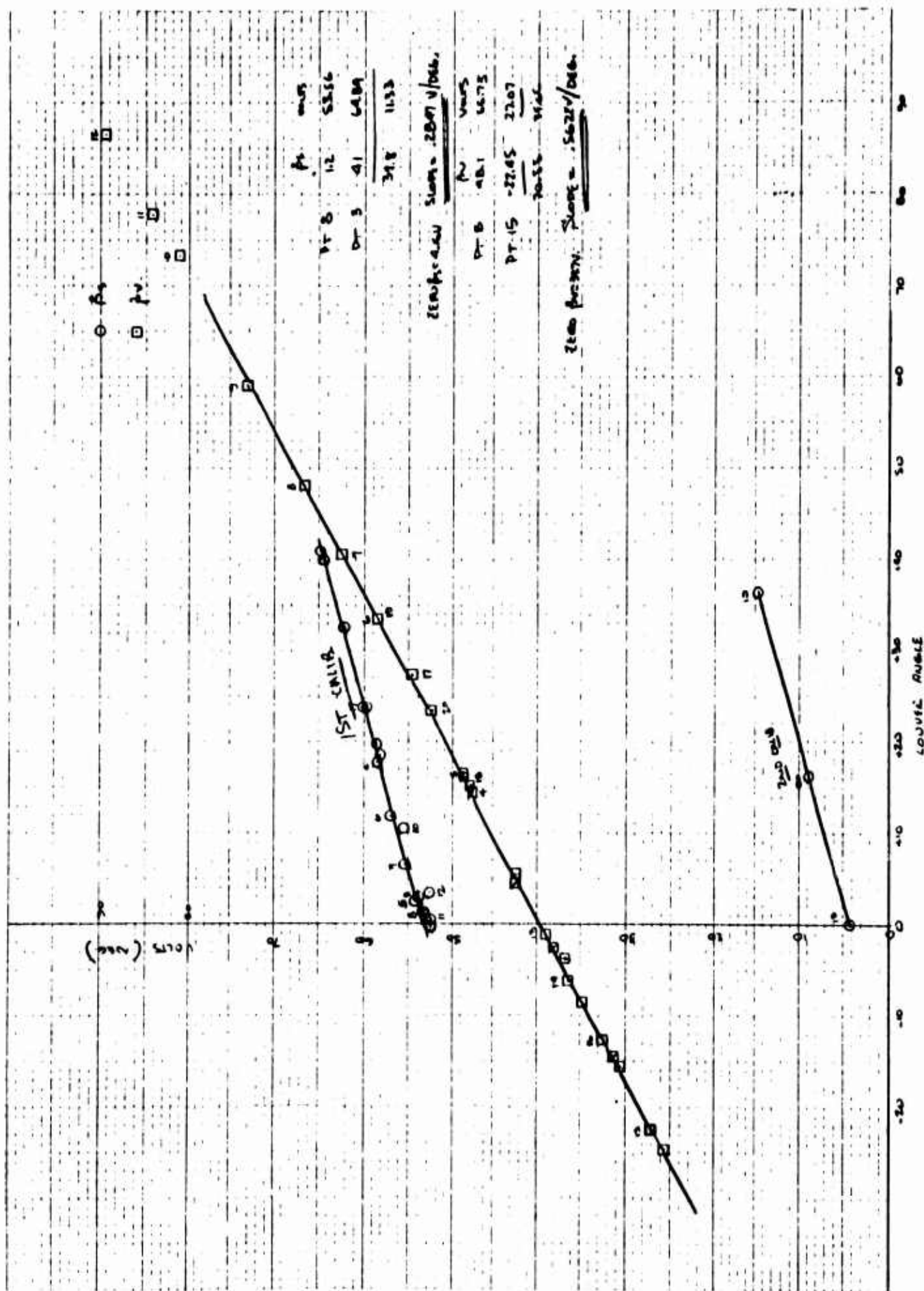Figure 133 Right Wing Vector/Stagger Calibration
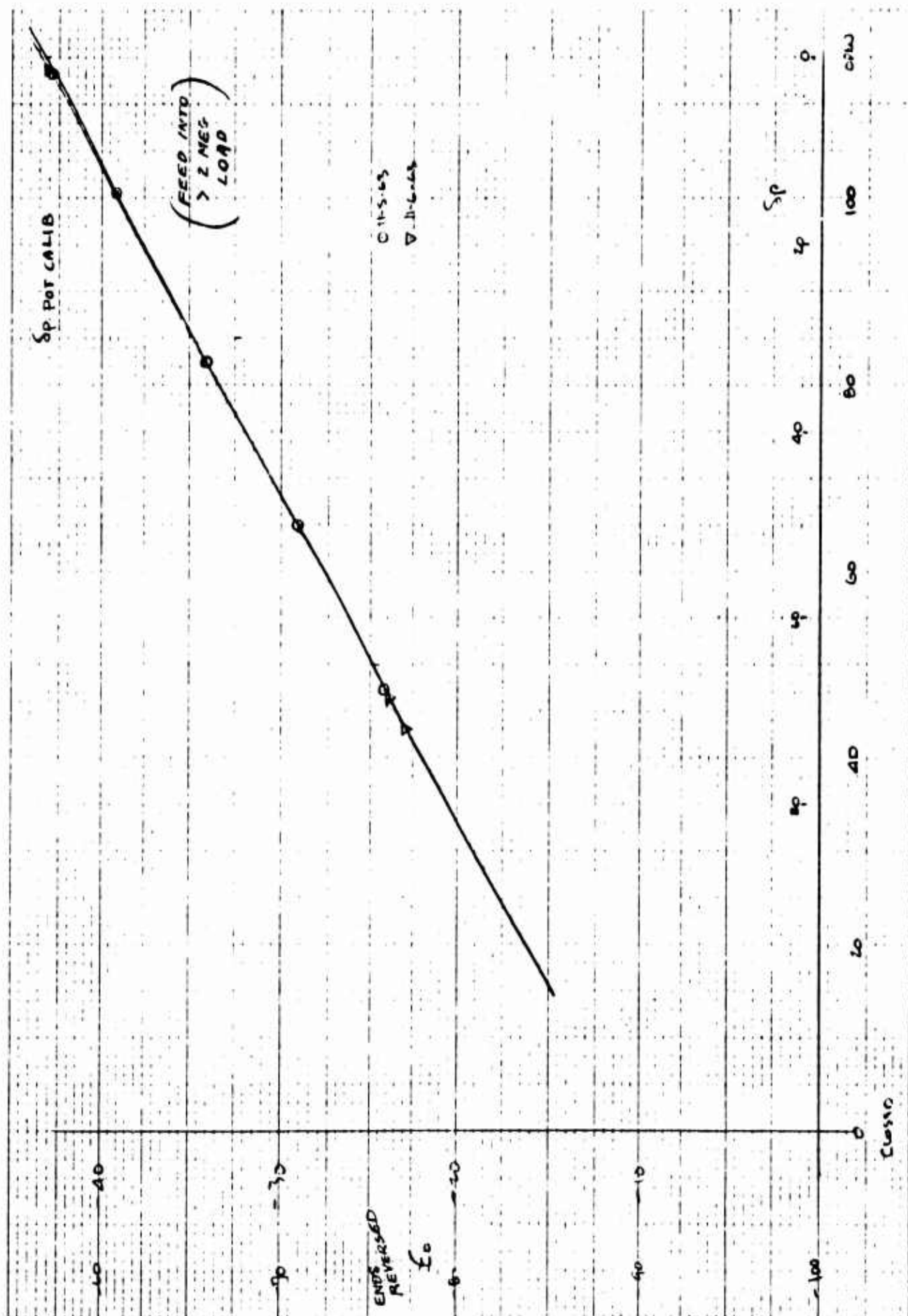
201

Figure 134 Left Wing Vector/Stagger Calibration

Figure 135 Nose Fan Reverser Door Calibration

BLANK PAGE

2.9 SIMULATION CHECKOUT

In a large simulation such as this, it is essential that sufficient verification be performed so that all persons involved develop confidence that the conclusions drawn from the simulation are valid. The steps followed in checking out this simulation after it was designed and wired were as follows:

1. A complete check of computer-generated functions by comparison with the original data.

2. A complete static check, where all variables are assigned values. The output of each amplifier is computed, and the actual output is compared. The accuracy of the individual contributions to the forces and moments are thus directly measurable, as well as the accuracy of their sums. In the case of this simulation, where two sets of aerodynamic data were being generated, it was necessary to choose the static check parameters in the region where the data phasing was taking place. If this had not been done, two separate static checks would have been required.

3. After the static check procedure, a considerable number of longitudinal trim points were determined, over the whole range of fan-powered flight speeds, as well as for low-speed conventional flight. These trim points were compared to data derived by independent calculations of another group. As part of this effort, the fan speed changes resulting from vector and stagger were compared to hand-calculation data. Several detailed calculations were made at various trim points to verify results which were questioned, and in this manner further confidence was gained in the validity of the simulation.

4. Once the static validity of the simulation was demonstrated, four dynamic check conditions were set up. These consisted of uncoupled three-degree-of-freedom cases for a near-hover condition and a moderate transition speed condition, such that one set of two cases used the high speed fan-powered aerodynamics, and the other set used the low speed fan-powered aerodynamics. Very good agreement was finally obtained between the analog responses and an independent digital computer time history for the same cases.

Initial difficulty was experienced in the digital computer hovering time histories, which used the aerodynamic force and moment equations originally presented to the Systems Analysis Group. It was felt that the digital time history should use the equations as originally presented so as to provide a check on the validity of the approximations used in the development of the low speed forces and moments. As it turned out, the digital solution at hover in no way compared to the analog solution. This was found to be caused by the fact that as soon as a small side velocity occurred, $T_c{}^\text{S}$ was slightly less than 1.0, and the change of $C_N{}^\text{S}$ with angle of attack was no longer equal to zero. Since angle of attack is defined as

$$\alpha = \tan^{-1}\left(\frac{w}{u}\right),$$

it can be seen that if u is zero, α is either undefined, $+90°$ or $-90°$.

We thus have a case where angle of attack switches rapidly from + to $-90°$, and the small moment resulting in the roll axis is enough to completely stabilize the vehicle so that no side velocity can build up.

The digital program was then modified to use the low speed momentum terms, and the two solutions then agreed closely.

The low-speed vehicle dynamics thus obtained agree well with the Langley free-flying scale model data.

After all of these checks were performed, pilot checks were flown to compare the simulation with the previous pilot evaluated simulations.

At this time the simulator was declared operational.

Since the complete static check required from 4 to 6 hours to complete, a "short form" static check was developed which required only about 10 minutes to complete each morning, unless there was an equipment malfunction.

The short check was accomplished at both ends of the fan-powered flight spectrum, i.e., hovering and β_V = maximum.

The check consisted of determining the trim velocity attainable at 100 per cent power, maximum collective setting, c.g. = 243 and it = $+20°$, using the two vector settings. A switch was provided to make $\theta = \alpha$, or

$\gamma = 0$ for these checks. Readouts included β_v, N_g, δ_e, N_{NF}, V_T, α. In addition, the values of stagger and vector for both wing fans were checked at $\beta_v = 0$ with max. and min. collective settings. The nose fan door travel was also checked at zero β_v and max. forward and aft stick.

Any significant malfunction thus became apparent as a loss in speed or a large change in one of the readouts. This check gave reasonable assurance in a short time that the simulation was functioning.

About every 1-1/2 weeks of operating time. the major static check was performed.

2.9.1 Simulation Checkout Detail

To check the simulation for error, several methods were employed. These methods are:

Static Check

To check the simulation statically, the following initial conditions were chosen:

$$N_g = 98\%$$

$$i_t = +20°$$

$$\delta_e = \delta_a = \delta_r = 0$$

$$\beta_v = 10° \text{ (actual)}$$

$$\beta_s = 27°$$

$$C_D S_{\text{Fuselage}} = 320$$

$$\rho = .00205$$

$$V_T = 60 \text{ fps}$$

$$u = 53 \text{ fps}$$

$$v = w = 20 \text{ fps}$$

$$p = q = r = .20 \text{ rad/sec}$$

$$\delta_p = +35.7°$$

$$\varphi = \theta = .2 \text{ rad}$$

$$K_T \eta_T = .80$$

$$\text{Sin } \Psi = \text{Cos } \Psi = .707$$

The fan parameters corresponding to these choices of initial conditions are as follows:

$$P_F = 3.04 \times 10^6 \qquad\qquad P_{NF} = .42 \times 10^6$$

$$C_p^s / C_{p_0}^s = .9874 \qquad\qquad \left(C_{p_0}^s / C_p^s \right)_{NF}^{2/3} = 1.003$$

$$\Delta C_{p_{\beta_s}}^s = -.057 \qquad\qquad \left(T_{0/A} \right)_{NF} = 193 \text{ psf}$$

$$\frac{T_{000}}{A_F} = 230 \text{ psf} \qquad\qquad R_{q_{NF}} = .0187$$

$$R_q = .0158 \qquad\qquad T_{c_{NF}}^s = .981$$

$$T_c^s = .9842 \qquad\qquad N_{NF} = 96.5\%$$

$$N_F = 91.3\%$$

The outputs of all amplifiers, diode function generators, and electronic multipliers were computed using these initial conditions.

The initial conditions were set up on the simulator and the computed values of outputs of the above components were checked against the simulator values. All critical functions read within 5% of the computed values. No component was more than 10% in error.

Dynamic Check

As a check on the dynamic characteristics of the simulation, a digital dynamic program was written and longitudinal and lateral time responses starting from the same initial conditions were run on both digital and analog simulations. The results from both sources in hover and in low speed flight matched closely, being different by no more than 10% in either frequency or time to double amplitude.

As a further check, filmed results from the wind tunnel test of the NASA .18 scale free flight model made in the 30' x 60' wind tunnel at NASA-Langley, showing the aircraft doing a stick fixed divergence in fan mode forward flight, were compared to results of a similar test run on the analog simulation. The comparison of these tests also showed no more than a 10% difference in either frequency or time to double amplitude.

Control Power Checks

To check the control portion of the simulation, both aerodynamic and fan control, control powers for 1/2 and full stick inputs at hover and at a forward speed condition were checked against predicted values. All control power values were good to 10% or better.

Trim Checks

As a final check on the over-all accuracy of the simulation, trimmed flight conditions were run for a range of speeds from hover to the highest fan mode flight speeds for the 2,500 ft. altitude, 93.7°F day. A plot of these conditions is shown in Figure 136. This plot agrees closely with predictions made by the Aerodynamics Group.

Maximum lift over the entire range of forward flight speeds attainable by the computer was also determined. These figures agreed with values predicted by the aerodynamics group to an accuracy of 5% or better. Trimmed drag figures taken over the same range of speeds agreed with predictions to within 5% also.

Stability Augmentation System Checks

To check out the stability augmentation system, roll, pitch and yaw rate signals were fed into the appropriate SA channel and sensitivity and authority limitations for each channel were checked.

Root locus plots were made for the aircraft in hovering flight and maximum gains for stability determined from these plots were compared to values determined on the simulation. The results for these tests in pitch and roll are shown in the root locus sections of this report. Close agreement was obtained between these results.

"Feel" System Checks

To check the feel system, the stick and rudder force gradients in hover and at a forward speed were measured in the cockpit. These checks completed the initial checkout of the simulator.

Daily Check

In order to make certain that computer failures did not compromise the results of the systems study made on the completed simulation, a quick check was made of the simulation each morning, and if this check was not satisfactory, the simulation was completely static checked.

This morning check consisted of two trimmed condition checks, one at 0° vector and one at 47.5° vector. Also checked was the nose fan door travel for full pitch stick inputs at hover.

Variations in the checked parameters at each of the trim conditions did not exceed 3% over the length of the simulator study.

Parameters checked at each of the trim conditions were:

δ_e V_T

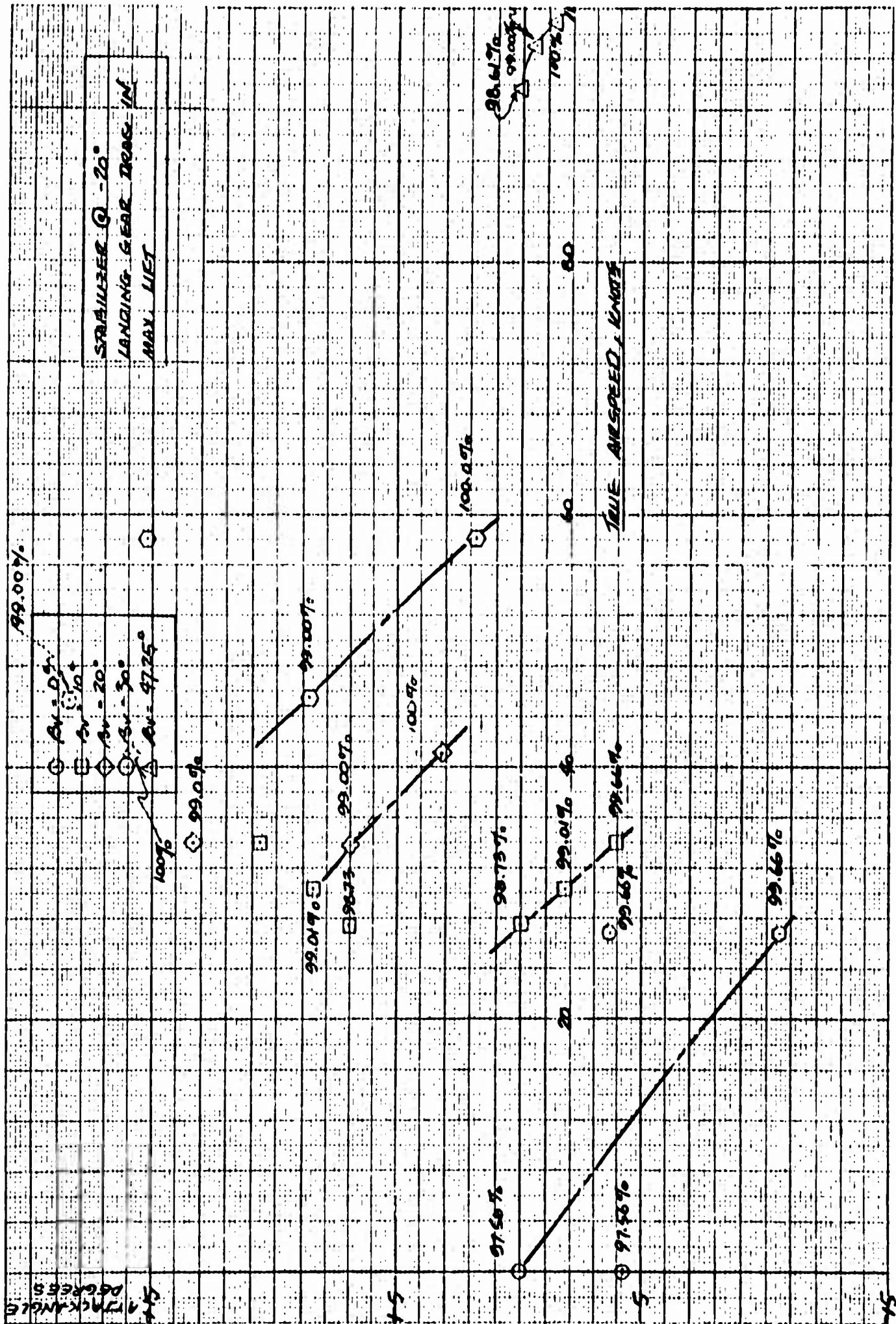N_g α^o

N_{NF} δ_p

Figure 136 Trim Condition Check

BLANK PAGE

2.10   SIMULATOR CHANGES PRIOR TO STUDY PROGRAM

After checkout of the simulator, but prior to commencement of the planned simulator study program, several changes were made in the simulation.

One change, made on the basis of updated information provided by General Electric, was to increase the fan power available at various turbojet rpms.

The increases are shown in Figure 137 and Figure 138, and are approximated closely by adding a constant increment of fan power to each of the old curves.

A constant voltage corresponding to this change is added to the generated fan powers by pots P12 and P13, shown in Figure 85 of Paragraph 2.6.

A second change was made to solve a problem that showed itself in the initial familiarization flights of the simulator made by the pilots prior to the study program.

More effective nose fan thrust reverser doors were required if sufficient pitching moment were to be developed thru the critical transition region at the c.g. positions acceptable for conventional flight.   See Reference 17.

To solve this problem, General Electric was consulted and a new thrust reverser effectiveness curve was determined.

Shown in Figure 139 is the new thrust reverser effectiveness which curve was generated on diode function generator F61.

All further changes to the simulator were made on the basis of the studies shown in Volume II.   These changes are summarized in Paragraph 3.8.
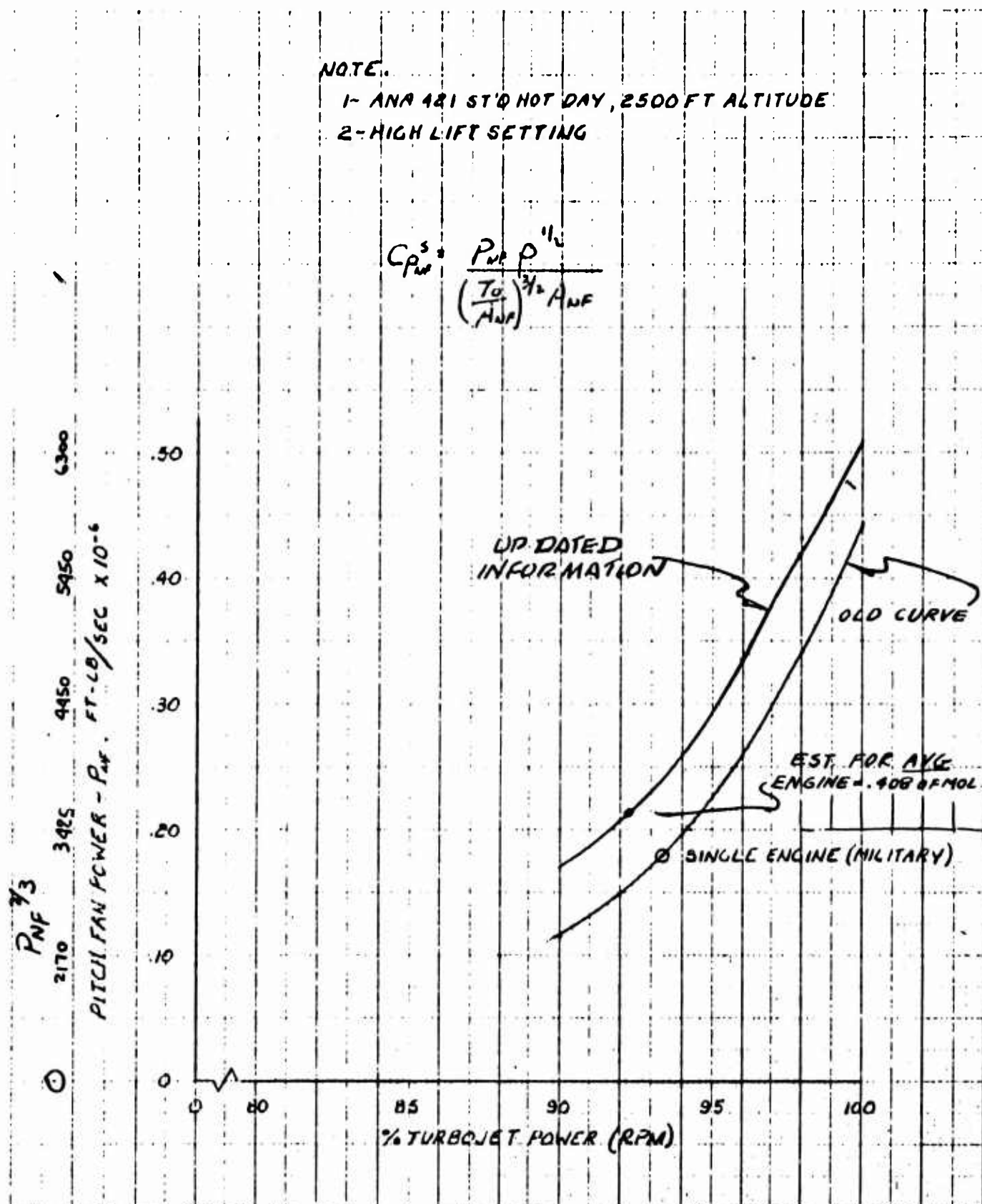
NOTE:
1 - ANA 421 ST'Q HOT DAY, 2500 FT ALTITUDE
2 - HIGH LIFT SETTING

$$C_{P_{NF}}^S = \frac{P_{NF}\, \rho^{1/2}}{\left(\frac{T_0}{A_{NF}}\right)^{3/2} A_{NF}}$$

Figure 137 Pitch Fan Power Curve

NOTE:
ANA A21 STD HOT DAY, 2500 FT. ALTITUDE

$$C_P{}^s = \frac{P_F \, \rho^{1/2}}{\left(\frac{T_{gas}}{A_F}\right)^{3/2} A_F}$$

UPDATED
6-6-63

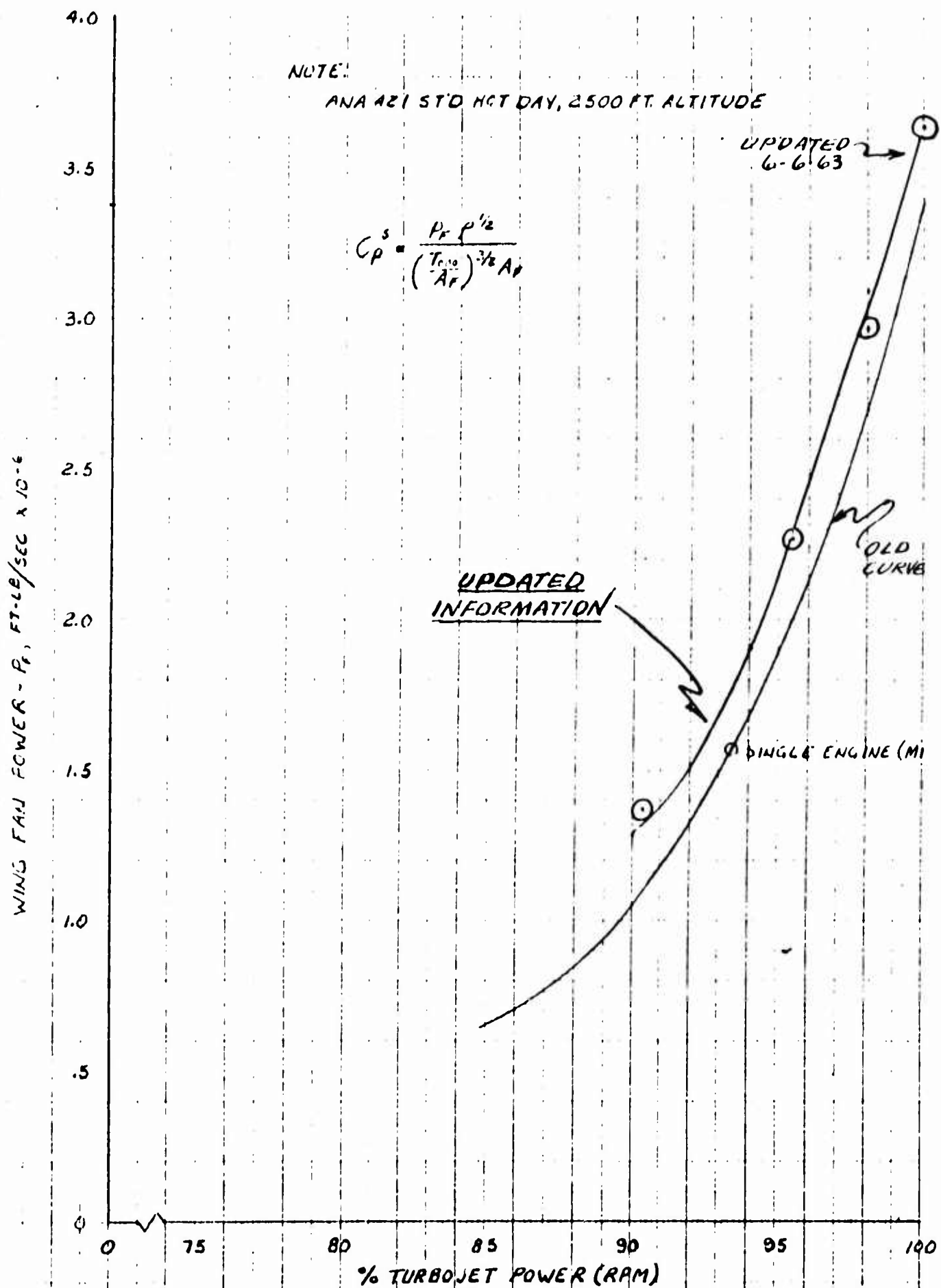UPDATED
INFORMATION

OLD
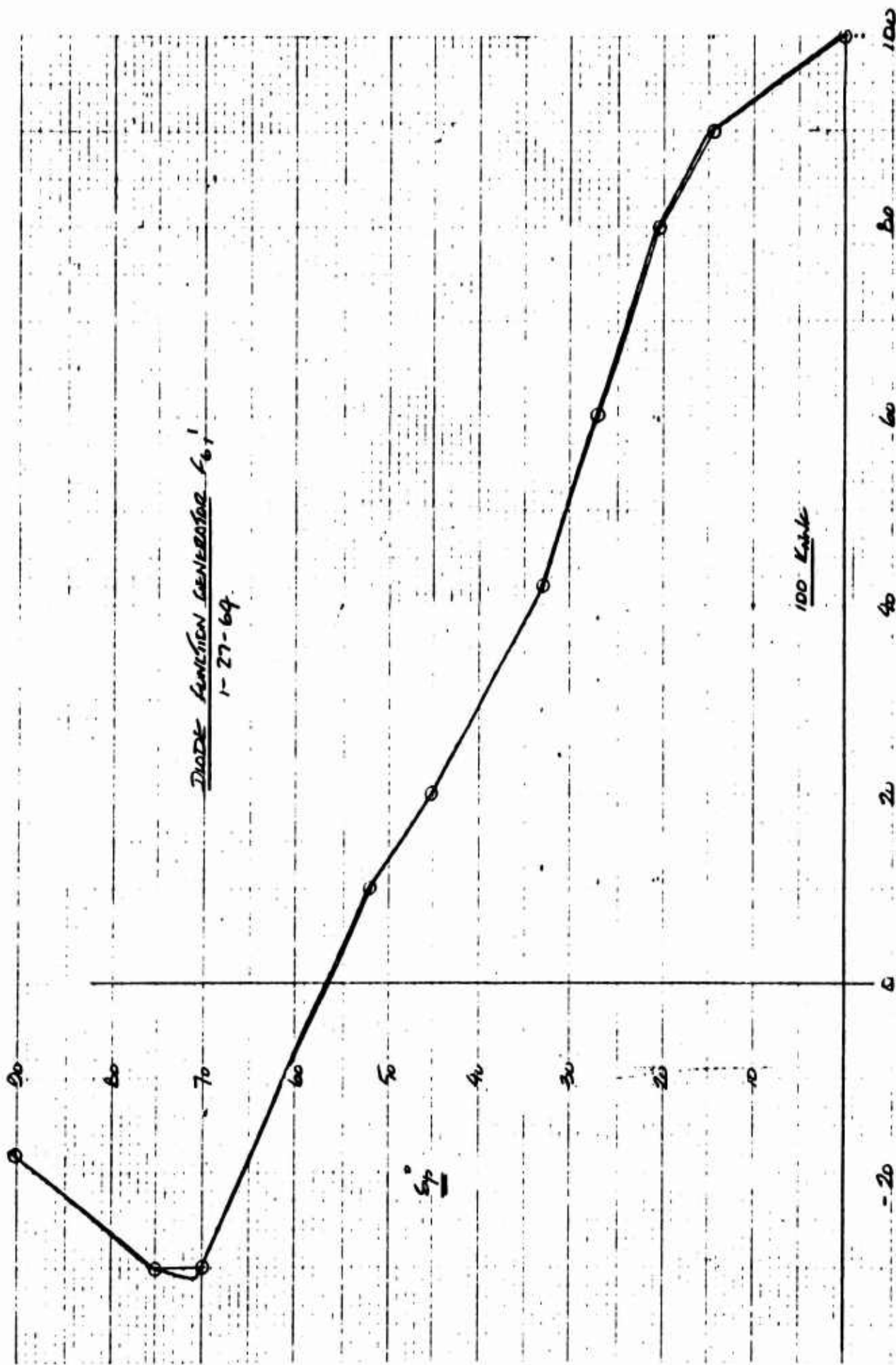CURVE

SINGLE ENGINE (MI

Figure Wing Fan Power Curve

215

Figure 139 New Nose Fan Thrust Reverser - 30% Reverse Capability